

JPRS-JST-89-006 - II

16 MARCH 1989



**FOREIGN  
BROADCAST  
INFORMATION  
SERVICE**

# ***JPRS Report***

**DISTRIBUTION STATEMENT A**

Approved for public release;  
Distribution Unlimited

# **Science & Technology**

***Japan***

4TH INTELLIGENT ROBOTS SYMPOSIUM

VOLUME II

19980630 091

22161

NTIS  
ATTN: PROCESS 103  
BEVERLY FARRADAY  
5285 PORT ROYAL RD  
SPRINGFIELD, VA

22161  
45

REPRODUCED BY  
U.S. DEPARTMENT OF COMMERCE  
NATIONAL TECHNICAL INFORMATION SERVICE  
SPRINGFIELD, VA. 22161

**DTIC QUALITY INSPECTED 1**

JPRS-JST-89-006 - II

16 MARCH 1989

## SCIENCE & TECHNOLOGY

### JAPAN

#### 4th INTELLIGENT ROBOTS SYMPOSIUM VOLUME II

43064062 Tokyo 4TH INTELLIGENT ROBOTS SYMPOSIUM PAPERS in Japanese  
13-14 Jun 88

[Selected articles from the 4th Intelligent Robots Symposium held 13-14 June  
1988 in Tokyo] [Final volume]

#### CONTENTS

|   |    |
|---|----|
| Surveillance Robot for Nuclear Power Station.....                                       | 1  |
| Water Cooling Condenser Pipeline Cleaning Robot for Nuclear<br>Power Stations.....      | 5  |
| Traveling Path Configuration for Pipeline Maintenance Robots.....                       | 11 |
| Autonomous Path--Harunobu No 4.....   | 25 |
| Cruise Control of Parallel Two-Wheeled Vehicle With Steering<br>Mechanism.....          | 37 |
| Helios--Terrain-Adaptive-Type Crawler Vehicle Developed.....                            | 47 |
| KR-I--Articulated Body Mobile Robot.....  | 55 |
| Dynamically Restructured Robotic System With Positioning Accuracy,<br>Joint Torque..... | 66 |
| Rotary Shoe Configuration for Mobile Robot.....   | 78 |

|  |     |
|--|-----|
| Development of Long-Arm Manipulators.....  | 91  |
| Active Positioning Systems Using Laser Beams, Corner Cube<br>Reflectors.....     | 104 |
| Network for Self-Contained Mobile Robots Involved in Cooperative<br>Motions..... | 117 |
| Programming Language for Sensor-Raised Mobile Robot Motions.....                 | 128 |
| Attitude Stabilization System for Mobile Robots.....                             | 139 |
| High-Speed Line Tracing Technique Using CCD Camera.....                          | 149 |
| Mobile Robot Position Referencing Using Map-Based Vision Systems....             | 160 |
| Safety Evaluation of Man-Robot System.....                                       | 171 |
| Fuzzy Path Pattern of Automatic Vehicle With Ultrasonic Range<br>Detector.....   | 182 |
| Bilateral Control of Smart Manipulators.....                                     | 189 |
| Closed Loop Displacement Control of Multilink Dynamic Robot Arms....             | 199 |
| Obstacle Avoidance Teaching Techniques for Two-Link Manipulator.....             | 212 |

## Surveillance Robot for Nuclear Power Station

43064062 Tokyo 4TH INTELLIGENT ROBOTS SYMPOSIUM PAPERS in Japanese  
13/14 Jun 88 No 113 pp 133-135

[Article by Takasuke Nakajima and J.R. White, Nippon Rimotekku]

[Text] 1. Introduction

In a nuclear power station, many pieces of equipment and piping are installed in a limited space. The inspection and maintenance of the equipment are carried out in an environment which is affected by radioactive rays not only from the piece of equipment being inspected, but also from nearby equipment.

Attempts have been made in recent years to keep the inspectors and maintenance staff from being affected by radioactive rays through automation and remote control.

The robot discussed in this report was developed to collect data and carry out inspection and simple maintenance in a radioactive environment in place of workers. Function confirming tests conducted in a nuclear power plant have proven that it is capable of providing sufficient functions.

## 2. Configuration and Functions of Robot System

This robot system is composed of a robot which enters areas affected by radioactive rays to collect data and carry out tasks including inspection, a portable operation control board to manipulate the robot from a distance, and equipment to house and carry the robot to another room, keeping clean areas from being polluted by radioactive substances emitted from the robot's surface.

Robot manipulation is conducted outside the work area so that the operator and the operation control board will not be contaminated by radioactivity. The operation of the robot is displayed on a graphic display incorporated in the operation control board according to real time. A TV monitor shows the work and the state of the surrounding area. Various measured data are indicated on the graphic display and recorded.

The robot can travel from the transportation equipment to a designated site, and is equipped with a TV camera to monitor the surrounding areas of the floor. The measurement equipment of the robot includes an air dust sampling device composed of a blower and a filter, a thermocouple to measure the temperature of the environment, a dose-rate meter to measure the dose rate of the environment, a directive microphone to detect abnormal noise from steam, water, or rotary devices, and a TV camera with an elevator to monitor the upper work area without having to traverse the stairs. The elevator incorporates lights, and can go up and down, revolve and turn with the camera.

The power for the robot is supplied through a cable connecting the operation control board and the robot. When more power is needed, e.g., for lighting, additional power is supplied by batteries built into the robot. These batteries are charged by a portion of the electric power supply, through the cable, while the load is low.

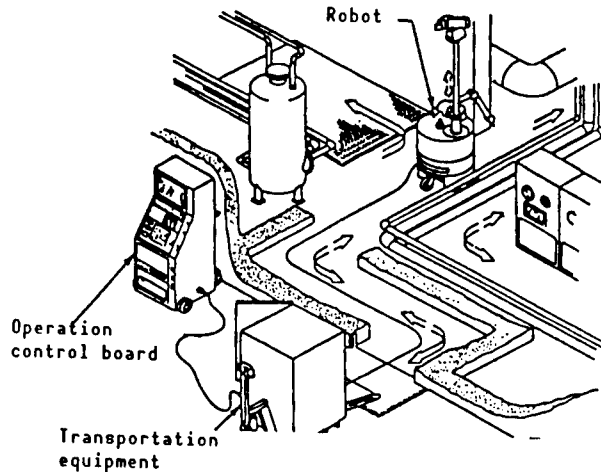


Figure 1. Configuration of Robot System

### 3. Robot

The robot is cylindrical with slight irregularities, facilitating the elimination of radioactivity from its surface in case the robot is polluted. It is 0.8 m in diameter, 1.4 m in height, and 270 kg in weight.

The robot runs on two driving wheels and a trailing wheel. The driving wheels, driven by separate electromotors, are capable of going back and forth and rotating on the same spot. The traveling speed can vary between 0-18 m/minute. Instructions on the driving direction are given by the operation control board's joystick, by input into a computer incorporated in the board, or on the touch screen of the graphic display. Winding and unwinding the cable while the robot is running is done by a computer so that no tension is put on the cable. Figure 2 [not reproduced] shows the robot traveling.

Electronic computers, such as a radioactive dose-rate meter, and a TV camera, are installed in the upper part of the robot.

The TV camera, along with the lights and a microphone, is loaded on a mechanism that can be extended to a height of 4.5 m. It can go up and down, turn and rotate. The ascent and descent of the camera are made after the robot stops to prevent damage from occurring through obstacle interference. The position of the camera is indicated on the graphic display.

The robot has electromotive arms with a capacity of 10 kg and 7 degrees of freedom. These arms can inspect surface contamination of floors and walls, open and close valves, retrieve fallen objects, and deal with jigs. The robot arm is an application of a master slave manipulator arm, which was developed for the maintenance of equipment and piping in an isolated room (cell). The robot arms are solely driven by a servomotor. The motion of the arms, when the robot has two arms, is illustrated in Figure 4. "Reaching up" and "crossed-over arms" in the figure are motions that cannot be made by the conventional master slave manipulator. These robot arms have functions more similar to those of human arms. They are manipulated either by remote manual operation during visual confirmation on the TV monitor or by automatic operation by the computer. The positions of the robot arms are indicated on the graphic display at real time. Figure 5 [not reproduced] illustrates work accomplished by the robot arms.

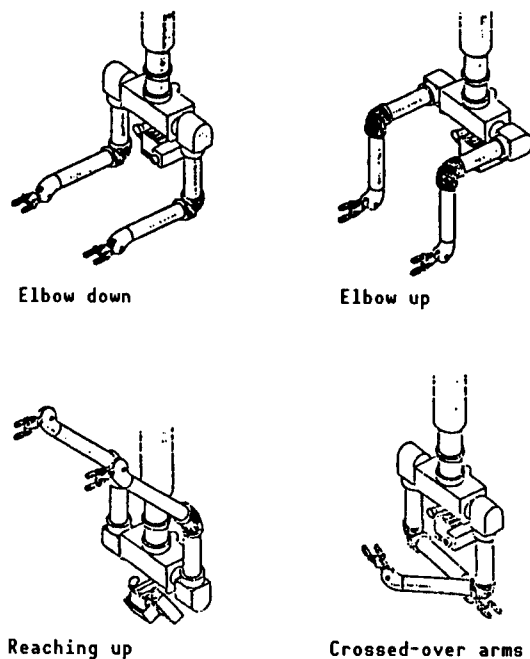


Figure 4. Robot Arm Motions When Two Arms Are Provided

Measured data are transmitted by the cable or through optical fibers to the operation control board to be processed.

#### 4. Operation Control

Operation of the robot is done solely on the operation control board by either remote manual operation or automatic operation by the computer. A main operation component is located in the central part of the front side of the operation control board. The upper part of the board houses a touch screen-type graphic display which is capable of showing the robot functioning in terms of the work area and the robot's position, the travel distance, the traveling direction, the position of the robot arms, and measured data, such as the radioactive dose rate, according to real time.

The board incorporates TV monitors for travel observation and visual confirmation. Figure 6 [not reproduced] is a photograph of the operation control board. When the robot travels automatically, it returns to the spot it started with an error of 5 cm. Manual operation of the robot arms can be learned through a brief training period and does not require special skills.

The scope of the TV camera for visual confirmation from 4.5 m overhead involved no problems, but the failure to zoom left the image unclear.

The combined use of the highly directional microphone and visual confirmation makes it possible to detect abnormal noise and specify the source in a short time, while the same work based entirely on the noise entails an error of  $\pm 35^\circ$ .

The functions of the system were fully proven by the experiments in a nuclear power station.

#### 6. [sic] Conclusion

Judging from the results of the experiments conducted in the nuclear power station and a comparison between the cost of employing workers and the cost of introducing the system, the robot is worth introducing.

However, the robot, as it is, cannot always be given full play in a nuclear power station with its many stairs and levels. Therefore, a robot with a caterpillar instead of wheels has been newly developed.

## Water Cooling Condenser Pipeline Cleaning Robot for Nuclear Power Stations

43064062 Tokyo 4TH INTELLIGENT ROBOTS SYMPOSIUM PAPERS in Japanese  
13/14 Jun 88 No 114 pp 137-140

[Article by Katsuhei Tanemura, Isamu Sano, and Jusei Shimada, Tokyo Electric Power Co.,; and Yoshio Sumitani, Katsuki Otake, Yasuo Fujitani, Masaaki Fujii, Shigeo Oda, and Shigeru Kajiyama, Hitachi, Ltd.: "Development of a Water Cooling Condenser Pipeline Cleaning Robot for Power Stations, Report No 2--Expansion of Work Areas"]

### [Text] 1. Introduction

A condenser, which is the main heat exchanger of a turbine plant for power generation, usually uses natural sea water for cooling. Therefore, the inner surface of its pipeline accumulates considerable dirt, including marine organisms, which attach themselves to the surface. Usually, such a pipeline is cleaned regularly by an employee using a nylon brush. The cleaning work, however, is so harsh that the demand exists for it to be automated. The basic development of a water cooling condenser pipeline cleaning robot for the purpose of automation of the work was discussed in Report No 1, "Prototype Manufacture of Components." Report No 2 will center on the subsequent development in terms of expanding the work areas.

### 2. Work To Be Automated

Cleaning condenser pipelines is done with a brush by a worker faced with a vertical pipeline board, 6 m high and 4 m wide. From 8,000-10,000 pipelines must be cleaned, using a scaffold (Figure 1). It takes a worker 30 seconds, on the average, to clean one condenser pipeline. Cleaning them all requires many hours of labor. The narrow work site and the danger of gas generating from the organisms present even greater difficulties for the worker.

The robot is intended to build and dismantle the scaffold, set a brush, and clean with it (Figure 2). It is aimed at mechanizing a substantial part of the cleaning work by automatically traversing the vertical pipeline board and cleaning the pipelines with a brush.

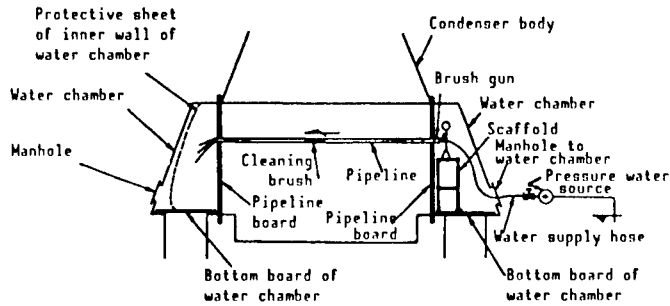


Figure 1. Conceptual Chart of Water Cooling Condenser Pipeline Cleaning

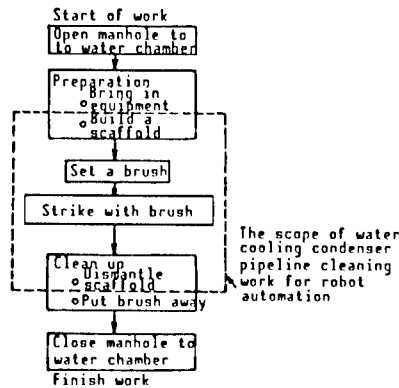


Figure 2. Cleaning Process With a Brush and Scope of Robot Automation

### 3. Configuration of Water Cooling Condenser Pipeline Cleaning Robot

As illustrated in Figure 3, the robot consists of a pipeline board surface traveling mechanism to travel on the pipeline board surface by gripping the pipes, a work arm to be mounted on this mechanism to place a brush striking nozzle in the pipeline hole, a brush feeder and a brush supply hose to provide a brush, a brush striking nozzle to supply water under pressure with a brush, a unit to control the devices, and a power supply unit.

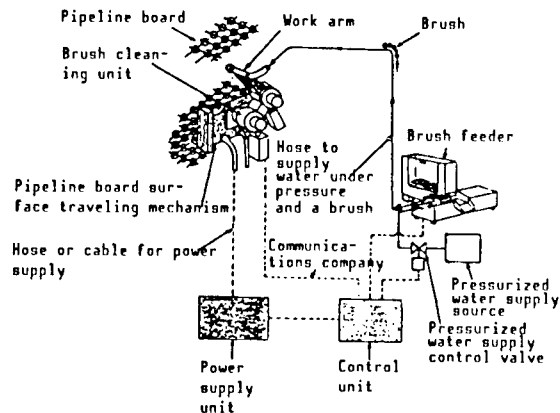


Figure 3. Configuration of Water Cooling Condenser Pipeline Cleaning Robot

## 4. Components of Condenser Pipeline Cleaning Robot

### 4.1 Pipeline Board Surface Traveling Mechanism

This apparatus is composed of two traveling parts--one for the vertical (Y) direction and the other for the horizontal (X) direction. These parts enable the apparatus to move on the vertical pipeline board. Each traveling part incorporates four pairs of clamp feet, which grip a pipeline. It can move the feet in and out of the pipelines, as well as grip them. The principle involved in traveling upward is illustrated in Figure 4 as an example. Air cylinders driven by  $12 \text{ kg/cm}^2$  are used as actuators to drive the body, move the clamp feet in and out of the pipelines, and open and close the feet.

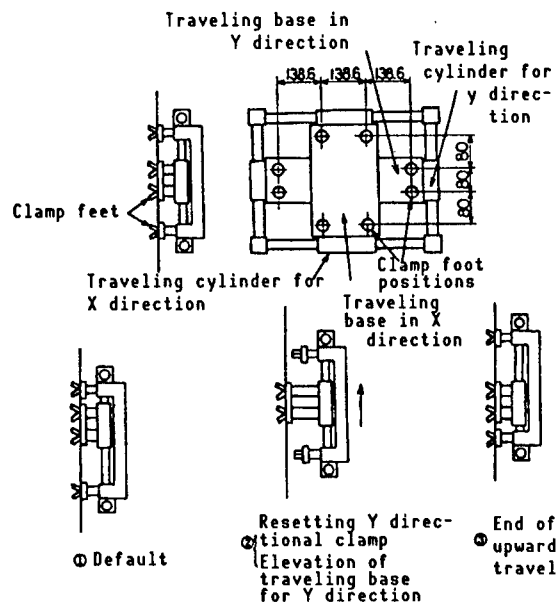


Figure 4. Principle Involved in Pipeline Board Surface Traveling Mechanism

### 4.2 Work Arms

This apparatus consists of two (Nos 1 and 2) arms, as shown in Figure 5. The brush striking nozzle (at the tip of arm No 2) is placed at a specified pipeline hole near the pipeline board surface traveling apparatus when a certain turning angle is assigned to these arms. The effective length of the work arms is 245 mm for arm No 1, and 265 mm for arm No 2, totaling 510 mm.

### 4.3 Brush-Cleaning Unit

A brush-cleaning unit sets a cleaning brush in the hole of a pipeline, supplies it with pressurized water, drives the brush through it, and cleans it.

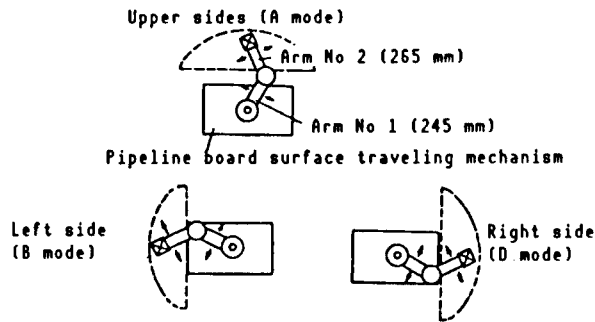


Figure 5. Location Method for Work Arms

The cleaning brushes are set, one by one, in a brush supply hose, which extends from a brush feeder to the brush striking nozzle, by the brush feeder's supply function. They are then inserted into a pipeline through the hose and the nozzle by pressurized water supplied in the brush feeder. The continued supply of pressurized water from the nozzle to the pipeline makes the cleaning brush travel through and clean the pipeline. The brushes are flexible so that they can move through the bent hose. The pressure of the water is equivalent to that of the water used in power generation plants.

Photograph 1 [not reproduced] shows the exterior of the water cooling condenser pipeline cleaning robot incorporating the above apparatuses.

## 5. Work Control and Record

The following points should be taken into consideration when the robot is used to clean an actual condenser pipeline.

- (1) Preventing dry portion due to the irregularities of water cooling pipeline configurations.
- (2) Preventing blockages in water cooling pipeline (an inevitable phenomenon in a sea water-type heat exchanger due to leakage around pipe plug or adhesion of marine life).
- (3) Recording the results of cleaning work for each cooling pipeline location.

For this purpose, the following control and recording devices have been developed. (The devices are controlled by a 16-bit personal computer and a sequencer.)

### 5.1 Travel Control

At first, a basic traveling route on the pipeline board is set up, taking into account the pipeline configuration and known plug parts. This is recorded as data (Figure 6). If while working the robot encounters an obstacle (a blockage) which was not anticipated, the adhesion of the robot and the pipeline board must be measured to determine whether the pipeline



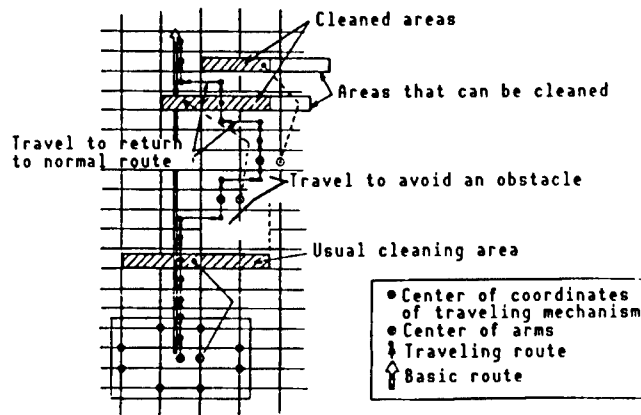


Figure 8. Cleaning Area When Route Is Changed To Avoid an Obstacle

## 6. Operational Test

Operational tests of the robots conducted on a mock-up principle board, modeled after a condenser for which the robot will be used, proved that the robot is able to deal with a given mock plug (obstacle) by controlling its traveling and brush striking operations. It was also proven that this robot is capable of working as fast as a human worker.

Photograph 4 [not reproduced] illustrates the operational tests.

## 7. Conclusion

This research helped establish the technology necessary to expand the work areas of a water cooling condenser pipeline cleaning robot, i.e., a function to control traveling and obstacle avoidance during the brush striking operation, and a function to record work results. It has been confirmed that the robot is capable of performing the job as fast as a human worker for the entire pipeline board surface, as long as there are no mechanical limitations.

Our research group plans to add intelligence to the control devices and conduct research on and the development of a function to set a traveling route more efficiently. We also intend to expand the function to apply the robot to the nondestructive inspection of pipelines (a turbulence flow detection test).

## References

1. Tanemura, Oda, et al., "Development of Water Cooling Condenser Pipeline Cleaning Robot (Report No 1. Prototype Manufacture of Components)," The 5th Symposium of the Japan Robotics Society, 1987, p 545.

## Traveling Path Configuration for Pipeline Maintenance Robots

43064062 Tokyo 4TH INTELLIGENT ROBOTS SYMPOSIUM PAPERS in Japanese  
13/14 Jun 88 No 115 pp 141-146

[Article by Toshi Fukuda and Hidemi Hosogai, Tokyo University of Science, and Masashi Osuka, Toshiba: "Task-Level Based Traveling Path Configuration for Pipeline Maintenance Robots"]

### [Text] 1. Introduction

The piping (pipelines) widely used in petrochemical plants and nuclear power stations requires inspection and maintenance to preclude accidents due to leakage or corrosion. However, the work is dangerous and difficult for humans to perform.<sup>1</sup> We conducted research on autonomous robots that would perform these tasks in place of human workers. Having designed and produced three types of robots, we studied the technologies relating to maintenance robots, such as performance evaluations, movement control methods, and diagnostic systems involving pipeline abnormalities.<sup>2-7</sup>

This report will focus on the third robot. First, its structure and basic movement will be explained, and then, obstacle detection and the configuration of a joint path to travel involving a low torque will be discussed. A method to pass by each obstacle will also be mentioned.

Path surveillance is a prerequisite in order for a robot to move automatically on pipelines configured similarly to a three-dimensional labyrinth. Most of the research on path surveillance by moving robots deal with travel on a plane, and research on three-dimensional travel, such as in pipelines, is difficult to find. We built an expert system for robots traveling in a three-dimensional pipeline system using Prolog, which generates the traveling path and commands automatically while the work is being planned. This system will also be discussed.

## 2. Structure and Basic Movement

### 2.1 Structure

Figure 1 shows the third robot schematically. This robot is composed of two pairs of gripper-type arms, a body connecting them, and sensor units to recognize the environmental status and diagnose pipeline conditions. The

body, equipped with a straight movement joint and a joint that twists the body along the circumference of a pipeline surface, is able to make intermittent movements in the direction of the length and on the circumference of a pipeline. The body and the arm units are connected by a rotary joint. This enables either arm to grip a pipeline and lift the entire robot, including the other arm. The robot is composed of five links and four joints, in addition to that governing the opening and closing of the arms, as well as the sensor units.

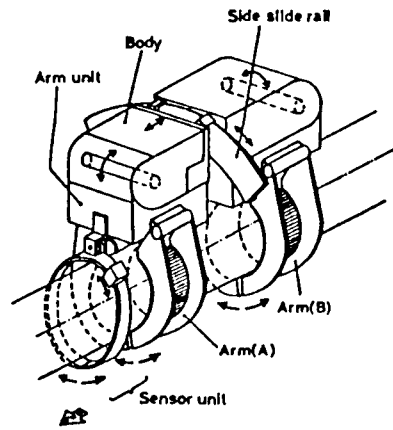


Figure 1. Schematic View of Third Robot

## 2.2 Basic Movement

Straight movement is made in stages, caterpillar-like, by gripping a pipeline with alternating arms and extending and shrinking the body. When it passes over a flange or an L-shaped pipe, it twists the body on the foundation of one of the arms, grips the pipe with the other arm, and twists the body again on the foundation of the latter arm. Figure 2 illustrates how it passes over an L-shaped pipe. These movements enable the robot to pass over a T-shaped pipe and transfer to an adjacent pipe.

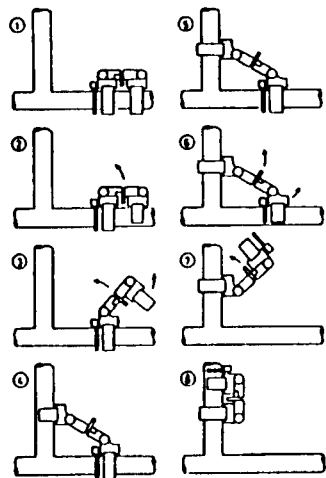


Figure 2. L-Shaped Pipe Traversing Mode

While gripping a pipeline with alternating arms, the whole robot can be controlled as one manipulator with a foundation, i.e., the arm gripping the pipe, and an end effector, i.e., the other arm. The robot moves by repeating two modes, one for the state in which the front arm functions as the foundation and the other for the state in which the rear arm serves as the foundation. We call this dual mode control. The joints are controlled in each mode.

### 3. Minimum Joint Load Torque Method

This robot passes over an L-shaped pipe by gripping it with the alternating arms, and traverses other types of pipes by using varying movements. As for (4) of Figure 2, there is more than one target value since the arms can grip anywhere in the range of the pipeline, as indicated in Figure 3. Therefore, the influence of the link weight should be converted into coordinates, so that the posture with the minimum static joint load torque can be selected.

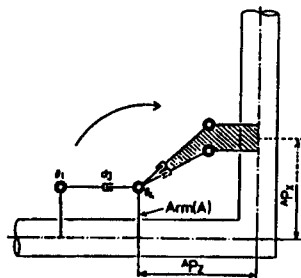


Figure 3. Gripping Range

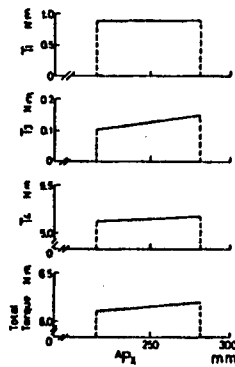


Figure 4. Calculation Results of Joint Load Torque

The calculation results of the load torque of each joint in Figure 3 ( $A_P = 300$  mm) are shown in Figure 4. The target value of the joints is calculated in this way.

## 4. Configuration of Optimal Path by Dynamic Planning Method

### 4.1 Formulation of Evaluation Function

The target angle of each joint was determined in the previous chapter. A path configuration method for the target angle will be suggested in this chapter. Joint control without advance planning is not efficient, since the joint torque might draw a long locus. Therefore, the relationship between the joint torque and a target value error was formulated as an evaluative function, and a joint path with a lower torque was determined by a dynamic planning (DP) method.<sup>9</sup> The evaluation function  $g(\theta, t)$  involves the total torque of each joint, the total of the target value differentials, and weight  $w$ . A joint path  $\theta(t)$  that minimizes  $g$  during time  $0-T_\theta$  is determined under the constraints of the starting and ending point conditions of each joint, the mobile range of each joint, the speed range, and the torque limits of each joint. These constraining conditions affect the static situation. As for the speed, only the range is given. In some cases, the target value is not attained by one DP. In those cases, DP is calculated first according to time (the right direction). If the target value is not reached, DP is calculated from the target value relative to the default value (reverse direction). Since the case evaluation is made in either direction, although the expressions differ, the calculations will definitely coincide at some point. Therefore, a comprehensive evaluation is made by the two directions.

If the evaluative function of the right direction is  $F(t)$  and that of the reverse direction is  $B(t)$ , when  $\Delta t$  is infinitesimal, they are expressed as follows:

$$\begin{aligned} F(t+\Delta t) &= \min (F(t) + \Delta t g(t+\Delta t)) \\ B(t-\Delta t) &= \min (B(t) + \Delta t g(t-\Delta t)) \end{aligned}$$

First, the right direction is checked. If the target value is not achieved, the reverse direction is checked. A final evaluative function,  $I_{cri}$ , is given as the total of  $F(t)$  and  $B(t)$  at the point at which the two calculations meet at time  $t = t^*$ . Along with these calculations, the sums of the torque and the error are calculated as  $T_{cri}$  and  $E_{cri}$ , respectively.

### 4.2 Simulation

A passage simulation involving an L-shaped pipe in control mode B, equivalent to the example in chapter 3, was carried out. Figure 5 shows the case when the path  $\theta(t)$  increased monotonously without using DP. Figures 6 and 7 indicate DP results when  $w = 0.2$  and  $0.8$ , respectively.

The evaluative function is as follows:

|          | $I_{cri}$ | $T_{cri}$ | $E_{cri}$ |
|----------|-----------|-----------|-----------|
| Figure 5 | --        | 141.9     | 228.2     |
| Figure 6 | 148.7     | 129.7     | 153.5     |
| Figure 7 | 120.5     | 98.9      | 206.9     |

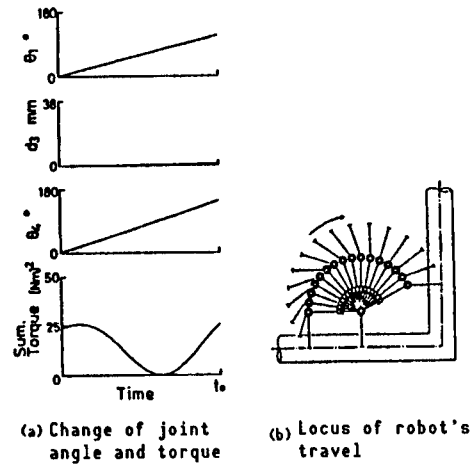


Figure 5. When DP Is Not Used (Monotonous increase to target value)

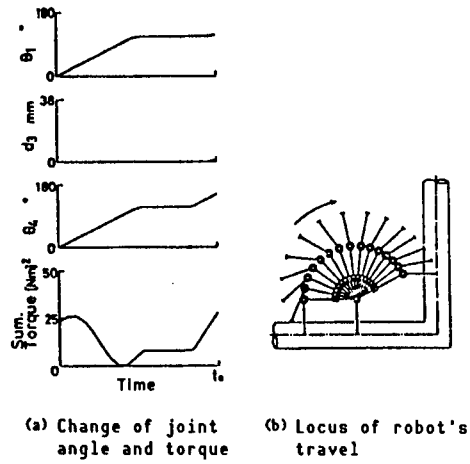


Figure 6. Results of DP ( $w = 0.2$ )

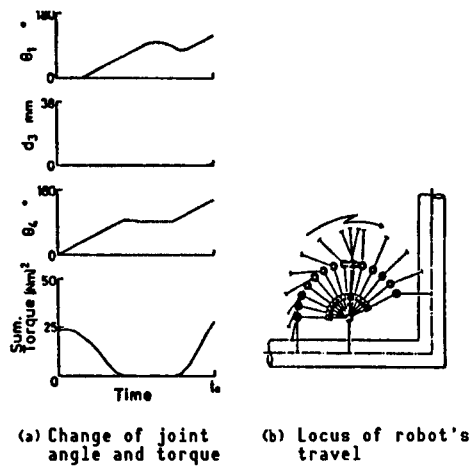


Figure 7. Results of DP ( $w = 0.8$ )

$E_{cri}$  of Figure 6 ( $w = 0.2$ ) is small because it is focused on the joint angle error, while  $T_{cri}$  of Figure 7 ( $w = 0.8$ ) is small because the joint torque is given priority. In either case, the result is smaller than that in Figure 5, proving the effectiveness of DP. An optimal path for a given weight  $w$  can be determined in this way.

## 5. Path Planning Expert System

### 5.1 Outline of PPEs (Path Planning Expert System)

A main objective of this system is to automatically generate a traveling path for a robot in a plant with a given environment. The operator assigns a task, ordering the robot to "go to site A, and inspect for abnormalities." The system breaks it down into subtasks of "1) going to site A, 2) carrying out an inspection, and 3) coming back," and makes a subtask plan. In this report, the traveling tasks of 1) and 3), i.e., path planning, will be discussed.

The configuration of this expert system is illustrated in Figure 8. It consists of a map operation portion to register and revise plant maps for path planning, a graphics part to confirm the maps and paths, and a path planning execution portion.

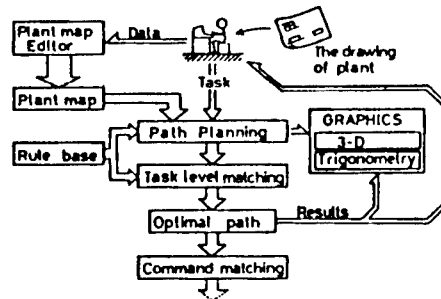


Figure 8. Configuration of PPES

### 5.2 Information Necessary for Pipeline Maintenance

Usually a plant has an intricate pipeline system which is further complicated by a variety of fittings. A maintenance robot requires certain information to enable it to move on the pipelines autonomously and perform the tasks. The necessary information is broken down below. In practice, however, it is imperative to add detailed data to each item.

#### (1) Information concerning a pipeline system

- Pipeline path (direction of straight pipes, position and direction of joints, connections with objects other than pipes (walls, tanks, etc.))
- Information on fittings (straight pipes, flanges, valves, supports, meters, pumps, tanks, etc.)

- Exterior environment (temperature of the room, humidity, intensity of illumination, noise level, etc.)

(2) Information concerning the robot system

- Information on location (current location, time, and distance of travel, path taken by the robot)
- Performance of the robot (
  - total length, total height, total width, weight
  - moving range of the joints, speed range
  - sphere within the reach of the arms
  - performance of the sensors and the diagnostic instruments)

(3) Information concerning execution of tasks

- Contents of tasks (moving the robot, inspection, diagnosis (spots and items for inspection), repair)
- Difficulty of task execution (time taken for execution, task level)

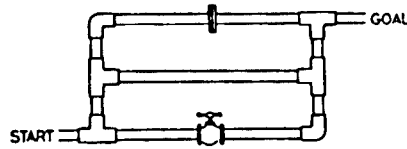
Possessing the above information in a data base and utilizing it enable autonomous travel and maintenance to occur.

### 5.3 Plant Map Operation Portion

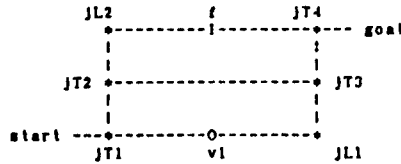
A map must be input as data prior to path surveillance. The plant map operation portion is composed of a registration part, a main part into which pipe connections can be easily input, a correction part to correct input mistakes, a display part, a partial measure part, and a retrieval part which retrieves the data contents. The plant map considers such distinctive points as L-joints, flanges and valves to be nodes, and a pipe between two nodes to be an arc. For example, the plant map of a pipeline system like that shown in Figure 9(a) is given in Figure 9(b).

### 5.4 Graphic Display Portion

Since the data input in the previous section is hard for people to understand, it is very important to confirm it visually on a graphic display. The system is capable of displaying both three-sided charts and three-dimensional bird's-eye graphics. The proper use of these types of graphics promises efficient confirmation. Figure 10 shows examples of graphic display. The graphics can also be used to confirm the results of path planning.

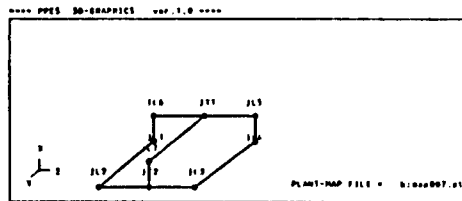


(a) Example of pipeline system

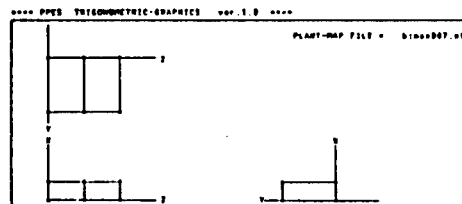


(b) Plant map

Figure 9.



(a) Three-dimensional map



(b) Three-sided chart map

Figure 10. Graphic Display

## 5.5 Path Planning

### (1) When the picture can be drawn with a single stroke

First, a task to "show a path from the start to the goal" in the case of Figure 9(b) was assigned to the robot. In the first step the path is not allowed to repeat itself. This problem can be solved in the same manner as are well-known graph surveillance problems. Prolog matches patterns and prepares an answer that meets the required conditions. The above question and its answer are as follows:

```

?-go(start,goal,Way).
Way = [start,jt1,v1,jl1,jt2,jl2,f,jt4,goal];
Way = [start,jt1,v1,jl1,jt3,jt4,goal];
Way = [start,jt1,jt2,jt3,jt4,goal];
Way = [start,jt1,jt2,jl2,f,jt4,goal];
no
?-

```

(2) When the picture cannot be drawn with a single stroke

If an inspection point is located in a dead end, the task cannot be performed in the foregoing way. In this case, "nodes the robot would have to go through (Mx) on the way to the inspection point (Mt) are found first, then a single stroke picture is drawn from the start to the goal by way of Mx, and the intervals between Mx and Mt are added. Figure 11 is an example of this situation. Mx is defined on Prolog so that it is obtained when Mt is given. For example, if 7 and 8 in Figure 12 are assumed to be Mt, 6 and 4 turn out to be the respective Mx, and the route is found as shown below.

```

! ?-findx(1,5,[7,8],Mx).
Mx= [4,6]
yes
! ?-possibly_gox(1,5,UAY,[7,8]).
UAY= [1,2,6,8,6,9,4,7,4,3,10,5];
no
    
```

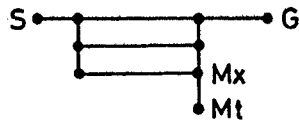


Figure 11. Nodes the Robot Would Have To Pass Through

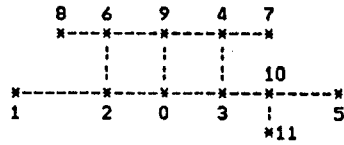


Figure 12. Map With Dead Ends

(3) Task Level

The method discussed in the preceding section made it possible to generate a path that goes to more than one inspection point. However, more than one path candidate may exist if the system deals with a complicated pipeline system or if the robot transfers from one pipe to an adjacent pipe. In such a case, an optimal path must be selected. Here, the concept of "task level" is used as an evaluative criterion. The total task level is calculated for each path, and the path with the lowest level is chosen. The task level defined by the formula below refers to the difficulty of the robot's motions, such as passing over a flange and a T-shaped pipe, transferring to another pipe, and going straight, depending on the positions of the robot and pipes.

$$L_{task} = w_1 E + w_2 T + w_3 V + w_4 S \quad (1)$$

- $L_{task}$ : task level
- E: change of potential energy during the ascent and descent of the robot
- T: static joint load torque according to the weight of the robot
- V: traveling speed of the robot

- S: the number of steps required to alternate the grippers, and extend and shrink the robot
- $w_{1-4}$ : weight applied to each component

The task level can be predetermined, based on the change in the joint load torque and the potential energy needed to overcome an obstacle, as well as the traveling speed and the number of steps needed for travel. We anticipated the 8 basic patterns shown in Figure 13, and determined a total of 18 task levels (except for overlaps) for them when  $\theta = 0^\circ, 90^\circ,$  and  $180^\circ$ , provided that 1) gravity is applied in the vertical direction in each chart, 2) the robot travels on the upper side of a pipe and returns to the upper side after negotiating an obstacle, and 3) when traveling on a vertical pipe, it retains the posture it had immediately after transferring from the previous pipe, and 3) one of the branches of L- or T-shaped pipes is horizontal. These rules are appropriate for the practical control of the robot and cover the factors involved in robot travel, such as energy (electric power consumption, distance), speed (time), the number of steps (time, distance). Adjusting the weight  $w_{1-4}$  to the robot's characteristics enables the system to respond to such special tasks as minimum energy problems and shortest time problems. The display result of the hypothetical plant model illustrated in Figure 14 is indicated below. Figure 15 shows the same results chart form.

```

---- Specify start      point_A
---- Specify goal      point_B
---- Inspection spot? (end by [CR]): meter 1
---- Inspection spot? (end by [CR]):

**** Calculation in progress ****
**** Following three paths are possible ****
Use= point_A, j11, j12, j13, j13, flange1, nut2, flange2, j16, j19, j10, valve1, j15, j17, j19, j18, j17, j12, j14, meter1, j14, point_B Task level= 2685
Use= point_A, j11, j12, j13, j13, flange1, nut2, flange2, j16, j18, j17, j12, j14, meter1, j14, point_B Task level= 1654
Use= point_A, j11, j12, j14, nut1, j11, j17, j12, j14, meter1, j14, point_B Task level= 1554

**** Path with minimum task level is ****
Use= point_A, j11, j12, j14, nut1, j11, j17, j12, j14, meter1, j14, point_B Task level= 1554

**** End of route selection ****

```

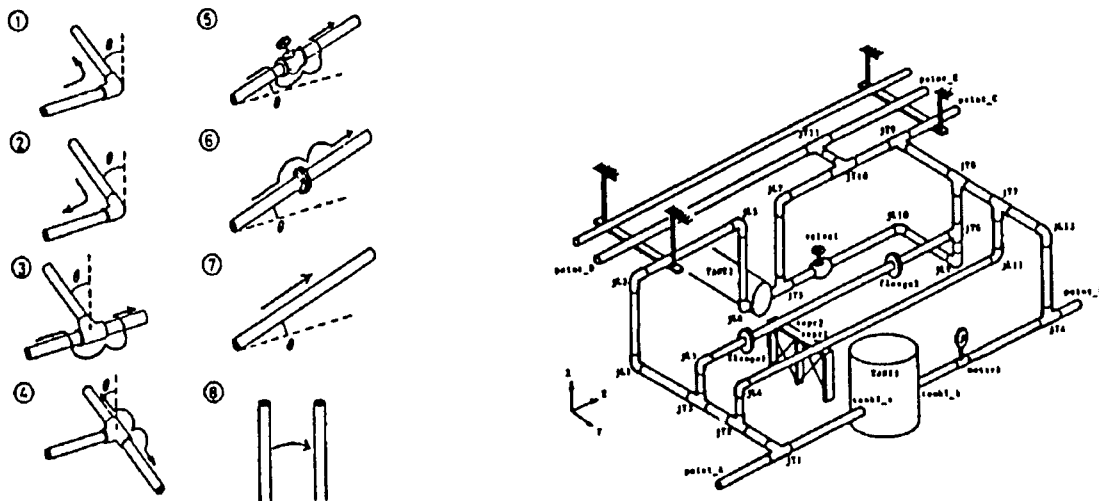
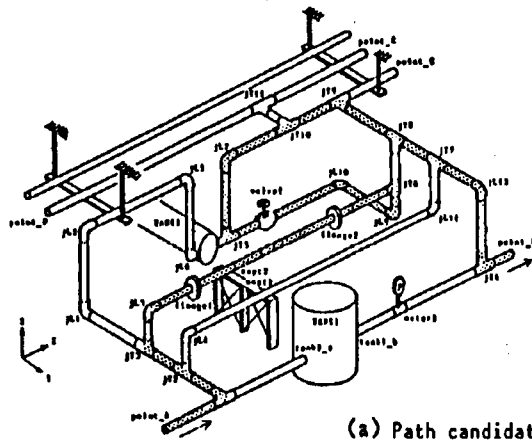
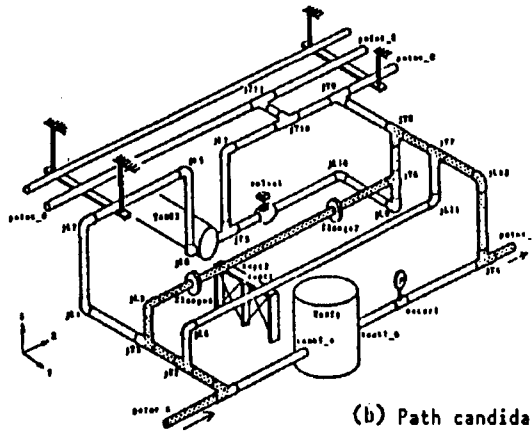


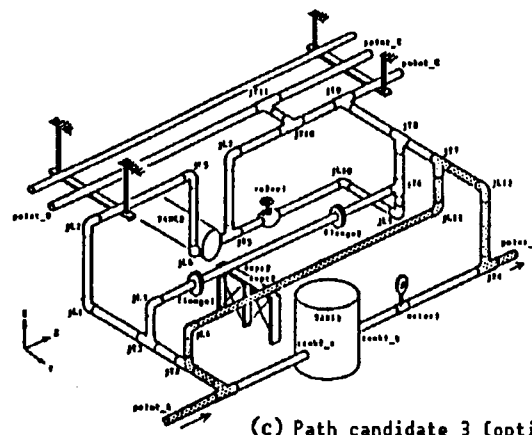
Figure 13. Basic Task Level Patterns Figure 14. Hypothetical Plant Model



(a) Path candidate 1



(b) Path candidate 2



(c) Path candidate 3 (optimal path)

Figure 15. Path Planning Results

Each pipe in the output path candidates is marked. Three possible path candidates are given for the model in Figure 14, among which candidate (c), with the lowest task level, is chosen. Here, however, transferring to another pipe is not taken into account.

Therefore, the use of the task level concept enabled the optimal path for a given weight to be generated automatically.

#### (4) Path Generation Allowing for Transfer

To this point, plans have been made involving pipes connected by joints. This method, however, is not applicable if the robot transfers from one pipe to another. Therefore, the method has been modified so that the robot, while on a pipe, can check whether it is possible to transfer to another pipe. The robot checks a few selected points on a pipe (in this report, near both ends and the pipe's center, since there would be an infinite number of path candidates if the robot kept checking all along the way, especially on parallel pipes that provide transfer opportunities at all points. Here, transfer is considered possible when the following conditions are fulfilled:

- (1) A pipe exists within 300-500 mm (in the case of the third robot) of the pipe on which the robot is currently located.
- (2) The two pipes should be parallel.
- (3) There is no obstacle between the two pipes.

If the system is instructed to show all the paths from s1 to the goal in the pipeline system in Figure 16 by using a program based on the above concept, the answer will be as follows:

```

I 1-test(s1,goal).
Way= [s1,Xp1(s2),Xp2(s4),Xp2(1/2),Xp2(s3),Xp3(s8),JL1,goal]
Task level= 224
Way= [s1,Xp1(s2),Xp2(s4),Xp2(1/2),Xp3(1/2),JL1,goal]
Task level= 204
Way= [s1,Xp1(s2),Xp2(s4),Xp2(JL1),JL1,goal]
Task level= 183
Way= [s1,Xp1(1/2),Xp2(1/2),Xp2(s3),Xp3(s8),JL1,goal]
Task level= 204
Way= [s1,Xp1(1/2),Xp2(1/2),Xp2(s4),Xp3(JL1),JL1,goal]
Task level= 183
Way= [s1,Xp1(s1),Xp2(s3),Xp2(s4),Xp2(JL1),JL1,goal]
Task level= 183
Way= [s1,Xp1(s1),Xp2(s3),Xp2(1/2),Xp3(1/2),JL1,goal]
Task level= 183
Way= [s1,Xp1(s1),Xp2(s3),Xp3(s8),JL1,goal]
Task level= 183
no
I 1-

```

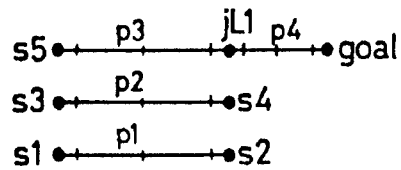


Figure 16. Pipeline System Requiring Robot Transfer

Six of these have task levels of the same level of difficulty. The only difference is the order of the motions. It does not matter which one of the six is chosen. In such a case, the system picks out the first path.

## 5.6 Basic Control Command

The traveling path of the robot in a plant is determined by the path planning method discussed above. However, it is impossible to control the robot by simply citing nodes.

It is necessary to translate the path into commands (a language) suitable to control the robot. The following six commands cover the control of all motion of the third robot.

FWD(L): Going forward (L: distance of forward movement (mm))  
 BWD(L): Going backward (L: distance of backward movement (mm))  
 SLD( $\theta$ ): Lateral sliding ( $\theta$ : sliding angle)  
 FLD( ): Going straight on flanges, T- (L-)shaped pipes  
 LJP( ): Turning on T- (L-)shaped pipes  
 TRS(L): Transferring between pipes (L: distance between the pipes (mm))

L and  $\theta$  are automatically substituted for by actual figures through matching with the plant map. The system converts the path shown in Figure 17 into the group of commands indicated below.

```

i ?-cmd_mch({start,'xp1(jL1)','xp3(jL2)',goal},Command).
Command= {FWD(900),TRS(360),SLD(+180),FWD(900)}
yes
i ?-
  
```

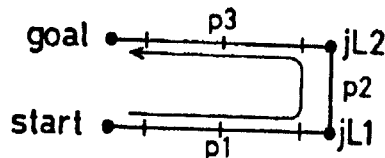


Figure 17. Example of Transferral Path

A matrix necessary for actual joint control is automatically derived from the group of commands. For instance, the matrix for moving forward 38 mm is as follows:

$$\text{FWD}(38) \rightarrow T_n = \begin{bmatrix} 1 & 0 & 0 & 0 \\ 0 & 1 & 0 & 0 \\ 0 & 0 & 1 & 38 \\ 0 & 0 & 0 & 1 \end{bmatrix}$$

In this way, the system generates not only the path, but also the control commands. It will be very useful in practical control.

## 6. Conclusion

This report has dealt with motional control methods, including the minimum joint torque method to determine a target position and arm locus determination method using two-directional DP, and the expert system PPES which generates not only a traveling path based on task level evaluation but also basic control commands. The PPES is employed to formulate a work plan, after which real-time control of the robot is employed.

The third robot has a structure capable of responding to a rather complicated pipeline system. However, some problems remain to be improved, since it lacks the flexibility to respond to pipe diameters and the capacity to traverse a tank. It is imperative that we continue to develop a more intelligent robot capable of more functions.

## References

1. Fukuda, "Intelligent Robot for Extreme Work," McGraw-Hill.
2. Hosogai and Fukuda, KIRON, 51-467, C(1985), pp 1655-1662.
3. Ibid., 53-486, C(1987), pp 399-406.
4. Fukuda, Hosogai, and Otsuka, Ibid., 53-492, C(1987), pp 1788-1794.
5. Ibid., 53-495, C(1987), pp 2235-2330.
6. Otsuka, Hosogai, and Fukuda, "The Third Intelligent Traveling Robot Symposium Papers," 1986, pp 111-114.
7. Fukuda, Hosogai, and Otsuka, "Japan Robotics Society Symposium Papers," 1985, pp 437-438, 1986, pp 211-212.
8. R.P. Paul, "Robot Manipulator, COLONA.
9. Sugiyama, "Dynamic Planning," Nikkagiren, 1976.
10. W.F. Clocksin, "Prolog Programming Microsoftware," 1983.

#### Autonomous Robot--Harunobu No 4

43064062 Tokyo 4TH INTELLIGENT ROBOTS SYMPOSIUM PAPERS in Japanese  
13/14 Jun 88 No 116 pp 147-152

[Article by Hideo Mori, Yukio Chino, Kazuhiko Saito, Masayuki Nagai, Gyosei Chin, Hiroshi Ishiguro, Shinji Kotani, and Bin Yasutomi, University of Yamanashi: "Autonomously Traveling Robot 'Harunobu No 4'"]

#### [Text] 1. Introduction

It is currently impossible to create a robot capable of appreciating a natural scene, such as the outdoors, just like a person does. However, if the objective is limited to traveling guided by vision, a robot exists which can accomplish this without comprehending images like a human being does. Honeybees are able to fly between their beehive and a flower carpet 2 km distant, remembering the sight of the surrounding environment. The traveling strategy we suggest was contrived based on a clue taken from the visual behavior of such a lower-order animal. In this strategy, a robot's behavior is comprised of the fixed behavioral forms of along-the-sign travel, i.e., traveling along a sign pattern such as a road line, to-the-sign travel, i.e., traveling to a sign pattern such as the entrance of a building, and obstacle avoidance, i.e., circumventing an obstacle like a parked car. A course from the start to a goal is expressed by some sign patterns and a sequence of fixed behavioral forms, which are then recorded on travel instructions. The robot reads the instructions while traveling, and behaves according to them. Error correction, such as that caused by losing sight of the sign patterns or the failure to pick them out, is also executed by fixed behavior. If Harunobu No 4, weighing 100 kg, follows the wrong course, it may destroy people or the environment. And if it gets broken in a collision, significant costs are incurred since the robot incorporates an expensive image processing system. A contact sensor and a supersonic wave sensor, in addition to a TV camera, are employed to prevent the destruction of the robot and the environment.

NavLab<sup>1</sup> of Carnegie-Mellon University of the United States and ALV,<sup>2</sup> jointly developed by the University of Maryland and Martin Marietta [MACHIN MARIETTA] are recognized as robots that can travel in an outdoor environment. They are based on a so-called artificial intelligence method, under which a robot understands an environment by integrating the results of image processing and a knowledge data base with a blackboard, plans a

path, and then issues a travel command. By contrast, the method discussed in this report does not require that a robot understand the environment or generate an environmental model.

The development of Harunobu is outlined as follows:

(1) The design and development of a picture interpretation language, PILS,<sup>3</sup> was begun in 1979. The language has been improved, and the latest one is the fourth version.

(2) The development of Harunobu, a robot which travels guided by vision, was begun in 1983 as an application of PILS. The third and the fourth models are currently being developed. The two models employ the same image processing system, but different unmanned carriers. While the third model is a lightweight, energy-conserving type, the fourth model, with its high power, consumes energy heavily. The third model is intended for indoor travel and cleaning work in hallways and classrooms. The fourth model is aimed at traveling on a university campus and on sidewalks.

(3) Efforts are currently being made to improve the energy efficiency of the mobile portion of Harunobu No 3 by using one-chip microcomputers. Software for indoor cleaning work is also being developed. The fourth model is in the phase in which its traveling system is being improved, and outdoor traveling tests are being repeated.

In this report, the details of image processing and the fixed behavior of the mobile part, which were omitted in our Robotics Society paper will be discussed.

## 2. Along-the-Sign Travel

The borders of a road, such as white lines, level differences, fences, and guard rails, are sign patterns for along-the-sign travel in an outdoor environment, such as on a campus street. The fixed behavior is to set the TV camera facing forward and a little downward (front-looking mode). The robot's travel of the robot must be controlled so as to keep a sign pattern in view in a certain spot of the lower half of the sphere of the camera.

Suppose that along-the-sign travel occurs through travel control by visual feedback while the distance between a sign pattern and the TV camera, which is fixed to the body and looking forward, is kept constant. The scope of the TV will fluctuate as the traveling direction of the robot changes, as illustrated in Figure 1(a). It will then be difficult to predict the sign pattern of the next picture, based on that of the current one. If the robot comes too close to the pattern and corrects its course, it may lose sight of the pattern and may be able to continue the along-the-sign travel.

It is necessary to maintain the direction of the optical axis once the camera catches sight of a sign pattern, even if the direction of the robot changes slightly, as shown in Figure 1(b). In other words, the direction of the TV camera should be adjusted by  $-\Delta\theta$  for the change  $\Delta\theta$  in the robot's

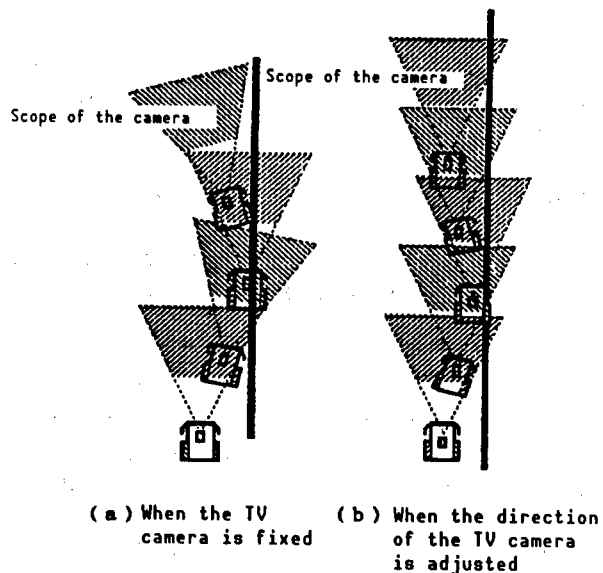


Figure 1. Directions of TV Camera and Robot

traveling direction. The same directional compensation is required in the to-the-sign travel.

### 2.1 Detection of Obstacles by Image and Avoidance Behavior

Suppose that the robot is following sign patterns. Parked vehicles and pedestrians may cut across sign patterns in the TV picture, as shown in Figure 3. The portion hiding the sign patterns is considered to be an obstacle. Things like a box lying on a street or fences preventing entrance from small areas enclosed in the street in the TV picture. The shadows of buildings and utility poles under a cloudless sky may also create an interrupted area or an enclosed area. In these cases, the robot must judge if these areas are obstacle candidate areas or not.

The fixed behavior of the robot, when an obstacle is detected by image processing, is to continue moving until it comes to within 3-4 m of the obstacle and to stop there. Then it determines the left and the right edges of the obstacle by image processing. If the width is more than 1 m it is regarded as a car, and if the width is less than 1 m, it is regarded as something else. A starting point for avoidance behavior is calculated from the width. The point should be quite far from a wide obstacle, while it may be near a narrow one. The robot proceeds to the point and gets around the obstacle to the right or left by arc movement. When the obstacle is recognized as a car, the robot goes past it, measuring the distance between the obstacle and itself, and resumes the fixed behavior it was following before taking the avoidance measures.

### 2.2 Travel Instruction

Suppose that the robot has exited to the side of a street. It needs to be instructed whether to go to the right or left. When it comes to an intersection, it must be instructed whether to go straight, or turn to the

right or left. These instructions for a course from its start to its designation in a form that the robot can understand are called a travel instruction note.

Harunobu No 4 divides a course from the start to the goal into sections in which the same sign pattern continues. The sections are defined in terms of the color (R,G,B) and the width (Width) of the road, with the border designated as a sign pattern (SPside) and the length (FarFrom). The travel instruction specifies fixed behavior for each section.

An example of a travel instruction note

(\*Conduct along-the-sign travel for 15.0 m. The color of the road is r = 0.47, g = 0.43, b = 0.45. The width is 4.0 m. Right side border is designated as a sign pattern. \*)

Moving along 15.0  
Curvature Straight  
Color (0.47, 0.43, 0.45)  
Width 4.0  
SPside Right

(\*Move straight for 2.0 m \*)  
Move-Line 2.0

### 2.3 State Codes and Fixed Behavior for Error Correction

Fixed behavior may fail to extract sign patterns, resulting in an abnormal state. The ending condition is expressed by four state codes. (NoPassageFound, SPmissed, CurveMismatch, ObstacleFound). The following are possible causes of abnormal conditions.

- (1) The sign pattern is out of view, because the road curves to the left. (SPmissed)
- (b) The sign pattern gets out of the TV camera's view toward the end of a section. (SPmissed)
- (c) The sign pattern is physically interrupted. (SPmissed)
- (d) The road cannot be extracted (NoPassageFound), or the image of the sign pattern cannot be grasped in the TV picture (SPmissed) due to the strong contrast between places in and out of the sun.
- (e) The robot took a wrong turn and ended up being faced with a building, a tree, or a lawn off the road. (NoPassageFound)
- (f) Something other than a designated sign pattern was erroneously extracted as a sign pattern. (CurveMismatch)
- (g) The robot followed a wrong course. (CurveMismatch)

(h) An obstacle is hiding a part or all of the sign pattern.  
(ObstacleFound)

While (e) and (f) are serious problems, other states are considered to be quasi-abnormalities which may arise even if the robot is traveling correctly. If the robot had to stop moving and return to the start for another attempt each time it ran into such a quasi-abnormal state, it would never reach the goal. The establishment of fixed behavior most suitable for error recovery occurring in each state, as shown in Table 1, would enhance the robot's chances of getting to the final goal without stopping.

Table 1. Fixed Behavior for Error Recovery

| State codes    | Fixed behavior for error recovery  |
|----------------|--|
| NoPassageFound | Sound alarm, wait 10 seconds, and process image again.<br>If this does not work, call operator   |
| SPmissed       | IF instruction note says 'curve to the left', THEN<br>Turn the head to the left and process image again.<br>If this does not work, turn the head to the front,<br>proceed for 1 m, process image again.<br><br>ELSE<br>IF toward the end of a section<br>THEN,<br>go straight through the remaining section<br>ELSE<br>Proceed for 1 m and process image again |
| CurvMismatch   | End along-the-sign travel forcibly and call operator   |

## 2.4 Navigation

The interrelationship of processes revolving around a navigator is illustrated in Figure 2. The operator inputs a travel instruction not in a file prior to travel. The navigator reads the travel instruction, section by section, from file (1), and starts a fixed behavioral process such as along-the-sign travel (2). If an obstacle is found while traveling, the robot stops when it arrives in front of the obstacle, the process is suspended, and the obstacle avoidance process is started (3). It resumes the former along-the-sign travel after circumventing the obstacle (4). If abnormal states such as NoPassageFound, SPmissed, or CurveMismatch arise during the travel, the fixed behavior for error recovery is started (5), referring to the travel history to that point (6) and the travel instructions for the next section (7). At the end of a section, it reads the travel instructions for the next section (8). Each time a process is finished, normally or abnormally, the name of the process, the position of the robot in relation to the sign pattern, and the travel distance are recorded on the travel history file.

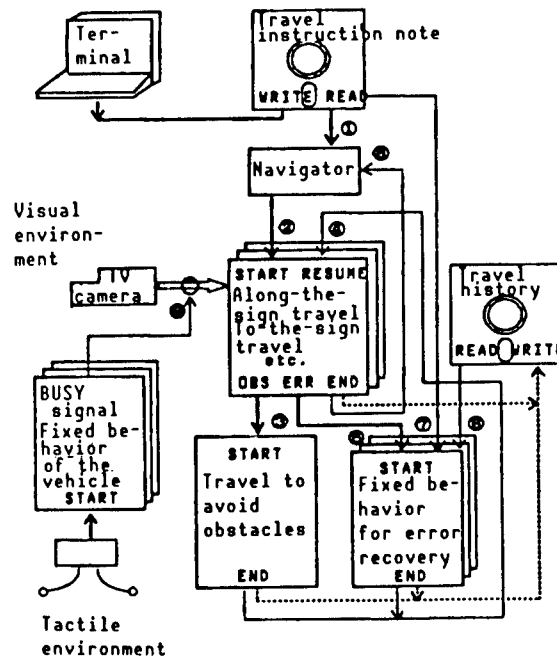


Figure 2. Configuration of System

The fixed behavior of the vehicle depends on the tactile environment. The vehicle acts independently of the fixed behavior of along-the-sign or to-the-sign travel that is affected by visual environment. However, during the fixed behavior of the vehicle, the input of images through the TV camera is controlled (9) because the TV camera may be facing the wrong direction.

### (3) Image Processing

The flow of image processing for along-the-sign travel is shown in Figure 3.

(1) The along-the-sign traveling process receives a sectional parameter from the navigator.

(2) The process enters from START, and exits from END.

If the process is suspended due to the detection of an abnormal state, the process is ended with ERR, and if an obstacle is found, it is ended with OBS. The process should then be started from the error recovery or the obstacle avoidance process. Along-the-sign travel is resumed from RESUME.

(3) A sign pattern is estimated on a screen based on sectional data. The sign pattern is expressed by a straight line:

$$X \cos \theta + Y \sin \theta = \rho \quad (1)$$

(4) The difference between the FIND and FOLLOW modes is that the former covers the entire screen while extracting a sign pattern, while the latter

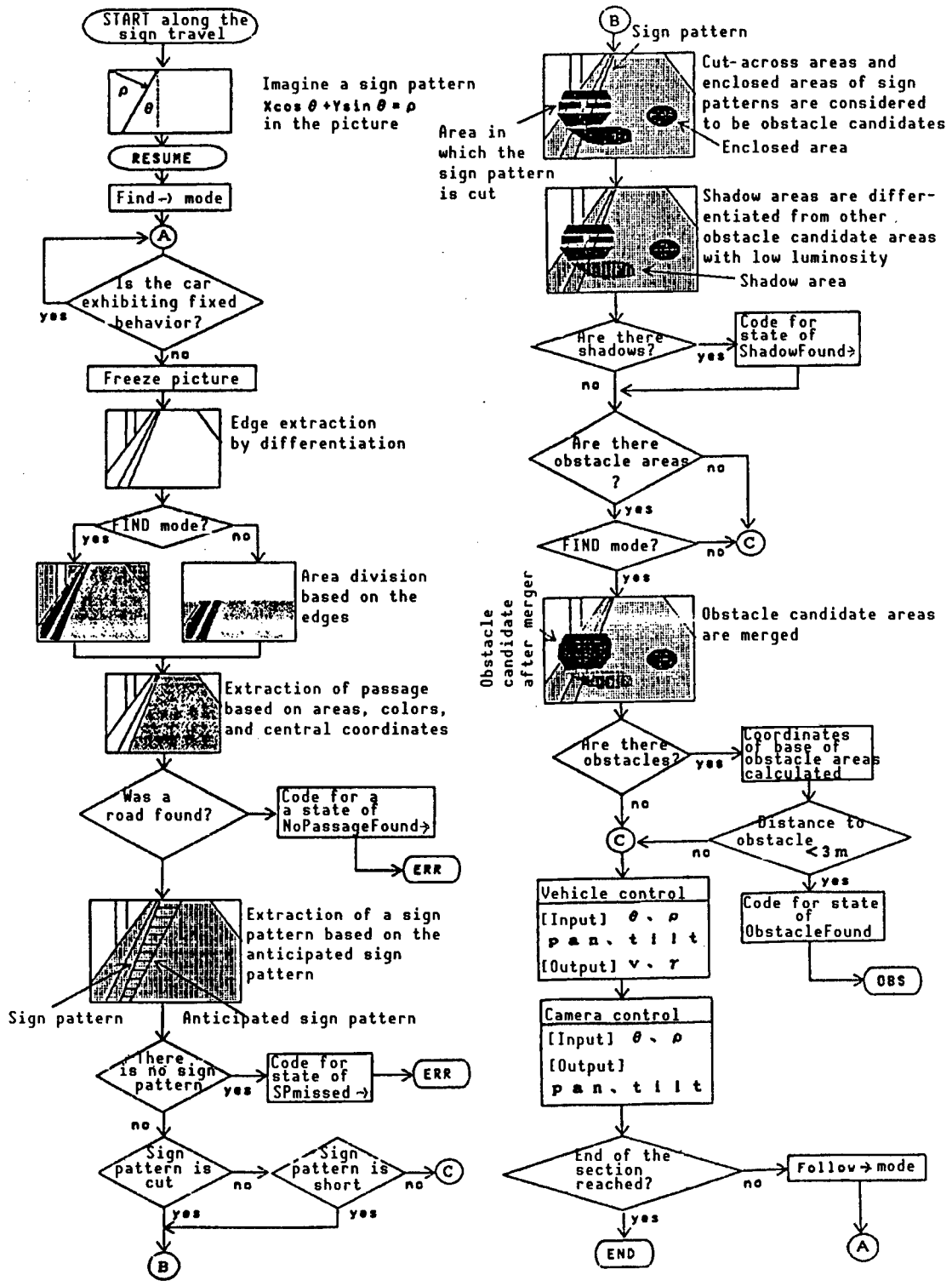


Figure 3. Process of Along-the-Sign Travel

covers only the lower half of it, and that the latter does not conduct the time consuming merging process. Therefore, the duration of the FOLLOW mode is less than half that of the FIND mode.

(5) Images are gathered (frozen) after the vehicle has finished its own fixed behavior.

(6) Images are differentiated to extract edges, which are then used as border lines in area division.

(7) Roads were extracted based on the sectional data recorded on the travel instruction note. Data on area, central coordinates, and color attributes is used for road extraction. If no road is found, NoPassageFound is set as a state code, and the task is suspended.

(8) An estimated line is used for sign pattern extraction. As shown in Figure 4, the estimated line is located farther inside an area than a real estimated line. The portion outside the line is scanned to find an edge, which represents a sign pattern. The same operation is conducted from the top through the bottom of the picture, and a row of points representing the sign pattern  $(x_1, y_1), (x_2, y_2), \dots$  is established. Then, an approximate line is drawn by excluding points with values varying from the raw ones. The line, expressed by formula (1), serves as a sign pattern.

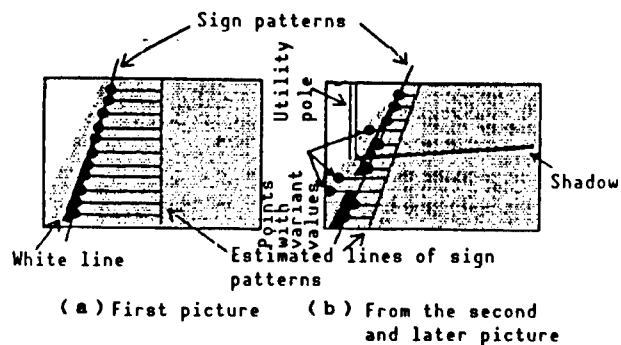


Figure 4. Sign Pattern Extraction

(9) When no sign pattern is found, SPmissd is set as a state code and the task is suspended.

(10) If a sign pattern is cut into two by some object (for example, the road and the sign pattern are cut by the shadow of the utility pole in Figure 4(b)), or either the upper part or the lower part of a sign pattern is hidden by something and shortened, the interrupted area is detected and regarded as an obstacle candidate.

(11) If there is an area with low luminosity or a black area in an obstacle candidate for obstacle, the judgment is made whether it is a shadow or a black object. Shadow areas are excluded from obstacle candidates and ShadowFound is set as a state code. The rest of the candidates are considered to be obstacles.

(12) An obstacle like a passenger car is usually divided into several small areas by the area division process. These small areas are integrated into one by merging.

(13) When an obstacle exists, the robot proceeds until it is 3 m from it, sets `ObstacleFound` as a state code, and the task is suspended. This exit is indicated as `OBS` in Figure 3.

(14) When an obstacle is found, the robot approaches until it is 3 m from it, and suspends the process.

(15) If no sign pattern is found, `SPmissed` is set as a state code and the task is suspended.

(16) If a sign pattern is found, the processes from (5) on are repeated until the travel distance reaches the length of the section.

#### 4. Fixed Behavior of Sensor Base

The accurate detection of obstacles and real-time processing are the advantages offered by a tactile sensor. A visual sensor is less accurate when there is background light or a shadow, and responds slower. Its processing time is 1 to 2 seconds at the shortest. The disadvantage of a tactile sensor is that its sphere for sensing a sign pattern is limited to very near the robot, or several centimeters. The sphere is far more limited than the sphere of image processing for sign pattern extraction, which ranges from 5 to 20 m.

##### 4.1 Fixed Behavior of Bumper

The vehicular system ignores travel instructions transmitted from the image processing system when the bumper switch is turned on, and initiates sensor base fixed behavior. Figure 5 shows the front and side views of the vehicular portion of Harunobu No 4, and indicates the shape and mounting location of the sensor.

The bumper switch is divided into three parts, right, left, and center, so that the part contacting an object is readily known.

(1) The front part of the bumper switch is on.

(Cause) It contacted a wall or an obstacle overlooked in the image processing process, or an obstacle which sprang out.

(Fixed Behavior) 1) Stop immediately. 2) Go backward for 10 cm to get away from the obstacle. 3) Stop and wait 10 seconds. (If the obstacle is an animal, it will go away.) 4) Resume former fixed behavior. 5) If the front bumper switch is turned on again on the same spot, the vehicle will go backward for 10 cm, turn around, draw a circular arc, and return in the direction it came from.

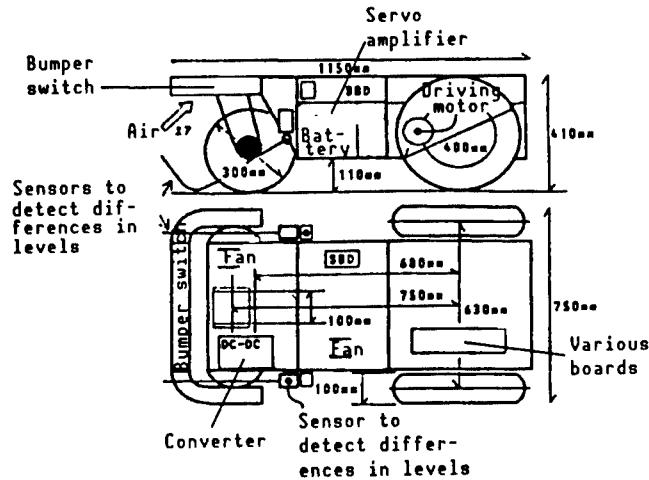


Figure 5. Vehicular Portion of Harunobu No 4

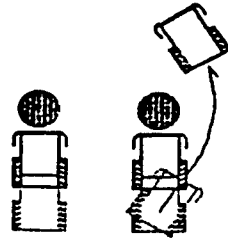


Figure 6. Fixed Behavior To Be Adapted When Front Part of Bumper Switch Contacts an Object

(2) The left (right) part of the bumper switch is on.

(Cause) It contacted a wall or an obstacle overlooked in the image processing process, or an obstacle which sprang out.

(Fixed Behavior) 1) Stop immediately. 2) Go backward for 10 cm to get away from the obstacle. 3) Temporarily modify the course to the right (left) by 30 degrees. 4) Resume former fixed behavior. 5) If the same part of the bumper switch is turned on within a specified time, the vehicle will stop, go 10 cm backward, stop there, and call an operator.

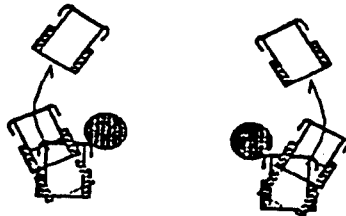


Figure 7. Fixed Behavior To Be Adopted When Left (Right) Part of Bumper Switch Contacts an Object

## 4.2 Fixed Behavior To Surmount Differences in Levels

The sensor detecting differences in levels is a limit switch made of an L-bent, 60 cm long, 3 mm thick stainless steel wire. This switch, mounted on the front of the vehicle, between the right and left tires, detects level differences 15 cm ahead of the front casters.

When the vehicle nears a change in level and the sensor SW1 is turned on, first a signal is cut in the CPU to retain the current location (X1, Y1) in memory. Suppose that SW2 is turned on then at the location (X2, Y2). If the distance between SW1 and SW2 is D, and if the angle formed between the direction of the difference in level and the direction of travel is  $\theta$ ,

$$\tan(\theta - 90) = \sqrt{(X1-X2)^2 + (Y1-Y2)^2}/D$$

(3) The sensor detecting changes in level is on.

(Cause) Difference in level was detected front right or front left, or a stone or a rise in the road surface was detected.

(Fixed Behavior) 1) If either of the tactile sensors is not on (when one of the casters is already on the higher level or there is a stone or a rise in the road surface that touches only SW1), the process is suspended. 2) When both tactile sensors are turned on, the angle  $\theta$  is calculated. 3) If  $\theta$  is  $90 \pm 10^\circ$ , the process is ended and former fixed behavior is continued. Otherwise, the vehicle stops once. 4) The distance to go backward, the spinning angle, and the distance to go straight to surmount the difference in levels are calculated from  $\theta$ . 5) The sensor is reset, and movements are made according to the results of the calculation. 6) After surmounting the difference in levels, the robot records the location of this difference (X1, Y1) and the direction  $\theta$  in the travel history and resumes normal travel.

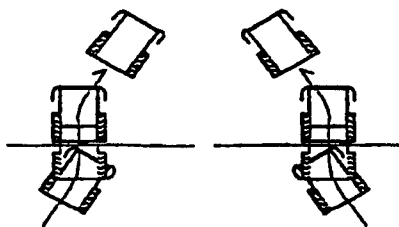


Figure 8. Fixed Behavior To Surmount Difference in Levels

## 5. Conclusion

An experiment on along-the-sign travel was conducted on campus by using the border line between the lawn and asphalt pavement as a sign pattern. The robot was able to extract the sign pattern and travel by following it. Image processing took about 3 seconds in the FIND mode and 2 seconds in the FOLLOW mode when MC68020 was employed as the CPU. The time involved seems short enough. However, the robot tends to lose sight of a sign pattern more often when it travels faster. This indicates the necessity to improve the

travel control method. While a shadow crossing a road, such as that of a utility pole, does not seriously affect the extraction of a sign pattern, a long shadow extending in the same direction as a sign pattern, such as that of a building, is often mistaken as the sign pattern.

Table 2. Image Processing Time

|                                    | FIND mode   | FOLLOW mode |
|------------------------------------|-------------|-------------|
| Image data transmission            | 0.2 second  | 0.1 second  |
| Edge extraction                    | 0.6 second  | 0.3 second  |
| Area division, abstract expression | 0.3 second  | 0.2 second  |
| Sign pattern extraction            | 2.0 seconds | 1.5 seconds |

#### References

1. T. Kanade, C. Thorpe, S. Shafer, M. Herbert, "Carnegie-Mellon NavLab Vision System," IEEE Int. Workshop on Machine Vision and Machine Intelligence, 1987.
2. A.M. Waxman, J.L. Moigne, L.S. Davis, E. Liang, and T. Siddalingaiaj, "A Visual Navigation System for Autonomous Land Vehicles," University of Maryland Center for A.R. Technical Report 139, 1986.
3. Hideo Mori and Akabane Hidetomo, "Picture Interpretation Language PILS," INFORMATION PROCESSING SOCIETY PAPER, Vol 23 No 4, 1982, pp 243-250.
4. Kazuhiko Saito, Masayuki Nakai, and Hideo Mori, "Classroom Cleaning Robots," The Fifth Japan Robotics Society Paper, 1987, pp 127-128.
5. Hideo Mori, Shinji Kotani, Hiroshi Ishiguro, Bin Yasutomi, and Yukio Chino, "Autonomously Moving Robot Traveling on Campus (A Strategy of Traveling Robot-Harunobu No 4)."

## Cruise Control of Parallel Two-Wheeled Vehicle With Steering Mechanism

43064062 Tokyo 4TH INTELLIGENT ROBOTS SYMPOSIUM PAPERS in Japanese  
13/14 Jun 88 No 117 pp 153-157

[Article by Kazumi Yamafuji and Takashi Kawamura, Denki Tsushin Daigaku; and Yasushi Miyagawa, Matsushita Electric: "Cruise Control Technique for Parallel Two-Wheeled Vehicle Equipped With Steering Mechanism"]

### [Text] 1. Introduction

This study is aimed at the upright stability control of a parallel two-wheeled vehicle, a kind of intelligent traveling robot, and its cruise control while steering it. The parallel two-wheeled vehicle has two drive shafts on a line perpendicular to the driving direction. A caster is installed on the outer side of each drive shaft. The wheel axle supports the main body. The vehicle can be compared to an inverted pendulum incorporating independently driven wheels. It is such an unstable system that it falls down uncontrollably.

In recent years, research has been conducted on stabilizing using feedback control systems, such as inverted pendulums,<sup>1-4</sup> feedback control systems, one-wheeled vehicles,<sup>5-6</sup> and two-wheeled vehicles,<sup>7-8</sup> which were unstable as they are. The authors succeeded in upright stabilization and cruise control of a coaxial two-wheeled vehicle which had one wheel on either end of an axle supporting the main body.<sup>8</sup> The vehicle, however, did not have a steering mechanism.

This research is aimed at upright stabilization and steering control of a parallel two-wheeled vehicle with independently-driven wheels.

### 2. Modeling of Two-Wheeled Vehicle and Equation of Motion

Figure 1 shows an inverted pendulum with a wheel modeled on a parallel two-wheeled vehicle. Here, equations of motion are set up on the assumption that both the right and left wheels rotate completely synchronously.

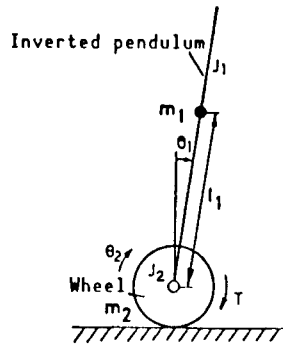


Figure 1. Inverted Pendulum Modeled on a Parallel Two-Wheeled Vehicle

(Key)

- $m_1$ : The mass of the mainbody (kg)
- $J_1$ : The inertial moment of rotation of the shaft of the main body ( $\text{kgm}^2$ )
- $m_2$ : The mass of the wheel (kg)
- $J_2$ : The inertial moment of rotation of the shaft of the wheel ( $\text{kgm}^2$ )
- $l_1$ : The distance between the shaft and the center of gravity of the main body (m)
- $r$ : The radius of the wheels
- $f_2$ : Viscosity friction coefficient related to rotation of the wheels (Nms)
- $T$ : Controlling torque applied to the wheel (Nm)
- $\theta_1$ : Inclination angle of the main body from a vertical line (rad)
- $\theta_2$ : Angle of rotation of the right wheel (rad)
- $\theta_3$ : Angle of rotation of the left wheel (rad)
- $k_1$ : Feedback coefficient against  $\theta_1$  (Nm/rad)
- $k_2$ : Feedback coefficient against  $\dot{\theta}_1$  (Nms/rad)
- $\xi$ : Torque conversion coefficient (Nm)
- $T_s$ : Sampling time (ms)

Based on the assumption of synchronized rotation of the two wheels,  
 $\theta_3 = \theta_2$

$$\text{(Main body)} \quad A \ddot{\theta}_1 + B \ddot{\theta}_2 - C \sin \theta_1 + f_2 (\dot{\theta}_1 - \dot{\theta}_2) = -T \quad (1)$$

$$\text{(Wheel)} \quad D \ddot{\theta}_2 + B \ddot{\theta}_1 \cos \theta_1 - B \dot{\theta}_1^2 \sin \theta_1 + f_2 (\dot{\theta}_2 - \dot{\theta}_1) = T \quad (2)$$

where,  $A = J_1 + m_1 l_1^2$ ,  $B = m_1 l_1 r$   
 $C = m_1 l_1 g$  ( $g$ : gravitational acceleration)  
 $D = J_2 + (m_1 + m_2) r^2$

### 3. Mechanism and Control System of the Experimental Two-Wheeled Vehicle

#### (1) The Mechanism of the Experimental Two-Wheeled Vehicle

Figure 2 illustrates the parallel two-wheeled vehicle produced. Two DC servomotors are incorporated in the upper part of the main body, and drive

the right and left wheels through a worm decelerator (deceleration ratio: 1/15). Each motor is equipped with an optical rotary encoder to detect the angles of rotation of the wheels,  $\theta_2$  and  $\theta_3$ . Both encoders are incremental types with a resolving power of 500 pulses/rev.

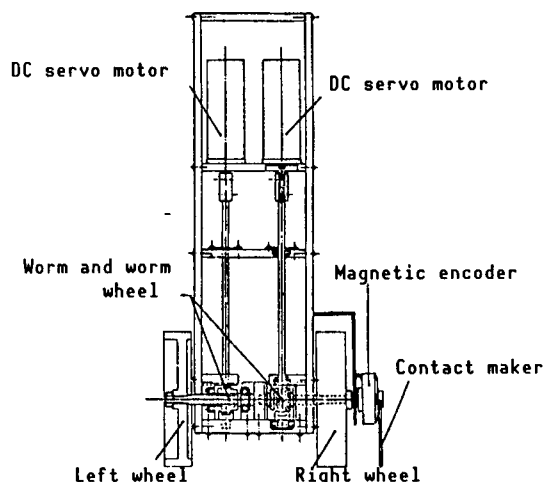


Figure 2. Schematic of Parallel Two-Wheeled Vehicle

The inclination angle of the main body from a vertical line,  $\theta_1$ , is detected by a magnetic encoder (an incremental type, 2,048 pulses/rev). The axis of the encoder is in line with the axis of revolution of the main body. Its housing is fixed on the side of the main body, when the revolution of the encoder's axis is stopped by a contact maker attached to the axis, the encoder's body rotates with the main body of the two-wheeled vehicle. This is how  $\theta_1$  is detected. The end of the contact maker contacting a floor is covered by a roller bearing. Measured values of the various parameters of the experimental two-wheeled vehicle are indicated in Table 1.

Table 1. System Parameters of Experimental Vehicle  
Suffixes f and b indicate fore and back spin.

|   |                               |
|---|-------------------------------|
| $m_1 = 3.38$ kg                         | $r = 0.07$ m                  |
| $m_2 = 0.96$ kg                         | $f_{2f} = 5.78 * 10^{-4}$ Nms |
| $l_1 = 0.201$ m                         | $f_{2b} = 5.16 * 10^{-3}$ Nms |
| $J_1 = 0.17$ kgm <sup>2</sup>           | $f_{3f} = 1.54 * 10^{-3}$ Nms |
| $J_2 = 2.54 * 10^{-3}$ kgm <sup>2</sup> | $f_{3b} = 4.59 * 10^{-3}$ Nms |

## (2) Configuration of Control System

The configuration of the experimental control system is shown in Figure 3. The controller is realized by software on a 16-bit personal computer (PC-9801E equipped with 8087 coprocessor). The inclination angle of the main body of the two-wheeled vehicle and the rotation angle of the wheels are detected by the foregoing encoder and transmitted to a microcomputer through a counter. The angular velocity is calculated by numerical differentiation based on the detected values of the angles. Input for control is calculated from the angle of the main body and a feedback

coefficient, which will be discussed in the following section. The input for control is transmitted from the personal computer through a D/A converter to a servomotor driver, which generates the necessary torque in each wheel in proportion to the control current.

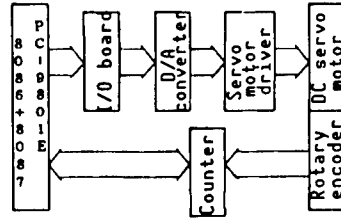


Figure 3. System for Experimental Control

#### 4. Posture Stabilization and Cruise Control

##### (1) Posture Stabilization Method

As for control rules for posture stabilization, the analysis of coaxial two-wheeled vehicles by Yamafuji's group<sup>8</sup> is applied. A feedback coefficient corresponding to the inclination angle of the main body is given by the formula:

$$mgl/\xi < k_1 < c/\xi T_s \quad (3)$$

The relationship between  $k_1$  and  $T_s$  is calculated with the parameters of the experimental vehicle. The results are shown in Figure 4. It is obvious that the range of the feedback coefficient changes according to the sampling time  $T_s$ .

##### (2) Control of Wheel Synchronization

The following control methods were attempted for driving the vehicle straight by synchronizing the right and left driving systems which have different characteristics.

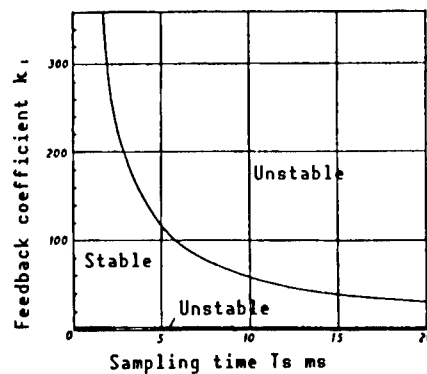


Figure 4. Relationship Between Feedback Coefficient Involved in Proportional Control and Sampling Time

### A. Follow-up Method

In this method, one of the wheels is chosen as a main wheel, subordinating the other. The inclination angle of the main body is fed back to the main wheel. The difference in rotation between the two wheels is fed back to the subordinate wheel, which follows the main wheel. Figure 5 is the block diagram.

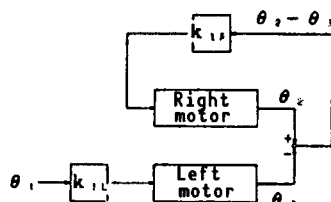


Figure 5. Block Diagram of Follow-Up Method

### B. Gain Adjustment Method

In this method, the feedback coefficient of input for control of the wheel driving motors corresponding to the inclination angle of the main body is adjusted for the difference in rotation between the wheels. Figure 6 is the block diagram.

#### (3) Cruise Control Method

The servo instruction method, as well as the gain changing method suggested in the previous report,<sup>8</sup> were tested. The gain changing method will also be mentioned below.

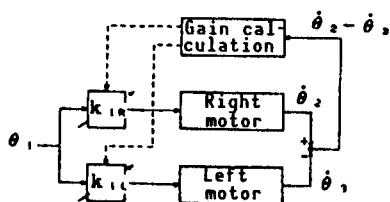


Figure 6. Block Diagram of Gain Adjustment Method

### A. Gain Changing Method

In this method, the posture stabilization control is cut, and the two-wheeled vehicle is allowed to incline toward the traveling direction to a certain degree. If the inclination exceeds the predetermined angle, the vehicle is controlled to recover its posture. In other words, the two-wheeled vehicle moves forward through recovering the posture of the main body.

## B. Servo Instruction Method

Control input based on servo instruction is given by the following formula:

$$u = k_1 \theta_1 - F(\theta_{2r} - \theta_2) \quad (4)$$

Assuming  $a$  to be a positive constant, and  $X = \theta_{2r} - \theta_2$ ,

$$\begin{aligned} F(x) &= a && (x > a) \\ &= x && (-a \leq x \leq a) \\ &= -a && (x < -a) \end{aligned}$$

The first term of the right side of formula (4) is input for posture stabilization, and the second is for servo cruising. The most stable gain for the sampling time is chosen from Figure 4 as gain  $k_1$  in the first term. The value of  $a$  was determined so that it does not exceed input corresponding to external turbulence in the early period,<sup>7</sup> that can convert with stability.

### (4) Steering Method

The vehicle can be moved along a given course by controlling the rotation speed of each wheel. The mechanism will be explained below. In Figure 7, the vehicle goes straight in section 1 and turns in section 2.

(Section 1)  $r\dot{\theta}_2 = r\dot{\theta}_3$ , therefore,  $\dot{\theta}_2 = \dot{\theta}_3$ .

(Section 2)  $r\dot{\theta}_2 > r\dot{\theta}_3$ , therefore,  $\dot{\theta}_2 > \dot{\theta}_3$ .

The radius of the turn  $R$  is:

$$R = w \dot{\theta}_2 / (\dot{\theta}_2 - \dot{\theta}_3) - w/2 \quad (5)$$

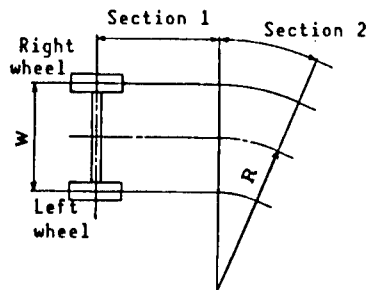


Figure 7. Radius of Turning

The two-wheeled vehicle can be moved at a given radius of turn by specifying the difference in angular turning velocity between the wheels.

## 5. Computer Simulation

Straight cruising of the two-wheeled vehicle was simulated by using the gain changing method. In this method, gain with high main body stability, which is found in the central part of the stable area in Figure 4, and gain with low stability are exchanged alternately, based on the detected results of

the inclination angle of the main body, in order to control the cruise. In the cruise control simulation, controlling the torque in formulae (1) and (2) are given by the formula:

$$\text{(Controlling torque) } T = k_1 \dot{\theta}_1 + K_2 \theta_1 \quad (6)$$

Formulae (1) and (2) were solved by Runge-Kutta Method and computer simulation was made by using the personal computer mentioned above. The time increase for the calculation  $\Delta T$  was 3 ms. The control was started on the main body inclined toward its traveling direction by 0.02 rad, taking external turbulence in the early period into consideration. At first, control occurred until the inclination angle of the main body recovered from 0.02 rad to 0.01 rad. When the inclination angle was less than that, the main body recovered a stable posture and the speed of the wheels decreased. Therefore, control is suspended until the inclination angle reaches 0.02 rad, permitting the main body to become unstable and inclined toward the traveling direction. When the inclination angle of the main body has reached 0.02 RAD, the foregoing control is resumed. Figures 8 and 9 show the results of the simulation made by assuming  $T_s = 3$  ms. From these figures, it can be understood that the main body is inclined forward and that the two-wheeled vehicle travels while correcting the inclination.

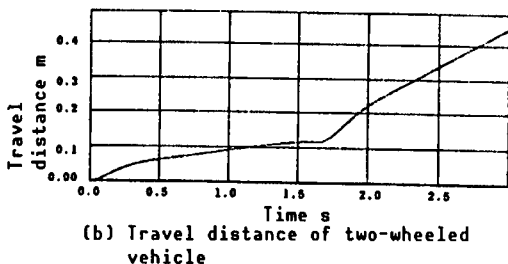
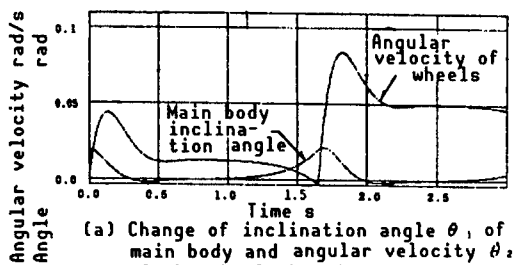


Figure 8. Cruising Simulation (1)

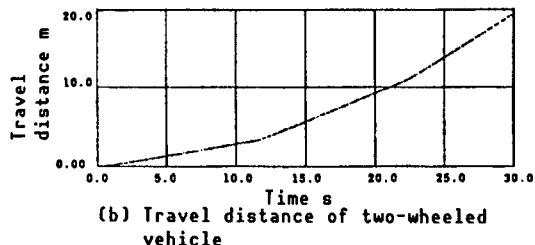
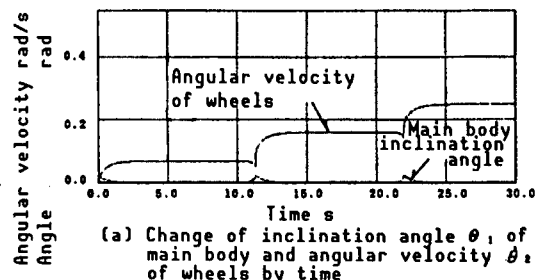


Figure 9. Cruising Simulation (2)

## 6. Results of Controlling Experiment

### (1) Posture Control by Follow-Up Method

The results of synchronization control of the wheels by the follow-up method are shown in Figure 10. A curve showing the difference in rotation between the two wheels, which is multiplied by 20, is also shown in the figure.

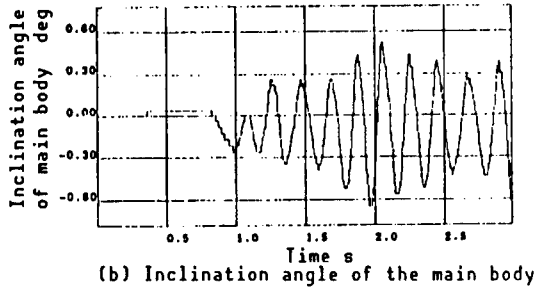
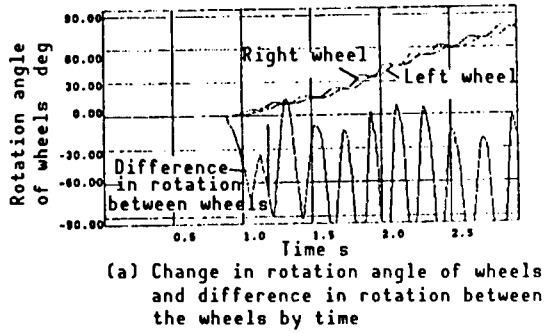


Figure 10. Results of Posture Control by Follow-Up Method

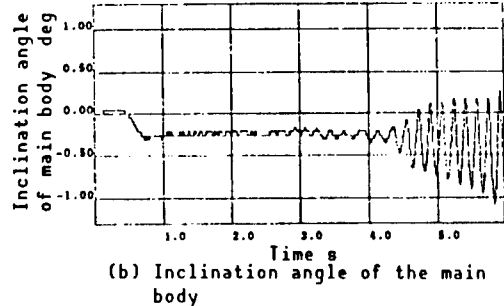
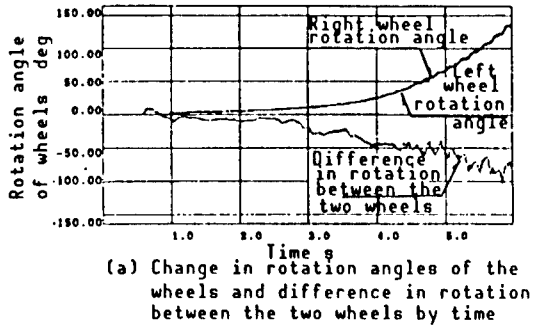


Figure 11. Results of Posture Control by Gain Adjustment Method

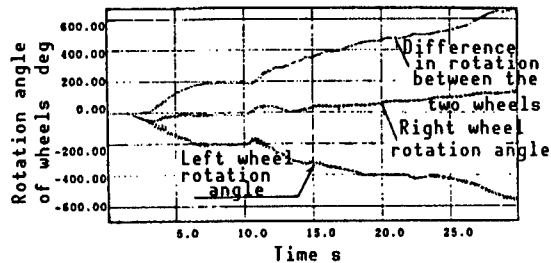
According to the figure, the vehicle does not move at all at first. About 0.9 s after the vehicle starts, a difference in rotation begins to arise between the two wheels. With follow-up control, the right wheel (the subordinate wheel) follows the left wheel (the main wheel) after a short delay. Although the posture of the main body is kept stable, it cannot remain in the same spot.

### (2) Posture Control by Gain Adjustment Method

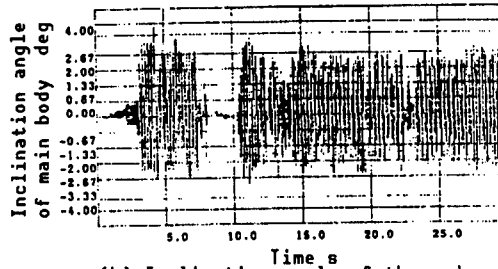
The results of synchronization control of the two-wheeled vehicle by the gain adjustment method are shown in Figure 11. A 30-fold difference in rotation between the wheels is shown in the figure. The two wheels rotate synchronously at first, but after a while the difference between the rotation angles of the two wheels begins. As the difference increases, the main body rocks wider and starts moving forward.

### (3) Steering Control

Figure 12 shows the results of traveling while steering the vehicle by controlling the rotation speed of the two wheels. In this case, the vehicle turns to the left when the right and left wheels rotate in opposite directions. Steering control is still being researched, and free steering control in any direction on any course has not yet been realized.



(a) Change in rotation angle of wheels and difference in rotation between the wheels by time



(b) Inclination angle of the main body

Figure 12. Results of Steering Control by Speed Control of Two Wheels

## 7. Conclusion

(1) An inverted pendulum-type vehicle with two parallel wheels driven independently by two motors was produced.

(2) Equations of motion were set up by using an inverted pendulum with a wheel as a model, and computer simulation of the cruise control was conducted by applying the gain changing method. As a result, it was learned that alternate applications of gain to stabilize the position of the two-wheeled vehicle and gain to unsettle it moves the vehicle forward as it corrects its posture, which is inclined toward the traveling direction. This was confirmed by experiments.

(3) Two methods to stabilize the posture by wheel synchronization were suggested, and experiments were conducted. Posture stabilization of the two wheeled vehicle was realized by both methods.

(4) Steering control was achieved by controlling the rotation speed of the two wheels. However, this is still being researched, and some problems have yet to be solved.

We would like to express our gratitude to CKD Co., Ltd., and Servo Land Co., Ltd., for their assistance with the experimental vehicle.

## References

1. S. Mori, N. Nishihara, and K. Furuta, "Control of Unstable Mechanical System; Control of Pendulum," INT. J. CONTROL, Vol 25 No 5, 1976, p 673.

2. Hayashi, Kano, and Masubuchi, "Posture Control of Inverted Pendulum," AUTOMATIC MEASUREMENT CONTROL SOCIETY PAPERS, Vol 13 No 5, 1976, p 425.
3. Sugie, Inouye, and Kimura, "Control To Stabilize Combined Inverted Pendulum," Ibid., Vol 14 No 4, 1978, p 425.
4. Kajiwara, Hosuge, and Furuta, "Position Control of Double Inverted Pendulum on Sloping Rail," Ibid., Vol 15 No 7, 1979, p 873.
5. Homma, Iguchi, Kondo, et al., "Research on One-Wheeled Rough Terrain Cruising Robots and Their Control," Vol 2 No 4, 1984, p 366.
6. Yamafuji and Inouye, "Research on Posture Control of One-Wheeled Vehicles," Papers of 1986 Precision Industrial Society Symposium in Yamanashi, 1986, p 4.
7. Yamafuji and Kawamura, "Research on Posture Control of Coaxial Two-Wheeled Vehicles," The Japan Mechanical Society, The 24th Symposium, 1987, p 189.
8. Yamafuji, Kawamura, and Miyagawa, "Cruising Control of Coaxial Two-Wheeled Vehicles Standing Upright," The Japan Robotics Society, The Fifth Lecture meeting, 1987, p 539.

## Helios--Terrain-Adaptive-Type Crawler Vehicle Developed

43064062 Tokyo 4TH INTELLIGENT ROBOTS SYMPOSIUM PAPERS in Japanese  
13/14 Jun 88 No 118 pp 159-163

[Article by Shigeo Hirose and Jun Miyake, Tokyo Institute of Technology; and Yoshihisa Aoki, Kogaku Seisakusho: "Development of a Terrain Adaptive Type Crawler Vehicle Helios"]

### [Text] 1. Introduction

The need is mounting, both in terms of safety and economy, for the robotization of the maintenance, inspection, and emergency work required in nuclear power stations, factories, chemical plants, etc. Those robots, unlike ordinary industrial robots, would have to move to a maintenance or an inspection spot to perform their jobs. Since the course may include uneven grounds to be traversed, such as stairs and bumps, adaptive cruising performance is required. A crawler vehicle newly developed for this purpose will be discussed in this article.

The crawler vehicle developed is primarily aimed at improving stability while negotiating stairs. Its features include 1) belt with flexibility that prevents it from slipping down, and 2) a posture control mechanism to maintain the levelness and stability of the body carrying materials (carrier). Each mechanism and the control method will be discussed below.

### 2. Introduction of Flexible Belt

A conventional crawler is capable of traveling stairs by hooking its nipple (the convex part of the belt) on the stair steps. However, when the nipple is located at the top of a step, it lifts the whole crawler and, as a result it falls down<sup>1</sup> (stranding effect). It has also been reported that, although a belt has many nipples, only a few of them actually bear the weight on the stairs, leaving the crawler unstable. Attempts made so far to solve these problems include 1) enlarging the grounding surface by making the crawler longer, 2) adjusting the space between nipples to the degree of slope of the stairs, and 3) creating a protrusion on the stairs to support the crawler. However, since the environment in which crawlers travel is usually narrow, elongating a crawler could result in the deterioration of its cruising performance. Measures such as 2) and 3) are effective only on specific stairs, and not on stairs in general.

The authors' group introduced the belt shown in Figure 1 [not reproduced], which has a flexible nipple. The nipple offers the following features:

- 1) Its structure is simple and solid, it is highly reliable as a grounding element, and it does not require any rubbing parts for support. It has good spring characteristics, exhibiting constant output, as shown in Figure 2.
- 2) Since the support mechanism employs a leaf spring, when it is sunk flexibly by forces applied from below, it can support and yet is not bent by lateral forces. Employment of this belt will eliminate the crawler's being lifted while traveling on stairs. Its cruising performance can be improved by sustaining its own weight with more than one nipple which conform to the stairs.

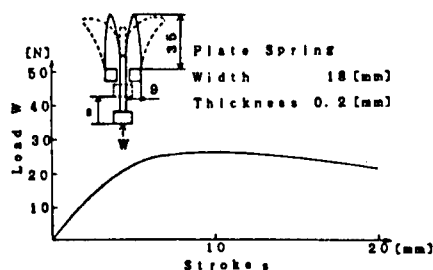


Figure 2. Characteristics of Suggested M-Type Leaf Spring

### 3. Introduction of Carrier Posture Control Mechanism

In most conventional vehicles, carriers loaded with materials are fixed on the crawler traveling part (thruster), as illustrated in Figure 3. If a vehicle of such a structure tries to go up or down relatively steep stairs, it falls down or becomes unstable, because the center of gravity of the entire vehicle moves out of the range of the crawler support. The volume and the weight of the loaded materials are especially increased in the case of traveling robots which are supposed to carry visual equipment, power sources, computers, etc. The center of gravity of these robots is raised accordingly, rendering them unstable. As a countermeasure against this instability problem, attempts have been made to lengthen crawlers, leading to the production of a crawler with four movable crawling mechanisms, and one that is variably-shaped.<sup>4</sup> Their shapes, however, are not suitable for travel on narrow stairs, as mentioned above. A system like the one in Figure 4 is also possible. In this system, the carrier and the thruster are separated, and the position of the carrier is actively controlled by its own straight movement. This system appears to be simple and realistic. On a slope, however, the carrier must be raised along the steep slope. Therefore, posture control alone requires a driving system with large output.

What is worse, the materials loaded on the carrier cannot be maintained horizontally. In these respects, this system is not desirable. Far better is the system shown in Figure 5, which keeps the carrier horizontal by turning it around the S-axis according to the inclination angle. In this system, even if the traveling part of the crawler is inclined on a road surface, the carrier's center of gravity is always located in a vertical

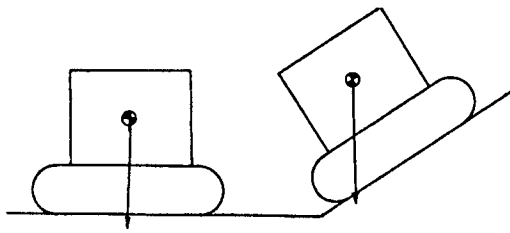


Figure 3. Conventional Crawler and Its Stability on a Slope

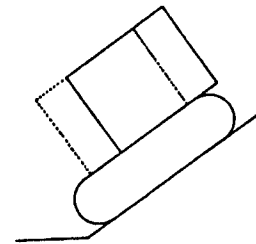


Figure 4. Crawler With a Mechanism for Straight Movement Posture Control

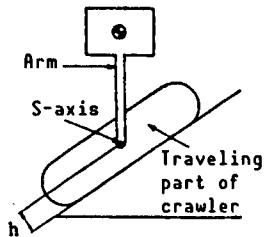


Figure 5. Crawler With an Inverted Pendulum-Type Carrier

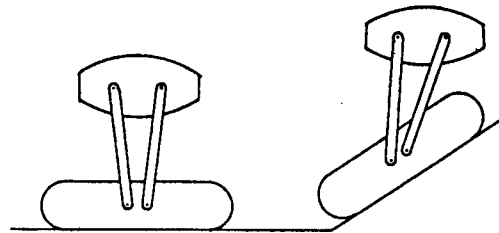


Figure 6. Crawler With a Four-Node Linking Mechanism

line with the S-axis if the posture of the carrier is controlled fast enough and the carrier is kept upright. In principle, the moment around the S-axis necessary for posture control of the carrier should be zero. Therefore, the driving system for posture control does not have to provide a substantial amount of power. A cell flock mechanism to prevent the carrier from being moved by external forces is necessary, but a driving system with a low deceleration ratio and limited power is sufficient. The fact that the posture can be controlled quickly by such a driving system is a very remarkable feature. Moreover, the stability of the loaded materials has been improved, since the carrier is always horizontal. However, in the mechanism in Figure 5, whenever the carrier is inclined, the center of gravity of the carrier moves downward in the crawler vehicle, due to height  $h$  between the S-axis and the road surface. This may cause the stability to deteriorate. To counter this problem, it is effective to introduce a mechanism that not only inclines the carrier, but also moves it horizontally at the same time. One concept, shown in Figure 6,<sup>5</sup> uses a four-node link. In this case, maintaining the carrier in a horizontal position moves the center of gravity forward structurally. However, substantial stress is concentrated in the support axis of the link when the carrier is inclined. In this report, we suggest a mechanism using a pulley, which is illustrated in Figure 7. The pulleys are fixed on the carrier and the traveling part of the crawler. The arm can revolve around the thruster. The rotation of the arm revolves the pulleys, and turns and drives the body. Relatively high tension is applied on the smaller pulley on the side of the traveling part of the crawler, but not as much as in the case of the four-node link.

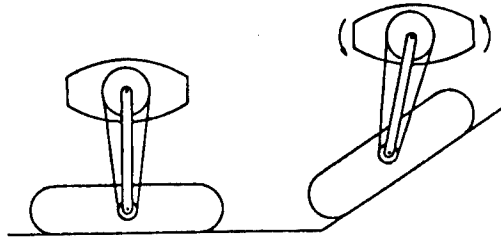


Figure 7. Pulley-Type Crawler Suggested

#### 4. Carrier Posture Control

The carrier posture driving mechanism introduced in the previous chapter requires appropriate carrier posture control using signals from a posture sensor. In this chapter, the optimal control method will be discussed on the assumption that the traveling part of the crawler is equipped with a gyro-type posture sensor. A regulator method by condition feedback is employed for control. First the system is modeled. The carrier and the thruster are bound with a belt. When the arm turns  $\theta_1$ , the carrier is supposed to turn  $k\theta_1$ . The coefficient  $k$  is obtained from the ratio of the diameter of the carrier and that of the thruster, or  $k = -\gamma_t/\gamma_o$ . The static characteristics of this system will be discussed first. When the traveling part of the crawler (thruster) is inclined by  $\phi$  due to the unevenness of the ground, as illustrated in Figure 8, the angle of the arm should be:

$$\phi - \theta_1 + k\theta_1 = 0 \tag{1}$$

based on the fact that the carrier is horizontal.

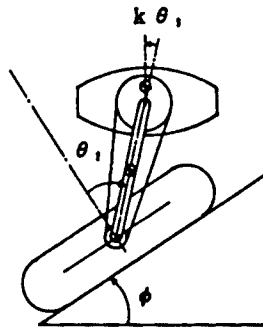


Figure 8. Model of Carrier Arm System Motion

The dynamic characteristics of the system involving such a static posture will be analyzed next. This can be led by the Newton Euler method. The torque  $u$ , which should be generated in the actuator of the shaft  $S$  of the arm, is:

$$\begin{aligned}
u &= \frac{1}{F_1} n_{1,} + I_1 F_1 \ddot{\theta}_1 + \mu_1 l_1^2 f_{1,} l [\dot{\theta}_1,] \\
&\quad + c_1 F_1 \dot{\theta}_1 \\
&= \frac{1}{F_1} \{ I_{1,} + (1-k) I_{2,} + F_1^2 I_1 \\
&\quad + (2-k) m_2 l_1 l_{02} \cos(k \theta_1) \\
&\quad + m_1 l_{01}^2 + m_2 l_1^2 \\
&\quad + (1-k) m_2 l_{02}^2 \} \ddot{\theta}_1 \\
&\quad - \frac{1}{F_1} m_2 l_1 l_{02} k (1-k) \sin(k \theta_1) \dot{\theta}_1^2 \\
&\quad - \frac{1}{F_1} [ m_1 l_{01} \sin(\theta_1 - \phi) \\
&\quad + m_2 ( l_1 \sin(\theta_1 - \phi) \\
&\quad - l_{02} \sin(\phi - (1-k) \theta_1) ) ] g \\
&\quad + c_1 F_1 \dot{\theta}_1
\end{aligned} \tag{2}$$

Table 1. Table of Keys

|   |          |                           |
|---|----------|---------------------------|
| Deceleration ratio                                  | $\xi_1$  | 300                       |
| Mass of arm   | $m_1$    | 2.37 kg                   |
| Mass of carrier                                     | $m_2$    | 4.09 kg                   |
| Viscosity resistance                                | $c_1$    | 0.0 N·m·s                 |
| Distance between arm axes                           | $l_1$    | 0.42 m                    |
| Distance between arm axis and center of gravity     | $I_{G1}$ | 0.21 m                    |
| Distance between carrier axis and center of gravity | $I_{G2}$ | 5.30e-3 m                 |
| Inertial moment of arm                              | $I_{1y}$ | 4.71e-2 kg·m <sup>2</sup> |
| Inertial moment of carrier                          | $I_{2y}$ | 7.94e-2 kg·m <sup>2</sup> |
| Inertial moment of motor                            | $I_m$    | 5.15e-5 kg·m <sup>2</sup> |
| Gravitational acceleration                          | $g$      | 9.8 m/s <sup>2</sup>      |
| Carrier rotation deceleration ratio                 | $k$      | 0.2615                    |

The keys used in this analysis are shown in Table 1, which also carry the specific figures of an actual machine to be used in the later analysis. The equation of state is found by linear equation of this formula near the equilibrium point. The result is as follows:

$$\dot{x} = Ax + Bu \tag{3}$$

$$x = \begin{bmatrix} \Delta \theta \\ \Delta \dot{\theta} \end{bmatrix}, \quad B = \begin{bmatrix} 0 \\ 1/\beta \end{bmatrix}$$

$$A = \begin{bmatrix} 0 & 1 \\ \alpha/\beta & \gamma/\beta \end{bmatrix}$$

However, 
$$\alpha = \frac{1}{F_1} \{ (m_1 l_{01} + m_2 l_1) \cos(k \theta_1) + m_2 l_{02} (1-k) \} g$$

$$\begin{aligned}
\beta &= \frac{1}{F_1} \{ I_{1,} + (1-k) I_{2,} + F_1^2 I_1 \\
&\quad + m_1 l_{01}^2 + m_2 l_1^2 \\
&\quad + (1-k) m_2 l_{02}^2 \\
&\quad + (2-k) m_2 l_1 l_{02} \cos(k \theta_1) \}
\end{aligned}$$

$$\gamma = c_1 F_1$$

The crawler vehicle HELIOS-1 has a potentiometer on its arm shaft, an inclinometer and an angular rate sensor in its thruster, and a tachogenerator in its motor. The equipment enables the vehicle to measure all of the coefficients for the foregoing equation of state. The volume of the state can be measured directly, and the equation of output is as follows:

$$y = Cx \quad (4)$$

$$C = \begin{bmatrix} 1 & 0 \\ 0 & 1 \end{bmatrix} \quad (5)$$

A system set up this way is controllable, and the regulator shown in Figure 9 is formed. Although the pole might have been determined by the introduction of a quadratic evaluation function, it was set so as to be settled as quickly as possible within the limits of the output torque of the driving motor. The optimal feedback coefficient, using the parameters of the actual machine shown in Table 1, is as follows.

$$[f_1, f_2] = [11, 2] \quad (6)$$

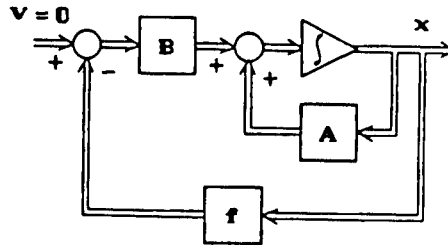


Figure 9. Regulator

## 5. Cruising Experiment

Based on the above results, the crawler vehicle HELIOS-1, which is shown in Figure 10 [not reproduced], was manufactured. It weighs 40 (kg), is 800 (mm) high, 1,000 (mm) long, and 600 (mm) wide. As for the driving mechanism, a pair of 120 (W) DC motors are installed in each crawler as a thrust system, and a 120 (W) DC motor for arm rotation and a 60 (W) DC motor to be used in the carrier's independent drive are mounted as posture control systems. The arm is driven through a worm gear with a cell flock mechanism. A piezo-type inclination angle sensor is installed in the carrier as a posture sensor.

The control system of HELIOS-1 is illustrated in Figure 11. HELIOS-1 can carry a range finder for three-dimensional measurement of its traveling environment, as shown in Figure 10 [not reproduced]. It is equipped with a supersonic wave sensor, enabling it to go up and down stairs automatically by measuring its distance from a wall.

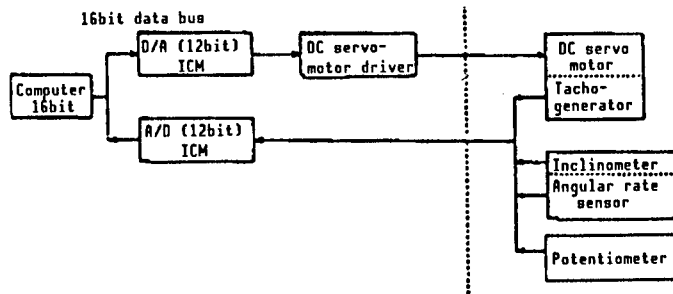


Figure 11. Control System of HELIOS-1

Experiments in which HELIOS-1 traveled up and down stairs were conducted, using two belts with conventional fixed nipples of different heights, and a belt with the suggested movable nipple. The stairs were ordinary ones, 200 (mm) wide and 150 (mm) high, with a slope of 30 degrees. As a result of the comparative experiment, the belt with the higher fixed nipple was found to exhibit a better supportive effect, but demonstrated instability when the nipple slipped off a step during stair travel. This phenomenon was not observed in the case of the movable nipple, which proved to have remarkable stability in going up and down stairs. As for the posture control system, an experiment involving getting over a bump was conducted using a brick similar to the one illustrated in Figure 12. The inclination angle of the carrier during the experiment was measured with a piezo-type inclination angle sensor mounted on the carrier, separate from the one for posture control. The results are shown in Figure 13. Figure 13(a) shows the reaction when the gain angular velocity feedback is 0, for reference. It is understood from Figure 13(b) that the regulator is capable of controlling the posture of the carrier within a deviation of  $\pm 8^\circ$ .

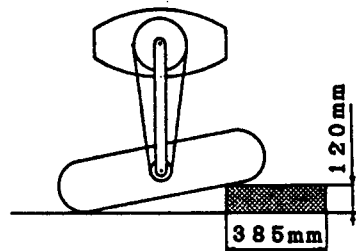


Figure 12. Experiment Involving Traversing a Bump

Figure 10 [not reproduced] shows the vehicle traveling on stairs exploring this posture control. A test of automatic ascent and descent between stair landings, or 10 steps (the dimensions are the same as above), was carried out. The manipulation was done by measuring walls using the supersonic wave sensor mentioned above. The vehicle was made to go up and down the stairs 20 times in fully automatic mode. It did not slip off at all during the test, and exhibited stability when ascending and descending. At the top of the stairs, the posture of the crawler changed drastically, both when ascending and descending. This created some concern, before the experiment, over whether the posture control system would work stably. In fact, however, the posture control was exerted quickly enough. It never lost its

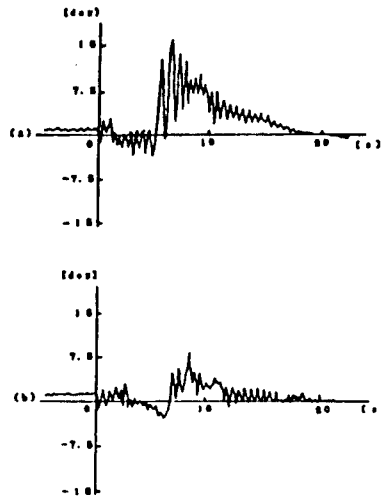


Figure 13. Rocking Carrier During Experiment Involving Traversing a Bump  
 (a) When the speed feedback coefficient is 0  
 (b) In the case of optimal feedback

balance on this spot. The elasticity of the movable nipple has the secondary effect of softening the collision of the crawler. This ultimately contributed to making the crawler's movement smoother at the top of the stairs.

#### References

1. Ohmichi, et al., "Proceedings of the Second Robotics Society Lecture Meeting," 1984, pp 233-234.
2. Takehara, et al., ROBOTICS SOCIETY MAGAZINE, Vol 2-3, pp 62-67.
3. Kohler, et al., Proceedings of 24th Conference on Remote System Technology, 1976, pp 196-218.
4. Iwamoto, et al., Proceedings of the Second Intelligent Traveling Robot Symposium, 1984, pp 33-38.
5. Kibata, et al., Proceedings of the Third Japan Robotics Society Lecture meeting, 1985, pp 417-418.

## **KR-I--Articulated Body Mobile Robot**

43064062 Tokyo 4TH INTELLIGENT ROBOTS SYMPOSIUM PAPERS in Japanese  
13/14 Jun 88 No 119 pp 165-170

[Article by Shigeo Hirose and Akio Morishima, Tokyo Institute of Technology; and Koichi Nagai, presently with Toshiba Corp.: "Articulated Body Mobile Robot 'Koryu KR-1'"]

### [Text] 1. Introduction

Advanced autonomous mobility must be added in order to realize a robot capable of infiltrating the natural environment or the interior of a building with complicated equipment and perform tasks there. This autonomous mobility must include loading capacity as well as ground adaptability as basic characteristics. This is because the environment in which the robot moves is, on the whole, uneven ground and because, to be able to perform assigned work autonomously, it must carry all necessary materials, including not only work equipment but also equipment for communication with the central control system, a computer, and a power source, and be capable of moving independently. Many previous studies on autonomous mobile robots have been primarily concerned with the problem of control, aimed at acquiring ground adaptability. However, few studies have been made from the standpoint of attempting to achieve ground adaptability and simultaneously improve loading capacity. Since the realization of a practical autonomous mobile robot is currently in demand, one cannot overlook the fact that research and development is being conducted from this inexhaustive position. In this paper, the authors will discuss the background behind the selection of the form of locomotion for "Koryu," the articulated body mobile robot we are attempting to develop<sup>4,5,6</sup> in order to realize a mobile robot combining ground adaptability and loading capacity, the results of a test on its basic actions, and the basic method employed in its force control.

### 2. Definite Examples of Locomotion Environment

The locomotion environment in an atomic reactor is one that requires the use of an autonomous mobile robot. In an atomic reactor with a high level of radioactivity, it is indeed necessary to use a mobile robot that can move freely and perform its work. A robot specifically designed to inspect and perform simple handling work as it tours passages and stairs in the reactor

is now being developed as a target for "atomic-related work robots" under the critical work robot development project of the Agency of Industrial Science and Technology. In this report, the target specifications of this development research are handled as a design example in order to definitely design and quantitatively study a mobile robot. These design specifications will be referred to hereunder as "reactor specifications." The reactor specifications are consolidated below.<sup>1</sup>

(1) The robot can carry materials, including a two-armed slave manipulator, a visual device, a communications device, a power source, etc. The total weight of these items cannot yet be predicted. Here, 500 kg is being used tentatively, based on estimates from the weight of conventional devices.

(2) It can ascend and descend a normal staircase with a gradient of about 40°, pass over a bump of a maximum height of about 300 mm that would be caused by pipes, etc., and travel a passage with a minimum width of about 600 mm, a height of about 1,500 mm, and with right-angle corners.

(3) It can have a locomotion speed of about 4 km/h, which is approximately the speed of human walk.

What must be noted in the above reactor specifications is that miniaturizing and high loading capacity are required as well as high adaptability.

### 3. Basic Configurations of Mobile Robot

The authors believe that three configurations, i.e., 1) a purely engineering configuration--wheel and track; 2) a configuration resembling the form of animal locomotion--leg; and 3) a similar configuration--articulated body, as shown in Figure 1, are the basic mobile robot configurations and that a highly practical mobile robot can be realized by one of these three configurations or by a hybrid combination of (1) and (2) or (1) and (3).<sup>2</sup> Here, configuration (1) of wheeled or tracked vehicles is structurally very simple, has a high loading capacity, and its locomotion can be controlled easily, but, in spite of these characteristics, it is inferior in ground adaptability. The leg configuration shows high ground adaptability, even on extremely uneven ground, because it can make effective use of its function to actively select its foot placement. However, its high degree of freedom results in a heavy leg drive system and its loading capacity is small, even if considerable efforts are made to improve the leg mechanism's energy efficiency, etc.<sup>3</sup>

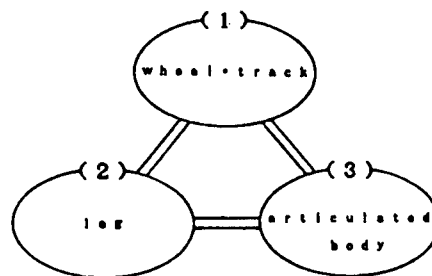


Figure 1. Three Basic Configurations of Mobile Robot

The above-mentioned locomotion configurations (1) and (2) are common themes of discussion, but the articulated body configuration has seldom been thought of as a basic configuration for a mobile robot. Nonetheless, this locomotion configuration has a number of characteristics,<sup>2</sup> as is clear from the observation of the locomotion of the snake, the animal after which it is modeled. When locomoting, a snake can: 1) proceed over heavily irregular ground or along a passage that is sinuous and too narrow for its body; 2) cross a crevice by stiffening its trunk into the shape of a bridge; 3) move stably in a marsh or on sandy ground by relaxing itself, and distributing its weight throughout its entire trunk. When these abilities are technologically composed in a mobile robot, it can conceivably 4) comprise a redundant and reliable device since it is a series of sections forming units. If a section is out of order, it can be left out. Also, the whole can be cut and used as two robots. For these reasons, the authors think that the articulated body should be regarded as one of the basic configurations of the mobile robot.

#### 4. Configurations With High Ground Adaptability and Loading Capacity

Autonomous mobile robots that satisfy the reactor specifications stated in Chapter 2 have been selected one by one from among the basic configurations in Chapter 3. The reactor specifications require ground adaptability, high-speed mobility, and a large loading capacity. The locomotion speed and loading capacity determine the eligibility of a tracked vehicle formula with documented results, and a configuration incorporating improvements of the characteristics of this formula and improved adaptability is believed to be a solution. However, passages in the target environments are narrow. According to 2) of the reactor specifications, the mobile robot must be designed with a width of not more than 600 mm, a length of not more than 600 mm, and a height of not more than 1,200 mm. Under these size conditions, it is difficult to design a tracked adaptable vehicle combining both characteristics: adaptability enabling it to safely ascend and descend a staircase and a loading capacity of 500 kg. Moreover, even if a tracked vehicle traveling with adequate ground adaptability could be produced at 500 kg, equalling the loading capacity, the total weight would be 1,000 kg and the specific gravity of the mobile robot would be 2.3. This would require a dense mechanism, almost completely filled with aluminum, to be designed (specific gravity: 2.7). It is by far more difficult, and unrealistic, to try to achieve an autonomous mobile robot incorporating the leg configuration, which is inferior to the tracked vehicle in loading capacity. One of the reasons for this is that the leg formula requires space for legs sway, and the load weight must be concentrated in the upper half of the allowable space. To be able to adopt the walking formula, it is necessary either to reduce the load weight drastically or to ease spatial restrictions.

Of course, we are not contending that the tracked vehicle and the leg-type locomotion mechanism are useless. These are generally exceedingly effective locomotion configurations. What we are arguing is that these two configurations cannot be adopted if it is necessary to convey large

quantities of materials through extremely small space and if the output/weight ratio of the actuator cannot be greatly improved.

By contrast, the articulated body configuration permits passage through narrow spaces, as stated above. Since it also permits dispersed loading and the drive system of each unit can be simplified, a large loading capacity is possible in this configuration. These and other characteristics, including high ground adaptability, can be expected by exploiting its linear body shape. It seems, therefore, that the formula using an articulated body as a basic configuration and hybridized with a wheeled or tracked vehicle for high-speed mobility is the most preferable configuration, satisfying the reactor specifications stated in Chapter 2.

## 5. Design of Articulated Body Mobile Robot and Traveling Test

### 5.1 Design

Some mobile robots close to the articulated body configuration have been tentatively produced so far.<sup>7,8</sup> However, their configurations, as they are, cannot produce mobile robots conforming to the reactor specifications. For instance, the oblique revolving mechanism we have already tentatively produced is unsuitable for passages that bend at right angles. Fukuda, et al.'s  $V_{roid}$ , as it is, has mobility only within the limits of the sagittal plane. Therefore, here we introduce the new mechanism illustrated in Figure 2. The articulated body mobile robot incorporating this mechanism is referred to here as "Koryu" (KR). KR is composed of many segments ((1) in the figure) of cylindrical and other shapes, and which are normally controlled vertically (2) as basic elements. The segments are connected serially. At their joints, segments can mutually make 2 degrees of freedom motions: translation in the direction of the vertical axis (z drive) and rotary motion around the vertical axis (2) ( $\theta$  drive). Wheels or tracked vehicles generating propulsive motion (s drive) (3) are provided under the segments.

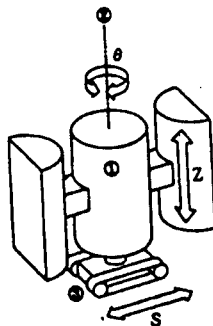


Figure 2. KR Unit Segment and Its Driving Mechanism

In KR, propulsive force is generated by all segments together. Therefore, if the output of each tracked vehicle is small, the total propulsive force produced is large. The height adjustment of each segment for the gravitational force is made by the cooperative control of the z-axis between adjoining segments. The distributed control of the dead weight can be made

independently because the drive system in the direction of gravitational force is separate. Operation in the direction of propulsion is made by the cooperative control of the  $\theta$  and  $z$  axes. The basic action consists of all segments following the locus of the foremost sign pattern segment.

Tracked vehicle three-axis rotation drive systems, shown as in Figure 3, are necessary for the accurate track control of a KR composed of segments of finite lengths. These include a drive system rotating actively around the vertical axis (yaw angle  $\theta_y$  drive), a drive system swinging tracked vehicle within the limits of the sagittal plane to cope with inclined faces, such as a staircase (pitch angle  $\theta_p$  drive), and a drive system swinging tracked vehicle within the limits of frontal plane for inclined faces (roll angle  $\theta_r$  drive). However, in the primary experimental model, the yaw angle is driven by a mechanism control causing the tracked vehicle to always face in the direction midway between the angle formed by the segment in order to simplify the mechanism of the model. A passive rotation axis with compliance is used for the pitch angle. The roll angle is fixed. These simplified mechanisms have been evaluated by a traveling test.

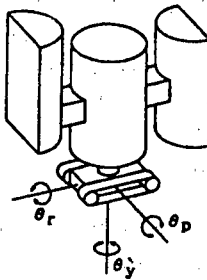


Figure 3. Additional Degrees of Freedom for the Track

## 5.2 Prototype Manufacture of Mechanical Model KR-I and Traveling Test

The mechanisms and specifications of the prototype mechanical model are shown in Figure 4 and Table 1. This mechanical model is referred to here as Koryu No I, KR-I. KR-I is composed of six segments. The diameter of each segment is 217 mm. Therefore, if studied for the uses stated in Chapter 2, the model is about one-third the size of the operational machine. The total number of degrees of freedom is 16, since 10 (= 2 x 5) 30 W DC motors are provided under the segments. The segments are composed of CFRP. The yaw angle drive of the tracked vehicles is realized by a pair of decelerators with a decelerating ratio of 1:2, as indicated in Figure 4. C language is used for all control programs, and the sampling time for the incorporation of angle information, etc., and target value instructions is 50 msec.

The traveling test for the KR-I is shown in Figures 5-9 [not reproduced]. Figure 5 [not reproduced] shows the action required to turn a right-angle corner. The track is indicated by the lamp attached to the foremost segment. The speed confirmed experimentally was 24 cm/sec. The maximum locomotion speed on a straight route was 40 cm/sec (1.44 kmh). If the bend angle is large, such as that at a right-angle corner, the direction

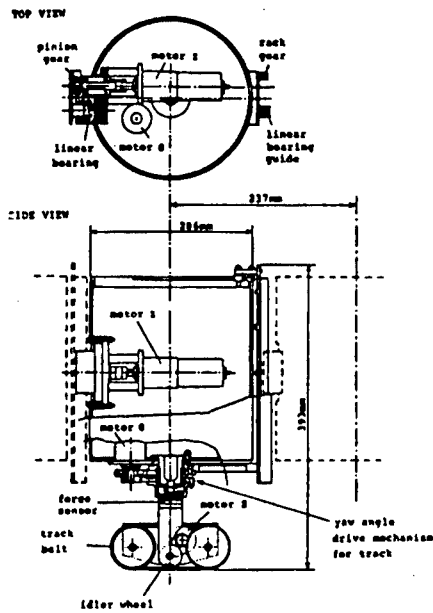


Figure 4. Mechanism and Dimensions of KR-I

Table 1. Specifications of KR-I

|                         |            |
|-------------------------|------------|
| <b>System</b>           |            |
| Total number of units   | 6          |
| Total length            | 1,391 mm   |
| Width                   | 206 mm     |
| Height                  | 393 mm     |
| Total weight            | 27.8 kg    |
| <b>Unit</b>             |            |
| Diameter                | 214 mm     |
| Weight (1st unit)       | 3.8 kg     |
| (2d-5th units)          | 5.2 kg     |
| (6th unit)              | 3.4 kg     |
| <b>Actuator</b>         |            |
| Z--Motion range         | 113 mm     |
| Velocity                | 7.9 cm/sec |
| Force                   | 18 kgf     |
| $\theta$ --Motion range | 90°        |
| Velocity                | 49°/sec    |
| Torque                  | 47 kgf/cm  |
| S--Velocity             | 532 mm/sec |
| Force                   | 4.4 kgf    |

corresponding to one-half of the angle structurally formed by the segments differs considerably from the direction of propulsion exerted solely by the yaw angle control of the tracked vehicles facing that direction. In the KR-I, to prevent the tracked vehicle sideslip in this situation, floating control by z-axis drive was used for segments with large errors in the

direction of their tracked vehicles. Since the only purpose is to remove weight, a slight z-axis displacement is sufficient. The direction of movement deviated by about  $20^\circ$  from the target track after turning a corner unless the synchronous flotation drive of the z-axis had been set into motion. However, it was confirmed that the synchronous control of the z-axis eliminated deviations almost completely. For an accurate motion sequence at corners, an angle target value is now given by providing a table according to the bend angle at the corner.

Figure 6 [not reproduced] illustrates striding over a pipeline as an obstacle. The locomotion speed was 30 cm/sec. Such actions as stopping in front of the obstacle and preparing to stride over it are not necessary. Also, the striding motion can be made without contacting the pipeline. From this, we confirmed that, although each segment of the KR-I is structurally very simple, smooth obstacle avoidance is possible through cooperative efforts of adjoining segments.

Figure 7 [not reproduced] demonstrates striding over a gap. The control is basically identical to that exerted when striding over an obstacle. It can be seen from this motion test that KR, with its long body, has maneuverability that differs from that of an ordinary mobile object with no length. The width of a gap that can be crossed by this motion must be less than half of the KR length for safety reasons.

Figure 8 [not reproduced] shows how KR climbs up or down stairs. We have learned that, if the stair steps are seemingly too small for the length of the tracked vehicles, the tracked vehicles conform to the stairs by the compliance of their pitch angle  $\theta_p$  and can travel smoothly and continuously. This indicates that, as long as large tracked vehicles are used for the stairs, one has only to induce passive compliance into pitch angle  $\theta_p$ .

Figure 9 [not reproduced] shows how KR-I crosses an inclined surface by assuming a wavelike form and increasing its stability in the lateral direction. Providing stability in all directions by this posture seems to be effective, except for when it passes through an extremely narrow passage. This form does not affect its propulsion since its tracked vehicle can turn up to one-half of the body bend angle. We have confirmed from this test that no serious problems arise in maintaining a stabilized posture, even if roll angle  $\theta_r$  is fixed.

In the above test, KR-I was not equipped with an external sensor, so we merely confirmed its motions by playback. Therefore, the motions differ from its actual motions. However, we believe that the high ground adaptability of the articulated body mobile configuration has been specifically verified from these tests.

### 5.3 Discussion of Loading Capacity

We shall now discuss the loading capacity of the prototype KR-I. The weights of its segments differ somewhat between that of the end segments and the intermediate segments, but, for a basic discussion, let us assume that all segments weigh 5 kg. The output of the z-axis drive system actuator,

which directly affects the loading capacity of KR, is 18 kg at a constant speed (8 cm/sec), or more than three times the dead weight. In case of a stall, 11 times the dead weight can be supported. Specifically, six times the dead weight can be easily driven if the z-axis drive is slowed somewhat.

In a configuration totaling 5 to 10 segments, which is believed to be adequate for practical use, the flotation support of two segments, at the most, is sufficient. This supporting posture is generated while striding, as shown in Figures 7 and 8 [not reproduced]. During the ordinary traveling of level ground or stairs, the bearing power at the z-axis is much less because it is controlled so as to distribute the load as much as possible. If, as above, all that is necessary is to be able to support six times the dead weight and the weight of two segments, probably twice the dead weight of a segment can be achieved as the load weight of each segment.

If an operational machine three times the size of the prototype KR-I is to be produced in the future, its weight probably can be about 50 kg, judging from the weight of the present drive systems and materials. In this case, the load weight of a segment would be 100 kg, provided that the relationship found in KR-I would apply here. If so, the load weight required in the reactor specifications can be achieved by connecting five or more segments. Of course, if the per-segment load weight is decreased by increasing the number of segments, stability improves and nimble high-speed locomotion becomes possible.

## 6. z-Axis Force Control

When KR travels uneven, irregular ground, it is necessary to effect force control for its z-axis drive system so that the dead weight may best be distributed throughout the different segments. However, KR contacts the ground due to its multiple segments and, generally, the distribution of its bearing power constitutes a problem of static indetermination. Therefore, the output torque of the z-axis drive actuator cannot be determined inclusively. Let us take, as a simple example, switching the z-axis drive systems of some segments in a straightened KR, as shown in Figure 7 [not reproduced], to servo systems, floating them, in order, from the front, propagating this to the rear, and thereby avoiding an obstacle. Here, the zero-segment-floating distance is assumed to simplify the analysis and, therefore, an optimum output and floor reaction force can be derived.

The symbols used in the analysis are as follows: For a KR model, such as that shown in Figure 10,  $F_i$  is the floor reaction force vector in the  $i$ -th unit,  $M_i$  is the floor reaction force moment vector in the  $i$ -th unit, and  $f_i$  is the vector of the force received by the unit at joint  $i$ , while,  $f_{z1}$  is the force generated by the  $\theta$  drive actuator,  $n_i$  is the vector of the moment received by the unit at joint  $i$ ,  $m$  is the unit mass (here, the same value is used for all segments for simplicity's sake),  $I$  is the vector of inter-unit distance (the same value is used for all segments and the center of gravity is taken in the middle) and  $g$  is the vector of gravity acceleration.

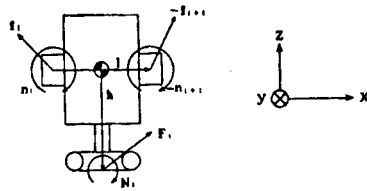


Figure 10. Vector Notation for the KR

If force and displacement vectors are defined as in Figure 10, restrictive conditions are derived from the balance of the force and moment. They are

$$F_i + mg + f_i - f_{i+1} = 0 \quad (i=0 \sim n) \quad (1)$$

$$\text{ただし } f_0 = f_{n+1} = 0$$

$$n_i - n_{i+1} + N_i + h F_i - \frac{1}{2} l (f_i + f_{i+1}) = 0 \quad (2)$$

$$\text{ただし } n_0 = n_{n+1} = 0$$

As an evaluative function for optimum motion, minimum energy consumption is used here. This evaluative function is

$$I = \sum_{i=1}^n \left( \sum_{j=1}^n F_{ij} - kmg \right)^2 \quad (3)$$

Equation (3) is derived as follows: Assuming the DC motor to be an actuator, its output power, P, is generally shown as

$$P = \frac{R_a}{K} T^2 + T\omega \quad (4)$$

Here,  $R_a$  is armature resistance,  $K$  is a torque constant,  $T$  is torque, and  $\omega$  is angular velocity. From this, the vertical drive for  $\theta$  driving can be ignored and, if the rotation of the motor is very small, the output power is proportional to the square of the torque and is

$$I \propto \sum_{i=1}^n T_i^2 \propto \sum_{i=1}^n f_{z,i}^2 \quad (5)$$

$f_{z,i}^2$  can be found from the recurrence formula of z-direction components in (1), thereby deriving Equation (3). This evaluative function corresponds to overall power consumption. The problem involves deriving a solution to  $F_i$  that will minimize Equation (3) on the basis of restrictive condition equations (1) and (2). This can be obtained by LaGrange's method of undetermined coefficients.

The results of the computation are shown in Figure 11. The posture in (b) is the one most requiring bearing power. The maximum generated power is 2 W, which is absolutely necessary. However, the torque generated by actuators between segments contacting the ground is distributed and, when compared with an example of other states of support, as in Figure 12, evaluative function I is smaller by about 20 percent. The basic control method for sending waves to the rear is clear from the results of the above discussion.

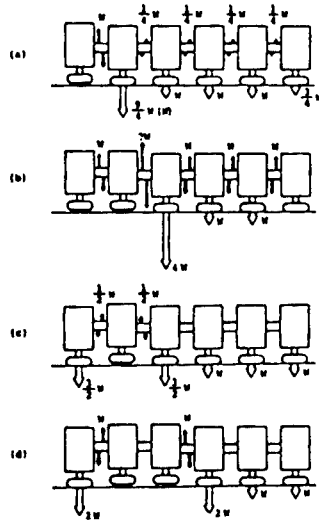


Figure 11. Optimum Producing Force and Resultant Floor Reaction for Wave Transmission Motion of KR

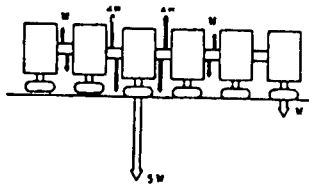


Figure 12. Another Example of Producing Force and Resultant Floor Reaction Corresponding to Figure 11(b)

## 7. Conclusion

In this paper, we first discussed the articulated body structure mobile robot, Koryu (KR), and compared it to the wheel and crawler formula and the leg formula, primarily with regard to using it in a nuclear reactor. As a result, it has been proven to have mobility, enabling it to exhibit high ground adaptability and loading capacity simultaneously. We produced a machine model KR-I prototype with a total length of 1,391 mm and a total weight of 27.8 kg, tested its mobility and studied its loading capacity. Finally, we studied how to derive an optimum solution with respect to force control involving the ground adaptability indispensable for locomotion. Figure 13 shows the conceptual diagram of the operational machine expected to be produced in the future. We are hopeful that a mobile robot satisfying the aforementioned reactor specifications may be realized in the near future by inducing this configuration, in which manipulators, measuring instruments, control devices, power sources, etc., are distributed to all segments.

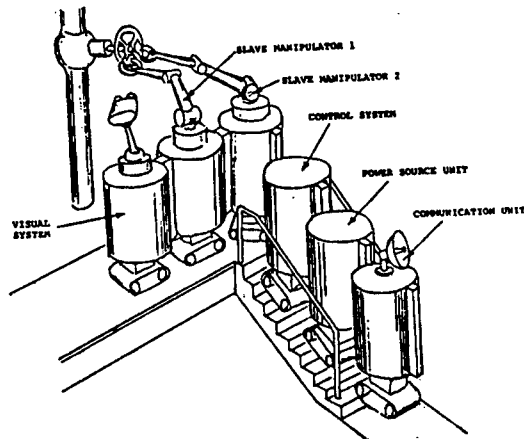


Figure 13. Anticipated View of Near Future Application of KR in Nuclear Reactor

#### References

1. Maki, "Research and Development of Atomic Energy-Related Work Robots," Major Project Results Announcing Meeting Papers, Osaka Science and Technology Center, 333/343, 1985.
2. Hirose, "Mobile Robot Technology," Keisoku to Seigyō 21-12, 1129/1134, 1982.
3. Hirose and Umetani, "Leg Configuration of Walking Machine and Locomotion Machine," "Biomechanism 5," Tokyo University Publishing House, 242/250, 1980.
4. Hirose, "Proposal of a Cable Active Mobile Robot," Third Japan Robotic Society Scientific Lecture Meeting papers, 275/276, 1985.
5. Hirose and Nagai, "Research on a Cable Active Mobile Robot," Fourth Japan Robotic Society Scientific Lecture Meeting Papers, 209/210, 1986.
6. Hirose and Morishima, "Research on a Cable Active Mobile Robot--Report No 3: A Few Studies for Improved Functions," 26th SICE Scientific Lecture Meeting Papers, 515/516, 1987.
7. Hirose, Oda, and Umetani, "A Cable Active Object Using an Oblique Revolving Mechanism and Its Control," SICE Collection of Papers, 17-6, 686/692, 1981.
8. Fukuda and Kobayashi, "Conception of Multiconfiguration Free Locomotion Mechanism ( $V_{roid}$ ) for Articulated Robot (Report No 1: Basic Conception and Basic Motion)," Second Japan Robotic Society Scientific Lecture Meeting Papers, 237/238, 1984.

## **Dynamically Restructured Robotic System With Positioning Accuracy, Joint Torque**

43064062 Tokyo 4TH INTELLIGENT ROBOTS SYMPOSIUM PAPERS in Japanese  
13/14 Jun 88 No 120 pp 171-176

[Article by Toshio Fukuda, Science University of Tokyo; and Seiya Makagawa, Sony Corp.: "Cell Structured Robot With Consideration for Positioning Accuracy and Joint Torque"]

### [Text] 1. Introduction

The dynamically reconfigurable robotic system, which is a new next-generation robotic system, can be wholly recomposed into an optimum configuration according to its work purpose and work environment by changing the sequence of cell combination in a self-organized manner when forming such items as the robot manipulator, mobile robot and its structure, using cells, which are its basic component.<sup>1,2</sup> DRRS is an autonomous distributed cooperative system, similar to that in the cellular structure of an organism, in both aspects of software and hardware, and permits communication, coupling and separation at the intercellular level. Therefore, it has redundancy that enables it to maintain its overall functioning by initiating self-repair before the partial failure or deterioration of the system occurs. DRRS can conform flexibly to changes in its work environment and to task diversification. Figure 1 shows the conceptual diagram of this new robotic system. To determine the type and sequence of cell connection during recomposition, we have proposed an optimum configuration selection method that can simultaneously determine the joint arrangement, degree of freedom, and link length. This article describes the test we conducted on the automatic approach, using Series II that incorporates improvements so that high positioning accuracy is not required during coupling as it is in Series I,<sup>1,2</sup> in order to realize this autonomous coupling and separation of cells in DRRS.

### 2. Basic Configurations and Functions of Cells

As hardware, a cell must have a connecting/disconnecting mechanism, enabling mechanical automatic coupling and separation as well as facilitating the coupling and separation actions. After coupling, this mechanism must be able to maintain high rigidity of the coupling surface. It must also permit the transmittance and exchange of force, energy, and information via the

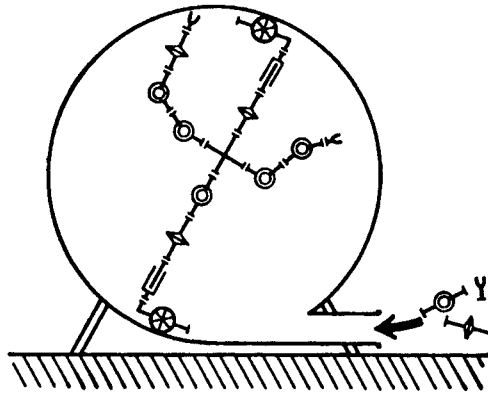


Figure 1. Conceptual Diagram of DRRS (Example of work in a tank)

coupling surface. The Series I cell, which meets these requirements, has had in its basic configuration and connecting mechanism, the disadvantage of requiring high intercellular relative positioning accuracy during coupling. Therefore, we produced Series II, incorporating a hook connecting mechanism, as illustrated in Figure 2. Whereas the basic configuration of the cell is rectangular parallelepiped in Series I, in Series II it has a truncated cone-shaped convex part on the front face and a concave part on the rear face, used for guidance during coupling, and its coupling effective ratio (area of potential coupling/area of coupling surface) is larger than that of Series I. Figure 3 [not reproduced] shows the external appearance of the cell produced. Table 1 compares the characteristics of Series I and Series II. Figure 4 shows the scope of potential coupling during coupling. If the center of the cell is in the area of the diagonals in Figure 4, the cell can pull in the target cell, using a hook, and couple with it. Series I lacked a connector for transmitting energy and information between cells, but Series II has a connector for this purpose, and energy and information can be transmitted through this. In Series II, a wheeled traveling cell, capable of moving on a smooth plane, and a cell without a traveling function to which the traveling cell is to be coupled (target cell), are provided. A castor is provided under the target cell to reduce friction with the floor while coupling.

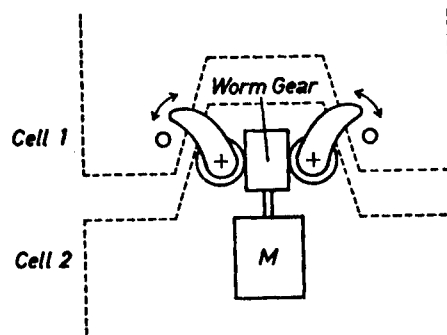


Figure 2. Hook Connecting Mechanism for Cells

Table 1. Data for Series I and Series II

|                             | Series I                               | Series II             |
|-----------------------------|--|-----------------------|
| Frame size (mm)             | 190 x 90 x 50                          | 176 x 126 x 90        |
| Weight (kg)                 | 1.2 (mobile cell)<br>1.2 (target cell) | 2.7<br>1.0            |
| Shape of connective surface | Flat                                   | Flat + truncated cone |
| Coupler type                | Small hocks x 4                        | Large hocks x 1       |
| Coupler actuator            | SMA                                    | DC motor              |
| Wheel actuator              | DC motor                               | Pulse motor           |
| Connectible area ratio (%)  | 0.3                                    | 4.0                   |

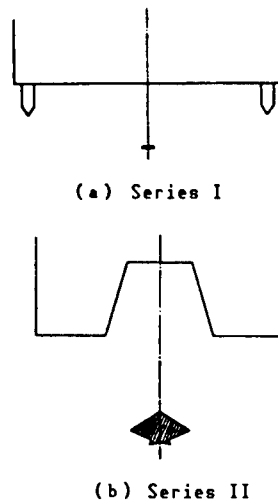


Figure 4. Scope of Potential Coupling

### 3. Sensor System and How To Control It

Let us now consider the two-dimensional approach--coupling and separation between the traveling cell and the target cell in Series II. The following five steps are set as the sequence for the approach and coupling of the two:

- STEP 1) After the target cell is selected, the traveling cell identifies the target cell from the group of cells and recognizes its position.
- STEP 2) It makes a general approach toward the cell selected as the target cell (primary approach).

- STEP 3) It recognizes the attitude of the target cell and moves to the side where the coupling surface of the latter cell is.
- STEP 4) It approaches the coupling surface of the target cell and enters the scope of potential coupling (secondary approach).
- STEP 5) It achieves coupling by operating the hook.

If obstacles (other cells existing singly) are within the limits of the locomotion plane of the traveling cell during the primary approach, the traveling cell recognizes and avoids them.

This report concerns our test on the sequence after Step 1: recognition of the position of the target cell. The sensor system used comprises three photodiodes of the infrared area-type (PD1, PD2, and PD3), and ultrasonic sensors--one for transmission and two for reception (HSS-T, USS-R<sub>R</sub>, and USS-R<sub>L</sub>), on the side of the traveling cell, and eight weak-directivity LEDs arranged radially at intervals of 45° on the side of the target cell. The sensor arrangement on each cell is shown in Figure 5. The traveling cell recognizes the position and attitude of the target cell by receiving LED light through the photodiodes and recognizes the other single cells as obstacles by the ultrasonic sensors.

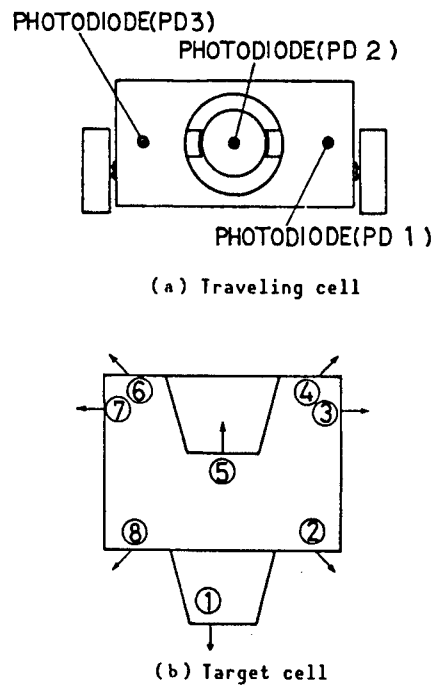


Figure 5. Arrangement of Sensors

Motions ending with coupling are tested by the following principles for Steps 1 through 5, using the control system shown in Figure 6. The

traveling cell initiates autorotation by the control algorithm shown in Figure 7, and recognizes the position of the target cell by the maximum output of PD2 (Step 1). Then, it proceeds straight, correcting its track for each set distance, until the output of PD2 reaches threshold value  $V_a$ . Track correction is made by controlling the wheels so that the output difference between the right and left photodiodes (PD1 and PD3) is minimal (Step 2). using the algorithm shown in Figure 8, the traveling cell recognizes the general attitude of the target cell by causing the successive emission of the eight LEDs of the target cell, follows the preset track, and

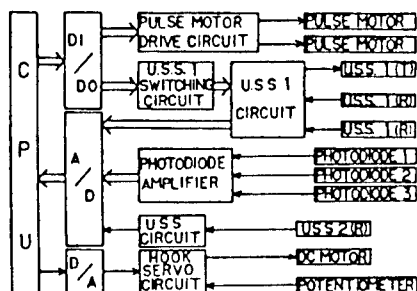


Figure 6. Control System

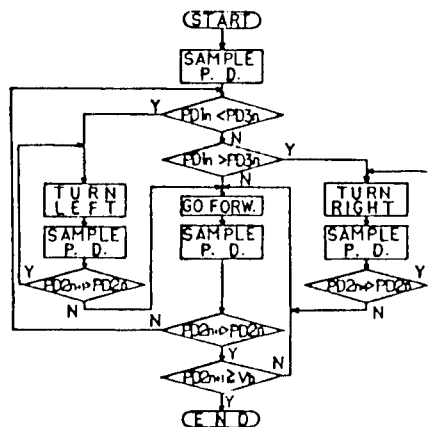


Figure 7. Control Algorithm for Steps 1 and 2

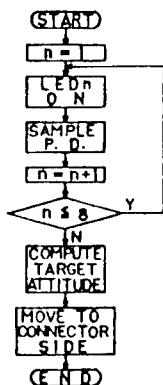


Figure 8. Control Algorithm for Step 3

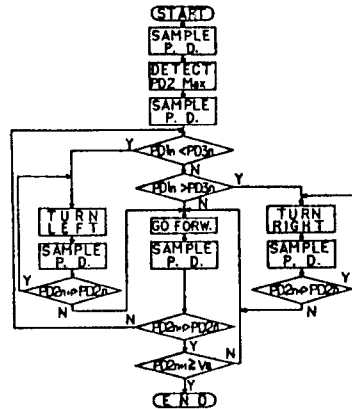


Figure 9. Control Algorithm for Steps 4 and 5

moves to the side of the coupling surface (Step 3). Then, the traveling cell advances to the position of potential coupling of the target cell through the control algorithm in Figure 9 (Step 4) and is coupled with the target cell (Step 5).

#### 4. Optimum Configuration

##### 4.1 Algorithm for Determining Optimum Configuration

The algorithm we propose for use in determining the optimum configuration is generally composed of two steps: the step to select configuration candidates which permit the execution of a task, and the step to select, from among these, the configuration that makes the evaluation function minimal. Figure 10 shows the algorithm for determining the optimum configuration of a cell structure manipulator. The first step is divided into the step to select the local candidate for each work point and the step to select the candidate common to all work points. The selection is made independently for a case using a fixed manipulator base and that using a movable manipulator base.

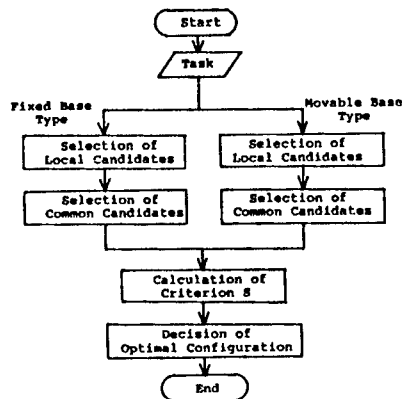


Figure 10. Algorithm for Optimum Configuration of Cell Structure Manipulator

## 4.2 Configuration Evaluating Function

Configuration evaluating function  $S$  is the sum of four parameters and is defined by the following equation:

$$S = \sum_{n=1}^N (a_1 P_n + a_2 H_n) + a_3 \sum_{n=1}^{N-1} L_n + a_4 C \quad (1)$$

Here,  $N$ : total number of work points  
 $P_n$ : positioning accuracy of the manipulator tip at work point  $n$   
 $H_n$ : attitude-maintaining torque of the joint cell at work point  $n$   
 $L_n$ : displacement of the joint cell when pose changes from work point  $n$  to work point  $n + 1$   
 $C$ : cost of cell  
 $a_1 \sim a_4$ : weight coefficient

The configuration candidate that makes this evaluation function minimal is the optimal configuration for the given task.

### 4.2.1 Positioning Accuracy of Manipulator Tip

The cell structure manipulator used comprises rigid cells connected by a coupling device with compliance and is modeled as indicated in Figure 11. Static deflection and torsion occur at the manipulator tip as an effect of gravity. Microdisplacement vector  $\Delta_i$ , accompanying the coupling near the base of the  $i$ -th cell, and  $F_i$  vector of force exerted there, are set as follows:

$$\Delta_i = [d_{ix}, d_{iy}, d_{iz}, \delta_{ix}, \delta_{iy}, \delta_{iz}]^T \quad (2)$$

$$F_i = [f_{ix}, f_{iy}, f_{iz}, m_{ix}, m_{iy}, m_{iz}]^T \quad (3)$$

Here,  $d_{ij}$ : micro-translation in direction of  $j$ -axis,  $\delta_{ij}$ : micro-rotation around  $j$ -axis,  $f_{ij}$ : translation force in direction of  $j$ -axis, and  $m_{ij}$ : moment around  $j$ -axis.

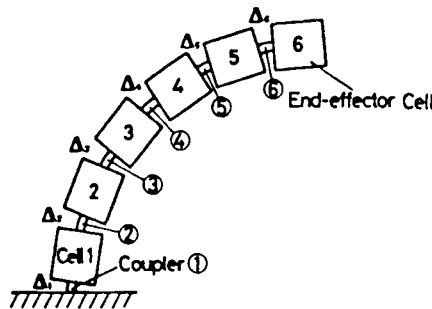


Figure 11. Model of Cell Structure Manipulator

Although the transformer matrix for the manipulator, the ordinary  $A$  matrix, is regarded as a completely rigid body,  $A'$ , the transformation matrix after deflection and torsion, is defined as follows:

$$A'_i = B_i \cdot C_i \cdot D_i \quad (4)$$

Here,  $B_i$ : transformation matrix from tip of cell (i-1) to center of coupling surface;  $C_i$ : micro-rotation translation matrix for transfer to center of coupling surface near base of cell i by  $\Delta_i$  displacement; and  $D_i$ : transformation matrix from center of coupling surface near base of cell i to own central coordinate system.

The  $C_i$  matrix is given, according to Equation (3), in the following form:

$$C_i = \begin{bmatrix} 1 & -\delta_{i,x} & \delta_{i,y} & d_{i,x} \\ \delta_{i,x} & 1 & -\delta_{i,y} & d_{i,y} \\ -\delta_{i,y} & \delta_{i,x} & 1 & d_{i,z} \\ 0 & 0 & 0 & 1 \end{bmatrix} \quad (5)$$

Using m as the total number of cells,

$$\Delta_i = K_i^{-1} \sum_{j=1}^m ({}^i Y_j D_j^{-1} \bullet F_j) \quad (6)$$

Here,  $\bullet$  is an operator.<sup>3</sup>

$\Delta_1 \sim \Delta_m$  vectors can be obtained by finding  $\Delta_1 \sim \Delta_m$  equations, using Equation (6), making them simultaneous and solving them. Displacement at the manipulator tip during the  $\Delta_1 \sim \Delta_m$  displacement occurring at cell coupling can be shown by vector expression as follows:

$$E_n = [d_{1,x}, d_{1,y}, d_{1,z}, \delta_{1,x}, \delta_{1,y}, \delta_{1,z}]^T \quad (7)$$

#### 4.2.2 Attitude Maintaining Torque of Joint Cell

Parameter  $T_n$  is obtained by finding the resultant force exerted in each joint cell by the mass and payload of the cell, taking the total of these resultant forces for all joint cells and making it scalar. This can be indicated by the following equation:

$$T_n = \sum_{i=1}^m \sum_{j=1}^m ({}^i Y_j^{(n)} X_j^{(n)-1} \bullet F_j^{(n)}) \quad (8)$$

At this time, parameter  $H_n$  is set as follows:

$$H_n = T_n^T W_n T_n \quad (9)$$

Here,  $W_n$ : weight matrix (6 x 6) for  $H_n$  at work point n.

#### 4.3 Simulation Results

The optimum configuration of the manipulator for a task requiring two work points, as shown in Figure 12, is given. It is assumed that the work space has no obstacles, the surface of the floor is smooth and the mobile carriage can move to any place (within the limits of the X-Y plane). Figure 13 shows

the configuration candidates for a manipulator capable of performing this task for the case with a fixed base and that with a movable base, and Table 2 shows the values of configuration function S for these, parameter by parameter. Positioning accuracy differs by axis direction and, according to the requirements of the task, the optimum configuration differs greatly.

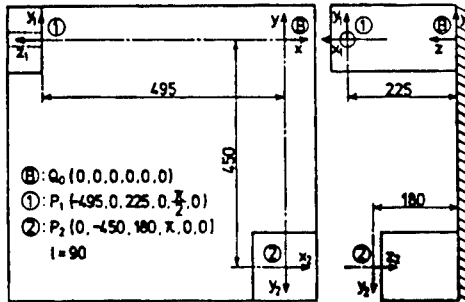


Figure 12. Positional Relationship Between Two Work Points and Base

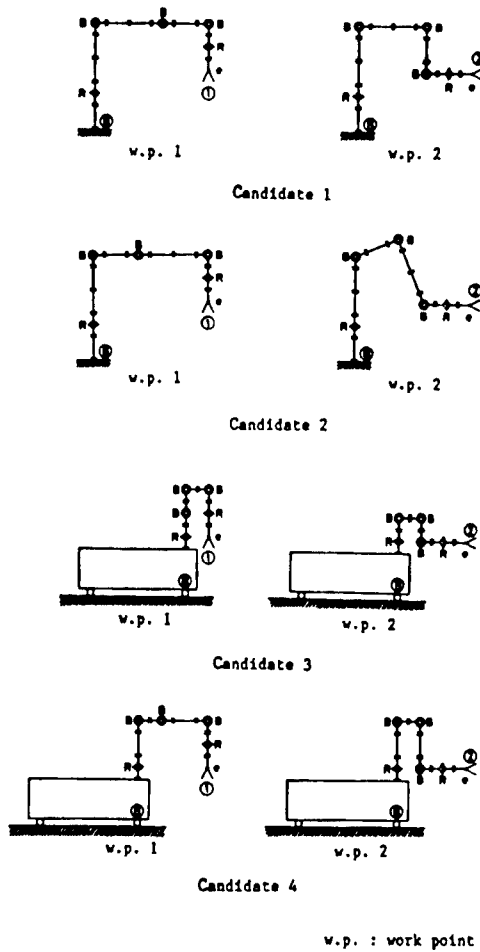


Figure 13. Configuration Candidates for Manipulator

Table 2. Values of Configuration Evaluation Function by Parameter

|             | P     | H   | L   | C  |
|-------------|-------|-----|-----|----|
| Candidate 1 | 13764 | 520 | 450 | 12 |
| Candidate 2 | 13758 | 593 | 450 | 12 |
| Candidate 3 | 13034 | 187 | 785 | 11 |
| Candidate 4 | 18819 | 291 | 648 | 13 |

P: Positioning accuracy; H: Holding torque; L: Joint displacement;  
 C: Cost

### 5. Test Results

Figure 15 shows the results of a test conducted to determine how a traveling cell on the circumference of a circle with a radius of 40 cm from its center, which is the center of the target cell as indicated in Figure 14, can recognize the attitude of the target cell. Figure 17 shows the results of testing the control of the approach, coupling, and separation when obstacles are not involved by arranging the traveling cell and the target cell, as shown in Figure 16. One can see from Figure 17 that, even in this sensor system and this sensor arrangement, cells can easily conduct automatic approach, coupling, and separation if their coupling effective ratio is increased by using concave and convex cell coupling surfaces, as is done in this Series II.

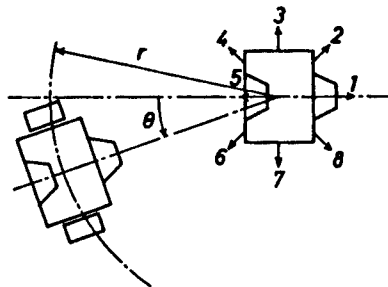


Figure 14. Cell Position Relationship in Attitude Recognition Test



Figure 15. Results of Test on Recognition of Attitude of Opposite Cell

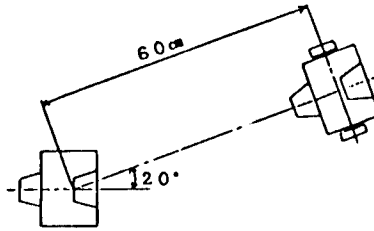


Figure 16. Initial Arrangement of Cells

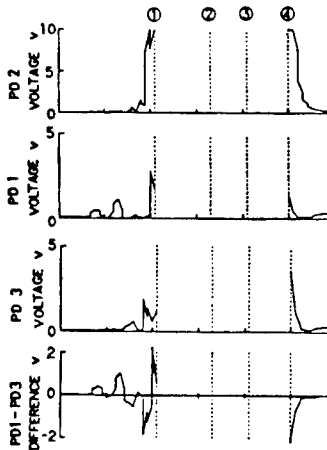
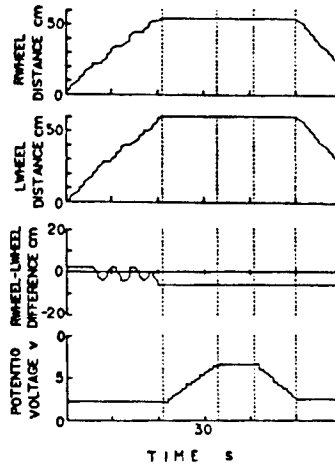


Figure 17. Results of Control Test

## 6. Conclusion

In this report, the following results were obtained on the realizability of the dynamically reconfigurable robotic system (DRRS):

- (1) We have devised and manufactured a connecting mechanism that does not require high positioning accuracy when coupling cells, and have proved the effectiveness of its operation.

(2) We have experimentally proved the possibility of practical two-dimensional automatic approach, coupling, and separation control using a traveling cell.

(3) We have proposed an optimum configuration selection algorithm to minimize the configuration evaluation function for the given task and proved its effectiveness by simulation.

Finally, we extend our heartfelt thanks to Ko Ezno who cooperated with us in conducting these tests.

#### References

1. Fukuda and Nakagawa, "A Self-Organized Robot With a Cell Structure-- Its Basic Conception, Methods of Control of Approach Between Cells, and Configuration Determination," *Dengakuron C-hen*, Vol 107 No 11, 1987, pp 1019-1026
2. Ibid., "A Dynamically Reconfigurable Robotic System (Concept of a System and Optimal Configuration)," *PROC. IECON'87*, 1987, pp 588-595.
3. P. Paul, translated by Yoshikawa, "Robot Manipulator," Corona Co., 1984, pp 45-46, 211-216.

## Rotary Shoe Configuration for Mobile Robot

43064062 Tokyo 4TH INTELLIGENT ROBOTS SYMPOSIUM PAPERS in Japanese  
13/14 Jun 88 No 121 pp 177-182

[Article by Yoshikata Rokusha, Wanbi Giken]

[Text] 1. Introduction

If a robot uses a locomotion mechanism and is operated outdoors, it must travel over uneven ground and bumps which cannot be traversed with wheels.

Specifically, a fruit picking robot, a farm work robot or a forest work robot must be able to traverse soft ground and snow-covered ground. Also, to the "welfare robot," an automatic vehicle for the physically handicapped, negotiating bumps and stairs is a major problem.

However, the crawler or walking mechanism previously used for uneven-ground vehicles was inefficient when traveling over level ground and involved excessive running resistance.

This report describes the newly-invented rotary shoe mechanism of the ground-adapted type and analytically proves that it combines the high speed of the wheel and the uneven ground traveling capacity of the walking mechanism by incorporating two modes, namely, a level ground traveling mode and an uneven ground traveling mode.

Careful observation of how a man uses his feet when he moves reveals that, as shown in Figure 1, when he walks ordinarily, he kicks the ground with the toe, turns the sole to the rear, brings the foot to the front, and, when approaching landing, turns the ankle and raises the toe. Then, he turns the sole to the front and lands, heel first.

Thus, when landing, he lowers the foot, heel first, and supports his weight with the entire sole but, when he kicks, he gains propulsive force by pushing the ground. So, the ankle sways back and forth, but is controlled well.

The reason that the human foot can traverse bumps, etc., better than the wheel can has much to do with the above-mentioned turn of the sole, and is because it can freely control the tread according to road conditions.

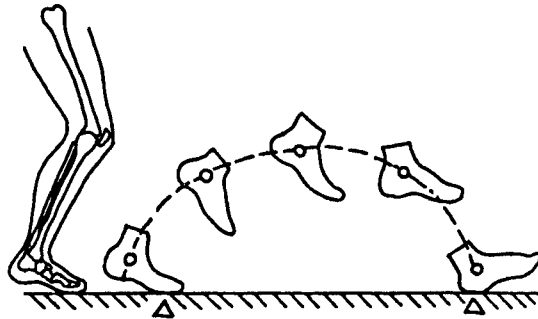


Figure 1. Foot Movement on Level Ground

The motion of the human foot can be compared with the rotary motion of the wheel.

Figure 2 likens a wheel to the walking shoe of a man, and its tire portion is divided and conceived as walking shoes configured in a circle.

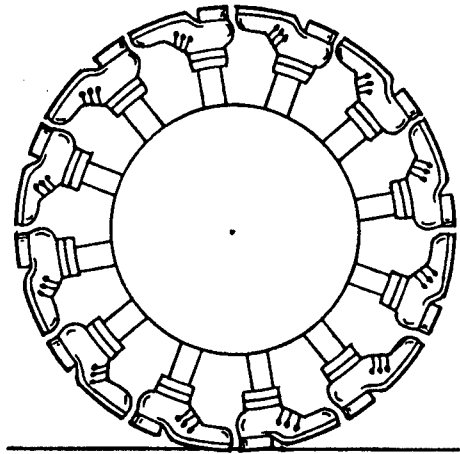


Figure 2. Rotary Shoe Wheel With Many Walking Shoes

Only one shoe is used when landing but, as soon as a shoe leaves the ground, kicking it with the toe, the heel of the next shoe touches the ground.

As far as its motion on and near the ground is concerned, this rotary wheel with many walking shoes resembles the walking motion on level ground and, if each shoe sways back to the front every time it completes its function as a propeller, it can timely begin to work again.

It does not matter what a shoe does after leaving the ground as long as it is prepared to function again as a propeller whenever and wherever necessary.

The attitude of the human shoe on and near the ground always changes according to road conditions and moving speeds. When a man traverses bumps on uneven ground, he increases his traveling capacity by raising his knees and turning the treads of his feet somewhat downward.

## 2. Example of Structure of Rotary Shoe Mechanism

The purpose of this rotary shoe mechanism is to improve its uneven ground travel capacity by pivot attachment of the shoes of the rotary shoe wheel so they can sway, rather than fixing them as in the conventional wheel, thereby enabling the mechanism to travel on ordinary paved roads with its shoes arranged in a circle like a wheel but, on uneven ground, changing the attitude of the rotary shoes and controlling the treads of the shoes in the manner of human walk.

Let us see a graphic example of this mechanism. In Figure 3, radial support 1 freely rotates around cylindrical axle 2 and is connected to motor 5 via gears 3 and 4. Rotary shoe 7 is attached to horizontal shaft 6 at the tip of support 1 so as to be able to sway freely and is coupled to pin 9 by link 8. Links 8•8•8...are bundled together in the center and fitted into axle 11 of rod member 10. Links 8•8•8...are bundled together in the center and fitted into axle 11 of rod member 10.

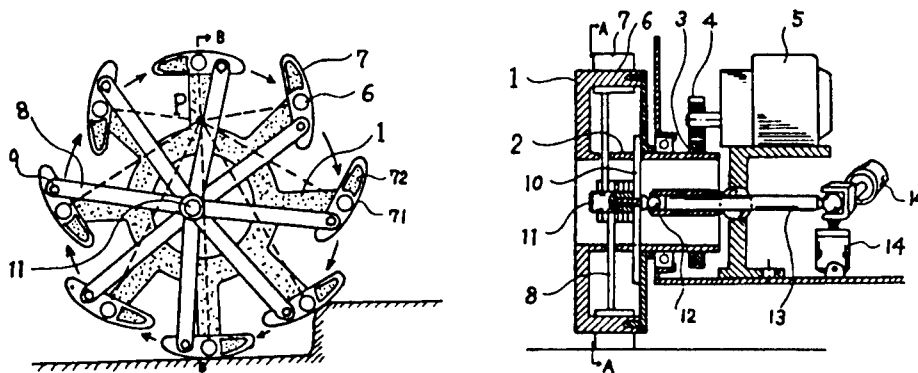


Figure 3. Structure of Rotary Shoe Mechanism  
(A-A line section and B-B line section)

The opposite side of rod member 10 is connected to lever 13 by spherical joint 12 and provided with fixed eccentricity adjuster 14 (two hydraulic cylinders, etc.).

The aforementioned rotary shoe 7 is provided with arc tread 71 and soft sponge 72 so as to absorb vibration from the road surface and has a tread pattern.

Because of this structure, motive power from motor 5 turns cylindrical axle 2 via gears 3 and 4 and revolves radial support 1 like a wheel when traveling on uneven ground.

Many a rotary shoe 7 is attached to the tip of support 1 and, therefore, revolves with the support, while able to sway by horizontal shaft 6, and the direction of tread 71 is controlled by link 8.

If locomotion adjustment is made of axle 11 of rod member 10 in the center, focusing point P formed by the crossing of a hypothetical line vertical to tread 71 shifts, and the bump traveling capacity increases in proportion to the height of point P.

When traveling over level ground, by lowering this point P and making it agree with the center of revolution of radial support 1, the treads 71 ... of the many rotary shoes 7 form a circular contour as a whole, and the mechanism can move as lightly as an ordinary wheel.

Furthermore, hypothetical line focusing point P can be shifted to the front if rod member 10 is moved by the eccentricity adjuster. By so doing, the tread of the lowest rotary shoe turns somewhat to the rear and, when traveling by giving a drive force to the rotary shoes, the shoes have increased force with which to kick the ground to the rear.

Therefore, the mechanism runs well on soft sandy or muddy ground with greatly increased drive and tractive force. Also, if it falls into a deep hole, it can easily get out by the reaction produced from vigorously pushing the sand or mud to the rear with its rotary shoes.

It is preferable that outdoor locomotion robots be able to travel uneven, snow-covered, sandy or muddy ground in order to pick fruit or harvest vegetables, or to accomplish forestry-related tasks, including afforesting, weeding, thinning, and felling. It is, of course, all the better if they can traverse bumps and ditches.

An outdoor locomotion robot will, by being equipped with this rotary shoe mechanism, be able to travel uneven, snow-covered, sandy or muddy ground using the uneven ground travel mode, and move along a paved road at high speed using the level ground traveling mode.

Crawler robots intended exclusively for uneven ground use have had difficulty with high-speed travel along urban paved roads, keeping pace with other means of transportation, and have been unable to locomote efficiently due to their excessive motional components. This rotary shoe mechanism will eliminate these disadvantages and drastically extend their range of operation.

Moreover, this mechanism can realize bump crossing and the quiet traveling of level ground for the welfare robot, making the vehicle suitable for operation in hospitals and institutions.

### 3. Analysis

The following describes this mechanism's motion and its analysis:

#### 3.1

As indicated in Figure 4, rotary shoes 7 make a circular motion around the center of the base of the lowest rotary shoe contacting the ground and present a cycloid locus.  $F$ , the force received from the tread of a rotary shoe, differs somewhat from the direction of motion of the shoe tread; therefore, it can be resolved into  $f_1$ , the force to vertically push the tread of the rotary shoe, and  $f_2$ , the force working toward a parallel slip to this tread.

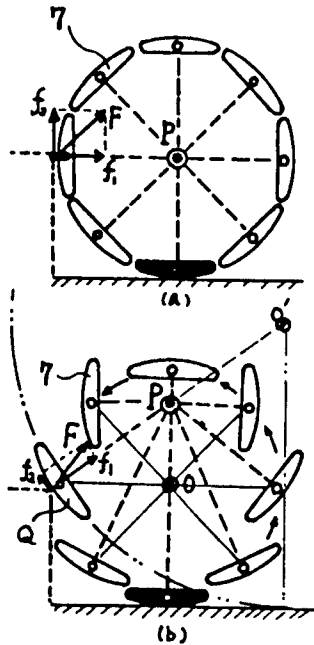


Figure 4. Traveling Capacity Increased by Raising Focus Point P

If a bump the height of the axle exists, if the rotary shoes are arranged circularly like a wheel, as in the upper diagram of Figure 4, the tread faces the front and, therefore, no catch can occur. In this case,  $f_1$ , the force component received from the tread, works to push back the axle and  $f_2$  becomes the force exerted precisely upward, making it impossible to step across the bump.

But if rod member 10 is moved by operating the eccentricity adjuster and theoretical focusing point P is shifted upward, the tread of the rotary shoe turns somewhat downward and, therefore,  $f_2$ , the component of force F working to cause slip, decreases and turns to the front. A catch then develops, even in a bump the height of the axle, making it possible to run onto the bump.

This effect is confirmed by the equivalent diameter wheel theory,

$$\sqrt{R^2 + r^2} : X - r : X - R$$

$$X = \frac{\sqrt{R^2 + r^2} \cdot R}{\sqrt{R^2 + r^2} - r}$$

and by the similarity in the right-angled triangle, using O as a real wheel axle center, O' as an equivalent wheel axle center, P as a focusing point and Q as a rotary foot in the lower diagram of Figure 4, and if OQ = R, OP = r, and O'Q = X are taken as measurements.

(An equivalent diameter wheel has a diameter double the diameter of a real wheel ( $X = 2R$ ) when  $R = \sqrt{3}r$ .  $r = 0.58R$ .)

### 3.2 Motion Locus of Rotary Shoe Rolling Over Ground

Figure 5 shows the motion loci of rotary shoes viewed from positions of rest. The upper diagram illustrates the case in which theoretical focusing point P in the center agrees with axle center O, and the lower diagram is for the case in which theoretical point P is raised.

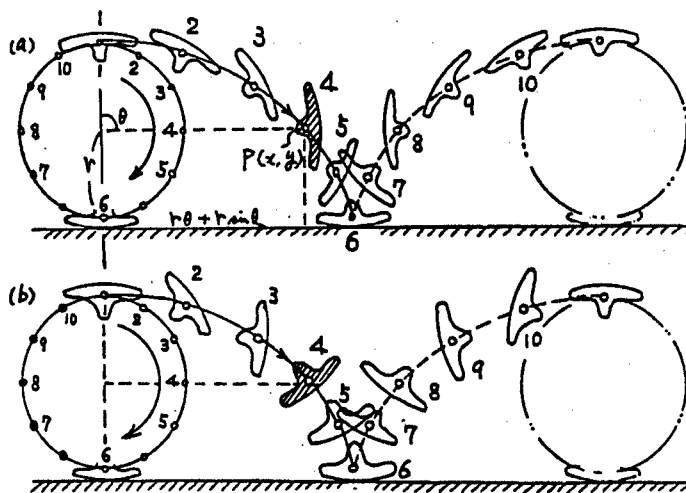


Figure 5. Motion Loci of Individual Rotary Shoes and Attitude

The x-axis is the axis of the ground on which the rotary shoes roll, while the y-axis is orthogonal to this. Using  $r$  for the revolving radius and  $\theta$  for the rotating angle, the coordinates of the above-mentioned rotary shoes Q ( $x$  and  $y$ ) are

$$\begin{cases} x = r\theta + r\sin\theta = r(\theta + \sin\theta) \\ y = r + r\cos\theta = r(1 + \cos\theta) \end{cases}$$

Hence, cycloid curves are expressed by the equation

$$x^2 + y^2 - 2\theta rx - 2xy + r^2\theta^2 = 0$$

The upper and lower diagrams differ in the shoe attitudes at each position. The attitudes of the shoes are particularly different at position 4.

In the upper diagram, the tread of the shoe at position 4 faces duly to the side, so its tread cannot traverse an obstacle. On the other hand, in the lower diagram the tread of the shoe at position 4 faces obliquely downward, so it can contact an obstacle and the mechanism can pass over it.

In the lower diagram, position 3, at which the tread faces the front, corresponds to the vicinity of position 4 in the upper diagram, and the height from the ground is so great that the traveling capacity on uneven, rugged, muddy or sandy ground is exceedingly large. Therefore, switching from the level ground traveling mode to the uneven ground travel mode denotes the ability to freely move off-road from a regular road, and has the effect of drastically extending the range of operation.

### 3.3 Angle of Inclination $\alpha$ and Angle of Sway $\beta$ of Rotary Shoes

Using  $O$  as a circling center,  $P$  as a theoretical focusing point,  $Q$  as a rotary shoe center,  $r$  as an eccentricity amount,  $R$  as a circling radius, and  $\theta$  as a rotation angle, in Figure 6,  $\alpha$ , the angle of inclination of the tread of the rotary shoe to the ground, can be computed as follows:

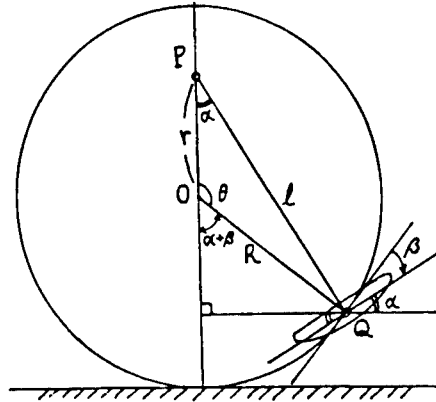


Figure 6. Finding Angle of Inclination  $\alpha$  (to ground) and Angle of Sway  $\beta$  (to axis) of Rotary Shoe

In  $\triangle OPQ$ , by the cosine theorem

$$R^2 = l^2 + r^2 - 2lr \cos \alpha \quad (1)$$

$$l^2 = r^2 + R^2 - 2rR \cos \theta \quad (2)$$

From (1)

$$\cos \alpha = \frac{l^2 + r^2 - R^2}{2lr} \quad (3)$$

From (2)

$$l = \sqrt{r^2 + R^2 - 2rR \cos \theta} \quad (4)$$

By substituting (2) and (4) for (3),

$$\begin{aligned} \cos \alpha &= \frac{r + R \cos \theta}{\sqrt{r^2 + R^2 - 2rR \cos \theta}} \\ \therefore \alpha &= \cos^{-1} \left( \frac{r + R \cos \theta}{\sqrt{r^2 + R^2 - 2rR \cos \theta}} \right) \end{aligned} \quad (5)$$

Figure 7 graphically shows angle of inclination  $\alpha$  of the rotary shoe. ( $\alpha$  is computed for 12-equal-points of the semicircle.)

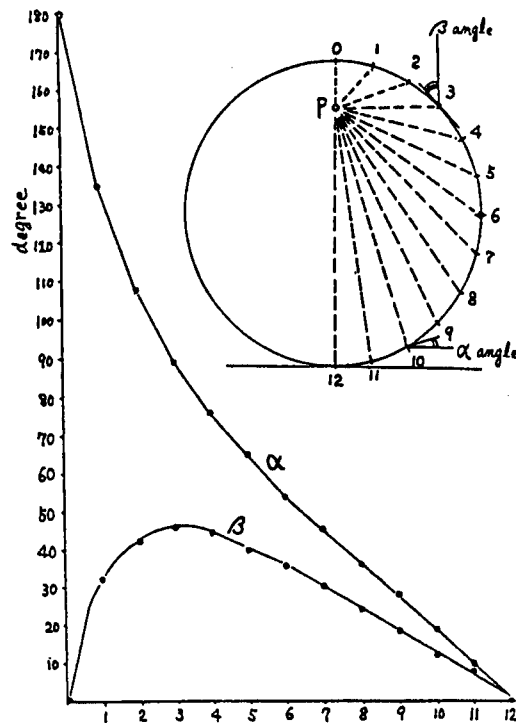
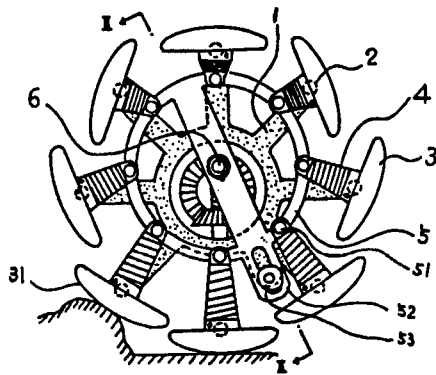


Figure 7. Graph of Angle of Inclination  $\alpha$  and Angle of Sway  $\beta$

Since the rotary shoes are not fixed to the wheel but are designed so as to sway, if angle of sway  $\beta$  of the pivotally attached rotary shoe is computed by Figure 6,

$$\alpha + \beta = 180^\circ - \theta \therefore \beta = 180^\circ - \theta - \alpha \quad (6)$$

Figure 7 shows this angle of sway  $\beta$  by a graph. As is clear from the change of angle of inclination  $\alpha$  and angle of sway  $\beta$  thus shown graphically, the swaying motion of the rotary shoe is fast at the upper positions 0-3, but at the other positions, 4-12, it is slow and progresses steadily.

If theoretical focusing point P is raised and r is brought close to R, the uneven ground travel capacity increases and the maximum of angle  $\beta$  increases to nearly  $90^\circ$ , but, in the degrees affected by the change, the return of the

attitude of the rotary shoe is sudden; thereby presenting structural problems.

Therefore, when designing, the maximum of  $r$  should be two-thirds  $R$  at the most, and preferably, it should not exceed one-half  $R$ .

To improve the traveling capacity even more, it is necessary to use a different mechanism that will be described later.

### 3.4 Action and Effect of Rotary Shoe Mechanism

If the wheel hits a protrusion, rotary shoe 7 receives reaction  $f_1$  from the protrusion, as indicated in Figure 8.

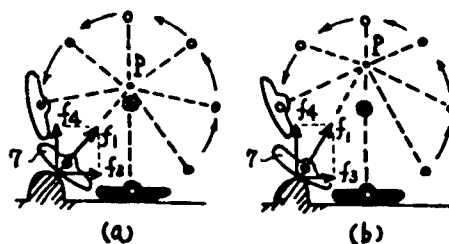


Figure 8. Resolved Into Horizontal Reaction  $f_3$  and Vertical Reaction  $f_4$

If this reaction  $f_1$  is divided into horizontal reaction  $f_3$  and vertical reaction  $f_4$ , the former acts to push back the vehicle body and the latter acts to lift it.

In the case of this mechanism, the direction of reaction  $f_1$  caused when it hits a bump, etc., is not the direction of the axle center, but the theoretical focusing point  $P$  mentioned above. Therefore, the proportion of the horizontal reaction decreases and the proportion of the vertical reaction increases accordingly.

If the vertical reaction increases, the force with which the tread pushes the bump downward increases and, therefore, the frictional force increases, making a slip difficult and facilitating the stride of the mechanism.

Then, as indicated in Figure 9, if a wheel proceeding at speed  $V_0$  hits a bump, it springs upward at speed  $V'$ . Using  $Q_0$  as the point of ground contact, the condition under which the wheel can manage bump height  $h$  is  $\theta > 45^\circ$  provided that angle of incident  $\theta$  composed mainly of the line of  $OQ_0$  is identical to angle of reflection  $\theta'$ . Therefore,

$$h < \frac{R - \sqrt{R^2 - V^2}}{2} R (\approx 0.3R)$$

which is very small. ( $R$ : circling radius)

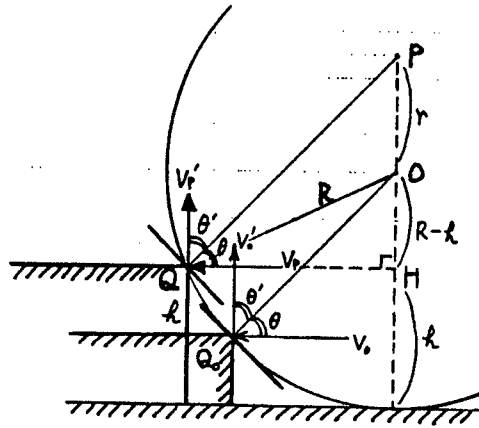


Figure 9. Height h of Pump That Can Be Traversed

However, if theoretical focusing point P is raised by distance r,

$$QH = PH = r + R - h \quad (1)$$

since  $\Delta PHQ$  is an isosceles right triangle.

$$QH^2 + OH^2 = QR^2$$

So, from (1)

$$\begin{aligned} (r + R - h)^2 + (R - h)^2 &= R^2 \\ \left\{ h - \left( R + \frac{r}{2} \right) \right\}^2 &= \frac{2R^2 - r^2}{4} \\ \therefore h &= R + \frac{r}{2} - \frac{\sqrt{2R^2 - r^2}}{2} \end{aligned} \quad (2)$$

If  $r = \frac{1}{2}R$ ,

$$h = \frac{5 - \sqrt{7}}{4} R (\approx 0.6R)$$

Therefore, the height of a bump that can be traversed is doubled.

In the rotary shoe mechanism, the treads of the shoes in front of and behind the lowest grounded shoe are turned downward. Therefore, settlement into soft sandy or muddy ground is proportionally small since theoretical focusing point P is high. The mechanism can thus engage in traveling that is all the more stabilized.

The tread of the lowest rotary shoe can be turned somewhat to the rear by shifting theoretical focusing point P from above to the front by means of the eccentricity adjuster, as shown in Figure 10, and the mechanism can travel soft ground well since its drive and tractive force increase, as happens when a man vigorously kicks the ground.

If it falls into a deep hole, it can easily get out due to the reaction generated from vigorously kicking the sand or soil with its rotary shoes.

In Figure 10(a),  $N$ , the force with which the tread of the rotary shoe pushes the ground, is directed precisely downward. Therefore, if the friction is small, the mechanism easily slips but, as in (b), slipping can be prevented by turning the tread of the rotary shoe somewhat to the rear and thereby increasing ground bite-in friction on snow-covered or sandy ground.

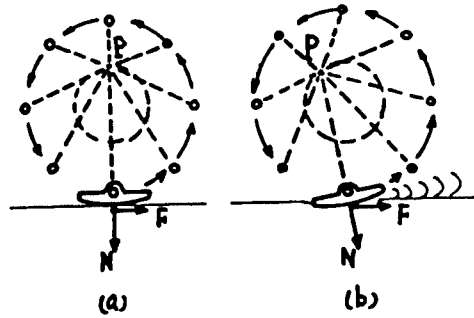


Figure 10. Increase of Drive and Tractive Force

Therefore, this mechanism can, of course, be used also as a locomotion vehicle in snowy districts or in deserts.

Something similar in structure and function to the walking shoe or the wheel tire is desirable as the rotary shoe material. It must be structurally soft and able to absorb shocks from the road surface.

#### 4. Conclusion and Future Image

The locomotion robot rotary shoe mechanism is a universal "foot" that enable the robot not only to travel efficiently on a paved road, but also to safely travel uneven ground, snow-covered ground and deserts.

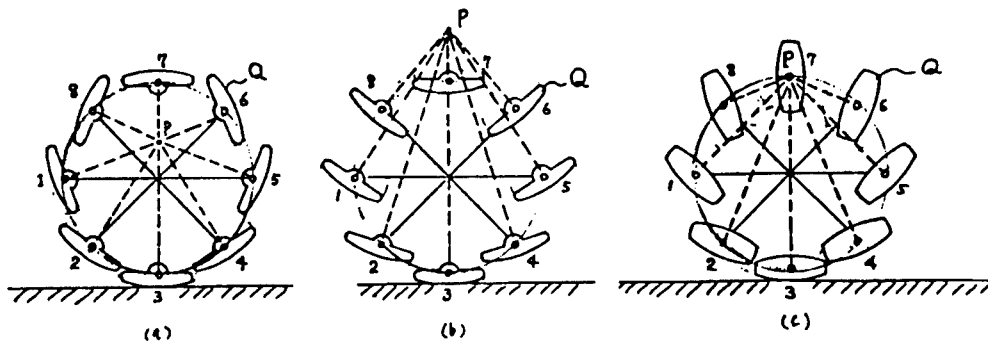


Figure 11. Three Forms of Rotary Shoe Mechanisms

Since its traveling capacity can be adjusted better than that of the mere wheel and it can freely move back and forth between level ground and off-road ground, it is suitable for robots used for rescue work, emergency disaster countermeasures, forest patrols, fruit picking, and transportation (Figure 12).

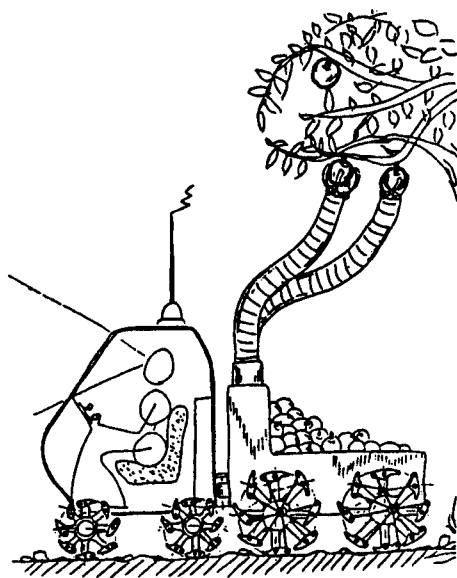


Figure 12. Fruit Picking and Transporting Robot

Theoretically, three types of rotary shoe mechanisms have been designed after the manner of human walk, imitating its high traveling capacity and noting the attitude assumed by man's shoes at their point of contact with the ground, as well as before and after.

These three types are shown in Figure 11. The (a) form is the one revolution/one rotation type, the (b) form is the one revolution swaying type, and the (c) form is the one revolution/half rotation type.

The (a) form rotary shoe mechanism has been described in detail in this paper. In the (b) form rotary shoe mechanism, eight rotary shoes Q revolve, but do not rotate. They sway, instead, and the axial attitude of the walking shoes are controlled so as to face theoretical focusing point P outside revolving circle O. It is characteristic for its striding capacity to be higher than that of the (a) type, since focusing point P is outside revolving circle O.

The (c) form rotary shoe mechanism is functionally between the (a) and (b) type. its rotary shoes Q characteristically make a half rotation for one revolution and do not sway. It clearly differs from the former two types in that its rotary shoes Q have a top/bottom symmetrical shape, permitting the use of both the top surface and the bottom surface.

What is common to all these forms of rotary shoe mechanisms is that they are far superior to the conventional wheel in traveling capacity in that they provide the shoes with a revolving motion, thereby controlling the attitude of the mechanism.

Here, the author has described all three forms, and the (a) form in particular.

---

### References

1. Patent application 1987-00326: Rotary Shoe Mechanism.
2. Patent application 1987-00403: Rotary Shoe Mechanism.

## Development of Long-Arm Manipulators

43064062 Tokyo 4TH INTELLIGENT ROBOTS SYMPOSIUM PAPERS in Japanese  
13/14 Jun 88 No 123 pp 187-192

[Article by Yoshio Nakajima, Kazuo Homma, Minoru Hiroshima, and Noriaki Okamoto, Hitachi Machine Research Institute; and Hiroshi Inemitsu, Hitachi Construction Machine]

### [Text] 1. Introduction

In the civil engineering and construction industries, labor reduction, safety, and high efficiency in the construction, maintenance, and inspection work are urgently required and various machines<sup>1</sup> have been developed for this purpose. As for cranes, a mobile work machine with a "long arm manipulator,"<sup>2</sup> able to handle an assortment of construction work including the arrangement of reinforcing bars and the delivery of materials into buildings under construction, is desired.

If rigid design, which is the design concept of conventional industrial robots, is applied to this kind of long-arm manipulator, its overall weight would be so large that it would be impractical as a mobile work machine. If, on the other hand, reduced weight design with priority on strength is practiced, an arm of flexible structure will result and the deflection of the arm and the deterioration of positioning accuracy due to vibration will become a problem. So, to solve this problem vibration control is necessary. Also, resolution speed control is necessary to enable a crane to operate so that the tip of its arm will describe a straight locus, as when inserting a material into a building.

We have, therefore, developed a lightweight, highly rigid structure designing technique and a technique to control long, flexible arms, and have realized a highly operable long-arm manipulator with light weight, low vibration, and resolution speed control.

This report presents the results of a test on vibration control and resolution speed control using an experimental machine, our design of a lightweight arm incorporating the vibration control effect and the mobile work machine we have developed.

## 2. Vibration Control System

### 2.1 Outline of Experimental Equipment

Figure 1 outlines the experimental equipment system used. This experimental machine is composed of arm Nos 1, 2, and 3 and hydraulic cylinders to drive them. The total length of the arms is about 16 m. The hydraulic circuit uses a servo valve as a hydraulic control valve and both ports of the hydraulic cylinders are provided with pilot check valves.

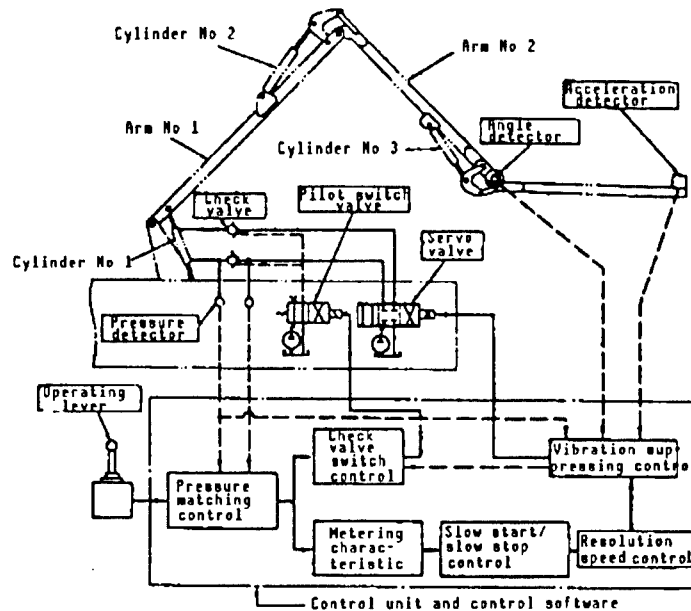


Figure 1. Conceptual Diagram of Total Control System

The control unit is input with spread command input signals from the operating lever, hydraulic circuit pressure signals, relative angle signals of the arms, and arm tip acceleration signals. The control unit processes these signals and outputs check valve switching signals and servo valve current signals. Strain gauges are attached to the vital parts of each arm in order to measure stress.

### 2.2 Vibration Suppressing Formula

The following two types of control are necessary when composing a long-arm manipulator with minimal vibration: 1) Pressure matching control, and slow start and stop control: these controls are designed to prevent vibration as much as possible when effecting the start or stop of each arm; and 2) vibration suppressing control: this control quickly attenuates vibration if it occurs for some reason, such as due to a disturbance.

#### 2.2.1 Pressure Matching Control

When a command to drive the hydraulic cylinders is received from the operating lever, the check valve is opened and a signal is simultaneously

issued to the servo valve. If, in that case, there is a great pressure difference before and after the check valve, a switch shock due to the flow of oil from the higher pressure side to the lower pressure side develops, and the arms vibrate.

Therefore, the check valve is opened after detecting rod-side pressure  $P_R$  and head-side pressure  $P_H$  of the cylinder with the check valve in the closed state, controlling pressure at both ports of the servo valve and thereby minimizing the cylinder thrust difference due to pressure differences before and after the check valve. The time wasted by employing switch valve operation is considered when opening or closing the check valve.

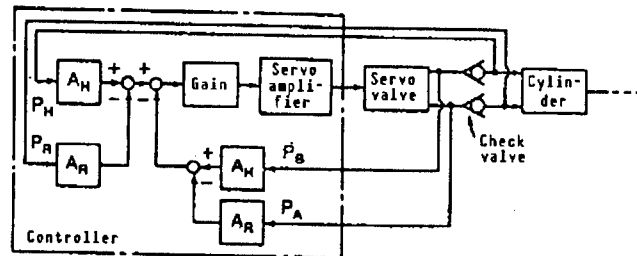


Figure 2. Block Diagram of Pressure Matching Control

### 2.2.2 Slow Start/Slow Stop Control

If the operating lever is used recklessly and if, in that state, the servo valve current is increased or decreased for the operating lever action, significant vibration is generated in the arm as the hydraulic cylinder accelerates or decelerates suddenly. Even in such cases, smooth shockless acceleration or deceleration can be achieved by limiting the maximum acceleration and deceleration caused during actuator acceleration and deceleration, the formula for this process is shown below.

The maximum value  $\Delta i_{\max}$  of the per-unit-time current increase is set for each servo valve corresponding to the actuator and, if the operating lever is set into operation suddenly, the operation is conducted at the maximum value  $\Delta i_{\max}$  while, if the lever operation is slow, the current value of the servo valve is increased or decreased according to that lever operating speed.

### 2.2.3 Vibration Suppressing Control

Attenuation characteristics can be improved by inserting a diaphragm or something similar into the hydraulic circuit or by feeding back arm tip acceleration. However, the former method is not recommended since it results in a decrease in circuit efficiency due to the change in hydraulic circuits, while the latter method makes control difficult because the motion interference between arms requires compensation.

Meanwhile, a pressure variation in the hydraulic cylinder is caused by the reaction to the external force exerted against the cylinder by the arm vibration. This varied pressure exhibits much the same behavior as does acceleration.

Therefore, attenuation characteristics are improved by computing the varied external force exerted against the cylinder from the cylinder pressure and exercising control to reduce this external force. Figure 3 is the block diagram of this process. In it, a by-pass filter is used to extract external force only.

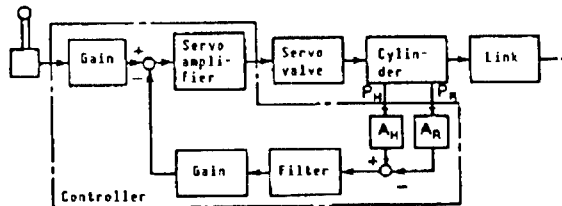


Figure 3. Block Diagram of Vibration Suppression Control

The study of vibration suppression using experimental equipment was limited to in-plane vibration because the equipment lacked a revolving mechanism. Out-of-plane vibration was tested using a mobile work machine, which will be described in Chapter 5.

### 2.3 Test Results

Figure 4 shows the slow start/slow stop characteristic. It was obtained by measuring the peak value of acceleration at the tip of the third arm when the three arms were stretched out straight and the first arm was operating while the values of  $\alpha_{max}$  were changing, limiting the maximum acceleration and deceleration.

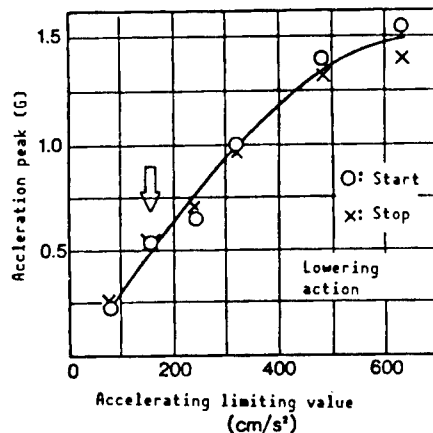


Figure 4. Results of Test of Slow Start/Slow Stop Control

One can see from Figure 4 that the acceleration peak naturally diminishes if the limiting value  $\alpha_{max}$  is reduced. However, if limiting value  $\alpha_{max}$  is too small, the start and stop become slow and operability deteriorates. Therefore, from the test results we decided on about 160 cm/s<sup>2</sup> (indicated with an arrow in the drawing), a value that did not impair operability. When this value was used, the arm tip lowered for about 38 cm and stopped about 0.7 seconds after the three arms had been stretched out straight and the lever had been suddenly returned during the lowering action at the maximum speed. Yet, no particular problems developed in positioning or other aspects.

Figures 5 and 6 are examples of test results without vibration suppression and with vibration suppression. The drawings show the behaviors of different components upon starting and stopping when the three arms were stretched out straight and lowered by driving the first cylinder. One can see that, without control, large acceleration peaks develop at both the start and stop and vibration attenuates very poorly but, with control, acceleration peaks are small and vibration attenuates rapidly. By suppressing vibration, we were able to raise the attenuation coefficient ratio from 0.06 to 0.31.

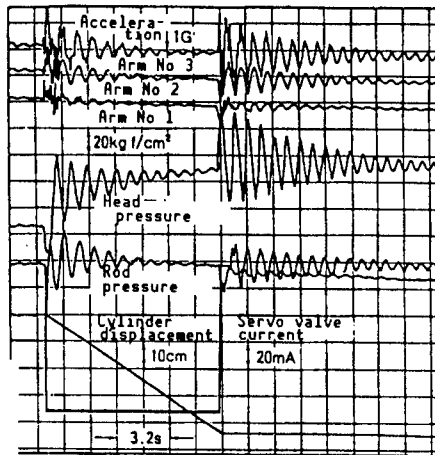


Figure 5. Test Results Without Vibration Suppression Control

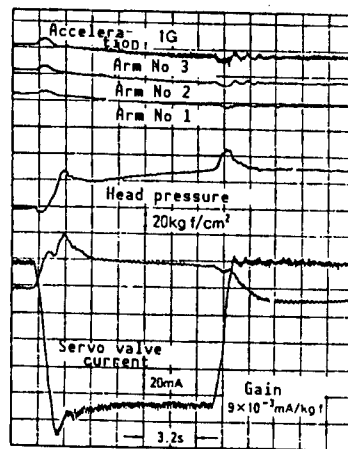


Figure 6. Test Results With Vibration Suppression Control

Figure 7 consolidates the distribution of values of maximum stress when the lowering action occurs. One can see from the drawing that the maximum value of vibration stress at both the start and stop can be reduced to about one-third by suppressing vibration.

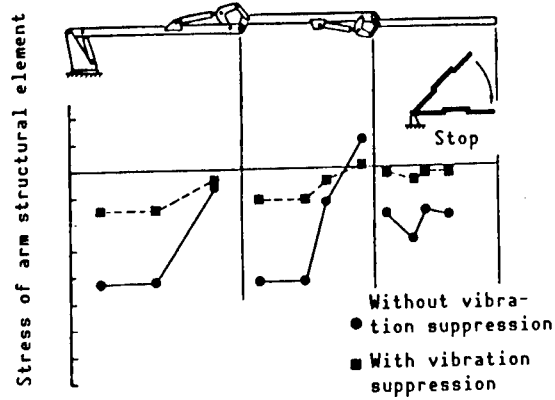


Figure 7. Vibration Stress Distribution I

### 3. Designing Lightweight Arm

#### 3.1 Vibration Response Analysis

Figure 8 shows the results of measuring the stress caused in the different components of the arms by dead weight and the maximum stress generated during arm lowering and stopping. In the first arm, the stress due to dead weight is greater than that due to vibration, but the reverse is the case with the third arm. This indicates that the ratio between stress due to vibration and stress due to dead weight differs from place to place. It is, therefore, impossible to achieve optimum design by estimating stress due to vibration, in which the analytical results of stress due to dead weight are multiplied by a certain coefficient. To make the appropriate structural design, particularly for weight reduction aimed at achieving minimal weight, as will be described later, it is necessary to correctly evaluate stress due to vibration. Therefore, we researched a method of vibration response analysis.

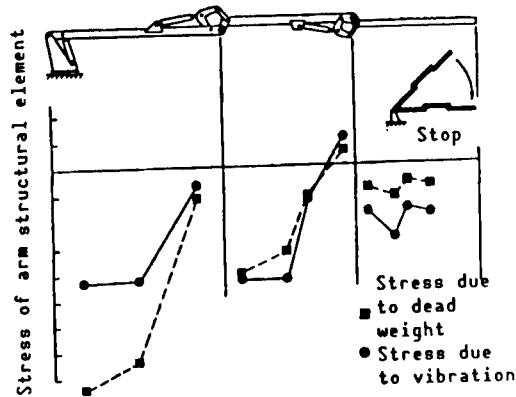


Figure 8. Vibration Stress Distribution II

Figure 9 shows a finite element model of the test equipment. The arm, hydraulic cylinder and link components were modeled by needle elements because they were too long for their cross sectional dimensions. In the model, the cross sectional areas of the arms have been changed, making axial rigidity equivalent, since the hydraulic cylinder has a spring characteristic in the axial direction due to the oil compressibility.

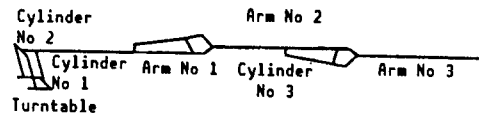


Figure 9. FEM Model

Figure 10 shows an example of the results of vibration stress analysis and test results during arm lowering and stopping. The maximum value in the analytical results is slightly smaller than that in the test results, but the transient response waveform of stress agrees well with the test results.

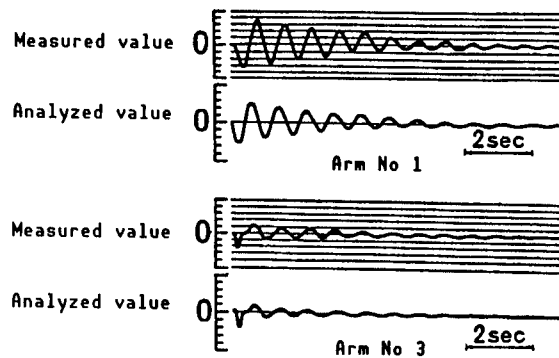


Figure 10. Analysis and Test Results

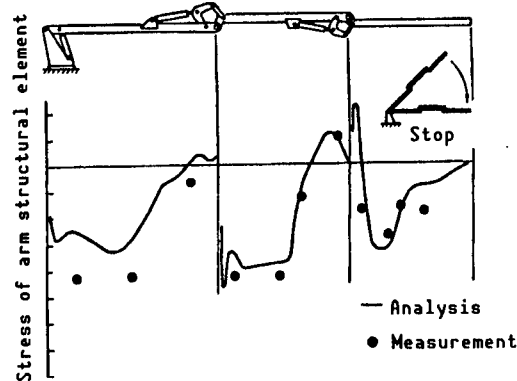


Figure 11. Vibration Stress Distribution III

Figure 11 shows the distribution of maximum stress values in the direction of the arm axis. The analytical results are smaller in the first arm, but agree well in the others. This is presumably because the first arm had many reinforcing plates of various widths welded to it, and its shape could not be modeled accurately.

### 3.2 Cross-Sectional Design of Arms

We designed the cross sectional shape of a box-structured arm according to the standards indicated in Table 1. We set design criteria by dividing the loading status into normal operation and abnormal periods.

Table 1. Design Criteria for Arm Cross-Sectional Shape

| Status                | Normal operation  |  |   | Abnormal periods  |                                       |                 |
|-----------------------|---|--|---|---|---------------------------------------|-----------------|
| Type of load          | In-plane static load  | In-plane dynamic load (time $\approx 1/3$ )                | Out-of-plane dynamic load (time $\approx 1/3$ ) | In-plane static load; In-plane dynamic load   | Out-of-plane dynamic load             | Earthquake load |
| Action                | —   | Lowering and stopping (with control)                       | Revolving and stopping (with control)           | Lowering and stopping (with control)  | Revolving and stopping (with control) | —               |
| Details of evaluation | Static strength<br>Elastic buckling<br>Fatigue strength   | Fatigue strength   |   | Final strength  |                                       |                 |
| Evaluating criteria   | Static strength $\sigma_s/k3$<br>Elastic buckling $\sigma_b/k1$<br>Fatigue strength $\sigma_f/k2$ | $\sigma_a$ : Allowable stress at repeat No $1 \times 10^6$ |   | $\left(\frac{M}{M_{s,}}\right)^2 + \left(\frac{T}{T_{s,}}\right)^2 \leq \left(\frac{1}{K4}\right)^2$<br><br>$M_{s,}$ : Maximum bending moment<br>$T_{s,}$ : Maximum twisting moment |                                       |                 |
|                       | $\sigma_s$ : Yield stress   | Elastic buckling stress                                    |   | Allowable stress taking frequency distribution into consideration   |                                       |                 |

Load during normal operation is that frequently exerted and comprises static load by dead weight and dynamic load generated upon starting and stopping. We used one-third of the figure without vibration suppression as our dynamic load value when taking the vibration suppression effect into consideration.

Load in abnormal periods refers to that generated only scores of times throughout the machine's life and comprises the dynamic load generated when the function to suppress vibration fails due to the breakdown of the controller, earthquake load, and others. Our evaluation of this load has been limited to final strength because we intended only to prevent the destruction of the machine.

We searched for a cross sectional shape that would minimize the box weight based on our stress analysis results for various load conditions, and sought to minimize the weight by adding the following restrictive conditions:

- (1) Plate thickness must be selected from standard sizes
- (2) Plate thickness must be uniform within the arm
- (3) Box width must be uniform within the arm

By the above cross sectional designing method, we reduced the weight of the original design by about 20 percent, based on past experiences.

#### 4. Development of Mobile Work Machine

##### 4.1 Outline of Work Machine

Figure 12 and Photo 1 [not reproduced] show our mobile work machine with reduced-weight arms. This work machine has arms with four joints and can be used for revolving work and underground work, and its range of operation is, indeed, large. In addition, its high performance makes it possible to use a truck as the traveling body.

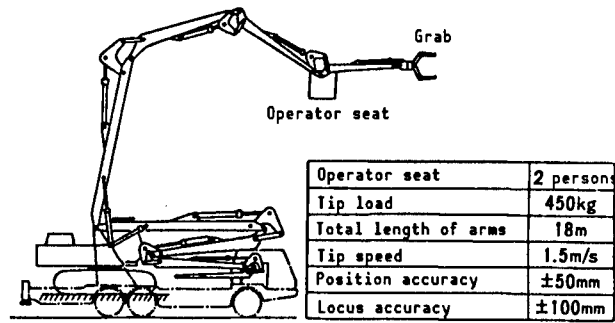


Figure 12. Mobile Work Machine

#### 4.2 Link Mechanism

Each arm is driven via a link mechanism. Depending on the link mechanism selected, such problems as a long hydraulic cylinder due to the wide operational range and abnormal force exerted against the arm can arise. Therefore, we studied the three types of link mechanisms in Figure 13 from various aspects. Figure 14 is an example of this, comparing displacements according to the dead weight of the arms. It indicates that the displacement in Type A is more than twice that in Type C. We also adopted Type B, a crescent ink mechanism, for such reasons as range of operation.

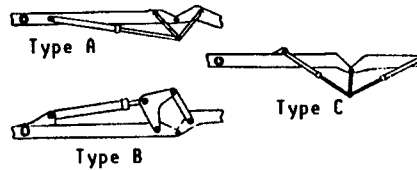


Figure 13. Link Mechanism

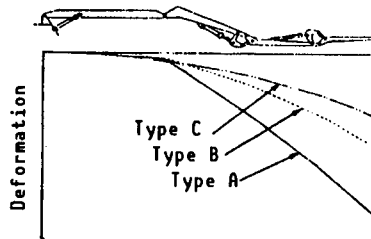


Figure 14. Link Shape and Deformation

### 5. Vibration Suppression for Revolving System

#### 5.1 Vibration Suppression Formula

A vibration suppression formula based on Figure 4 was effective for motions in the arm plane but this control formula cannot, as it is, be applied to the revolving system. The reason is as follows:

A revolver has great inertia, and the circuit pressure increases substantially when the revolver accelerates or decelerates. Therefore, as

indicated in Figure 15, the hydraulic circuit of the revolving system is provided with a crossover relief valve and the maximum value of acceleration is limited by the pressure set for this relief. Consequently, if the discharge from the servo valve comes out of the relief valve, the change of servo valve discharge by vibration suppression control merely results in changing the discharge form the relief valve and does not attenuate vibration.

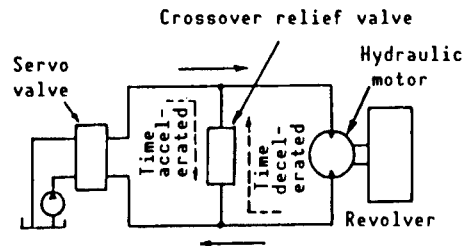


Figure 15. Hydraulic Circuit of Revolving System

Therefore, if the circuit pressure rises to the vicinity of the relief pressure, it is necessary to control the pressure cut-off,<sup>3</sup> reducing the discharge from the servo valve, regardless of whether the lever operation value is large or small.

Figure 16 is the block diagram of vibration suppression control for the revolving system, which was composed after taking the above into consideration. This formula comprises the pressure cut-off control and vibration suppression control shown in Figure 4.

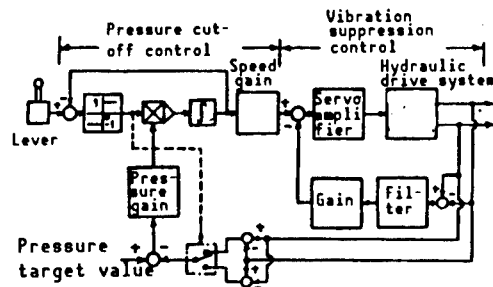


Figure 16. Vibration Suppression Control for Revolving System

## 5.2 Test Results

Figures 17 and 18 are examples of test results for the case without vibration suppression and that with vibration suppression. Both drawings show how the different components behaved when the four arms were stretched out straight and revolved. Without control, great acceleration peaks developed at both the start and stop, vibration attenuated very poorly and the revolving speed fluctuated pulsating. However, with control, the acceleration peaks were small, vibration attenuated quickly and the revolving speed fluctuated smoothly. By suppressing vibration, we were able to reduce the arm tip acceleration peak and vibration stress to from one-third to one-fourth that when control was not exerted.

## 6. Resolution Speed Analysis

### 6.1 Control Formula

Resolution speed control consists of controlling the speed of cylinders Nos 1-3 so that the lever operation values  $V_x$ ,  $V_y$ , and  $\phi$  may correspond to, respectively, the orthogonal components of the motion speed of the tip of arm No 3 and the attitude angle speed of arm No 3.

Figure 19 is the functional block diagram of resolution speed control. Both feedback control and feed forward control are used in the servocontrol section.

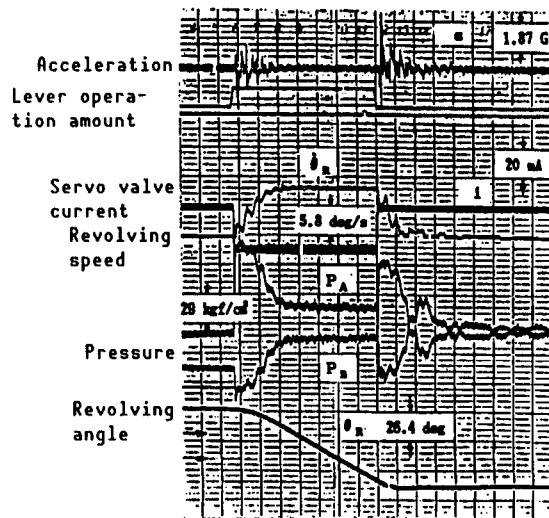


Figure 17. Results on Test Without Vibration Suppression

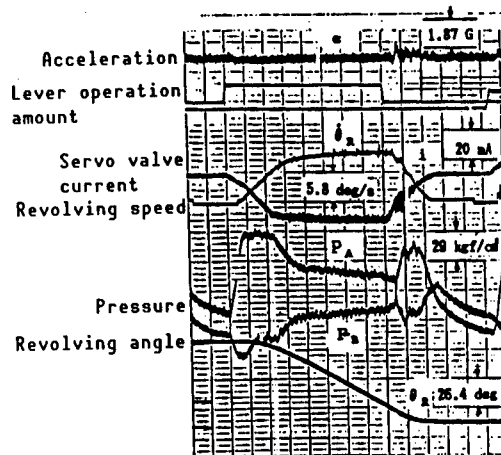


Figure 18. Results of Test With Vibration Suppression

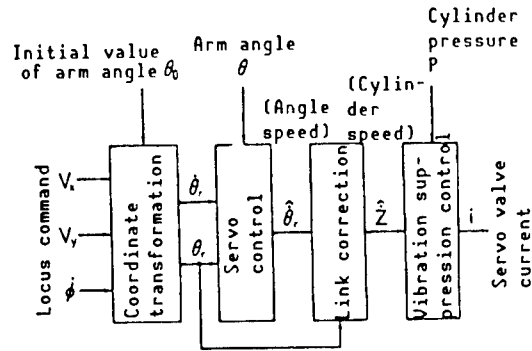


Figure 19. Functional Block Diagram of Resolution Speed Control

## 6.2 Test Results

Figure 20 is an example of test results when only basic control and feed forward control are exerted. In the test, the three arms were stretched out almost straight and, from the horizontal state, the tip of arm No 3 was reciprocated horizontally. In data reduction, Y-direction control error  $\Delta Y$  was computed from control errors  $\Delta\theta_1$  and  $\Delta\theta_2$ .

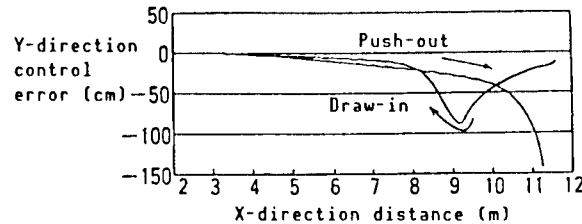


Figure 20. Test Results of Resolution Speed Control I (Basic control + feed forward)

As a result, the tip of arm No 2 lowered once at a point about 2 m from the start of control and, on the return trip, suddenly lowered at a point about 10 m away. The reason for this is that the value of the discharge command to the servo valve exceeded the allowable value and the discharge was saturated. Therefore, we introduced servo valve discharge saturation prevention control, i.e., if the servo valve discharge computed from the input speed command value were to exceed the allowable value, the input value would be recomputed to prevent the saturation of all servo valve discharges, while maintaining the resolution speed ratio.

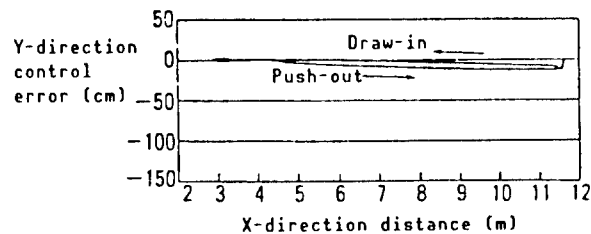


Figure 21. Test Results of Resolution Speed Control II (With vibration suppression and discharge saturation prevention)

Figure 21 shows an example of test results with this control in addition to vibration suppression control. As a result, track accuracy of 15 cm(p-p) for a stroke of about 8 m at an average locomotion speed of about 40 cm/s was achieved.

## 7. Conclusion

The conclusion of this report is summarized as follows:

- (1) We applied an arm in-plane vibration suppression system, composed of pressure matching control, slow start/slow stop and vibration suppression control, to our experimental machine, and confirmed that the system had a satisfactory vibration suppression effect for all degrees of freedom.
- (2) Weight reduction by robot 20 percent became possible by minimizing the arm weight while taking into consideration the effect of vibration suppression.
- (3) We applied an arm resolution speed control system, composed of a basic computation section, vibration suppression control, and servo valve discharge saturation prevention control, to the experimental machine and confirmed its effects.
- (4) Based on the above achievements, we developed a mobile work machine with a "long-arm manipulator," which has large working scope and is capable of handling various types of construction work.
- (5) We applied an arm out-of-plane vibration suppression system, offering pressure matching control, slow start/slow stop, pressure cut-off control, and vibration suppression control, to the machine and confirmed that the system could suppress vibrations satisfactorily.

## References

1. Mori, et al., "Examples of Robot Application by This Company," ROBOT, Vol 38, November 1983, pp 62-68.
2. Nakajima, et al., "Control of Long-Arm Manipulator," 5th Robotic Society Scientific Lecture Meeting, November 1987.
3. Homma and Nakajima, "Control of Static Hydraulic Drive System by Microcomputer," 1982 Autumn Lecture Meeting (November 1982)

## Active Positioning Systems Using Laser Beams, Corner Cube Reflectors

43064062 Tokyo 4TH INTELLIGENT ROBOTS SYMPOSIUM PAPERS in Japanese  
13/14 Jun 88 No 210 pp 193-198

[Article by Toshihiro Tsumura, Masabumi Hashimoto, and Naobumi Fujiwara, University of Osaka Prefecture: "Laser and Corner Cube Active Positioning Method for Locomotion Robot (Composition of Laser Acquisition/Tracking Control System)"]

### [Text] 1. Introduction

In guiding a mobile object (locomotion robot), it is basically important to determine the robot's position accurately. Accurate position measurement can be realized by finding a landmark from the traveling environment in some manner and observing its direction and distance in relation to the mobile object.

In the past, the positioning formula involving setting in the environment, as a landmark, a facility to emit information; on the mobile object, i.e., light, ultrasonic wave or electric wave, and receiving the information emitted from it, has often been proposed.<sup>1-3</sup> This formula permits accurate position measurement, but is expensive to install and maintain.

The formula involving the use of existing objects in the environment as landmarks for position measurement has recently begun to be actively studied. This includes, for instance, the active method in which a position is obtained by emitting ultrasonic waves or laser beams from a mobile object and measuring the distance to an object around the mobile object and its direction,<sup>4,5</sup> and the passive method in which a position is determined by extracting a landmark from the scene obtained by a TV camera mounted on the mobile object.<sup>6,7</sup> These are ideal methods for realizing autonomous guidance, but it seems to be rather difficult to recognize landmarks accurately within the actual environments.

Therefore, we are studying an active positioning method using laser beams and corner cubes in order to measure accurate positions by recognizing landmarks accurately, even in the actual environment, while minimizing the set up and maintenance cost of environmental landmarks.<sup>8-10</sup>

As indicated in Figure 1, this consists of setting up corner cubes at two fixed points in the environment, emitting laser beams from two laser scanners mounted on the mobile object and determining a position by triangulation by observing the laser beam emission direction, i.e., the corner cube directions when the laser beams irradiate the corner cubes.

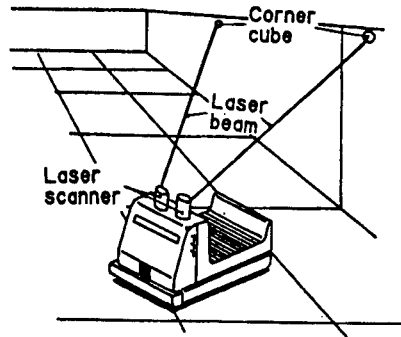


Figure 1. Configuration of Active Positioning System by Using Laser Beams and Corner Cube Reflectors

In this formula, corner cubes can be recognized as a simple method because, when a laser beam hits a corner cube, the reflected light is returned to the side of the laser scanner. Also, laser beams, with their acute directivity, characteristically enable the directions of the corner cubes to be observed with high accuracy.

To be able to measure accurate positions by this formula, even while the mobile object is traveling, it is necessary to acquire and track a corner cube and ensure that the laser beam always points to the center of the corner cube.

In this report, therefore, we propose methods to control acquisition/tracking and testing, using an experimental system manufactured for each method.

## 2. Outline of Laser Acquisition/Tracking Control

This acquisition/tracking control is outlined below, using a laser scanner with the structure shown in Figure 2.

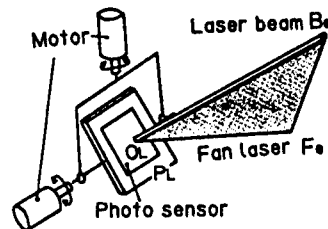


Figure 2. Configuration of Vehicle-Borne Laser Scanner

"Acquisition control" and "tracking control" are defined as follows:

Acquisition control:

Control in which a corner cube is found and laser beam  $B_0$  is directed in the general direction of the corner cube if  $B_0$ , with its acute directivity emitted from point  $O_L$  on plane  $P_L$  of the laser scanner, deviates from the corner cube.

Tracking control:

Control in which laser beam  $B_0$  is accurately directed to the center of the corner cube when  $B_0$  irradiates the corner cube.

Laser beam  $B_0$  is so narrow that prediction technology is necessary to control its acquisition. Furthermore, its acquisition control is quite lengthy if its prediction is inaccurate.

Therefore, when controlling acquisition, fan-shaped laser beam  $F_0$  is emitted along  $B_0$  from point  $O_L$ , as shown in Figure 2, and is caused to revolve (scan) around  $B_0$ , as shown in Figure 3(a). If  $F_0$  hits a corner cube while scanning, reflected light returns to the photosensor on  $P_L$  and, therefore, the corner cube is recognized by the light reception signal. The direction of the corner cube is obtained by observing the angle of rotation  $\phi$  of  $F_0$ . In addition,  $P_L$  is driven biaxially, based on the angle of rotation information. If this procedure is taken every time  $F_0$ , while scanning, irradiates the corner cube,  $B_0$  can be faced toward the corner cube.

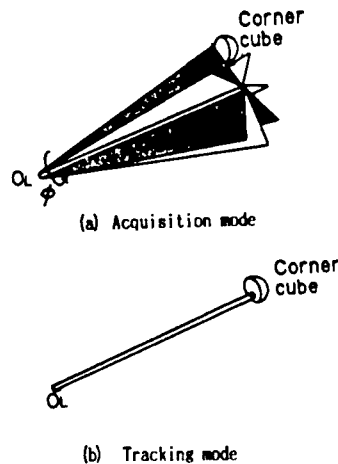


Figure 3. Control Modes in Laser Scanner

The control mode is switched from "acquisition" to "tracking" as laser beam  $B_0$  irradiates the corner cube (Figure 3(b)). A corner cube can "reflect incident light from a place with point symmetry for the center of the corner cube." Taking advantage of this property, the irradiation point of  $B_0$  of the corner cube is found by measuring the light reception point of the reflected laser beam returned onto  $P_L$ .  $B_0$  can be directed toward the center of the corner cube by controlling the direction of  $P_L$  in accordance with this information. When tracking,  $P_L$  direction control is made at prescribed intervals so that reflected light can be observed continuously.

Laser beam  $B_0$  can be directed toward the center of the corner cube by repeating the above acquisition/tracking control.

### 3. Acquisition Control Method

#### 3.1 Manufacture of Acquisition System Prototype

Figure 4 shows the composition of the acquisition laser scanner prototype manufactured, and Figure 5 is the block diagram of its drive system and observation system.

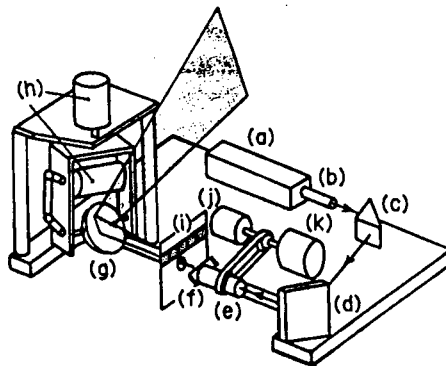


Figure 4. Configuration of Our Experimental Laser Scanner for Acquisition Control

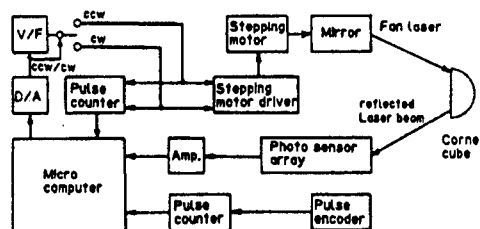


Figure 5. Hardware Configuration of Experimental System

The 5 mW He-Ne laser beam emitted from laser generator (a) is directed toward cylindrical lens (f) fixed at the tip of a hollow shaft via collimator lens (b), rectangular prism (c), total reflector (d), and hollow shaft (e), and becomes a fan laser beam with an opening angle of 2.8 degrees. Then, it is emitted to the outside via mirror (g) mounted on a biaxial gimbal. The gimbal is driven via a harmonic gear by two stepping motors(h). For this reason, the fan laser beam can be turned to any direction. Also, the fan laser beam can be scanned if the hollow shaft with a cylindrical lens is rotated by AC motor (j) via a timing belt and a pulley.

When the fan laser beam being scanned irradiates the corner cube (effective diameter: 6 cm; glass, the reflected light is returned in the direction from which it was emitted and received via mirror (g) by photo sensor train (i), 1 cm x 10 cm, attached to the plate shown in Figure 4. This light reception

signal is transmitted to a microcomputer (CPU:8086) as an interruption signal. Then, the scanning angle of rotation of the fan laser beam obtained by pulse encoder (k) at that time and the angle of rotation of the mirror obtained from the operation pulse to the stepping motors are incorporated into the microcomputer.

In the microcomputer, the amount of operation of the motors is determined from this information, and the motors are driven via D/A and V/F converters.

The scanning angle of rotation of the fan laser beam per pulse encoder pulse is 0.115 degrees, while the angle of rotation of the mirror per stepping motor pulse is  $1.278 \times 10^{-3}$  degrees.

### 3.2 Design of Acquisition Control System

Figure 6 shows the structure of a mirror drive equivalent to that of the prototype system.

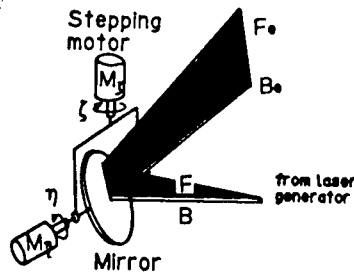


Figure 6. Illustration of Laser Scanner Equivalent to Our System

If a tracking system is added to a prototype acquisition system, as indicated in this diagram, tracking laser beam  $B$  from the laser generator falls into the center of the mirror along acquisition fan laser beam  $F$  from a direction orthogonal to the axis of rotation of motor  $M_3$  and is reflected there, and is then emitted to the outside as laser beam  $B_0$  together with fan laser beam  $F_0$ .

In acquisition control, therefore, one has only to drive the mirror, using as the target value the direction of the mirror when  $B_0$  irradiates the center of the corner cube.

For the system in Figure 6, a three-dimensional coordinate system  $(O_M;xyz)$ , with  $O_M$ , the center of the mirror, as the origin, the axis formed by laser beam  $B$  as the  $x$ -axis, and the axis of rotation of motor  $M_3$  as the  $z$ -axis, is defined in Figure 7. Now, using  $\zeta$  and  $\eta$  as slope line directions of the mirror in  $(O_M;xyz)$  specified by the drive of  $M_3$  and  $M_\eta$  in the motor when emitting laser beam  $B_0$ , and using  $\zeta^*$  and  $\eta^*$  as the same directions when  $B_0$  irradiates  $O_c$ , the center of the corner cube,  $\epsilon_\zeta$  and  $\epsilon_\eta$ , the directional deviations of the mirror, can be defined by the following equation:

$$\begin{aligned} \epsilon_\zeta &= \zeta^* - \zeta \\ \epsilon_\eta &= \eta^* - \eta \end{aligned} \quad (1)$$

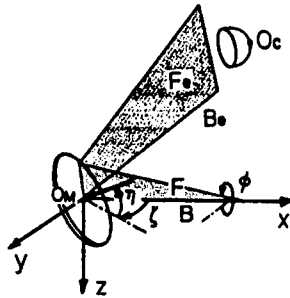


Figure 7. Coordinate System of Laser Scanner

Now, using  $\phi$  as the scanning angle of rotation from the xy plane of F when  $F_e$  irradiates  $O_c$ , the relationship between  $\phi$  and  $\epsilon_3$  and  $\epsilon_\eta$  can be obtained geometrically by the following equation:

$$\begin{bmatrix} \epsilon_3 \\ \epsilon_\eta \end{bmatrix} = \frac{\lambda}{2\rho} \begin{bmatrix} \sec^2 \eta & 0 \\ -\tan \zeta \tan \eta & -\sec \zeta \end{bmatrix} \begin{bmatrix} \cos \phi \\ \sin \phi \end{bmatrix} \quad (2)$$

Here,  $\rho$  is the distance from  $O_M$  to center  $O_c$ .

However,  $\lambda$  in the above equation is an indefinite positive number, and  $\epsilon_3$  and  $\epsilon_\eta$  cannot be determined universally. therefore, a system to drive the mirror in the direction in which  $\epsilon_3$  and  $\epsilon_\eta$  become zero has been constructed as an acquisition control system.

Now, the relationship between V/F converter input voltages  $u_3$  and  $u_\eta$  and mirror directions 3 and  $\eta$  is an integral system, as shown in the following equation:

$$\begin{aligned} \dot{\zeta}(t) &= 0.0198 u_3(t) \\ \dot{\eta}(t) &= 0.0244 u_\eta(t) \end{aligned} \quad (3)$$

Therefore, if control inputs  $u_3(t)$  and  $u_\eta(t)$  are

$$\begin{aligned} u_3(t) &= K \sec^2 \eta \cos \phi \\ u_\eta(t) &= -0.811 K (\tan \zeta \tan \eta \cos \phi \\ &\quad + \sec \zeta \sin \phi) \end{aligned} \quad (4)$$

K: feedback gain

it is possible to accomplish acquisition control, bringing laser beam  $B_e$  close to the corner cube.

### 3.3 Acquisition Test

The effectiveness of the above-mentioned acquisition control is shown by the test below:

In  $(O_M;xyz)$  of the laser scanner, corner cubes are set at 3 m apart in the direction of 43.4 degrees in the xy plane and acquisition control is made,

using about 0.7 and 0.6 degrees as, respectively,  $\epsilon_z$  and  $\epsilon_\eta$ , the initial deviations of the laser scanner in the direction of the mirror.

Figure 8 shows the state of mirror direction control for about 20 seconds after the start of acquisition in the case of corner cube acquisition, using feedback gain  $K = 0.5$  and fan laser beam scanning frequency  $f = 3$  Hz. One can see the effectiveness of the proposed method of acquisition control although, in the test, the mirror vibrated as it followed its target value (see diagram) because no tracking control system was added.

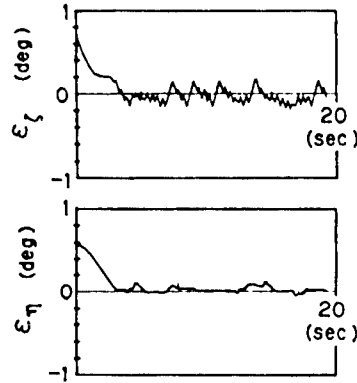


Figure 8. Experimental Results of Acquisition Control

#### 4. Method of Tracking Control

##### 4.1 Manufacturing Tracking System Prototype

Figure 9 shows the configuration of the tracking laser scanner. The drive system of mirror (f) in this laser scanner is similar to that for the acquisition laser scanner shown in Figure 4.

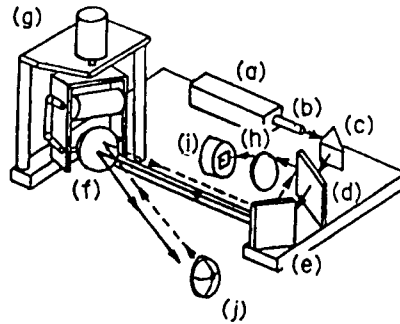


Figure 9. Configuration of Experimental Laser Scanner for Tracking Control

The 1 mW He-Ne laser beam emitted from laser generator (a) is directed toward mirror (f) mounted on the gimbals via collimator (b), rectangular prism (c), half-mirror (d), and total reflector (e), is reflected there, and is then emitted to the outside.

When the laser beam is irradiating corner cube (j), reflected light is led via mirror (f), total reflector (e), and half-mirror (d), converged by lens

(h) and detected by two-dimensional optical position sensor (i). Light reception position information obtained by the optical position sensor and angle information from the mirror are incorporated into the microcomputer at prescribed intervals. The operation of the stepping motors is determined from this information, and the mirror is driven via D/A and V/F converters.

The resolution in light reception point measurement by the optical position sensor is  $2.4 \times 10^{-4}$  cm.

#### 4.2 Design of Tracking Control System

Figure 10 shows the structure of an optical system equivalent to our prototype system. Here, laser beam B from the laser generator is adjusted to pass through the center of the optical position sensor and fall into the center of the mirror from the direction orthogonal to the axis of rotation of motor  $M_3$ .

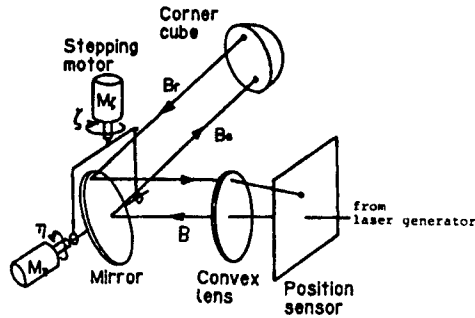


Figure 10. Illustration of Laser Scanner Equivalent to Our System

Now, let us consider the two coordinate systems:  $\{O_M;xyz\}$  and  $\{O_S;y_s z_s\}$ , shown in Figure 11, in the optical system shown in Figure 10.  $\{O_M;xyz\}$  is similar to that defined in Section 3.2, while  $\{O_S;y_s z_s\}$  is a two-dimensional coordinate system in which  $O_S$ , the center of the optical position sensor, is defined by the origin, and the  $y_s$ - and  $z_s$ -axes parallel-shifted on optical position sensor plane  $P_s$ .

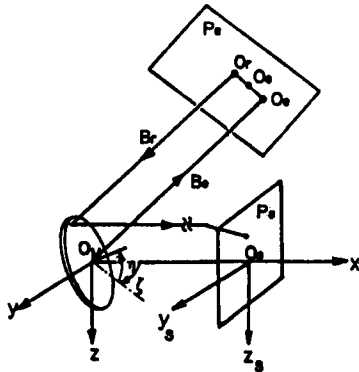


Figure 11. Coordinate System on Laser Scanner

In tracking control, too one only needs to find  $\epsilon_3$  and  $\epsilon_\eta$ , the mirror direction deviations defined by Equation (1), and construct a control system assigning zero to these deviations.

Let us first see how to compute  $\epsilon_3$  and  $\epsilon_\eta$ .

Using  $P_c$  as a plane parallel to the surface of the mirror and which passes through corner cube center  $O_c$ , the relationship between  $B_e$ , the incident laser beam into the corner cube, and reflected light  $B_r$  is as follows according to the corner cube recurrence:

- (1)  $B_r$  is parallel to  $B_e$
- (2)  $O_e$ , the intersection of  $B_e$  and  $P_c$ , and  $O_r$ , the intersection of  $B_r$  and  $P_c$ , are point-symmetrical for  $O_c$ .

Taking advantage of these properties, the relationship between ( $y_s$  and  $z_s$ ), the light reception points of reflected light  $B_r$  on the optical position sensor, and deviations  $\epsilon_3$  and  $\epsilon_\eta$  can be obtained geometrically by the following equation:

$$\begin{bmatrix} \epsilon_3 \\ \epsilon_\eta \end{bmatrix} = \frac{1}{4\rho\mu} \begin{bmatrix} \sec^2 \eta & 0 \\ -\tan \zeta & \tan \eta \end{bmatrix} \begin{bmatrix} y_s \\ z_s \end{bmatrix} \quad (5)$$

Here,  $\rho$  is the distance from  $O_M$  to  $O_c$ , and  $\mu$  is a constant determined by the positional relationship between the optical position sensor and the condensing lens. In our prototype,  $\mu = 0.147$ .

Therefore,  $\epsilon_3$  and  $\epsilon_\eta$  can be determined universally from  $\rho$ , computed from the position of the mobile object obtained when laser beam  $B_e$  irradiates the corner cube, ( $y_s$  and  $z_s$ ) obtained from the optical position sensor, and ( $\zeta$  and  $\eta$ ), the present direction of the mirror.

Then, a system in which the laser emitting direction agrees with the direction of the center of the corner cube is designed by rotating the mirror.

Expressed by a discrete system the relationship between  $\zeta$  and  $\eta$ , the angles of rotation of the mirror, and  $u_3$  and  $u_\eta$ , the input voltages into the V/F converter, is obtained from Equation (3) as follows:

$$x(k+1) = x(k) + \alpha u(k)$$

where,

$$\begin{aligned} x &= \zeta \quad \text{or} \quad \eta \\ u &= u_\zeta \quad \text{or} \quad u_\eta \\ \alpha &= 0.0198 \tau \quad \text{or} \quad 0.0224 \tau \end{aligned}$$

(6)

Here,  $\tau$  is the control period.

Now, a ramp follow-up system is designed on the assumption that, when a mobile object moves slowly,  $x^*$  ( $= \zeta^*$  or  $\eta^*$ ), the target value of  $x$  ( $= \zeta$  or  $\eta$ ), changes to a state of slow acceleration, namely, a ramp state, within a very small period of time.

The following extended system for Equation (6) has been conceived as  $\epsilon(k) = x^*(k) - x(k)$ :

$$\underline{x}'(k+1) = \underline{A} \underline{x}'(k) + \underline{B} u'(k) \quad (7)$$

Here,

$$\underline{x}'(k) = \begin{bmatrix} x(k) - 2x(k-1) + x(k-2) \\ \epsilon(k) - \epsilon(k-1) \\ \epsilon(k) \end{bmatrix}$$

$$u'(k) = u(k) - 2u(k-1) + u(k-2)$$

$$\underline{A} = \begin{bmatrix} 1 & 0 & 0 \\ -1 & 1 & 0 \\ -1 & 1 & 1 \end{bmatrix}, \quad \underline{B} = \alpha \begin{bmatrix} 1 \\ -1 \\ -1 \end{bmatrix}$$

Then, the problem of designing a tracking control system of the ramp follow-up type involves obtaining an optimum regulator with which to find  $u'(k)$ :

$$J = \sum_{k=0}^{\infty} [\underline{x}'(k+1)^T \underline{Q} \underline{x}'(k+1) + u'^2(k)] \quad (8)$$

where,  $\underline{Q}$  is the weight, as the minimal evaluative function. Therefore,  $u(k)$  can be computed by the following equation:

$$u(k) = 2u(k-1) - u(k-2) + K_1[x(k) - 2x(k-1) + x(k-2)] + K_2[\epsilon(k) - \epsilon(k-1)] + K_3 \epsilon(k) \quad (9)$$

Here, feedback gains  $K_1$ ,  $K_2$ , and  $K_3$  are given by

$$[K_1, K_2, K_3] = -[\underline{B}^T \underline{S} \underline{B} + 1]^{-1} \underline{B}^T \underline{S} \underline{A} \quad (10)$$

and  $\underline{S}$  is the solution of the following equation:

$$\underline{S} = \underline{Q} + \underline{A}^T \underline{S} \underline{A} - \underline{A}^T \underline{S} \underline{B} [\underline{B}^T \underline{S} \underline{B} + 1]^{-1} \underline{B}^T \underline{S} \underline{A}$$

### 4.3 Tracking Test

We conducted a tracking test, using the device shown in Figure 12, and causing the corner cube to revolve around point 0 at constant angular velocity  $\omega$  by means of a DC motor. The distance between point 0 and the center of the corner cube was 26 cm. The device was installed 10 m distant to enable  $O_M 0$  to be in the direction of 30 degrees within the xy plane of ( $O_M;xyz$ ) of the laser scanner and orthogonal to the locomotion plane of the

corner cube. Our test caused the corner cube to move at constant angular velocity  $\omega$  from a point precisely under point O, as illustrated. At the start of the corner cube's locomotion, the laser beam was made to irradiate the center of the corner cube.

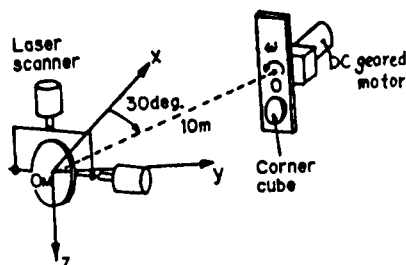


Figure 12. Hardware Set Up for Experiment

In the test, control period  $\tau$  was 25 seconds and feedback gains were computed on the assumption of weight  $Q = \text{diagonal}(10^5, 10^4, \text{and } 10^4)$ .

Figure 13 shows the state of direction control of the mirror for about 5 seconds after the start of locomotion of the corner cube in a test made by causing the corner cube to move at  $\omega = 34.4$  degrees/second. The deviation at the start of the corner cube's locomotion was large because the corner cube was started suddenly by giving step input to the motor used to move the corner cube. However, later, the directing of the mirror followed the target value with high accuracy. This indicates the effectiveness of the proposed method of tracking control.

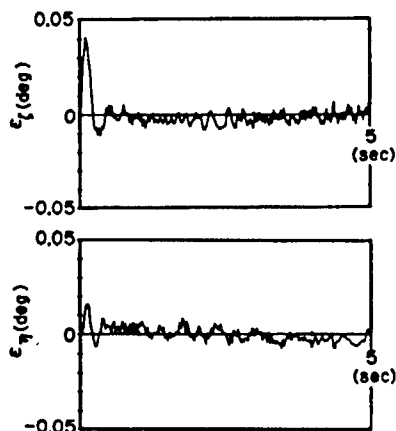


Figure 13. Experimental Results of Tracking Control

## 5. Conclusion

In this report, we proposed methods of acquisition and tracking control to direct a laser beam from a mobile object toward a corner cube installed in the environment as important for the realization of an active positioning method using laser and corner cubes, and proved the effectiveness of the proposed methods by tests using a prototype system.

It is believed that these control methods can also be applied to the means of securing transmission circuits for the laser space communications system<sup>11,12</sup> which has become important in recent years.

Finally, we wish to express our gratitude to Hitachi Kiden Kogyo Co., Ltd., and Akira Ishida, ex-graduate student at the University of Osaka Prefecture (now serving with Matsushita Electric Industrial Co., Ltd.) for their assistance in conducting this research.

#### References

1. Examples of Introduction of Unmanned Vehicle Conveyance Systems, Shoryoku to Jidoka (1986).
2. Arai and Nakano, "Development of Locomotional Vehicle-Mounted Position and Direction Measuring Equipment and Evaluation of Their Performances," Society for Instrumentation Automatic Control Papers, Vol 18 No 10, 1982, p 1013.
3. Ochi, "Position Detection of Locomotion Robot Using Point-Symmetrical Revolving Laser Beam," JAPAN ROBOTIC SOCIETY JOURNAL, Vol 5 No 5, 1987, p 339.
4. Matsumoto and Aburada, "Locomotion Robot Autonomous Traveling System According to Route Maps," Ibid., Vol 5 No 5, 1987, p 351.
5. Osono, "An Example of a Visual Sensor for Traveling Robot Guidance Control," SENSOR GIJUTSU, Vol 4 No 7, 1984, p 69.
6. Kameshima, Ogawa, and Nakano, "Visual Guidance of Locomotion Robot Using Recurrent Picture Processing Mechanism," Ibid., Vol 5 No 5, 1987, p 343.
7. Tsubouchi and Aburada, "Environment Recognition of Locomotion Robot by Colored Pictures," 3d Intelligent Locomotion Robot Symposium Papers, 1986, p 67.
8. Tsumura, Hashimoto, and Ishida, "Laser Tracking Method for Active Positioning of Mobile Object Using laser and Corner Cubes," Society for Instrumentation Automatic Control Papers, Vol 23 No 10, 1987, p 1017.
9. Tsumura, Hashimoto, and Fujiwara, "Laser Acquisition/Tracking Control for Active Positioning of Mobile Objects," Papers for 24th Autumnal Convention Jointly of Kansai and Chubu Chapters, Japan Aerospace Society, 1987, p 189.
10. Ibid., "Active Positioning of Three-Dimensional Mobile Object Using Laser and Corner Cubes," Japan Robotic Society Papers, Vol 6 No 1, 1988, p 26.

11. "Feasibility Research Report on Phototechnology Using System VI--Light Link Technology," Hikari Sangyo Gijutsu Shinko-kai, 1984, p 155.
12. Gaguliardi, (translated by Namarikawa and Morinaga): "Optical Communication System," McGraw-Hill, 1983.

## **Network for Self-Contained Mobile Robots Involved in Cooperative Motions**

43064062 Tokyo 4TH INTELLIGENT ROBOTS SYMPOSIUM PAPERS in Japanese  
13/14 Jun 88 No 211 pp 199-204

[Article by S. Premvuti and Shinichi Yuta, University of Tsukuba: "A Network System for Self-Contained Mobile Robots and a Proposal of Their Communications Protocols"]

### **[Text] 1. Introduction**

Autonomous movements of mobile robots and the cooperation among them as a whole can expand the range of their applications. In order to make this possible, an inter-robot communications network system is indispensable. This study is aimed at enabling a group of mobile robots to converse with one another. When individual mobile robots are moving autonomously, it is deemed that the natural human conversational speed suffice for the inter-robot communications. This article proposes the communication protocols for self-contained robots and describes examples where these protocols are loaded on the "Yamabiko-IX," a mobile robot being developed by the authors.

### **2. Hierarchization of Self-Contained Inter-Robot Communication Protocol**

#### **2.1 Features Required for the Protocol**

The features required for a communication network used for cooperative motions among self-contained robots are:

- (1) Information transfer medium without a signal line
- (2) Network structure without a host or a monitoring node
- (3) Easy entrance into and withdrawal from the network of each node
- (4) Positional information control of robots at the network system level
- (5) Real-time exchange of mutual information

#### **2.2 Hierarchization of Protocols and Features of Individual Layers**

In order to design, improve, and maintain a communications system with ease, the division and hierarchization of the system are indispensable. In this article, the authors propose protocols for the following four layers as the robot communication protocols:

### **(1) Physical layer<sup>1</sup>**

This layer conducts communications through an electric wave with a single frequency which does not disturb robot motions, permitting simple hardware construction. This shared frequency can be thought of as a shared bus, and this mode can be referred to as an electric wave bus mode.

### **(2) Data link layer**

The primary function of this layer is to secure information transmission lines among multiple robots. The access mode, the formats for information units and their semantics, and the communications procedure for this electric wave bus are controlled by this layer.

### **(3) Network layer**

This layer provides for the mutual exchange of messages between the processes of different robots, which is called a logical link between processes. The user process is required to utilize these links with ease. To this end, this layer defines network functions for communications.

### **(4) User layer**

A user can write various application programs for cooperative motions by several robots by using network functions.

## **3. Protocol for Data Link Layer**

### **3.1 Data Link Method**

The necessary consideration for this layer is in what way a collision between pieces of information should be prevented and how information exchange among several robots should be conducted. The information unit selected for this protocol mostly based on the HDLC frame while the Token-passing method has been adopted for medium access. The reasons for this are to permit the ensured reliability of communications, to confirm robots joining the network, and to ensure the constant mutual exchange of the positional information of individual mobile robots, which is indispensable for their cooperation.

This mode permits the positional information regarding a robot to be announced to every robot within the network by passing a token accompanying its positional information to the next robot. The positional information is controlled by the data link layer. In other words, pieces of positional information regarding all the robots within the network are constantly in the memory of the network controller and their values are updated to be the latest for each token circulation. This eliminates the need for the user to transfer its positional information to other active robots within the network or to request the positional information regarding other robots. This layer can be divided into the token circulation control sublayer and the information transmission control sublayer.

### 3.2 Frame Construction

This protocol uses the HDLC frame as its information unit. However, the bit configuration of the address field is different from that of the control field.

- (1) Flag: The start and end of the frame contain a flag pattern, a binary number of 01111110.
- (2) Transmit/receive destination address field: this field contains the addressees of a transmitting and a receiving station.
- (3) Control field: This field contains identification codes for frame types.
- (4) Information field: This field contains the information to transmit.
- (5) Error checking field: This field contains the CRC value of the frame.

### 3.3 Token Circulation Control Sublayer

The major procedures of this sublayer are the activation of the network, a token creation procedure, a token circulation procedure, an error recovery procedure, and offering an information transmission line to the information transmission control sublayer.

#### 3.3.1 Frames To Be Used

- (1) G frame: This frame declares that a token has been secured.
- (2) R frame: This frame passes the token to the following node.
- (3) A frame: This frame authorizes the entry of new nodes into the network.
- (4) D frame: This frame eliminates the node from the network.
- (5) C frame: This frame transmits an entry request of a new node into the network. When no requests are made, it passes the token to the first node in the token circulation sequence.
- (6) Q frame: This frame presents an entry request.

#### 3.3.2 Procedures

##### (1) Normal token passing

The normal token passing procedure is presented in the time chart shown in Figure 1.

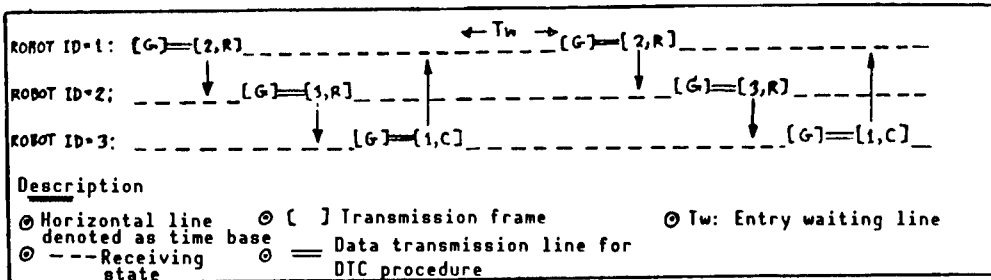


Figure 1. Normal Token Passing

(2) Procedure for a robot entry into the network

When a robot's switch is put into the ON position, it conducts the following procedure:

- a. The robot enters the receiving state.
- b. The robot searches for the HDLC frame.
- c. When the HDLC frame is not found within the time  $T_s$ , the robot activates the network to enter the normal token passing state by a single robot.
- d. When the HDLC frame is found within the time  $T_s$ , the robot enters the network, according to the "Append Robot to Network" procedure.

(3) Append robot to network procedure

Figure 2 presents a time chart for other robots to enter a network comprised of more than one robot.

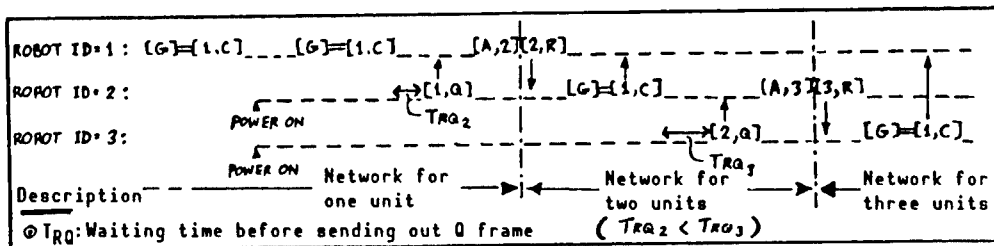


Figure 2. Append Robot to Network Procedure

(4) Error recovery

The conceivable errors in the token circulation control procedure include the following, with each provided with a recovery procedure.

- a. In passing the token to the following robot, the robot is deleted when it is absent.
- b. When the token is lost in an accident, it is deleted.

### **3.4 Information Transmission Control Sublayer**

This sublayer transmits the information to be transferred to other robots using the information transmission line provided by the token circulation control sublayer.

#### **3.4.1 Frames To Be Used**

- (1) I frame: The frame entered by the information to be transferred
- (2) RR frame: The frame for answering the I frame reception.

#### **3.4.2 Procedure**

This procedure makes it possible for messages to be exchanged between robots using the message transmission line provided by the token circulation control procedure. Transmitting and answering data are conducted when the individual robots are provided with a token.

### **4. Network Layer Protocol**

As network functions to implement communications between user processes for different robots, the protocol proposes the following network functions:

#### **(1) Message transmission**

A message is transferred using the `send_vis_net` function. Then, the `recv_mess (NETWORK)` function sends information regarding whether the message has been transferred correctly to the receiver.

#### **(2) Message receive**

The `recv-mess (NETWORK)` function awaits messages provided from the network controller. When a message from another robot is received, the pointer indicated by the message is passed to the user process.

#### **(3) Request for positional information**

The pointer indicated by the positional information regarding the robot specified by the `ask_position` function can be obtained.

#### **(4) Request for a list of the robots within the network**

The `ask_robot_list` function makes it possible to obtain the pointer indicated by the list of the robots within the network.

### **5. Loading on Yamabiko-IX**

#### **5.1 Yamabiko-IX and the Creation of Each Network Layer**

Yamabiko-IX has adopted a distributed function modular architecture (Figure 3). The functions, such as travel and sensing, have been created by modules

provided with respective dedicated processors and are linked to the central master through serial communications. Each module receives commands from the master, executes tasks specified by those commands, and replies to the master as required. The master CPU is loaded with an operating system, termed the modularized operating system for robotic architecture (MOSRA).<sup>2</sup> This operating system offers multiprocess processing and an interprocess communications function. It is also equipped with a module monitor, as a system process, corresponding to each module. The role of the module monitor is to link a user process with each module. Viewed from the user process, the module monitor acts as if it were a module itself.

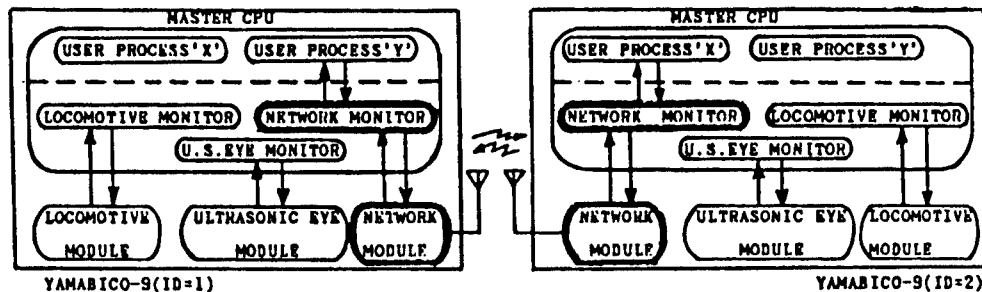


Figure 3. Yamabiko IX's Modular Configuration and Network Modules

The communications network system loaded on the Yamabiko is designed as a module, termed a network module, and the MOSRA is provided with a network monitor. The inter-robot communications network supports the message communication between user processes. In other words, a user process can execute message communication with its counterparts via the network monitor. Table 1 presents the hardware and software for creating each layer of the proposed protocol.

Table 1. Communications Network Layers and Corresponding Positions in the System

| Layer number and name | Position in system        |
|-----------------------|---------------------------|
| 4. User layer         | User process in master    |
| 3. Network layer      | Network monitor in master |
| 2. Data link layer    | Network module's software |
| 1. Physical layer     | Network module's hardware |

## 5.2 Network Module Hardware

The hardware configuration of the network module is presented in Figure 4. The HDLC controller creates frames of the HDLC standards and interprets them. In transmitting, the modem enters the HDLC controller's digital signals into the radio transmitter after their audio frequency modulation. In receiving, the modem enters the digital signals obtained by demodulating the acoustical signals output by the radio receiver not the HDLC controller. FM transceivers were used as the radio equipment. Table 2 presents the I/O hardware specifications for the network module.

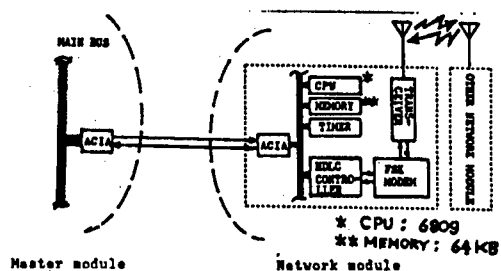


Figure 4. Configuration of Network Module Hardware

Table 2. Interface Between Network Modules

|                   |   |
|-------------------|---|
| Mode              | Serial communication  |
| Medium            | FSK modulated signals are transmitted through UFB-band FM waves (1 channel) |
| Transmission rate | 1,200 bps   |
| Information unit  | HDLC frame  |

### 5.3 Network Module Software

#### 5.3.1 Configuration

For communications implementation as proposed by the protocol, several processes must be executed almost simultaneously. To this end, the MOSRA, a compact real-time operating system, has been adopted as the operating system for the network module. The MOSRA's 11 processes have enabled a data link layer protocol to be created. The following are descriptions of the functions of the individual user processes. The data flow between major processes is illustrated in Figure 5. The programs were written in C, totaling about 4,000 lines, with its object size being about 36 K bytes.

#### 5.3.2 Individual Processes on Network Module

##### (1) Start process (STARTUP)

This process activates TMON, TIMER, AND STARTNET.

##### (2) Terminal monitor process (TMON)

TMON offers the interface between each process and an operator mainly for debugging purposes.

##### (3) Timer process (TIMER)

This process offers a timer function.

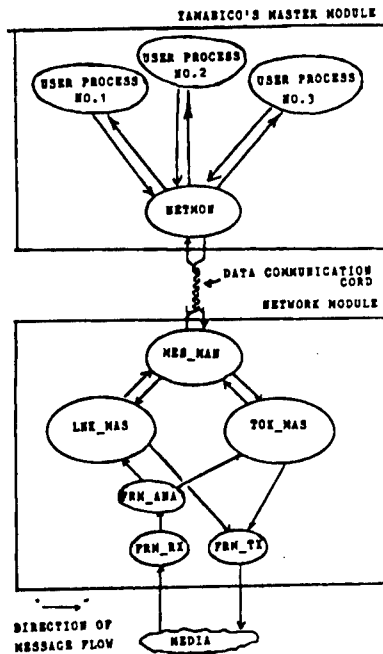


Figure 5. Software Structure of Yamabiko's Network System

**(4) Startup the network (STARTNET)**

This process activates the following processes required for the network function: MES\_MAN, FROM\_RX, FROM\_TX, TOK\_MAS, LNK\_MAS, FROM\_ANA, and WCH\_DOG.

**(5) Watch dog process (WCH\_DOG)**

This is a monitoring process to inform the programmer of the cause of errors occurring during the real-time debugging operation.

**(6) HDLC frame transmitter process (FROM\_TX)**

This process receives frame transmission requests by TOK\_MAS or LNK\_MAS and executes tasks for them. FROM\_TX transmits HDLC frames using the HDLC controller.

**(7) HDLC frame receiver process (FROM\_RX)**

This process receives HDLC frames using the HDLC controller and passes to FROM\_ANA only those which have been received correctly.

**(8) Received HDLC frame analyzer (FROM\_ANA)**

This process analyzes the address fields of the frames it receives from FROM\_RX. Frames with unrecognizable addresses are removed. It passes frames whose destination address fields hold global addresses (sFF) to TOK\_MAS. When the value of a destination field is the same as its address, it passes the frame to LNK\_MAS.

**(9) Token circulation maintenance master process (TOK\_MAS)**

This process executes the token circulation control sublayer. It conducts such tasks as creating tokens, token circulation the procedures for appending robots to and deleting them from the network, creating and managing a list of robots within the network, an error recovery procedure, and offering an information transmission line to LNK\_MAS. The possible number of robots to be appended to the network is determined by this process, with eight units currently entering.

**(10) Link management for user data transferring master process (LNK\_MAS)**

This process executes the information transmission control sublayer. Its primary task involves connecting itself to the seven other robots. In other words, it manages even links. The user information from MES\_MAN is transferred to the other robots through this process. LNK\_MAS always waits for a request from MES\_MAN, and when MES\_MAN makes a request for information transmission, it checks whether the linkage between the specified robot to which the information is being transferred and itself has been established. When the linkage has been established but no information is waiting to be transmitted, LNK\_MAS accepts the message as information waiting to be transmitted. Otherwise, it replies to that effect and refuses the transmission request. After processing the information waiting to be transmitted, it returns the success or failure message to MES\_MAN.

**(11) Messages management process (MES\_MAN)**

This process interfaces the network module to the network monitor process (NET\_MON) in Yamabiko-IX's master CPU. MES\_MAN receives commands from NET\_MON, analyzes and executes them, and replies to NET\_MON.

**6. Examples of Simple Cooperative Motion Programs and Their Experimental Results**

Examples of simple cooperative motion programs for two Yamabikos are presented in Figure 6. In executing these programs, the two robots, in turn, make a round trip over a distance of 1 m. First, robot A sends a message to robot B. Upon receiving the message, robot B advances 1 m, rotates 180 degrees, and stops. Then, it sends the message to robot A. Upon receiving the message from robot B, robot A operates in the same way as did robot B. In this way, cooperative motions can be programmed with ease using the basic network functions--ASK\_ROBO\_LIST, SEND\_VIA\_NET, and RECV\_MESS (NET\_WORK)--contained in the WAITRXMESS and WAITTXRSLT functions.

The execution of these programs by two Yamabikos resulted in synchronous motions, as had been expected. It was confirmed that in such simple examples, the time necessary for communication, when compared to the time required for the robots to travel, was short enough to be negligible.

```

Program for Robot A
main()
{
  struct mess *m, *n;
  struct list_mess *lst;
  int kh, ll;
  char word, messid;

  set_timer(500);
  timer_wait();

  a_send_mess(TALEMON,3,0x81,0x81,0x81);

  word=0x81;
  messid=0;

  /*****
  STS1: do {
    list_mess robot list();
    kh=lst->que[SLPRID]; kh=kh&0xff;
    ll=lst->que[TOURID]; ll=ll&0xff;
    nfree(lst);
    while ( (kh==0xff) || (ll==0xff) );
    /* up-down link connected */
    send_term("Try to call 001");

    Preparation
    for trans-
    mitting
    message
    m=malloc( L1+3 ); /* L1=14 */
    m->lang=L2+3; /* L2=9 */
    m->nt_body[0]=word;
    m->nt_body[1]=2;
    m->nt_body[2]=3;
    send_via_net(TOURID,TOURID,messid,m);
    Transmitting
    message
    if ( waittxrslt[3]==0 ) goto STS1 ;};
    word++;
    Waiting
    for message
    to be
    received
    m=waitrxmess(messid);
    /* Message received */
    a_send_mess(TALEMON,1,n->nt_body[0]);
    nfree(n);

    1 m advance
    180 degree
    rotation
    mchi(MGO,0,0,0,0);
    mchi(MSTOP,100);
    mchi(MSTRT);
    mchi(MSPIN,180);
    mchi(MSTATUS,'N');
    mchi(MSTATUS,'S');
    mchi(MSET,0,0,0);
    mchi(MWAIT);

    messid++;
    goto STS1;
  }
  /*****/

Program for Robot B
main()
{
  struct mess *lst, *m, *n;
  int kh, ll;
  char word, messid;

  a_send_mess(TALEMON,3,0x81,0x81,0x81);

  word=0x81;
  messid=0;
  /*****
  STS0:
  m=waitrxmess(messid); Waiting for message
  /* Message received */ to be received
  a_send_mess(TALEMON,1,n->nt_body[0]);
  nfree(n);

  1 m advance,
  180 degree
  rotation
  mchi(MGO,0,0,0,0);
  mchi(MSTOP,100);
  mchi(MSTRT);
  mchi(MSPIN,180);
  mchi(MSTATUS,'N');
  mchi(MSTATUS,'S');
  mchi(MSET,0,0,0);
  mchi(MWAIT);

  /*****/
  STS1: do {
    list_mess robot list();
    kh=lst->que[SLPRID]; kh=kh&0xff;
    ll=lst->que[TOURID]; ll=ll&0xff;
    nfree(lst);
    while ( (kh==0xff) || (ll==0xff) );
    /* up-down link connected */
    send_term("Try to call 001");

    Preparation
    for trans-
    mitting message
    m=malloc( L1+3 ); /* L1=14 */
    m->lang=L2+3; /* L2=9 */
    m->nt_body[0]=word;
    m->nt_body[1]=2;
    m->nt_body[2]=3;
    send_via_net(TOURID,TOURID,messid,m);
    Transmitting
    a message
    if ( waittxrslt[3]==0 ) { goto STS1 ;};
    word++;
    Waiting for transmission
    result
    messid++;
    goto STS0;
  }
  /*****/
}

```

Figure 6. Yamabiko's Cooperative Motion Program Examples

### 7. Conclusion

The authors have proposed a communications protocol for self-contained robots. This communication procedure is intended for the cooperative motions by multiple robots. This protocol features the following: A compact four-layer configuration is adopted; electric waves are used as an information transmittal medium which does not constrain robot travel; token passing is utilized for the medium access; a radio network with a token bus configuration is structured; positional information significant for mobile robots is attached to tokens and managed at the data link level, and the procedures appending robots to and deleting them from the network are simple.

The authors loaded Yamabiko-IX with the protocols proposed in order to study their scope. The network controller on Yamabiko\_IX became a network module in terms of form. The software for the network modules are the several processes on the MOSRA. An experiment regarding simple cooperative motions was conducted successfully.

### References

1. S. Premvuti, W. Yuta, "Radio Communication Network on Self-Contained Mobile Robots for Cooperative Motions," PROC. SICE'87, Vol II, pp 1025-1028.
2. Nakayama and Yuta, "Application Program Execution Environment in Yamabiko-X," 5th Japan Robotic Society Academic Meeting Papers.

## Programming Language for Sensor-Raised Mobile Robot Motions

43064062 Tokyo 4TH INTELLIGENT ROBOTS SYMPOSIUM PAPERS in Japanese  
13/14 Jun 88 No 212 pp 205-210

[Article by Shoji Suzuki, Shinichi Yuta, and Maki K. Habib, University of Tsukuba; and Junichi Iijima, The University of Electrocommunications: "A Programming Method for Describing Mobile Robot Motions and a Programming Language Suitable for Describing Programs Based on It Are Proposed"]

### [Text] 1. Introduction

A mobile robot is different from a fixed counterpart in that, since it moves around, its environment can change instantly, and it is impossible to forecast the changes. For this reason, it is necessary for robot control programs to be able to respond sufficiently to changes in the environment and, therefore, the contents of motions described in the programs will be quite different in nature from general computer programs.

The specifications for conventional programming languages have been determined by referring to general computer languages on the premise that robot motions can be expressed in principle as a sequential arrangement of groups of small motions. However, when a robot is likely to encounter quite major changes in its environment and responds to each of them, its motions must be expressed by attaching more importance to its serial motions, responding to each possible change, than to sequential motions. For programs for such a mobile robot, a programming language suitable for responding to such possible changes is required. This report proposes a method of programming to describe the motions of such a mobile robot, and a programming language appropriate for describing programs based on the method.

### 2. Motions Expected for Intelligent Robots

In order to move a manipulator to a certain position, a conventional robot language would describe as follows, for example:

MOVE intended position

However, this instruction is only that the manipulator hand should be moved to the intended position, and no definition is given with respect to

problems likely to occur on the way. Therefore, no description regarding the manipulators expertise when colliding with an obstacle during its movement is provided in the program. However, ideal environments free from obstacles are rare among the actual environments in which intelligent robots are employed, and the presence of those obstacles is not necessarily known when the programs are produced.

A general procedure for preventing a robot from colliding with an obstacle is: The environment is examined using a vision sensor, etc., before actuating a manipulator, a locus which makes the robot free from collisions is designed, and motions, as designed, are executed. Even if the robot moves as planned, the environment may change in a short time or the robot may not move along the designed orbit due to an error in the sensor information. Therefore, the robot must be monitored by sensors during its operation to prevent it from colliding. Also, it is necessary to provide a robot program, in advance, that offers a method for discriminating between a normal and an abnormal piece of sensor information and the expertise for dealing with anomalies.

Of course, the use of sensor information during its motion is indispensable not only for preventing collisions, but also for enabling a robot to change its motions dynamically, in a more general sense of the word, based on sensor information. In particular, when a mobile robot moves in environments with unknown parts, the following problems are created, necessitating dynamic changes in motion as required, based on sensor information.

(1) Accidental errors occur without fail during travel, and it is preferable that the robot be able to correct them dynamically while traveling.

(2) Upon encountering an obstacle during its travel, it is desirable that the robot change its course dynamically and avoid it without stopping. However, the number of obstacles to be encountered cannot be anticipated in time to change its course in many cases.

(3) If the robot cannot reach its intended position, it becomes necessary for it to change its basic motions through the appropriate appraisal of its environment.

(4) In addition, a method to dynamically change its motions cannot always be determined on a general basis. For example, it cannot be left to be dealt with "suitably" in the MOVE statement. A significant point of programs for intelligent robots with sensors seems to lie in the expertise involved in expressing the use of such dynamic sensor information and resulting changes in the robots' motions.

What about the case in which the robot has avoided an obstacle and resumes its course? In this case, since the robot's positions before and after its avoidance movement are not the same, the problem is what segment of the program it should resume in order to travel along the original course.

Therefore, avoiding obstacles cannot be regarded as a simple interruption program.

As stated previously, one cannot describe robot motions, including the monitoring of sensor information and the programming responding to that information, by arranging individual motions for chronological sequential execution similar to the process followed in general computer programs. The description of motions based on sensor information cannot apparently be dealt with by conventional robot languages and their level of sophistication and, therefore, it is necessary to study their description method.

### **3. Description of Intelligent Robot Motions**

#### **3.1 Program Layers**

An intelligent robot is equipped with such sensors as a telecamera and ultrasonic and tactile sensors, and is also equipped with various actuators, such as a manipulator and wheels. Of course, making them function necessitates specific programs since the hardware instruments, such as an ultrasonic transmitter-receiver and a motor, must be actuated according to specific procedures. These programs can be regarded as independent from those for executing robot motions, so it is recommended that they be produced in advance. The sensor and actuator functions created in these pieces of hardware are called robot basic functions. Also, the programs to control the hardware functions producing robot functions are termed programs to create basic functions. Robot motions are to be directed using these basic functions. Therefore, programs for an intelligent robot can be divided into two layers--a program to create robot basic functions and one to direct the robot to perform motions.

#### **3.2 Robot Basic Functions**

The external specifications of the robot basic functions become significant in this respect. In general, the more perfect the basic functions and the more sophisticated their contents, the easier the programs to direct motions can be written on them. However, as stated above, it is not appropriate to provide the basic functions of the intelligent robot described here by such descriptions as "MOVE intended position" in conventional robot languages. The reason is that, in order to express those functions, a large number of monitoring conditions and the expertise to deal with each case must be added as parameters, and it is almost impossible to define and create them in advance.

To this end, the robot basic functions will be created by the autonomous actuator system and the autonomous sensor system, which can be described as follows:

##### **(1) Basic functions of the actuator system**

The travel system and manipulator, segments corresponding to the hand and foot of a robot, have been regarded as belonging to the autonomous actuator system, and move independently. This refers to positions, speeds, and loci,

generating strength and torque to direct the target, which are provided by higher-order programs. Once a target position, etc. is given, the actuator system controls itself to coincide with the target, based solely on its internal sensor. This actuator system can be thought of as a type of intelligent servo system. A direction not to move is indicated by providing a target in which the robot is to remain at the current site.

Of course, as long as a robot moves to unknown environments, this motion target value cannot necessarily be achieved. However, this autonomous actuator system is not responsible for the failure to achieve this target, and all that is required for the system is to control itself according to the target value. When the target value cannot be achieved due to obstacles, etc., higher-order programs deal with the case.

Incidentally, the travel system is provided, as a basic function, with a position recognizing function through dead reckoning, and the position locus of a target can be given, not in terms of an angle of rotation of the wheel, etc., but, for example, in the form of coordinates on a two-dimensional plane.

## (2) Basic function of the sensor system

The robot's function recognizing sensor information or environments in general requires a certain amount of time for measuring and processing. However, the robot sensor system studied here is regarded as one constantly operating autonomously, which recognizes its environment and always retains updated values.<sup>7</sup> These updated pieces of sensor and environmental information are written into the blackboard system by which they can be referred to by higher-order programs. Therefore, the sensor system can be thought of as a blackboard on which values are always updated.

### 3.3 Robot Motion Expressing Method Using Motion Modes

As previously noted, a series of robot motions features the following:

- (1) A robot always obtains external information through its sensors while performing a task.
- (2) A robot selects the task to be performed next according to the sensor information obtained and its current situation.

Incidentally, a set of the tasks currently being conducted, sensor information and the state of the robot for which conditions change during work, as well as directions for the next task to be performed on that occasion, is termed a "motion mode." A series of robot motions can be described by defining each motion mode i.e., by the transition among modes due to the tasks and conditions in each mode.

This robot motion expressing method expresses the parallel quality, etc., of a robot waiting for specific conditions according to the sensor information in the natural form, enabling the basic functions of an intelligent robot to function effectively.



Mode 3: The robot examines the following conditions to stop.

When the obstacle ahead is removed, proceed to Mode 1.

When more time has elapsed than the ordinary standard, proceed to Mode 5.

Mode 4: The robot examines the following conditions to stop.

When the obstacle ahead is removed, proceed to Mode 2.

When more time has elapsed than the ordinary standard, declare termination and proceed to Mode 5.

Mode 5: The robot stops its motions.

Figure 3.2 presents the transition among the modes in this example.

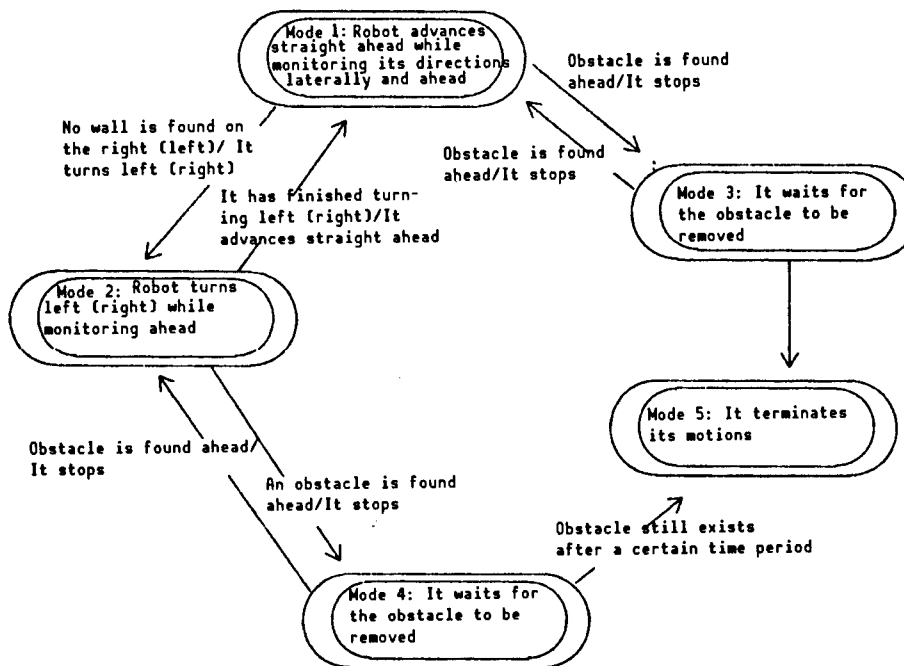


Figure 3.2 Concept of Robot Motions

#### 4. Programming Language ROBOL/O To Describe Intelligent Robot Motions

The robot language ROBOL/O for programming robot motions has been defined based on the concept and description in Chapter 3. ROBOL/O describes robot motions using motion modes while using robot basic functions as functions.

## 4.1 Robot Basic Functions and Functions To Be Utilized

### (1) Actuator functions

The actuator functions are defined as functions providing each of the basic functions of the actuator system stated above with target values for motions. When a target value is changed by this function, the actuator system autonomously achieves the given target value.

This function only gives a direction while the actuator receiving the direction starts a motion, but it terminates the function execution before terminating the motion. Therefore, the execution of every actuator function terminates instantaneously. The actual hang-up and termination of the actuator motions are conducted by the "stop" motion direction given by an actuator function.

### (2) Sensor functions

The functions to determine the results of measuring and processing by the aforementioned autonomous sensors and the environmental recognition functions are defined as sensor functions. Sensor functions only read the blackboard, so they are executed instantaneously.

## 4.2 Expression of Motion Modes

Robot motions are programmed by arranging the definitions of motion modes, which are defined in the following format:

```
Mode (mode name)

    Execute statement 0

    WAIT

    WHEN (conditional statement 1) EXEC Execute statement 1; NEXT
    next mode

    WHEN
    .
    .
    .
MEND
```

Table 4.1 and Figure 4.1 present ROBOL/O's reserved words and their semantics and the grammatical definitions, with C language as the standard, respectively.

### 4.3 Program Example

Figure 4.2 presents an example of the motions stated in Chapter 3 described in ROBOL/O.

Table 4.1 ROBOL/O's Reserved Words and Their Semantics

| Reserved word | Semantics  |
|---------------|--|
| MODESDEF      | Declares the initiation of the mode definition segment             |
| STARTM        | Specifies the mode to execute first                                |
| MODE          | Declares the beginning of the definition of a mode                 |
| WAIT          | Declares the beginning of the condition waiting segment            |
| WHEN          | Declares a condition   |
| EXEC          | Declares a statement to execute when the condition is met          |
| NEXT          | Specifies the mode to execute next                                 |
| WCONT         | Specifies to continue the same condition without changing the mode |
| MEND          | Declares the end of the definition of a mode                       |
| MODESEND      | Declares the end of the mode definition segment                    |

```

#define   OBST  50
#define   WALL 150

MODESDEF

  go_straight();

MODE straight
  WAIT
  WHEN (front_distance() <= OBST) EXEC stop();
    NEXT waiting_st
  WHEN (left_distance() >= WALL) left_turn();
    NEXT turning
  WHEN (right_distance() >= WALL) right_turn();
    NEXT turning
MEND

MODE turning
  WAIT
  WHEN (front_distance() <= OBST) EXEC stop();
    NEXT waiting_tr
  WHEN (endof_turn() == TRUE)
    EXEC go_straight(); NEXT straight
MEND

MODE waiting_st
  c = get_time();
  WAIT
  WHEN (front_distance() > OBST)
    EXEC go_straight(); NEXT straight
  WHEN (get_time() > c+10) EXEC stop() NEXT end
MEND

MODE waiting_tr
  c = get_time();
  WAIT
  WHEN (front_distance() > OBST)
    EXEC recover(); NEXT turning
  WHEN (get_time() > c+10) EXEC stop() NEXT end
MEND

MODE end
  end_motion();
MEND

```

Figure 4.1 Example of Program Description in ROBOL/O

```

<program>::=(global variable declaration)<modes definitin><procedures definition>
<global variable declaration>::=<variable declaration>
<variable declaration>::= refer to C language
<modes definition>::=#MODESDEF [<modes variable declaration>]
                        [<initialization>][<first mode>]<modes> MODESEND
<modes variable declaration>::=<variable declaration>
<initialization>::=<statements>
<statements>::=<statement>[<statements>]
<statement>::= refer to C language:<procedure call>:<robot function call>
<procedure call>::= refer to function call in C language
<robot function call>::=<sensor function call>:<actuator function call>:<cooperation function call>
<sensor function call>::= refer to robot's function table
<actuator function call>::= refer to robot's function table
<cooperation function call>::= refer to robot's function table
<first mode>::=STARTM <mode name>
<mode name>::=<name>
<name>::=<string of alphanumeric>
<modes>::=<mode>[<modes>]
<mode>::=MODE [<mode initialization>] WAIT <condition statements> MEND
<mode initialization>::=<statements>
<condition statements>::=<condition statement>[<condition statements>]
<condition statement>::=WHEN <condition> EXEC <execution statement> <next mode>
<condition>::=<logical expression>
<logical expression>::= refer to C language
<execution statement>::=<statements>
<next mode>::=NEXT <mode name>;WCONT
<procedures definition>::=<procedure definition>[<procedures definition>]
<procedure definition>::= refer to function definition in C language

```

Figure 4.2 Grammar of ROBOL/O With C Language as Its Standard Language

## 5. Language Processing in Autonomous Robot Yamabiko and Its Execution System

### 5.1 Yamabiko's Architecture

The Yamabiko hardware is comprised of independent modules for its individual basic functions, with its master system designed to retain motion direction programs and the autonomously operating sensor and actuator system combined in the form of a star. Yamabiko is not presently equipped with a blackboard, but its sensor modules constantly retain updated sensor information, so inquiries to the sensor modules are answered immediately, as required.

### 5.2 Language Processing System

The ROBOL/O processing and execution system of the above-mentioned Yamabiko was test manufactured. The software for Yamabiko is being developed in C language on the OS/9. ROBOL/O created C language as the standard language in order to utilize Yamabiko's software library.

The reserved words of ROBOL/O can be defined in C language. However, this alone makes the debugging of grammatical errors almost impossible. For this

reason, a method to convert ROBOL/O into C language while checking its grammar was adopted. A program written in ROBOL/O is first translated into C language, and then the C compiler creates an imperative program, which is executed by Yamabiko's robot basic functions.

## 6. Conclusion

ROBOL/O, a language with new specifications designed to describe robot motions based on sensor information, has been devised since it is extremely difficult to describe them in either conventional robot languages or in their sophisticated versions. ROBOL/O has initiated its specifications on the authors' self-contained robot Yamabiko, and its effectiveness as a programming language is currently being evaluated.

## References

1. E.A. Puente, C. Balaguer, and A. Barrientos, "LRS: A High-Level Explicit Programming Language for Sensor-Based CARA Type Robot," "Languages for Sensor-Based Control in Robotics," NATO ASI Series, Springer, 1987, pp 25-44.
2. A. Brooks Rodney, "A Robot Programming Scheme for a Mobile Robot," Ibid., pp 509-522.

## Attitude Stabilization System for Mobile Robots

43064062 Tokyo 4TH INTELLIGENT ROBOTS SYMPOSIUM PAPERS in Japanese  
13/14 Jun 88 No 213 pp 211-216

[Article by Ryosuke Masuda and Shinichi Hinuma, Tokau University: "An Autonomous Stabilization System Studied Using a Fluid-Filled Gyroscope"]

### [Text] 1. Introduction

R&D on mobile robots for use on irregular ground and unlevel routes is actively being conducted, while the majority of robots are being designed and manufactured in pursuit of improved mobility. On the other hand, for a robot which travels to achieve a certain goal, attitude stabilization during its travel creates a major problem. Conceivable methods of providing attitude stabilization during its travel include giving it a heavy inertia and a stabilizer, as well as attitude detection and balancer control. This research studied the configuration of a system permitting autonomous stabilization using a fluid-filled gyroscope for the robot's attitude stabilization while traveling.

### 2. Outline

Various studies have been conducted to date to stabilize the robot attitude, some of which have been put to practical use. A gyro compass used for ships and aircraft, for example, enables directions to be found at any attitude since the gyro itself, floating in a fluid, is always directed toward the gravity. However, this cannot ensure the stabilized attitude of ships and aircraft, although the stabilization of the gyroscope itself can be maintained. A gyroscope cannot be utilized effectively unless it is combined with a sensor. In addition to this, those used practically include stabilizing instruments, such as one using a weight and one which stabilizes the body by controlling its suspension. However, their structures are so complex that they cannot be mounted with ease on vehicles and ships. Therefore, a fluid-filled gyroscope has been mounted whose structure is relatively simple, but which provides great output, enabling the body of a vehicle or ship to be stabilized with virtually no structural changes.

The great advantage of mounting this type of gyroscope is that the scale of the attitude stabilizing instrument does not need to be large and that a vehicle or a ship can be stabilized by merely mounting this instrument.

Mounting a gyroscope, whether fluid or rigid, makes the visual inertial mass greater, which naturally leads to the stabilization of a robot on an irregular route surface. If this is the goal, the use of a heavy vehicle suffices. However, when a robot with a rigid gyroscope or one with a heavy body travels along a route with holes on its surface at a relatively low speed, a wheel may be off the route in one of these holes. However, a fluid-filled gyroscope has a function preventing the attitude from changing, so that the body may tilt slightly, but the tilt can be minimized.

### 3. Basic Principle

The stability of a fluid-filled gyroscope against an impact has been theoretically analyzed in an approximate manner by dividing the gyroscope's ring into  $n$  equal parts and regarding one of them as a thin circular cylinder. It is presumed that the entire ring and this section are as presented in Figures 1 and 2, respectively.

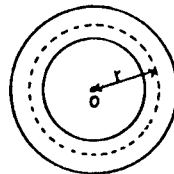


Figure 1. Entire Ring

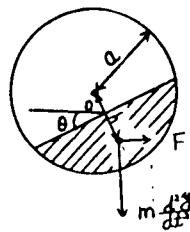


Figure 2. Ring Section

- (1) The ring's total length:

$$L = 2\pi r \quad (1)$$

- (2) The width of the ring divided into  $n$  equal parts:

$$H = \frac{2\pi r}{n} \quad (2)$$

- (3) Let a revolution of the gyroscope around the Z-axis be  $\omega$  [rad/sec]. A centripetal force  $F$ , which works upon the center of the mass of a fluid (mass,  $m$ ) in one-nth of the ring, can be expressed as:

$$F = mr\omega^2 \quad (3)$$

- (4) A horizontal deflection angle  $\theta$  of a fluid in a horizontal stationary rotary ring can be expressed as:

$$\theta = \tan^{-1} (F/mg)$$

and the radius to the center of the fluid mass,  $r + h$ , is

$$F = m(r+h)\omega^2$$

$$\therefore \theta = \tan^{-1} \left\{ \frac{(r+h)\omega^2}{g} \right\} \quad (4)$$

(5) The gyroscope's behavior when force  $F$  works upon its central axis  $\ell$  for  $\Delta t$ :

a. Gyroscope's behavior when a fluid is not injected

Suppose that a gyroscope is a circular cylinder, the inertial moment around the X-axis and the gyroscope's mass are  $I$  and  $W$ , respectively, and

$$I = \frac{Wr^2}{4} + \frac{Wa^2}{3} \quad (5)$$

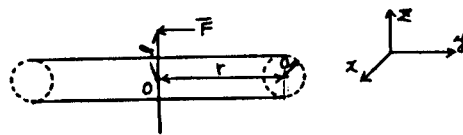


Figure 3. Sectional View of Ring Segment

Then, when the force  $F$  works as in Figure 3, let an angular acceleration and an angular velocity be  $\alpha$  and  $\omega$ , respectively, and, from the equation of motion  $I\alpha = F$ ,

$$\alpha = \frac{F}{I}$$

$$\therefore \omega = \frac{12F}{W(3r^2 + 4a^2)}$$

Therefore, when a force is applied for  $\Delta t$  seconds, the tilt of the gyroscope's axis  $\beta$  can be expressed as:

$$\beta = \frac{l}{2} \cdot \frac{12F}{W(3r^2 + 4a^2)} \cdot \Delta t^2 \quad (6)$$

b. Gyroscope's behavior when a fluid is injected

The gyroscope will tilt, as presented in expression (6), over a period of  $\Delta t$  seconds. However, since the internal fluid has inertia, the center of its mass, which is presented in Figure 5, moves as shown in Figure 4.

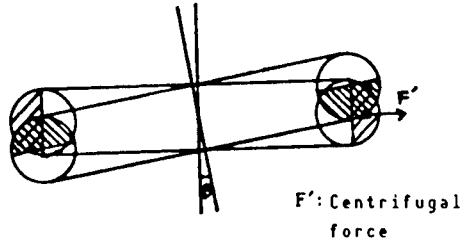


Figure 4. Gyroscope's Stability

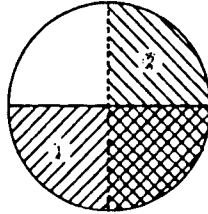


Figure 5. Section of a Ring Divided Into Equal Parts

At first, the fluid is pushed against the ring side due to the action of centrifugal force. However, when an external force acts upon the gyroscope, the fluid in segment (2) in Figure 5 moves to segment (1) in order to retain the center of its mass. Meanwhile, the internal fluid will move to the ring side due to the action of the centrifugal force. Therefore, from the law of the conservation of momentum, the ring is pushed down and, if its tilt  $\beta$  is small, the gyroscope can return to its original rotatable shaft.

The then returning force, i.e., the drag on the gyroscope's radius  $r$ , can be expressed as follows: Assuming that the gyroscope tilts at microangle  $\beta$ , since the mass of the fluid divided into  $n$  equal parts is  $m$  at  $r$  in the Y-axis direction, work  $J$  performed by the ring divided into  $n$  equal parts can be expressed as:

$$J = m (r+h)\omega^2 \cdot 2h \sin 45 \quad (7)$$

Then, since the circle is divided into  $n$  equal parts, the total work conducted by the ring and the drag acting for  $t$  seconds can be expressed respectively as:

$$J' = 2mh(r+h)\omega^2 \sin 45 \cdot \sum_{k=1}^{n-1} \frac{1}{k} \quad (8)$$

$$N = J'/t \quad (9)$$

#### 4. Experimental Method

In order to confirm the effectiveness of a fluid-filled gyroscope, basic data was collected using the experimental instrument presented in Figure 6, and an experiment was conducted to measure the properties of a fluid-filled gyroscope based on the following three grounds:

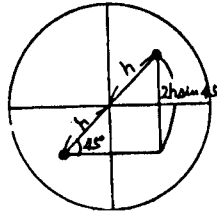


Figure 6. Movement of Level

(1) In order to measure the stability of a fluid-filled gyroscope against the revolution, the revolution alone was changed, with the quantity of mercury left contact.

(2) The experiment was repeated while changing the fluid quantity to measure the stability of a fluid-filled gyroscope against the fluid quantity.

(3) A comparison of the stability when impact was applied was made between a fluid-filled and a rigid gyroscope, under the same conditions, to determine the comprehensive properties of a fluid-filled gyroscope.

The following describes the experimental method in detail.

**(1) Revolution-to-stability property**

The ring used for the fluid-filled gyroscope presented in Figure 8 was mounted on the instrument presented in Figure 7. The quantity of mercury in the ring was kept constant and, as shown in Figure 7, a spring balance was attached to the ring. The spring balance was pushed to a point where the gyroscope tilted as much as had been preset and the value was then read. As can be seen from Figure 7, the gyroscope could only move in one direction.

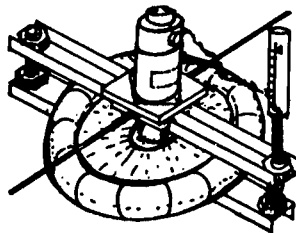


Figure 7. Experimental Gyroscope Instrument

**(2) Fluid quantity-to-stability property**

More mercury was injected into the ring shown in Figure 8, and the stability property was measured.

**(3) Experimental comparison between a rigid and a fluid-filled gyroscope's properties**

The experimental instrument is presented in Figure 9. The dynamic difference in the force required to recover an attitude between a rigid and

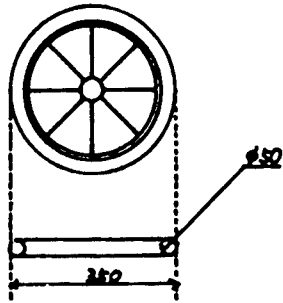


Figure 8. Drawing of Fluid-Filled Gyroscope's Ring Segment

a fluid-filled gyroscope was measured, based on the conditions selected in Guideline Nos (1) and (2). As presented in Figure 9, an experiment equivalent to that in Guideline Nos (1) and (2) was conducted using a metallic weight instead of a ring for use in a rigid gyroscope.

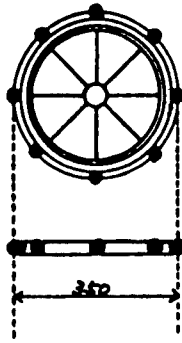


Figure 9. Drawing of Rigid Gyroscope's Ring Segment

## 5. Results of Measurement

The following are graphs drawn based on the data obtained in Guideline Nos (1), (2), and (3) above.

## 6. Study of the Results

A comparative study of the values of the experimental results and those obtained by the simulations was conducted. As a result of a simulation using expressions (6) and (8), the properties presented in Figure 11 were obtained. A comparison between Figure 11 and the experimental results indicates that the simulation matches the trend of measured values. The difference between the simulation and the measured values can be attributed to insufficient revolution and the nonuniformity of the ring.

The properties for actually used revolutions, which were not measured this time, are presented in Figure 12. The data used for this simulation was that of this experimental instrument.

Figures 11 and 12 present the calculated forces required to tilt a gyroscope 30 degrees/second. The simulation has found that when 3-kg mercury is injected into this experimental instrument and revolved at 3,000 rpm, tilting a gyroscope 30 degrees/second requires a force of about 70 kg.

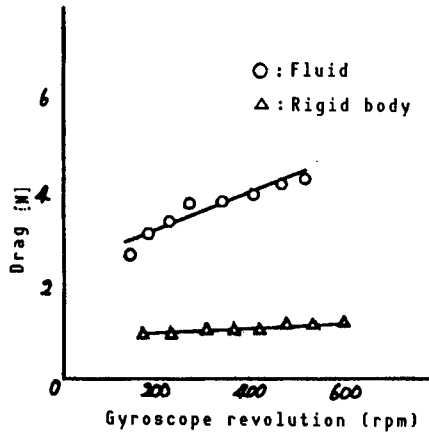


Figure 10.1 When the Mercury and the Rigid Body Each Weigh 1 kg

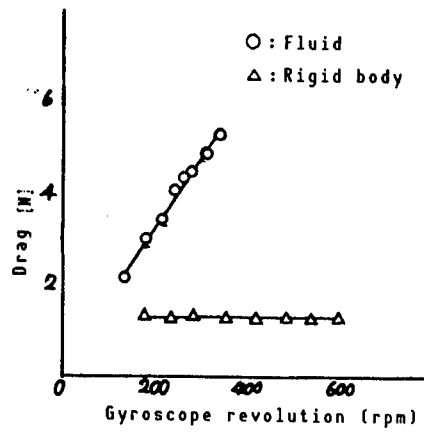


Figure 10.2 When the Mercury and the Rigid Body Each Weigh 2 kg

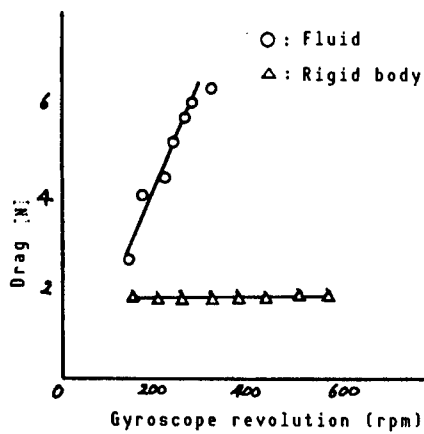


Figure 10.3 When the Mercury and the Rigid Body Each Weigh 3 kg

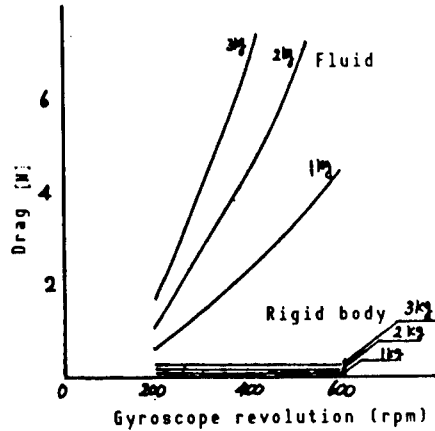


Figure 11. Simulation Results

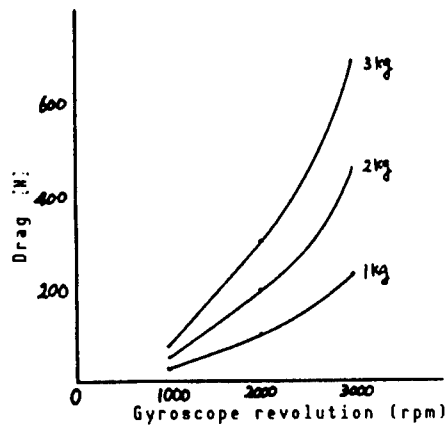


Figure 12. Fluid-Filled Gyroscope Property During High-Speed Revolution

The above results can be summarized as follows: Not very great stability could be obtained for about 600 rpm, although it is expected that a fluid-filled gyroscope with a diameter of 35 cm and injected mercury quantity of about 3 kg is likely to maintain the attitude of a compact robot when it is revolved at 3,000 rpm.

## 7.2 Bidirectional Stabilization

The adoption of this method makes it possible to cancel the Coriolis force, a disadvantage for both fluid-filled and rigid gyroscopes. The addition of this function makes it possible to cancel yawing as well as pitching.

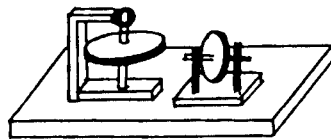


Figure 13. Bidirectional Stabilization Gyro System

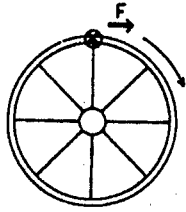


Figure 14. Force Working Upon Gyroscope

### 8. Applications of a Fluid-Filled Gyroscope

This system was designed to stabilize the attitude of a mobile robot. The increased number of revolutions of a gyroscope makes it possible to obtain quite large apparent inertial mass despite its compactness. Therefore, it is believed that the system can display its effectiveness not only in the case shown in Figure 15, but also in the cases presented in Figures 16 and 17.

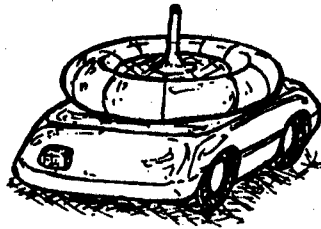


Figure 15. Gyroscope Mounted on a Vehicle



Figure 16. Safety Voyage for Small Vessels

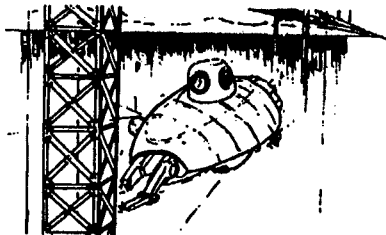


Figure 17. Attitude Stabilization for Underwater Working Robot

Only a few application examples could be presented in this article, but it is deemed that a fluid-filled gyroscope capable of producing a great output despite its relative compactness can find applications in a quite wide portion of the mobile robot field.

## 9. Conclusion

The application of a fluid-filled gyroscope to the attitude stabilization of a mobile robot has been studied, and a basic experiment has confirmed its effectiveness. However, some problems remain to be solved, such as the weight of the gyroscope body, the dynamic load on the gyro shaft, travel controllability, and the selection of a bandwidth to permit robot attitude stabilization. Also, the autonomous stabilization alone of a gyroscope fails to deal with some situations. However, it is deemed that a better performance can be displayed by combining a robot with an active stabilization system. For example, it may be effective to combine a robot with a system which detects, through its sensors, the tilt of a floating-type fluid-filled gyroscope with a double spherical structure, transmits the value to its shock absorber, etc., thereby controlling the robot attitude. In the future, the above problems will be studied, necessary improvements will be made, and experiments of a high-speed-travel-type mobile robot equipped with a system to stabilize the robot attitude will be conducted.

## References

1. Barclay's Physics Course, "Dynamics," (Maruzen Co.).
2. Pros and Cons, "Fluid Rotor Gyros," CONTROL ENGINEERING, 1963, pp 105-109.
3. Kanai, Tahara, Hayakawa, and Nagasono, "Attitude Sensors," JAPAN AEROSPACE SOCIETY JOURNAL, Vol 30 No 336, January 1982, pp 15-21.
4. Roger F. Gans, "Dynamics of a Near-Resonant Fluid-Filled Gyroscope," AIAA JOURNAL, Vol 22 No 10, October 1984, pp 1465-1471.
5. O.M. Grodestskii and D.M. Klimov, "Applicability of the Quasi-stationary Method for Investigating the Dynamics of a Gyroscope With a Liquid Suspension," J. SOLID, Vol 17, 1982, pp 4-6.

## High-Speed Line Tracing Technique Using CCD Camera

43064062 Tokyo 4TH INTELLIGENT ROBOTS SYMPOSIUM PAPERS in Japanese  
13/14 Jun 88 No 215 pp 223-228

[Article by Chie Kasuga and Taiya Nomura, Shibaura Institute of Technology;  
and Fumio Harajima, the University of Tokyo: "A Modification Method of  
Control Signals for Curve Tracing Mobile Robots Is Proposed"]

### [Text] 1. Introduction

With regard to a curve tracing mobile robot using guidance lines, it has been demonstrated that it is possible for a robot to travel markedly faster than when using the conventional method involving detecting a guidance line directly below the robot, by directing the curvature of a guidance line ahead of the robot and by allowing the robot to travel in a manner approximate to it using an arc of circle. In this case, more accurate and faster travel following the curve becomes possible through the adequate modification of control signals, in which the time from the detection of the curvature of the guidance line to the output of control signals and the time lag during control motions are studied. This report proposed a method to modify such control signals, with its effectiveness confirmed through simulations.

### 2. Curve Tracing Mobile Robot

As presented in Figure 1, a CCD camera is mounted on the projected segment of a mobile robot's forehead and is directed toward the floor surface ahead. The robot uses a two-wheel vehicle. The length between the wheel shaft center and the focal distance is L.

#### 2.1 Guidance Line Curvature Detection by CCD Camera

As presented in Figure 2, given that the mobile robot at point A detects point E on the guidance line perpendicular to line AB on the extended line ahead at point B at a distance L from point A, let the distance BE be Y. Suppose that the mobile robot directed toward point B at point A passes point E on an arc in  $\Delta t$  seconds, and the radius of curvature of the circle is R, with

$$R = \frac{M}{2\cos(90^\circ - \theta)} \quad (1)$$

where

$$M = \sqrt{L^2 + Y^2} \quad (2)$$

$$\theta = \tan^{-1} \frac{Y}{L} \quad (3)$$

Figure 3 presents a locus of the outer and inner wheels of a mobile robot while traveling from point A along an R-radius circle to point E. If  $\angle AOE$  is  $\alpha$ , the travel distance P of the outer wheel can be expressed as:

$$P_o = \alpha \left( R + \frac{T}{2} \right) \quad (4)$$

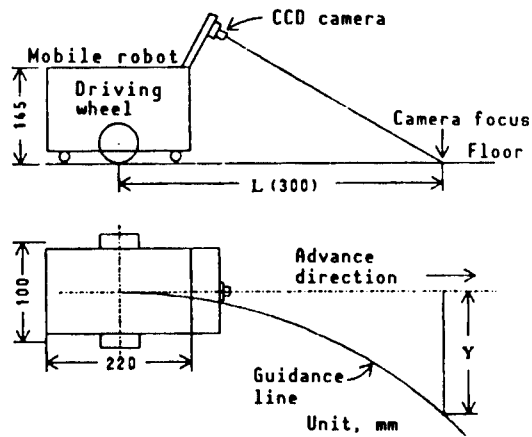


Figure 1. CCD Camera Mounting Position and Focal Distance L

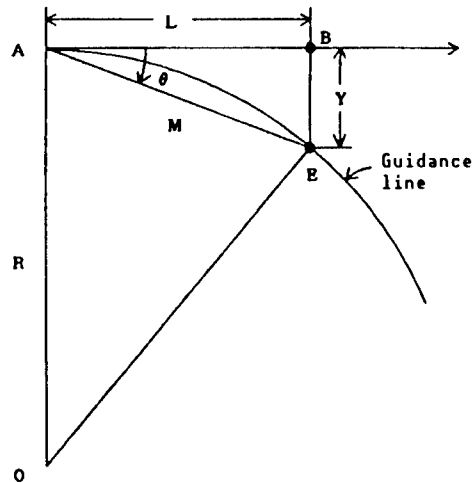


Figure 2. Diagram of the Radius of Curvature Being Obtained From the Slippage of the Robot Advance Direction

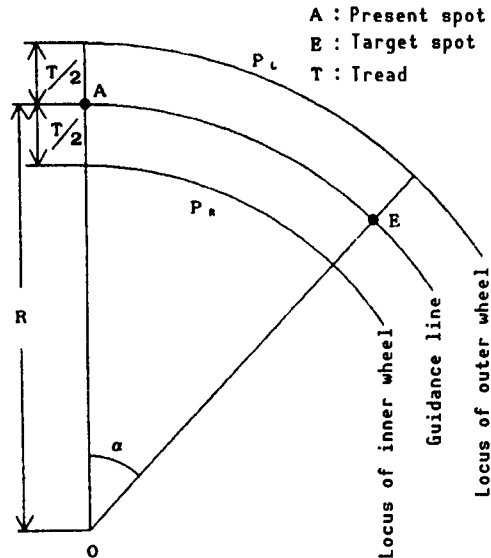


Figure 3. Loci of Right/Left Wheels

The travel distance of the inner wheel can be expressed as:

$$P_R = \alpha \left( R - \frac{T}{2} \right) \quad (5)$$

Let the angular velocities of the outer and inner wheels be  $\theta_L$  and  $\theta_R$ , respectively, and the wheel radius be  $r$ . Then, the travel distances of the two wheels in  $\Delta t$  seconds can be expressed as:

$$P_L = \theta_L \cdot r \cdot \Delta t \quad (6)$$

$$P_R = \theta_R \cdot r \cdot \Delta t \quad (7)$$

Therefore, the speed ratio of the outer wheel to the inner wheel necessary for the circular movement with the radius of curvature  $R$  can be expressed as:

$$\frac{\theta_R}{\theta_L} = \frac{P_R}{P_L} = \frac{R - T/2}{R + T/2} \quad (8)$$

The right and left wheels are driven by separate DC motors and their speeds are proportional to the voltage impressed to each motor. Therefore, let the impressed voltage of the motor to drive the outer wheel and that of the motor to drive the inner wheel be  $V_L$  and  $V_R$ , respectively, and

$$V_R = \frac{R - T/2}{R + T/2} \times V_L \quad (9)$$

In order to allow the robot to travel as fast as possible, the largest rated value is given to the impressed voltage of the motor driving the outer wheel.

## Simulation

The system presented in Figure 1 can be shown using a block diagram as shown in Figure 4. Reference (3) was used to calculate the coordinates of the centers of the vehicle's wheels driven by motors.

### 3.1 Control Signals Not Taking Time Lag Into Consideration (Method 1)

Figure 5 presents a locus of the center of the wheel shaft of a mobile robot. Let the sampling time to detect the line and the time between its detection and the generation of a signal be  $DT_2$  and  $DT_1$ , respectively. At point  $A_1$ , the mobile robot detects point  $E_1$  on the guidance line at a point a distance  $Y_1$  away from point  $B_1$  perpendicular to line  $A_1B_1$ , and finds from expression (1) the radius of curvature  $R_1$  of the circle, with its center perpendicular to line  $A_1B_1$ , at  $A_1$  which passes point  $E_1$ . Then, from expression (9), it finds the impressed voltage of the inner wheel. During this period, after detecting the guidance line at point  $A_1$ , the robot starts to move according to the new signal beginning at point  $A_1'$ . Therefore, it travels from point  $A_1'$  to point  $A_2$  according to the new signal, and the time required for this is  $DT_2 - DT_1$ . Then, it detects point  $E_2$  at point  $A_2$  in the same manner as before and finds the radius of curvature  $R_2$ . It travels up to point  $A_3$ , according to the previous signals, along the radius of curvature of  $R_2$ . The time chart to generate these signals is presented in Figure 6. The first radius of curvature  $R_1$  can be found as follows: From Figure 7, let the point be  $E(x_E, y_E)$ , which is distance  $Y$  away, in the perpendicular direction, from point  $B$ , a distance  $L$  ahead of the present position  $A(x_1, y_1)$  where the radius of curvature  $R_1$  and the guidance line meet. The radius of curvature of the arc which passes  $AE$  can be expressed as:

$$R_1 = \frac{M}{2\cos(90^\circ - \psi)} \quad (10)$$

where

$$a = x_1 \cos \theta_1 - y_1 \sin \theta_1 - R \cos \theta_1 \quad (11)$$

$$b = -2R(x_1 + L \sin \theta_1) + (x_1 + L \sin \theta_1)^2 + (y_1 + L \cos \theta_1)^2 \quad (12)$$

$$Y = -a \pm \sqrt{a^2 - b} \quad (13)$$

$$M = \sqrt{L^2 + Y^2} \quad (14)$$

$$\psi = \tan^{-1} \frac{Y}{L} \quad (15)$$

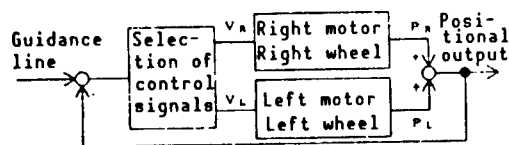


Figure 4. System Block Diagram

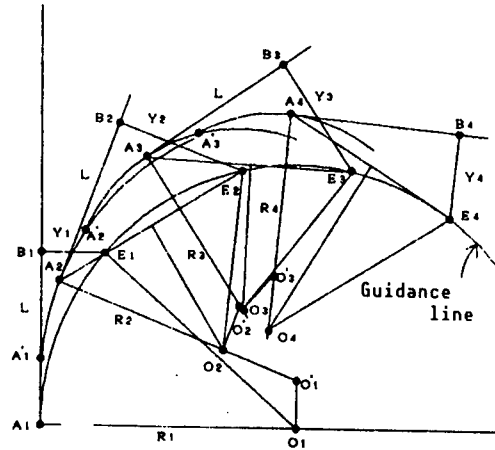
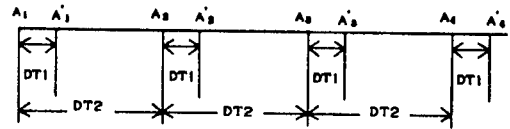


Figure 5. Locus of Vehicle Shaft Center



$A_1, A_2, A_3, A_4, \dots$   
 Center of vehicle when observing guidance line  
 $A'_1, A'_2, A'_3, A'_4, \dots$   
 Center of vehicle when starting to move according to a new signal

Figure 6. Time Chart of Sampling Periods and Time Lag

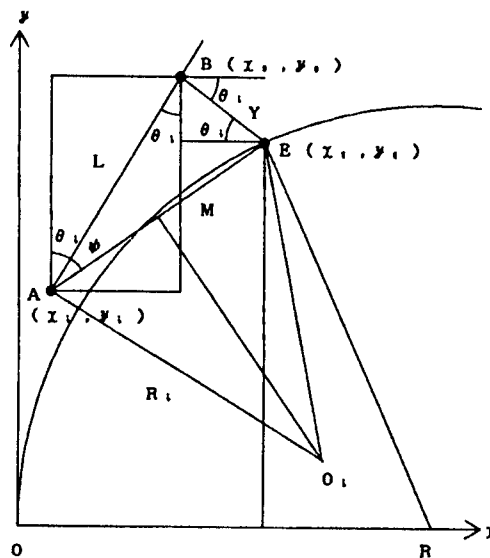


Figure 7. Method To Find Radius of Curvature  $R_1$

Figure 8 presents the critical value  $DT2$  of the sampling period while gradually departing from the circle with a radius curvature of  $R$  and while converging when  $DT1$  is changed in the time chart in Figure 6. This indicates that when a time lag is the same, the longer the distance for detection, the longer the sampling period and the wider the range of stability.

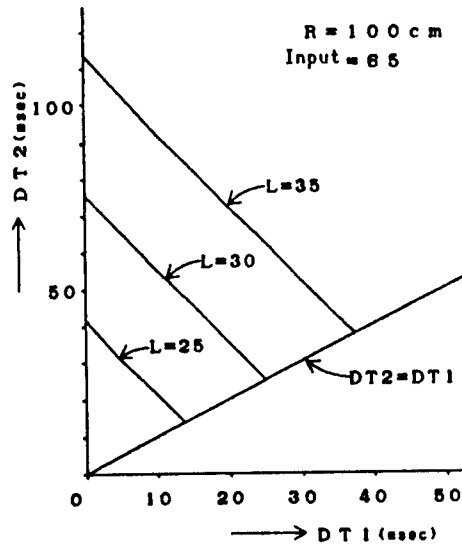


Figure 8. Critical State Sampling Period for Time Lag (Method 1)

### 3.2 Control Signals Taking Time Lag Into Consideration (Method 2)

Figure 9 presents a method to find signals for a mobile robot, taking the time lag into consideration. Suppose that the robot detects point E ( $x_E, y_E$ ) on the guidance line at a point a distance  $Y_0$  away perpendicular to line  $A_1B$  from point B, a distance  $L_0$  away from point  $A_1$ , and moves to point  $A_1'$  ( $x_N, y_N$ ) for a period of  $DT1$  according to the previous signals. Let the intersection of the robot advance direction at  $A_1'$  and the perpendicular from point E be C. Here, radius  $R_1$ , which makes it possible for the robot facing the direction of point C at point  $A_1'$  to pass point E, is found, and a control signal resulting in a radius of curvature of  $R_1$  is input. Let line  $A_1'E$  be M, and

$$M_2 = (x_E - x_N)^2 + (y_E - y_N)^2 \quad (16)$$

then, let  $\angle EA_1'O_1$  be  $\beta + \theta_N$ , and

$$R_1 = \frac{M}{2 \cos(\beta + \theta_N)} \quad (17)$$

where  $\theta_N$  is an angle in the vertical direction to the robot, and

$$\beta = \tan^{-1} \frac{y_E - y_N}{x_E - x_N} \quad (18)$$

Figure 10 presents sampling periods in a critical state for time lags obtained using this method. The relationship between time lags and sampling periods is the same as presented in Figure 6. The difference between methods 1 and 2, however, is that in method 1, the signal to be changed after a delay of  $DT1$  is obtained through the radius of curvature passing both the position at the time of observation and the observation point, while in method 2, the signal is obtained by assuming a position the robot may advance to according to the signal over the period of  $DT1$  and by finding

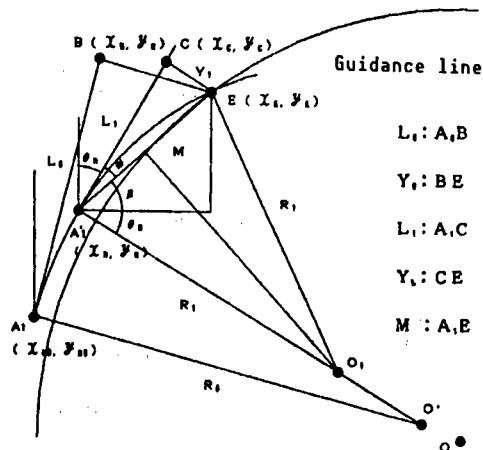


Figure 9. Method for Finding Radius of Curvature When Time Lag Is Taken Into Consideration

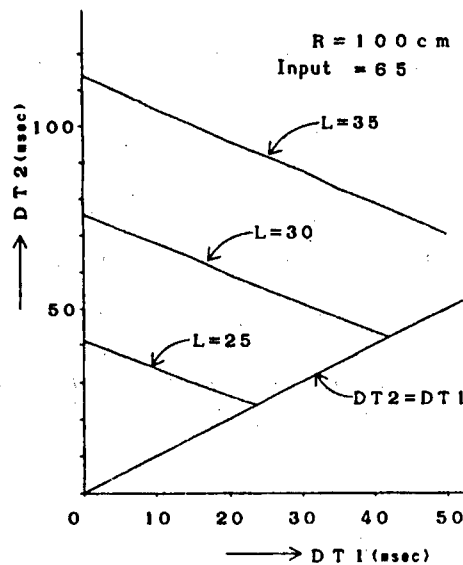


Figure 10. Sampling Periods in Critical State for Time Lag (Method 2)

the radius of curvature which passes both the position (point) and the observation point.

Figure 11 compares the sampling periods in a critical state obtained using both methods 1 and 2. When periods below the line of method 1 are selected for DT2, both methods result in stable sampling periods. When periods between the lines of the two methods are selected, method 2 results in stable sampling periods, while method 1 causes them to diverge. When periods above the line of method 2 are selected, method 2 also causes the divergence.

Figures 12(a) and (b) present values of the vertical slippage of the center of the mobile robot's vehicle shaft from the line on which the radius of curvature is 100 cm. Figure 12(a) indicates that given  $DT1 = 10$  msec, when  $DT2$  is a value of (b), method 1 results in damped oscillations.

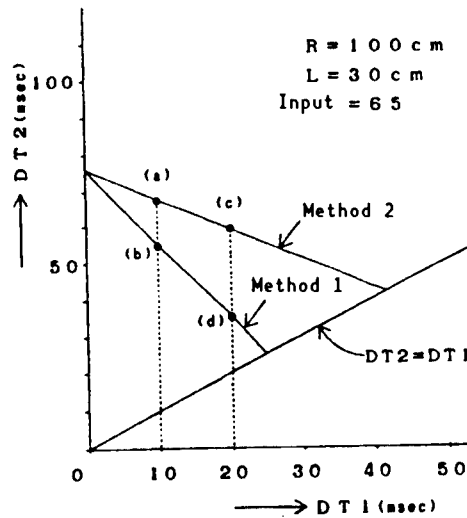


Figure 11. Comparison Between Sampling Periods by Methods 1 and 2

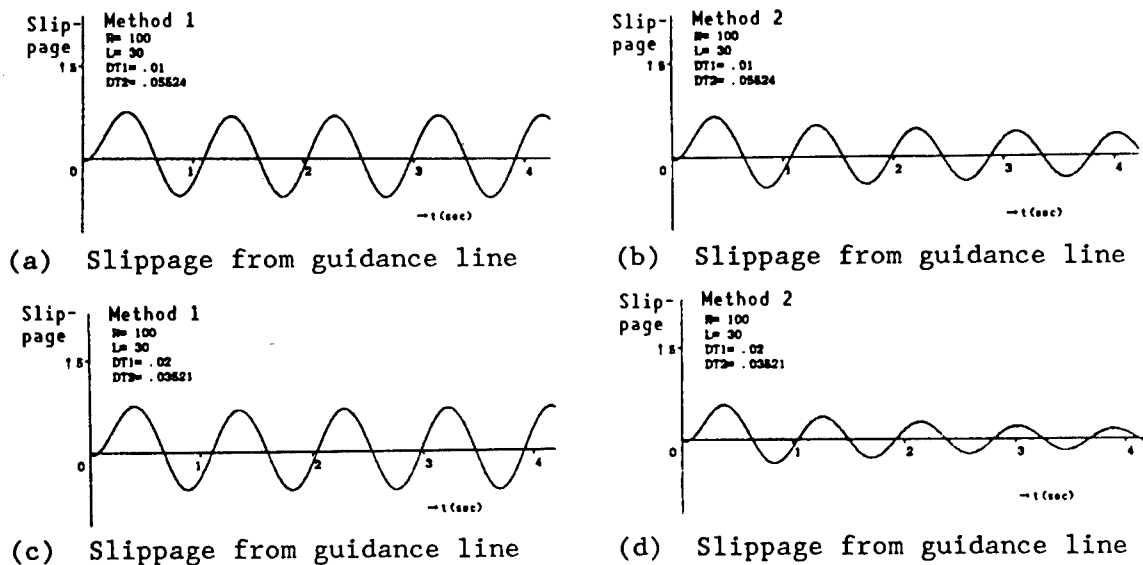
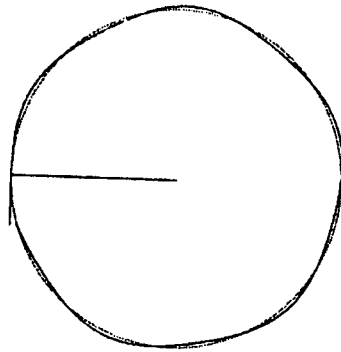


Figure 12.

Figure 12(b) indicates that given  $DT1 = 10$  msec, when  $DT2$  is the same value as (a), method 2 results in continuous oscillations. When  $DT2$  is a value of (a), method 2 results in continuous oscillations and method 1 results in the divergence. The greater  $DT1$  is, the greater the damping effect by method 2 is.

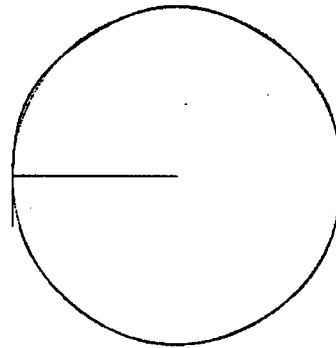
Figure 13 presents the locus of the center of the vehicle shaft of a mobile robot which moves along a 100-cm radius circle. Figure 13(a) presents a case where  $DT1 = 0.02$  second and  $DT2$  is the value of (d) in Figure 11 for method 1, which results in continuous oscillations. Figure 13(b) presents a case where  $DT1 = 0.02$  second and  $DT2$  is the same as by method 1, which results in damped oscillations.

Method 1  
 R= 100  
 L= 30  
 DT1= .02  
 DT2= .03521



(a) R = 100 cm, Method 1

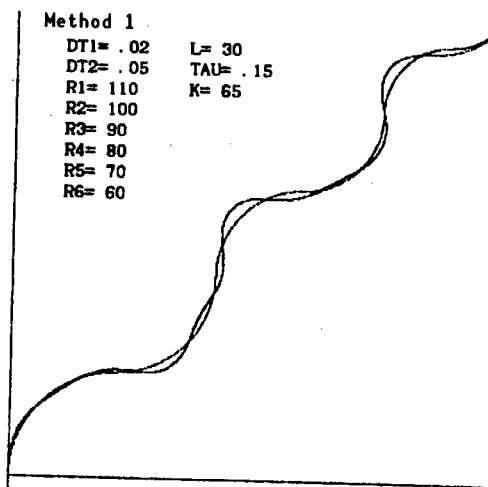
Method 2  
 R= 100  
 L= 30  
 DT1= .02  
 DT2= .03521



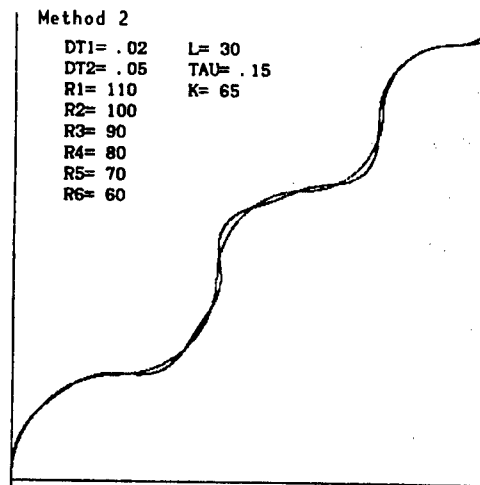
(b) R = 100 cm, Method 2

Figure 13. Locus Along a Circle With a Radius of Curvature of R

Figure 14 presents a locus of the center of the vehicle shaft of a mobile robot which moves along a combination of quarter circles with different radius of curvature. Figure 14(a) is that obtained by method 1 and Figure 14(b) by method 2. For both, DT1 = 0.02 second and DT2 = 0.05 second, with DT2 being between (d) and (c) in Figure 17, however, since R varies, method 1 does not cause the robot to get off the course.



(a) Method 1



(b) Method 2

Figure 14. Locus Along Quarter Circle

### 3.3 Relationship Between Observation Points and Speeds

In Figures 8 and 10, it was found that when the value of L was large, the sampling period DT2 can be lengthened. Then, a study was made of whether the travel speed could be accelerated, given constant DT2 and the larger L. Since speeds are proportional to impressed voltages, the relationship between L and the magnitude of voltages impressed to the motor of the outer wheel was studied (Figure 15). Impressing voltages greater than this causes the robot to stray from curves with a radius of curvature of 100 cm. It is found from this figure that, in both methods, the speed is nearly

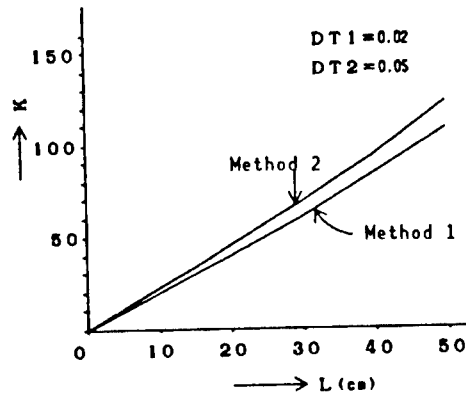


Figure 15. Observing Points and Speeds ( $R = 100$  cm)

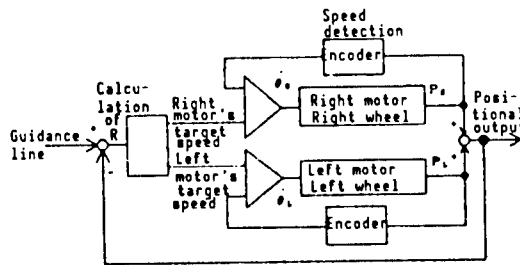


Figure 17. System Block Diagram

proportional to  $L$ , and also in both methods, the speed is stable for values of  $K$  below the graph lines.

#### 4. Travel Experiment

Figure 16 [not reproduced] presents the exterior of the robot used for the experiment. The CCD camera detects a line 30 cm ahead of the center of the robot's vehicle shaft, with a tread of 10 cm. Figure 17 presents a block diagram of the system. Capable of detecting slippage to widths of about  $\pm 10$  cm for  $L$  of 30 cm, the robot can theoretically travel along curves with  $R$  of up to 50 cm. However, since the width of the slippage actually becomes greater due to the direction of the vehicle body and the slippage from curves, the radius must be greater. In the experiment, the robot could travel at a speed of about 1.1 m/seconds along a combination of curves with  $R$  of 75 cm and above by method 1 for  $DT1$  and  $DT2$  of 5 m/seconds along a combination of curves with  $R$  of 75 cm and above by method 1 for  $DT1$  and  $DT2$  of 5 m/seconds and 40 m/seconds, respectively. The CCD camera uses a linear image sensor with 128 signal image elements. In the experiment, the use of a battery caused the voltage value to change before and after travel. The rate of the voltage impressed on the motors was determined by changing the pulse width, however, changes in the pulse height prevented the motors from revolving at target speeds. For this reason, the rotation angles of the motors were detected by the encoders and actual pulse widths were determined in order to achieve target speeds.

## 5. Conclusion

It was confirmed that the method taking into consideration the time lag between the detection of the slippage of the guidance line against the robot advance direction and the selection of control signals results in stable sampling periods, when compared with the method which did not take the time lag into consideration for the same sampling periods. In other words, it can be said that when sampling periods are stable, the former method can increase speeds when compared with the latter.

## References

1. Kasuga, Suzuki, and Harijima, "High Speed Line Tracing by Mobile Robots," 4th Japan Robotics Society's Academic Meeting, 1986, pp 201-202.
2. Kasuga, Takata, Gotoh, and Harajima, "Line Tracing Using CCD Linear Image Sensor," 5th Japan Robotic Society's Academic Meeting, 1987, pp 119-120.
3. Tsumura, et al., "Automatic Guidance of Mobile Equipment Through Directions of Mapped Courses," SYSTEMS & CONTROL, Vol 25 No 3, 1981, pp 167-174.

## Mobile Robot Position Referencing Using Map-Based Vision Systems

43064062 Tokyo 4TH INTELLIGENT ROBOTS SYMPOSIUM PAPERS in Japanese  
13/14 Jun 88 No 216 pp 229-234

[Article by Takashi Tsubouchi and Shinichi Yuta, University of Tsukuba:  
"Reference of Positions More Precise Than Those Through Dead Reckoning Using  
Maps, Picture Images, and Positions Through Dead Reckoning"]

### [Text] 1. Introduction

The authors have previously presented a structuring method for a vision system using maps and a color image processing method based on it<sup>1,2</sup> for mobile robots, followed by proposals of a mapping method<sup>3</sup> and a matching method for actual visual images obtained with ones obtained from a map.<sup>4</sup> This visual system was devised for mobile robots traveling in indoor environments, such as corridors in buildings, to recognize picture images produced by a telecamera and mapped environments and to identify their own positions. Its configuration is presented in Figure 1.

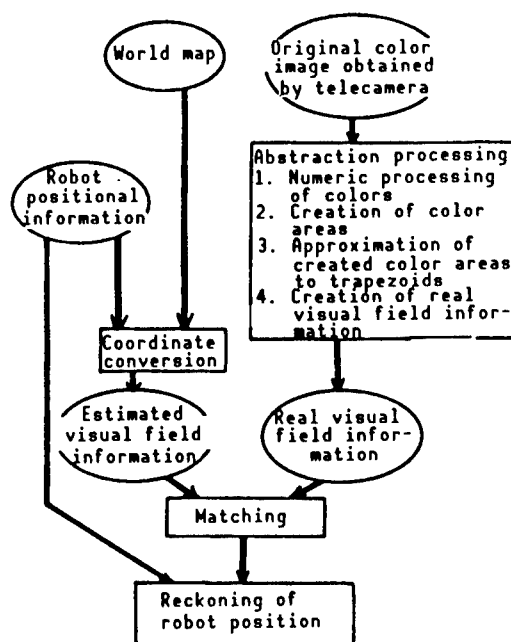


Figure 1. Configuration of Visual System

This visual system's color telecamera is mounted on the front of a mobile robot so that the camera's optical axis is parallel to the floor and is directed ahead of the robot. The system fetches picture elements colored through the fetching processing of hue values of individual picture elements from color picture images obtained by the telecamera, collects adjacent isochromatic picture images, and creates color areas. Since in corridors in buildings, for example, parallel sides of a large number of objects look like perpendicular trapezoids, the system approximates color areas it creates in such trapezoids. In this way, the colored object included in a given picture image is approximated to a trapezoid of the same color and abstracted as the value of the color (hue value) and the vertices of the trapezoids on an image plane (Figure 2 [not reproduced]).

A map of the environment a mobile robot travels in is provided so that colored objects can be created as a group of trapezoids, in the same form as real visual field information, when their observing positions are provided on the map. A group of trapezoids created using this map and their observing positions on the map is called "estimated visual field information." A mobile robot can find its position through dead reckoning based on the accumulated revolutions of its wheels. When the matching of the estimated visual field information, created using the observing position based on dead reckoning, with the real visual field information obtained from picture images actually obtained at their observing positions, regards these two pieces of visual information as identical, the present position of the robot is believed to have been confirmed. This matching process is conducted at high speeds through comparing the colors of trapezoids and the positions of the vertices. However, if this matching process determines that the real visual field information provided matches the estimated visual field information, the observing positions used to create the estimated visual field information do not necessarily agree with the observing positions of the real picture images based on values containing accumulated errors obtained through dead reckoning, which are used for the former. In other words, from the authors' experience, it is apparent that it is quite difficult technically for a mobile robot, after traveling 10-odd meters, to control accumulated positional errors to within several tens of centimeters. Therefore, in a comparison between the real and estimated visual field information which were determined to be matching, as presented in Figure 3, the position on the image plane of the trapezoid judged to be corresponding to the object dislocates, which reflects an error between the observing position obtained through dead reckoning and the actual observing position. It is believed, however, that a more precise observing position can be reckoned from the slippage in positions of corresponding trapezoids, the observing position used to create the estimated visual field information, and the object position indicated on the map. This article describes robot position referencing and related experimental examples.

On the other hand, Charila, et al.,<sup>5</sup> and Takeuchi, et al.,<sup>6</sup> have been conducting studies aimed at finding as precise a robot position as possible, based on the information from external sensors, such as a range finder, and its position obtained through dead reckoning, while taking errors to be caused by these sensors into consideration, when no map is available to

provide information regarding travel environments for mobile robots or when the map available is imperfect. This article describes a study for referencing a more precise robot position than that available through dead reckoning, using a map, picture images, and its position obtained through dead reckoning when, with regard to the travel environment of mobile robots, information necessary for a robot to recognize an environment can be provided, in advance, as a map.

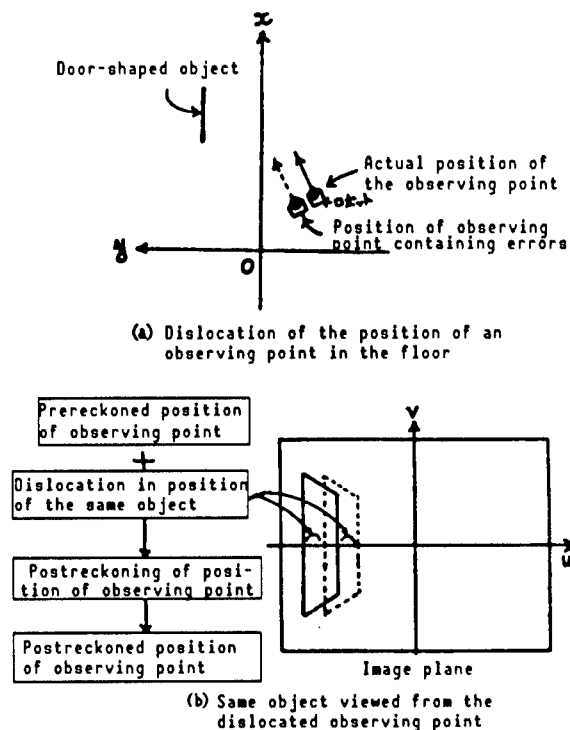


Figure 3. Reckoning of Robot Position

Incidentally, finding the position of an observing point through dead reckoning in order to create the estimated visual field information will be referred to as "prereckoning of observing point," and the position of an observing point as "prereckoned position of observing point." Also, the algorithm to be described later in this article is referred to as "postreckoning of observing point," and the position of an observing point thus obtained as "postreckoned position of observing point."

## 2. Reckoning of the Position of the Observing Point of Input Picture Image

### 2.1 Algorithm for Postreckoning of Observing Points

As stated above, a telecamera mounted on a mobile robot has its optical axis parallel to the floor surface. As for the degree of freedom of the attitude of a telecamera, since a mobile robot only travels on the floor surface in a two-dimensional manner, the following 3 degrees of freedom are sufficient to take into account the degree of freedom of the attitude of a telecamera --2 degrees of freedom for the position in two-dimensional planes involving the floor surface, and 1 degree of freedom for the rotation around the

vertical axis. After taking these degrees of freedom into consideration, the only dislocation remaining in the position of an observing point is that of the trapezoids in the visual field information in the direction of the horizontal axis on the image plane. Therefore, the dislocation in the position of an object in the direction of the horizontal axis is the only consideration that need be taken. Hereunder, let the horizontal axis of an image plane and the axis perpendicular to it be the u-axis and v-axis, respectively.

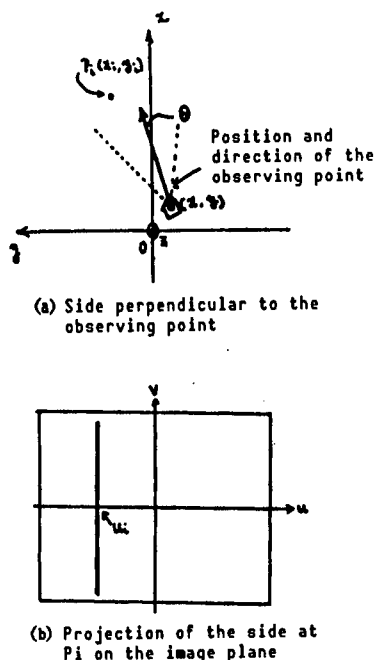


Figure 4. Parallel Side to Z-Axis and Its Projection on Image Plane

As in Figure 4, consider the plane x-y in a map corresponding to the floor plane on which a mobile robot moves, with the z-axis perpendicular to it. Suppose that the position of the observing point of the robot in this coordinate system lies at  $(x, y, \theta)$ --x and y represent the x- and y-coordinates and  $\theta$  the angle formed by the camera's optical axis and x-axis. Also, suppose that a side of the object in this coordinate plane parallel to the z-axis lies at  $P_1(x_1, y_1)$ , and the side becomes a line parallel to the u-axis on the image plane. The value of the u-coordinates of the line,  $u_1$ , can be obtained as follows

$$u_1(x, y, \theta) = -r \frac{(x_1 - x) \sin \theta - (y_1 - y) \cos \theta}{(x_1 - x) \cos \theta + (y_1 - y) \sin \theta} \quad (2.1)$$

where, r is a constant for the angle of the visual field of a camera lens. This calculation is conducted when creating the estimated visual field information,  $x_1$  and  $y_1$  are obtained from the map, and values obtained from the robot's travel system, etc., through dead reckoning are used for x, y, and  $\theta$ .

Suppose that, from the corresponding relationship among trapezoids in two items of visual field information obtained through matching the real visual

field information with the estimated visual field information, the value of the  $u$ -coordinates of the side of the object corresponding to the side  $P_i$  is found to be  $u_i$ . With regard to  $n$  sides of such an object, let  $x$ ,  $y$ , and  $\theta$  be a postreckoned position which minimizes the error function for the  $u$ -coordinate value, which is expressed as

$$N = \sum_{i=1}^n w_i (u_i' - u(x, y, \theta))^2 \quad (2.2)$$

where  $w_i$  represents the weight corresponding to  $u_i'$  and  $u_i$ . A postreckoned position will hereafter be represented as  $(X, Y, \Theta)$ . A postreckoned position  $(X, Y, \Theta)$  can be obtained through the following calculation. If the slippage between a postreckoned position  $(X, Y, \Theta)$  and a prereckoned position  $(x, y, \theta)$  is  $\Delta x$ ,  $\Delta y$ , and  $\Delta \theta$ , and setting

$$X = x + \Delta x, \quad Y = y + \Delta y, \quad \Theta = \theta + \Delta \theta \quad (2.3)$$

we can find  $\Delta x$ ,  $\Delta y$ , and  $\Delta \theta$  through a calculation by providing a condition to make the value of expression (2.2) minimal, and reckon  $X$ ,  $Y$ , and  $\Theta$ , based on the values of expression (2.3) and the known values of  $x$ ,  $y$ , and  $\theta$ . If the values of  $\Delta x$ ,  $\Delta y$ , and  $\Delta \theta$  are extremely small, they can be expanded as

$$u_i(X, Y, \Theta) = u_i(x, y, \theta) + A_{ix}\Delta x + A_{iy}\Delta y + A_{it}\Delta \theta \quad (2.4)$$

where

$$A_{ix} = \frac{\partial u_i}{\partial x}, \quad A_{iy} = \frac{\partial u_i}{\partial y}, \quad A_{it} = \frac{\partial u_i}{\partial \theta}$$

Substituting expression (2.4) for expression (2.2), we have

$$N = (\mathbf{U} - \mathbf{A}\Delta\mathbf{x})^t \mathbf{W}(\mathbf{U} - \mathbf{A}\Delta\mathbf{x}) \quad (2.5)$$

where  $\mathbf{A}^t$  represents the transposition of  $\mathbf{A}$ .  $\mathbf{W}$  and  $\mathbf{A}$  are matrices and can be expressed as

$$\mathbf{W} = \begin{pmatrix} w_1 & & & \\ & w_2 & & 0 \\ & & \ddots & \\ & & & w_{n-1} \\ & & & & 0 \end{pmatrix} \text{ (weight matrix)}$$

$$\mathbf{A} = \begin{pmatrix} A_{1x} & A_{1y} & A_{1t} \\ A_{2x} & A_{2y} & A_{2t} \\ \vdots & \vdots & \vdots \\ A_{n-1x} & A_{n-1y} & A_{n-1t} \end{pmatrix}$$

$$\mathbf{U} = \begin{pmatrix} u_1' - u_1 \\ u_2' - u_2 \\ \vdots \\ u_{n-1}' - u_{n-1} \end{pmatrix}$$

$$\Delta \mathbf{x} = \begin{pmatrix} \Delta x \\ \Delta y \\ \Delta \theta \end{pmatrix}$$

Suppose that in expression (2.5),  $M$  is  $M + \delta M$  when  $\Delta X$  changes into  $\Delta X + \delta \Delta X$ . Then, ignoring the secondary term and above of  $\delta \Delta X$ , we have

$$\delta M = -2(\mathbf{U}^T \mathbf{W} \mathbf{A} - \Delta \mathbf{x}^T \mathbf{A}^T \mathbf{W} \mathbf{A}) \delta \Delta \mathbf{x} \quad (2.6)$$

For the above expression to hold for any  $\delta \Delta X$ , we need

$$(\mathbf{U}^T \mathbf{W} \mathbf{A} - \Delta \mathbf{x}^T \mathbf{A}^T \mathbf{W} \mathbf{A}) = 0 \quad (2.7)$$

Therefore, the requirement for  $\Delta X$  is

$$\Delta \mathbf{x} = (\mathbf{A}^T \mathbf{W} \mathbf{A})^{-1} \mathbf{A}^T \mathbf{W} \mathbf{U} \quad (2.8)$$

From this expression,  $\Delta X$  or  $(\Delta x, \Delta y, \Delta \theta)^t$  can be obtained and, from expression (2.3),  $(X, Y, \theta)$  can be computed as the postreckoned position of the robot.

## 2.2 Evaluation of Postreckoning of Observing Points Through Accuracy Simulation

A simulation to find a postreckoned position of an observing point through a simple environmental model using expression (2.8) was conducted to examine how accurately the postreckoning of the position of an observing point could be carried out using the above algorithms.

As an environmental model, a simple, corridor-looking environment presented in Figure 5 was used. The doors in both walls of the corridor are the objects in this environment. On this model, observing point A was set at  $(x, y, \theta) = (-39.5, 65, 12.2^\circ)$ , while the other, B, was set in the periphery of A, and the values for the u-coordinates of the sides parallel to the z-axis of every object on the image plane were obtained using expression (2.1) from each observing point. The difference in the values of the u-coordinates of the sides of the same object resulted from the dislocation occurring between the positions of the two observing points and, based on these values and the position of observing point B, the position of observing point A was computed using expression (2.8), where weight matrix  $W$  was regarded as a unit matrix. Sufficient accuracy was given to variations necessary for calculations, using double precision floating point numbers. The angle of the visual field of a camera was supposed to be 50 degrees, which would respond to a camera with a 2/3-inch image pickup tube using a lens of approximately 8 mm. Also, a simulation was conducted with 1/256th of the length of the area on the u-axis of the image plane within the camera's visual field as the unit length (a picture element length) of the image plane.

The result of this simulation is presented in Figure 6. Figure 6(a) presents the difference between the actual position and the postreckoned position of observing point A ( $\delta x, \delta y, \delta \theta$ ) when observing point B was moved

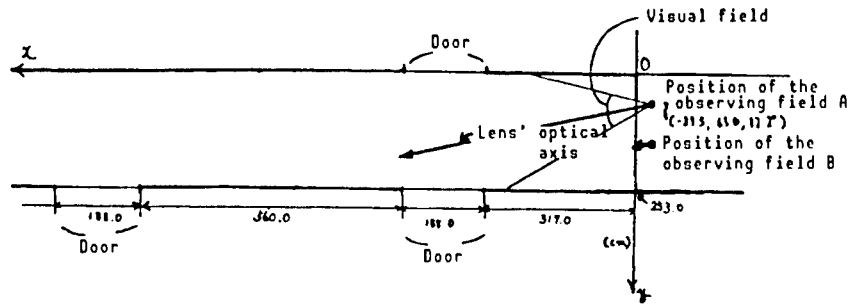


Figure 5. Model in Actual Environment Used for Simulation

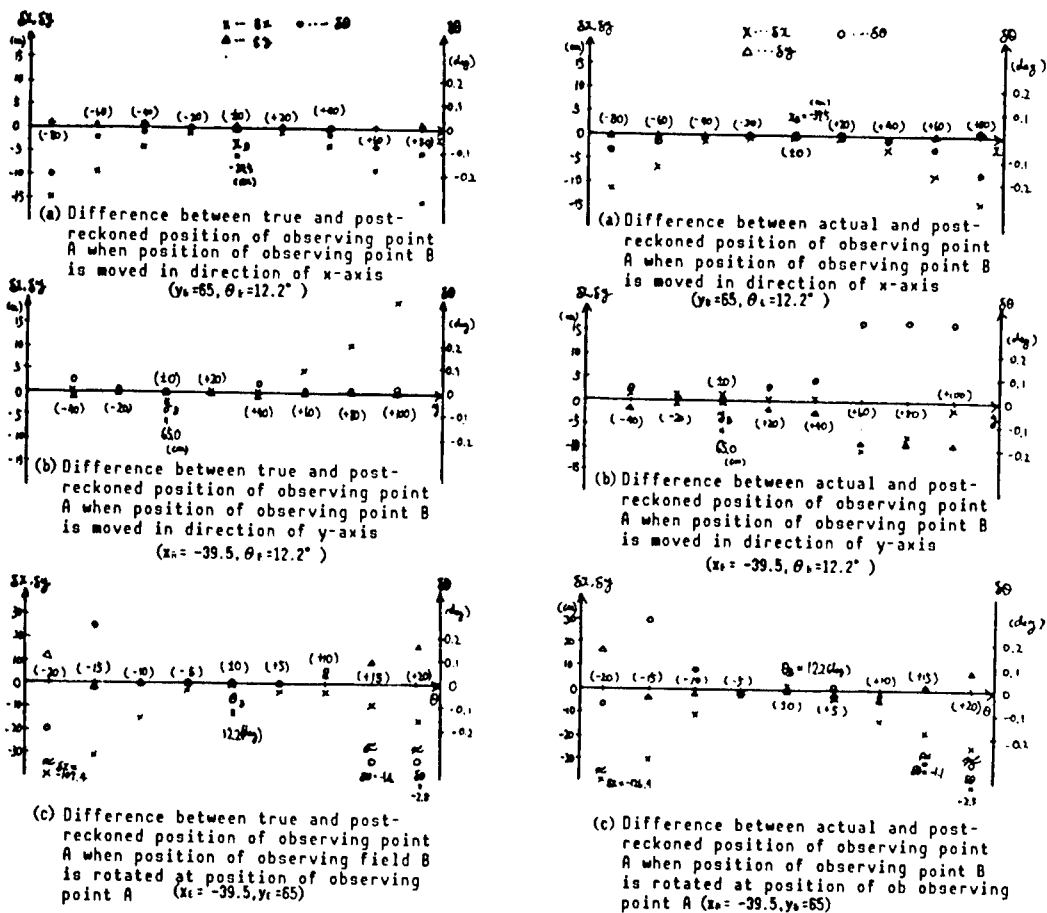


Figure 6. Simulation for Precision Evaluation 1

Figure 7. Simulation for Precision Evaluation 2  
(When errors are provided in the picture images of the objects viewed from observing point A)

from the position of observing point A in the direction of the x-axis. Figure 6(b) presents the difference between the two when observing point B is moved from observing point A in the direction of the y-axis, while

Figure 6(c) presents the same when observing point B is rotated at the position of observing point A. These figures indicate the nearer  $\delta x$ ,  $\delta y$ , and  $\delta \theta$ , the more precise the postreckoned value. As can be seen from Figure 6, in the example presented here, the postreckoned value of the position of observing point A is obtained allowing an error of several centimeters for the actual position of observing point A when the position of observing point B dislocates several tens of centimeters from the position of observing point A. From this, it has been found that when the calculation of observing points is precise enough, the robot position can be calculated with sufficient precision.

In addition, a simulation taking practical problems into account was conducted. Sufficient precision can be achieved for the position of an object on the image plane in the estimated visual field information, while for the position of the object on the actual picture image, precision with a unit of one picture element of the image can be achieved at best. Then, the precision of the values of the u-coordinates of the object was experimentally decreased by regarding the object on the image plane obtained at observing point A under the above experimental conditions as included in the actual visual field information. In other words, errors of uniform distribution of below  $|1/2|$  were provided to the values of the u-coordinates, and the same simulation experiment as above was conducted. The postreckoned position of the observing point obtained as a result of the experiment is presented in Figure 7. It has been found that when a dislocation of several tens of centimeters occurs between the positions of the observing points in the plane where the robot travels, the difference between the position of the actual observing point and that of the postreckoned observing point is about 10 cm, although the precision is decreased by providing uniform distribution errors to the values of the u-coordinates obtained at observing point A on the image plane of the object.

Considering that a robot frame is as large as several tens of centimeters square, an error of about 10 percent of the size of the robot frame is believed to be allowable. From the authors' experience, the positions of parallel sides of trapezoids in the real visual field information acquired through processing actual color picture images can be obtained with an error of about one picture element through averaging those positions and the positions of corresponding objects in the actual picture image.

### 3. Postreckoning Experiment of Positions of Observing Points

#### 3.1 Postreckoning Experiment of Positions Observing Points in Actual Environment

A postreckoning experiment involving a robot position was conducted in an actual corridor, as shown in Figure 8. A picture image by the telecamera actually used is presented in Figure 9(a) [not reproduced]. This picture image was fetched by a resolution of 256 x 240 picture elements. Figure 9(b) [not reproduced] presents a group of trapezoids based on the actual visual field information created through processing this original picture image. Table 1 presents errors between the positions of the u-coordinates

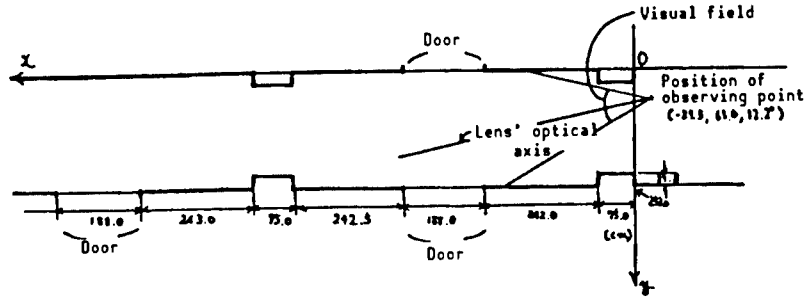
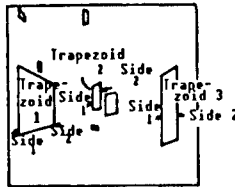


Figure 8. Example of Actual Environment

Table 1. Slippage in u-Axis Direction Between Actual Picture Images and Objects in Real Visual Field Information

|    | Ob-ject zoid 1 | Ob-ject zoid 2 | Ob-ject zoid 3 |
|---|----------------|----------------|----------------|
|   | Side Side      | Side Side      | Side Side      |
| Dislocation in positions of trapezoids in real visual field information based on positions of objects in actual picture image (picture element) | ±0 ±0          | -1 +2          | -1 -2          |

Group of trapezoids in Figure 9(b)

of the parallel sides of the trapezoids in the actual visual field information and the positions of the corresponding sides in the original picture image. A maximum error of about two picture elements is produced. Postreckoning of the positions of observing points was also conducted through actually measuring the positions of the telecamera, using a tape measure, providing the positions adjacent to the positions of those observing points as the prereckoned positions, and using the values of the u-coordinates of objects calculated from a map of this environment experimentally constructed in a computer and the positions of the objects based on the actual visual field information.

Table 2. Experimental Results in Actual Environment

| Measured position of observing point<br>x (cm) y (cm) θ (deg.) | Prereckoned position of observing point |      |      | Dislocation caused by calculation |       |     | Postreckoned position of observing point |      |      |
|--|---|------|------|-----------------------------------|-------|-----|--|------|------|
|  | x                                       | y    | θ    | Δx                                | Δy    | Δθ  | x  | y    | θ    |
| -39.5 65.0 12.2  | -20.0                                   | 65.0 | 10.0 | -10.4                             | -4.9  | 3.2 | -30.4                                    | 60.1 | 13.2 |
|  | -40.0                                   | 90.0 | 12.0 | -5.1                              | -27.7 | 1.0 | -45.1                                    | 62.3 | 13.0 |
|  | -60.0                                   | 95.0 | 12.0 | 14.7                              | -34.0 | 1.1 | -45.3                                    | 60.2 | 13.1 |
|  | 0.0                                     | 25.0 | 10.0 | -32.0                             | 31.7  | 3.4 | -32.0                                    | 58.7 | 13.4 |

These results are presented in Table 2. Also, in this example, while the difference between the prereckoned and the measured position of the observing points is approximately 10 cm, the difference between the postreckoned and the measured position of the observing points is several centimeters. The directions of the observing points are calculated with a difference of about 1 degree. Taking into consideration the results presented in Section 3.1, this is an appropriate value and it has been found that a mobile robot's precise position can be calculated using the methods described above.

### 3.2 Study of and Time Required for Processing

The algorithm for calculating the positions of this robot's observing points has been described in C language, which operates through an OS9/68000 on the AVAL Co.-made computer CX10. The above calculations took about 0.2 second, which is thought to be a sufficient speed on a practical basis despite the fact that the computer used was not very fast. Although most numeric calculations were conducted using a double precision floating point operation, they were executed at this high speed. Therefore, the time required for calculations can be reduced to tenths of the above value through the integral processing of the operation and the use of a fast numeric operation processor and, therefore, real-time processing can be expected.

### 4. Conclusion

For the mobile robot visual system using a map as proposed by the authors, an algorithm was presented to calculate seemingly more precise observing point positions using the dislocation between the matching positions of mutually corresponding trapezoids existing in the actual and reckoned visual field information. In addition, a simulation using this algorithm and an experiment in an actual environment were conducted. The experimental results have been presented, demonstrating that the robot position referencing method proposed in this article is effective.

### Acknowledgement

The authors wish to express their gratitude for the guidance received from Junichi Iijima, an assistant at the Information Engineering Department, University of Electrocommunications. They also wish to express their thanks to Nexus Co. for their cooperation regarding the peripheral equipment of the image input display unit.

Incidentally, part of this research has been conducted based on the bounty research (A)62790203, the subvention for the scientific research expenditures by the Ministry of Education.

### References

1. Tsubouchi and Yuta, "Visual System Building Method for Robots Moving in Indoor Environments Using a Map and Color Picture Images," Electronic Information and Communication Society's paper journal D (RESEARCH NEWS), Vol J 70-D, No 8, 1987, pp 1685-1688.
2. T. Tsubouchi and S. Yuta, "Map Assisted Vision System of Mobile Robots for Reckoning in a Building Environment," PROC. OF IEEE INT. CONF. ON ROBOTICS AND AUTOMATION, 1987, pp 1978-1984.
3. Ibid., "Visual Sense for Map-Assisted Mobile Robots (2): Expression Method of a Map and Creation of Reckoned Visual Field Information," Japan Robotic Society 4th Academic Meeting Papers, 1986, pp 345-348.

4. Ibid., "Visual Sense for Map-Assisted Mobile Robots (3): Algorithm for Matching Abstracted Real Picture Images With Picture Images Created From a Map," Japan Robotic Society 5th Academic Meeting Papers, November 1987.
5. R. Chatila and J.P. Laumond, "Position Referencing and Consistent World for Modeling Robots," PROC. OF IEEE INT. CONF. ON ROBOTICS AND AUTOMATION, 1985, pp 138-144.
6. Takeuchi, Iijima, and Yuta, "Unknown Environment Probing Method Using Mobile Robots: Simulation Using Sensor Models," 4th Intelligent Mobile Robots Symposium Papers, June 1988.

## Safety Evaluation of Man-Robot System

43064062 Tokyo 4TH INTELLIGENT ROBOTS SYMPOSIUM PAPERS in Japanese  
13/14 Jun 88 No 217 pp 235-240

[Article by Yoshinobu Sato, Industrial Safety Institute; and Koichi Inoue, Kyoto University: "Report No 6--Configuration of the Hazard Control System in Mobile Robots"]

### [Text] 1. Introduction

An intelligent mobile robot is expected to contribute positively to safety and maintainability, such as through alternative execution of hazardous, harmful work including in-pile work and its application as a rescue system in emergency situations.<sup>1</sup> Also, the wide use of robots in our daily lives in the future has been studied.<sup>2</sup>

However, while the expectations for robots are on the rise, it is an unavoidable fact that potential hazards exist in the interference between robots and the environment. When viewed from the standpoint of safety, the intrinsic difference between a conventional system and robot lies in the latter's flexibility. While a conventional system is used exclusively for a single functional purpose, a robot is sometimes used for purposes beyond its manufacturer's intentions. Each stage of a preliminary safety schedule must be made, based on a systematic methodology, according to such procedures as 1) the identification of hazards, 2) a study of means to restrain hazards, 3) stable safety analysis, and 4) quantitative safety analysis.<sup>3</sup> This study has previously reported a hazard identification model,<sup>4</sup> a comprehensive logic model involving accidents caused by strikes by robots,<sup>5</sup> a quantitative model for safety evaluation,<sup>6</sup> and evaluations of actual systems<sup>7</sup> in order to contribute to preliminary safety schedules for robot systems. In the previous report, hazard restraint processes were systematized as the hazard restraint principle (HRP), the configuration principle of a hazard control system (HCS) was generalized as a dissociation principle for action chains, and a conceptual design method of an HCS was proposed.<sup>8</sup> In a so-called information processing system (IPS) comprising sensors and a signal processing segment, significant elements of an HCS, a major difference exists, from the standpoint of safety, between the so-called safety detection-type IPS (SIPS), which avoids hazards caused by power source cutoff interlock and emergency stop through IPS zero output (containing relatively lower output than that for nonavoidance of hazards),

and a hazard detection-type (IPS (DIPS) which avoids those hazards through other means in addition to IPS zero output. The configuration of a SIPS is aimed at achieving a fail-safe signal system in a limited sense, while that of a DIPS is based on maintaining functions through multiple designs. The former has properties excellent from a safety standpoint, such as a generally simple structure and little need to take simultaneous failure in a redundant system into consideration, when compared with the latter. However, which of the two should be adopted depends on conceivable hazards and the entire structure.<sup>9</sup> This report will mention two conceivable types of major hazards involving autonomous mobile robots and will discuss using an A-C model with the configuration of an HCS.

## 2. A-C Model for HCS Conceptual Design Method

### 2.1 Symbol Definition

System components:

R: Autonomous mobile robot  
 ST: Structural system element  
 ES: Power source for R  
 SE: External sensor system for R  
 SI: Internal sensor system for R  
 CP: IPS processing segment of R  
 CA: IPS output segment of R  
 DR: Drive function of R  
 BR: Braking function of R  
 SR: Steering function of R  
 BL: Equilibrium function of R  
 TR: Mobile function of R  
 RS: Skid state of R  
 RB: Equilibrium state of R  
 O: Stationary target  
 M: Mobile target  
 G: Gravity  
 D: External disturbance factor such as surface condition  
 S: Skid promotion factor  
 T: Overturn promotion factor

Action chains and their dissociation models:

$X u_i \rightarrow W$ : Action  $u_i$  is transferred from action factor X to acted-upon factor W ( $u_1=a, u_2=b, u_3=c, u_4=d, u_5=e, u_6=f$ ).

$X u_j \rightarrow W(\odot)$ : Direct cause action  $u_j$  causes damage in W.

$Y u'_j \rightarrow X$ : Dissociation action  $u'_j$  is transferred from dissociation factor Y to X ( $u'_1=a, u'_2=b, u'_3=c, u'_4=d, u'_5=e, u'_6=f$ ).

$(Y g' \rightarrow X) \& (Y g' \rightarrow Y g'' \rightarrow V)$ : Dissociation action  $g' \& g''$  is transferred from Y to X.

- $Y_1 u_k \rightarrow Y_2$ : Control action  $u_k$  is transferred from control factor  $Y_1$  to  $Y_2$  ( $u_1="a"$ ,  $u_2="b"$ ,  $u_3="c"$ ,  $u_4="d"$ ,  $u_5="e"$ ,  $u_6="f"$ ).
- $X u_k \rightarrow W$ : Action chain ( $u_k$ ) is dissociated through dissociation principle  $P_\xi(\xi=1,2,3,4)$ .
- $m, n, q$ : Chaining order of individual chains from the direct cause action chain ( $m=0$ ) ( $m, n, q = 1, 2, 3, \dots$ ).
- $Y_1 \rightarrow X, Y_2 \rightarrow Y_1$ : A dissociation or a control action chain is a single directional control action chain (SFAL).
- $Y_1 \rightleftarrows X, Y_2 \rightleftarrows Y_1$ : A dissociation or a control action chain is a bidirectional control action chain (DFAL).

#### Abbreviations:

- A-C model: Action-change and action chaining model  
 DFAL: Bidirectional control action chain  
 DIPS: Hazard detection type information processing system  
 DP: Dissociation principle  
 EDFAL: Externally dependent bidirectional control action chain  
 HCS: Hazard control system  
 HRP: Hazard restraint principle  
 IPS: Information processing system  
 SFAI: Single directional control action chain  
 SIPS: Safety detection type information processing system

## 2.2 HCS Configuration Principle

The major theorems of the information obtained in the previous report which are to be used in this report are presented below.

Auxiliary theorem 1: The hazard restraint process can be systematized into the following individual HRPs--1) Elimination of the action source; 2) restraint of changes; 3) prohibition of the action chaining creation phase transition; and 4) the dissociation of chainings manifested after the transition of the creation phase.

Theorem 1: The action chains of a (energy propagation), b (information transfer), c (transition of action causing matter), d (supply inhibition), and e (existing form) types of action chains are dissociated by either  $OPP_1$  (control of action source),  $P_2$  (control of action path), or  $P_3$  (control of action source and path), while f (functional default)-type action chains are dissociated only by  $DPP_4$  (alternative control of default functions).

Theorem 2:  $DPP_1$ ,  $P_2$ , and  $P_3$  appear through dissociation actions of a' (energy propagation), b' (existing form), c (transition of action causing matter), and d' (supply inhibition), while DPP appears only through the dissociation action of the g' and g" (alternative function) type.

Auxiliary theorem 2: When an EDFAL (a DFAL whose action involving the fluctuating directions of properties and strength depends on those of other DFALs exists in the HCS, at least one restraint chain, comprising a DFAL linking the EDFAL and the DFAL it depends on, must exist in the HCS.

Theorem 7: An SFAI can be constructed in principle from any restraint or dissociation action chains, while a DFAL cannot be constructed from dissociation or restraint action chains of the f' or f" type.

Auxiliary theorem 3: In order for a SIPS to be constructed in principle in the HCS, every action chain involved in transferring signals (or information) between the elements composing the IPS must be capable of being constructed as an SFAL.

### 3. Hazard Identification

Various hazards have been identified for a prototype intelligent mobile robot. This report specifies the following hazards occurring during autonomous travel by a mobile robot--1) its collision with stationary target  $O \rightarrow Ra \rightarrow O(\omega)$  and 2) collision of moving target M with it  $\{Re \rightarrow Ma \rightarrow R(\omega)\}$ . These hazards can be identified by an A-C model, as shown in Figures 1 and 2.

### 4. HCS Configuration

#### 4.1 Application of HRP<sup>3</sup>

##### 4.1.1 Hazard (1)

The system phase can be divided into the robot's stop and motion mode. Since only collisions caused by the robot's autonomous motions are taken into consideration, inducing action chains  $(DRa \rightarrow), (ESa \rightarrow), (DRe \rightarrow)$  are the requirements for  $(Ra \rightarrow)$  in Figure 1.  $(DRe \rightarrow)$  can be dissociated through  $P_1$  in principle (Theorem 2). A power source cutoff interlock system can be constructed as an HCS comprising the following control chain:

$$Ou \rightarrow SEu \rightarrow CPu \rightarrow CAu \rightarrow DRe \rightarrow R \quad (1)$$

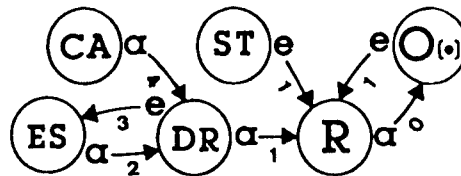


Figure 1. Identification of Hazard (1)

The dissociation action chain  $(CAu \rightarrow)$ , as well as other restraint action chains, can be made an SFAL solely in the direction of the power source cutoff. This HCS can construct a SIPS in principle (Theorem 7). Figure 3 presents the configuration of an HCS using a SIPS.

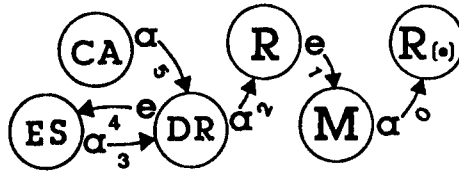


Figure 2. Identification of Hazard (2)

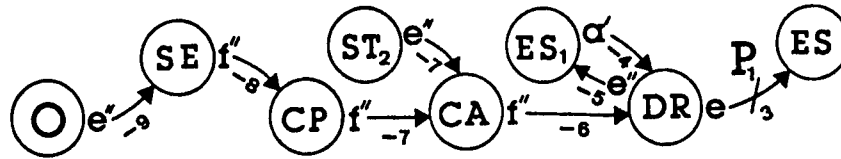


Figure 3. HCS's Main Segment Applying HRP (3) Against Hazard (1) (SIPS)

#### 4.1.2 Hazard (2)

The system phase can be divided into a mode in which a robot does not exist in the area, permitting its interference with target M, and one in which a robot does exist. First, the system phase is in the former's mode. Suppose that the robot does not interfere with M as long as it stays there, and the inducing action chain  $(DR \xrightarrow{e} M)$  is the requirement for  $(M \xrightarrow{e} R)$ . The only procedure required to restrain hazard (2) is to dissociate  $(DR \xrightarrow{e} M)$ . Therefore, an HCS comprising the following control chain can be constructed:

$$\text{Theorem 1: } M \xrightarrow{e} SE \xrightarrow{f} CP \xrightarrow{f} CA \xrightarrow{f} DR \xrightarrow{e} R \quad (2)$$

Similarly to the previous chapter, a control chain can be an SFAL directed solely toward the power cutoff, enabling both a SIPS and a DIPS to be constructed. Figure 4 presents a conceptual design of an HCS using a DIPS.

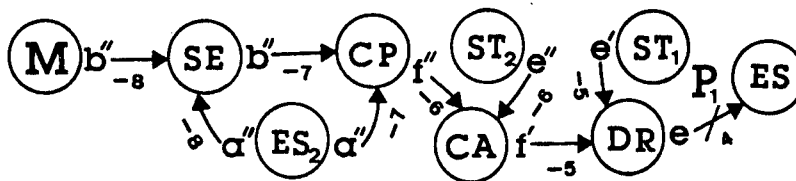


Figure 4. HCS's Main Segment Applying HRP (3) Against Hazard (2) (DIPS)

#### 4.2 Application of an HRP (4)

An HCS has been studied after the transition of the system phase to the robot motion mode or when a robot exists in the area, permitting its interference with M.

### 4.2.1 Hazard (1)

#### a. Avoidance of braking collisions

The direct cause action chain  $(Ra \xrightarrow{2})$  can be dissociated in principle by  $P_1$  (Theorem 1). In other words, when halting a robot does not cause other hazards, an HCS comprising the following control chaining can be constructed:

$$Ou \xrightarrow{3} SEu \xrightarrow{4} CPu \xrightarrow{5} CAu \xrightarrow{6} BRu \xrightarrow{7} Ra \xrightarrow{8} O \quad (3)$$

A control chain can be constructed through an SFAL solely in the stopping direction, and a SIPS can be adopted in principle (Auxiliary theorem 3). Figure 5 presents a conceptual design of an HCS using a SIPS (Theorems 2 and 7).

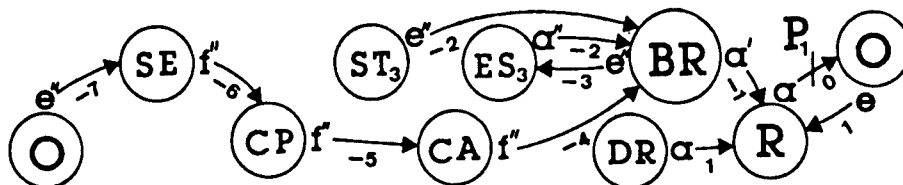


Figure 5. Main Segment of HCS To Avoid Hazard (1) Involving Single Braking Collision (SIPS)

#### a.1 System causing skid

Braking causes skidding to occur, depending upon the robot structure and the environmental conditions, making it necessary to take hazards resulting in collisions (Figure 6) into consideration. As a countermeasure against skidding, a method involving skid detection and the ON/OFF control of the braking force is being studied.<sup>11</sup> The action chain  $(BR \xrightarrow{2})$  can be dissociated through  $P_1$ , and an HCS comprising the following control chaining can be constructed:

$$RSu \xrightarrow{1} S \xrightarrow{2} CPu \xrightarrow{3} CAu \xrightarrow{4} BR \xrightarrow{5} S \quad (4)$$

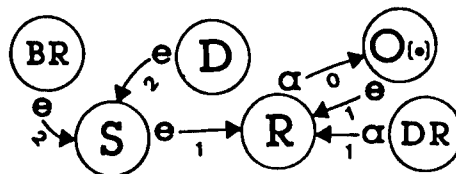


Figure 6. Hazard Involving Skid (1)

Here, the dissociation action chain  $(CAu \xrightarrow{3})$  becomes an EDFAL since it controls the ON/OFF of the braking force according to the control action  $(RSu \xrightarrow{1})$  of the skidding state, and every restraint action chain composing a control chaining (4) under the condition that no restraint chain linking  $(RSu \xrightarrow{1})$  and  $(CAu \xrightarrow{3})$  exist except for a control chaining (4) becomes a DFAL (Auxiliary



$$Qu \xrightarrow{1} SEu \xrightarrow{2} CPu \xrightarrow{3} CAu \xrightarrow{4} SRu \xrightarrow{5} R \xrightarrow{6} O, \\ (i=1,2,3,\dots)$$

(6)

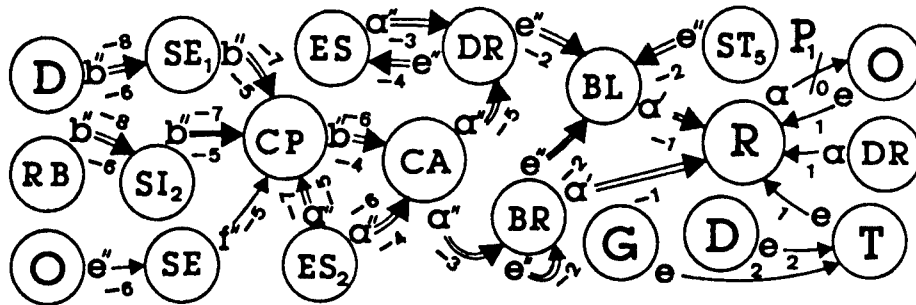


Figure 9. Main Segment of Collision-Avoidance HCS Through Multi-Braking Control Against Hazard (1) Containing Overturns

### b.1. Single target avoiding system

First, let us study a system for which only single object 0 needs to be avoided--an obstacle so small that a robot can avoid it through a single path changing operation. In this case, dissociation action chain  $(SRu, \vec{1})$  can be made at SFAI only in the direction in which a robot is separated from a target according to restraint action chain  $(0, u, \vec{1})$ . Control chaining can be constructed through an SFAL in principle, and an IPS can be made a SIPS in principle. Figure 10 presents an HCS using this system.

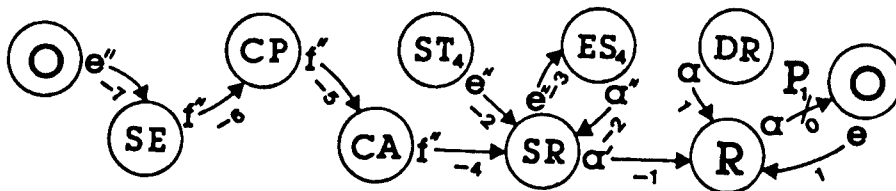


Figure 10. Main Segment of Single-Target Collision-Avoidance HCS Through Path Control Against Hazard (1) (SIPS)

### b.2 Multiple-target simultaneously avoiding system

Suppose a system where  $n$  single targets  $O_i$  ( $i = 1, 2, \dots, n$ ) are distributed over such a wide range that a robot cannot avoid them through a single path change. Dissociation action chain  $(SRu, \vec{1})$  cannot be constructed as an SFAI since a path must be controlled in both directions in order for the robot to avoid every target according to the restraint action chain  $(0, u, \vec{1})$  from multiple targets. Therefore, a SIPS cannot be constructed since every restraint action chain composing this control chaining must be a DFAL due to the condition that no restraint chaining linking  $(SRu, \vec{1})$  and  $(0, u, \vec{1})$  exists except for control chaining (6). Here, a conceptual design of the HCS in Figure 11 becomes possible.

#### 4.2.2 Hazard (2)

In hazard (2), inducing action chain  $(Re, \vec{1})$  is the requirement for direct cause action chain  $(Ma, \vec{1})$  to appear. Therefore, the manifestation of  $(Re, \vec{1})$  can be inhibited by dissociating  $(Ma, \vec{1})$ .  $(Re, \vec{1})$  can be dissociated through  $P_2$  from Theorem 1, namely, through a robot's traveling



are hazards which are caused by anomalies or failures in the HCSs. Of HCSs which conduct such formats for avoiding collisions against target 0 as C1 (simple braking), C2 (skid control braking), C3 (equilibrium control braking), C4 (path control single target), and C5 (path control multi-target), those theoretically constructable through a DIPS are displayed within area D, while those constructable through a SIPS appear within area S.

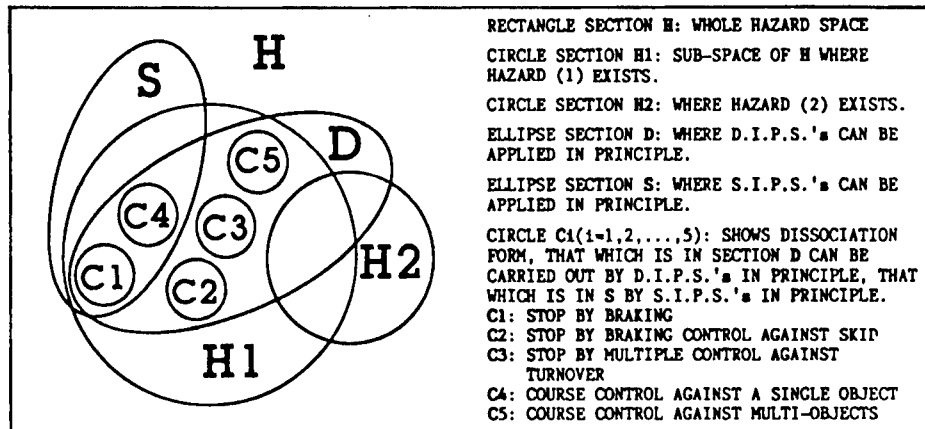


Figure 13. Scope of HCS Comprising DIPS and SIPS

It is impossible to construct an HCS capable of responding to every space H, so it is important to construct one rationally by determining the priority of the hazards involved.

## 5. Conclusion

A hazard control system for an autonomous mobile robot was constructed using the "A-C model," a conceptual design method for hazard control systems. This report discussed hazards involving a robot colliding with stationary targets and mobile robots colliding with a robot, after presenting a conceptual design of a hazard control system applying the hazard restraint principle (3). Then, applying the restraint principle (4) discussions were presented involving collision avoidance through simple braking, skid control braking, and equilibrium control braking, as well as avoiding collisions with a single stationary target and multitargets through path control, and a hazard control system to enable collisions with mobile targets to be avoided was described. In addition, the scopes of the safety-detection-type information processing system and the hazard-detection-type information processing system against individual hazards were explained.

## References

1. Furukawa, "Robots and Humans," NHK Books 475, NHK Publishing Association, Tokyo, 1985.
2. Katoh, "From Mechanism to My Robot," MACHINERY JOURNAL, Vol 89 No 792, 1984, p 1245.
3. Satoh and Inoue, "On Robot Safety," Ibid., Vol 90 No 827, 1987, p 1351.

4. Ibid., "Safety Evaluation of a Man-Robot System (1st Report)," Vol 51 No 468, C 1985, p 2188.
5. Satoh, Inoue, and Kumamoto, "Safety Evaluation of a Man-Robot System (2d report)," Ibid., Vol 52 No 475, C1 986, p 823.
6. Ibid., "Safety Evaluation of a Man-Robot System (3d report), Vol 52 No 475, C 1986, p 1110.
7. Ibid., "Safety Evaluation of a Man-Robot System (4th report)," Vol 52 No 482, C 1986, p 2754.
8. Satoh and Inoue, "Safety Evaluation of a Man-Robot System (5th report)," Excerpt of 911A of Kansai Branch 63rd Regular Convention Papers.
9. Ibid., (4), p 8.
10. Ibid., (4), p 2192.
11. Inui, "Car Electronics and Safety Problems--Current State and Potentials," Electronics and Communication Society Report, S-87-16, 1987, p 48.

## Fuzzy Path Pattern of Automatic Vehicle With Ultrasonic Range Detector

43064062 Tokyo 4TH INTELLIGENT ROBOTS SYMPOSIUM PAPERS in Japanese  
13/14 Jun 88 No 218 pp 241-246

[Article by Kaoru Hirota (regular member of the Society of Instrument and Control Engineers (I&C) and regular member of the Robotic Society) and Kinyo Arizume (student member of I&C), Hosei University]

### [Text] 1. Introduction

In realizing the automatic movement of intelligent robots, route seeking poses a big problem. Route seeking involves finding a route for movement from one point to another. In order for a robot to accomplish this action, which is easily conducted by human beings every day, many problems must be solved.

In general, the seeking methods are different according to the amount of information given to the robot seeking the route.<sup>1</sup> When partial route or environmental information is given, the very fact that the robot reaches the destination is important. When complete information is given, it is requested that the shortest route to the destination be selected in addition to reaching the destination. This is similar to the situation in which a man tries to get to his destination in a strange place by asking directions. In this case, it is important to arrive at destination regardless of the time and distance. On the other hand, if he has a detailed map, he tries to find the shortest route to the destination. When information, which is imparted at this time, is considered, the man can reach the destination simply by knowing the simple route information. However, it is expected that the robot will have difficulty reaching the destination if the same information is given. This is because approximately accurate information is given with regard to the direction and route, but information involving the routes is liable to be ambiguous. The man can handle intrinsically ambiguous values well, but for the robot, a fatal problem might arise through an error in information. In general, in regard to route problems, many intelligent robots have been designed with emphasis on the execution and accomplishment of given programs, while trials meant to approach human actions, such as the flexible handling of information received, are not conducted in many cases. The authors have tried to construct human-oriented route-seeking moving robots using a route-seeking problem as a model.

In development, it is being emphasized that the robot reach its destination, based only on the simple information given by the man, by realizing smooth straight advance and handling flexibly the ambiguous information given by the man. The route environment formed by such ambiguous information is referred to fuzzy routes.

Before discussing the main subject, the mobile robot HER01, which currently employs a sensor, is explained. The ETW/ETS-18 HER01 is an autonomous robot which does not require another control computer. An 8-bit microprocessor MC6808 is used for the intelligent information processing function. As a sensing function, an ultrasonic wave range finder, which can measure ranges up to 2.4 M, is mounted on the head. The following mobile functions are provided: running with one front driving wheel and two rear wheels; and head rotation. As human-mechanical information exchange functions, a teaching pendant, sounding function in combination with phonemes, a six-digit LED display, a hexadecimal keyboard, etc., are provided.

The outer configuration is shown in Photo 1 [not reproduced].

## 2. Input Data

Following is a description of the route information to be given to the HER01. The information given the HER01 combine the finite pieces of information about the approximate distance to an intersection, where the direction should be changed, the configuration of the intersection, and the advancing direction at the intersection. The configuration of the intersection and the route information for advancing must be correct, while the distance to the intersection can be the fuzzy distance given by a man.

Now the fuzzy information will be described. When one is asked how many meters it is from one intersection to another, it is hard to give the accurate distance unless the distance has already been measured. However, a human can utilize the distance as a reference even if it is vague. This is because the man intrinsically understands the distance information such as this to be vague.

In reflecting these considerations, a broad interpretation will be made, even if the distance is specified in detail in meters. An evaluating measure<sup>2</sup> called a vagueness, which is proposed by the authors, has been introduced in order to distinguish in the case when the man responding is confident from that when the man is not confident of his answer. This is the new evaluative measure, which has been proposed for inputting the data for a man-machine system. This is a method for inputting the secondary information regarding the degree of confidence with which the data are input. The vagueness is given as multiple finite values from 0 to 1. The value zero refers to the highest level of confidence. As the value approaches 1, the confidence decreases. In this study, quantizations were conducted in three stages in order to simplify the data input. For the case of "-meters without confidence," the vagueness value is specified as 1, while the allowance to be made with respect to the specified distance is  $\pm 50$  percent. In the case of "approximately -meters," the vagueness value is

specified as 0.5 and the allowance to be made is  $\pm 25$  percent. In the case of "exactly  $\sim$ meters," the vagueness value is specified as 0, and the allowance is set at  $\pm 12.5$  percent.

On the fuzzy route on which the HERO 1 runs, only the information on intersections where the direction is changed is given. Therefore, there is the possibility that another intersection might be encountered before the robot reaches the intersection at which the direction is changed. If the robot erroneously changes the route at such an intersection, it cannot reach its destination. In the HERO1, however, the detecting scope of the intersections is adjusted based on the reliability of the given information by using the vagueness. Therefore, the errors can be prevented to some extent. Since allowance is given for the distance to the destination, the accumulated error in the running distance can be allowed to some extent.

The longest distance to the next intersection to be covered during one advance is set as 30 m, taking into consideration traveling through building corridors. The eight kinds of intersection configurations are set under the following restrictions, including that of the direct advancing intersection. The advancing direction at the intersection, i.e., left, straight or right, is selected to determine the one direction in which the robot can advance.

The following restrictions have been imposed based on the HERO1 structure and problem simplification.

1. The ground on which the HERO1 advances should not enable wheels to slip and no step difference should exist.
2. Routes cross at right angles at intersections.
3. Obstacles to be measured with ultrasonic-wave range finders should not be found on the routes.
4. The walls of the routes are covered with a uniform material, and the step difference should be within 10 cm.
5. The width of the route is from 1.5 m to 3 m.
6. The total running distance is 1 km, due to the battery capacity.

### 3. Position Measurement

In order for the HERO1 to advance along straight routes such as corridors, the course must be corrected adequately. In this case, the following method has been selected. The robot advances so that the distance from the wall is kept constant based on the distance from the wall and the inclination with respect to the wall, and the robot advances straight ahead along the route. The distance information from the wall can be obtained by using the ultrasonic wave range finder mounted on the robot's head. What must be noted here is the fact that, when the ultrasonic wave hits the wall at a slant, sufficient reflection is not obtained with the ultrasonic wave range finder used in the HERO1 due to the ultrasonic wave properties. Therefore,

the distance cannot be measured. Measurement can be carried out only when the wave hits the wall approximately vertically.

One example of the distance measuring method using the ultrasonic wave range finder will be demonstrated here. The HER01 is placed approximately parallel with the wall. In measuring the distance with the ultrasonic wave range finder, the head is turned to the right. Since the wave hits the wall at a slant, the distance cannot be measured at first. When the head is turned about 90 degrees, the wave hits the wall orthogonally and the distance can be measured (Photographs 2.1 and 2.2 [not reproduced]). When the HER01 is placed at a slight incline in relation to the right wall, the turning angle of the head is smaller than that when the robot is parallel to the right wall and the wall is detected (Photographs 2.3 and 2.4 [not reproduced]). When the robot is inclined to the left side, the turning angle of the head increases. Based on the magnitude of the turning angle of the head, the amount of slant for the specific route can be found.

#### 4. Data Processing Method

The inclination and distance with respect to the wall can be detected by the method described above. Since the resolution of the ultrasonic wave range finder is poor, the values are liable to disperse. Therefore, the turning angle of the head and the distance to the wall were obtained by utilizing not the data at one point, but the data at multiple points. The HER01 was placed parallel to the wall, as shown in Photo 2.1 [not reproduced]. With the head turned toward the right, the distances to the right wall were measured. The examples of the head positions and the distances when the reflections were obtained are shown in Table 1.

Table 1. Positions and Distances in Right-Wall Seeking  
(Values are shown in hexadecimal expression)

---

|               |      |            |        |      |      |      |        |    |        |      |
|---------------|------|------------|--------|------|------|------|--------|----|--------|------|
| Head position | 8789 | 8A8B8C8E8F | 909192 | 9495 | 9899 | 9A9B | 9D9E9F | A0 | A2A3A4 | A7A8 |
| Distance      | 352F | 2F2E2D2A2A | 292928 | 2827 | 2727 | 2727 | 272727 | 27 | 272727 | 2828 |

---

As is apparent in the data, the errors due to the reflecting angles are decreased and resolution is improved when the direction approaches the vicinity of the wall (\$9F). Therefore, the same distance data appears many times. The distance data appearing the most is regarded as the most accurate distance to the wall. The midpoint between the first head position in the series of distance data and the final position is obtained, and is regarded as the representative value of the detected position. For example, in Table 1, the distance to the wall is \$27, which has appeared the most. The head position is \$9D, which is the midpoint between \$95 and \$A4.

#### 5. HER01 Course Correcting method

Based on the data detected by the method described above, the course can be corrected according to the following two objectives: 1) the robot is placed parallel to the wall; 2) the robot advances keeping the distance from the wall constant. At first, the HER01 moves slightly forward so that it

becomes parallel with the wall. Then it is made to advance about 1.5 m so that the distance from the wall approaches the objective value (about 40-50 cm). This step is repeated, and the HEROl seems to advance in a straight manner.

The caution exercised in this correction method is as follows: steering is not to be made in large amounts at one time, so that a smooth straight advance can be realized as in human driving, and corrections are not made in small amounts. In order to satisfy the requirement, the following method has been adopted. When the objective value of the distance is temporarily considered to be 40 cm, and the measured value at a certain time is 20 cm, this is clearly too close to the wall. When the distance is 38 cm, however, the value does not agree with the objective value and it is judged that it is too close to the wall. From the human point of view, 38 cm and 40 cm are felt to be about the same. As seen in human driving of a vehicle, the position is not adjusted based on the precise distance, but instead the distance is adjusted based on the impression of the course position. The distance is not adjusted at one time, but the objective value is approached slowly during the correction process. As a result, very smooth operation is performed.

When the same correction method is used, smooth movement can be made. Then, the numerical value is not used to express the position in relation to the wall, but the terms to express five stages (nine stages when greater distances are included), i.e., "approximately equal," "rather close," "slightly close," "close," and "very close," are used. The determination of the classification for the particular position is performed by distinguishing the distance from the wall, and the correction is made by the representative value.

Apparently smooth movement can be realized by this method.

## 6. Intersection Detecting Method

Using the method described above, the HEROl advances straight and approaches the intersection. When the HEROl arrives at a position before the point where the intersection is expected to be found the ultrasonic wave range finder is turned toward the wall under detection and the distance to the wall is detected, even during the running. At this time, the distance to the wall is shorter than that during straight advancing, supplying the state in which the robot can readily change its direction. When the reflection disappears during the running, it is assumed that the robot is at the intersection, and the configuration of the intersection is determined.

## 7. Evaluation of Intersection Configurations

When the intersection is detected, the configuration of the intersection is evaluated and, through comparison, a determination is made of whether the detected intersection agrees with the given intersection. In this evaluation, the ultrasonic wave range finder is used to determine whether walls are present to the right, left, and straight ahead for the respective

sections. The intersection configuration is evaluated based on the presence or absence of the walls.

When the robot is inclined more than 45 degrees with respect to the route, this evaluative method cannot be used. Since it is seldom that the HEROl is inclined more than 45 degrees with respect to the route, no problems in this respect are encountered in practical use.

When the intersection configuration is evaluated and agrees with the configuration of the given intersection, the robot advances in the specified direction. When the configuration is different, the robot advances straight if straight advance is possible. When the advancing direction is only that of the position the robot advances straight in that direction, continuing to seek the intersection.

## 8. Result of Operation

An example of the operational results is shown in Photo 9 [not reproduced]. The HEROl detects the direction to the wall, and the inclination is corrected by the method described above so that it is parallel to the wall. The distance from the wall is corrected, and the robot advances (Photographs 3.1, 3.2, and 3.3 [not reproduced]). The distance advanced is counted based on the number of rotating steps of the driving motor. When it is ascertained that the robot has arrived at a position before the point at which the intersection is expected to be preset, the hand is inclined, and the presence or absence of the wall is detected. The robot advances (Photographs 3.4 and 3.5 [not reproduced]). When the reflection disappears, it is judged that the intersection has been reached. The presence or absence of the wall is checked (Photographs 3.6 and 3.7 [not reproduced]). When the configuration agrees, the robot is steered toward the specified direction, and the direction is changed (Photographs 3.8 and 3.9 [not reproduced]).

In actual operation, problems occur when the HEROl steering hampered by fine irregularities on the floor, and the robot advances in a somewhat snake-like pattern. The program comprises about 1,300 bytes (750 steps).

## 9. Conclusion

The authors attempted to construct a human-oriented route-seeking robot by using the HEROl. We set several restrictions when conducting this experiment. Most route-seeking robots of this kind are guided by methods utilizing image processing, landmarks, etc. In this experiment, however, a low-level sensor such as an ultrasonic wave range finder was used, ambiguous information given by a man was processed flexibly, and the robot reached the destination based on its own judgment. Therefore, it can be said that satisfactory results have been obtained. Since the detection of the distance advanced was based on the number of rotations of the motor, several problems exist such as the difficulty in obtaining the accurate accumulated distance. In the future, we would like to promote improvements, using a good scanning detecting method as the central theme.

### References

1. Kobayashi Shigenobu, "Intelligent Processing in Autonomous Moving Robots," KEISOKU TO SEIGYO, February 1987, the Society of Instrument and Control Engineers, pp 128-133.
2. K. Hirota, "Extended Fuzzy Expression of Probabilistic Sets, Advance in Fuzzy Set Theory and Applications," M.M. Gupta, et al., eds, 1979, North Holland, pp 210-214.
3. Hirota Kaoru and Arizumi Kinyo, "Route Finding Robot," HOSEI DAIGAKU KOGAKUBU KENKYU SHUHO, No 24, March 1988, pp 69-78.
4. Ibid., "Fuzzy-Controlled Intelligent Robot," McGraw-Hill, 1985.
5. Ibid., "Fuzzy Robot," SURIKAGAKU, January 1987, Science Co., pp 70-74.

## Bilateral Control of Smart Manipulators

43064062 Tokyo 4TH INTELLIGENT ROBOTS SYMPOSIUM PAPERS in Japanese  
13/14 Jun 88 No 219 pp 247-250

[Article by Hiroshi Yamamoto, Yoshiro Nakajima, Taro Iwamoto, and Tatsu Aoki (all are regular members of the Society of Mechanical Engineers), Mechanical Laboratory, Hitachi, Ltd.]

### [Text] 1. Introduction

A master-slave manipulator, which can reproduce the movement of the human hand at a remote position as if a man were manipulating the manipulator, has been in demand in many fields, with space and nuclear applications as a core, as a useful means for conducting tasks safely in adverse environments (in space, seawater, and high radiation) in which man cannot survive. Under such environments, manipulators are often used in the fixed state. On the other hand, when the manipulator is used with a mobile mechanism without fixing it in one place, a broad area can be covered with one manipulator. Therefore, many specific jobs can be handled with the manipulator, diversified jobs can be executed, and the system performance is improved. For example, in space, as illustrated in Figure 1, it is planned that arms be attached to a flying body, which will fly around a space station freely and service it. With the movement of the flying body, its position and the attitude are changed. Therefore, the position and attitude of the mounted manipulator are changed for every task. It is believed that the position and attitude of the manipulator are changed with the movement of the flying body during the task. In the conventional method, the moving directions of the slave and the master, which are attached to the flying body, will become unmatched with the movement of the flying body. Therefore, degradation in steering is inevitable. It is preferable that the structure of the master be suitable for human manipulation. The structure of the slave must be suitable for various tasks. Therefore, the structures of the arms are different. Even in cases in which the different attitudes and different structures as such are used, the manipulator is controlled by a computer so that the positions and the forces of the tips of both during the corresponding movement always agree. In this way, the movement of the manipulator is controlled adequately. We will report here the "Smart Manipulator," which has been developed for this purpose.

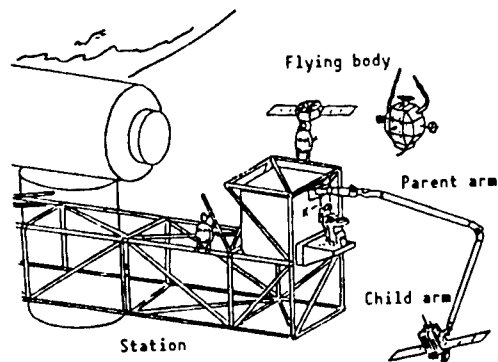


Figure 1. Application of Moving Robot in Space

## 2. Outline of Smart Manipulator

### 2.1 Developmental Objectives

Conventional master manipulators have been developed as motion transfer apparatuses, in which the joints of two arms with the same configuration are linked together in a ratio of 1:1, and the arms are operated in a servo mechanism. When the freedom constitution of the two arms and the ratios of the lengths of the arms are not equal, the motion is not transferred correctly. Due to these restrictions, problems arise with the manipulating property depending on the operating environment and the operating conditions. The basic concept of the smart manipulator is to link the master arm, with a configuration that is readily manipulated by a human operator, and a slave arm, which is suitable for tasks employing a computer, so that the motions of the tips of both arms are matched and the motion is transferred. When the matching methods of the tip movements can be changed in many ways, adaptability to the environment is enhanced and the performance of the manipulator is improved. These are the developmental objectives.

### 2.2 Basic Structure of Tip-Motion Matching and Controlling System

As shown in Figure 2, both arms are moved in a space with an imaginary common coordinate system so that the matching points, which are set in the grip of the master arm and in the end effector of the slave arm, agree. The coordinate transformation matrix  $T_{ms}$ , which indicates the relative positional relationship of the base coordinate systems of both arms, is set at the initiation of the associated movement. When controlling is carried out so that the matching point of the master arm always agrees with the matching point of the slave arm, in accordance with the following expression, the motion of the master grip is transferred to the hand of the slave:

$$T_{6m}R = T_{ms}T_{6s}, \dots \quad (1)$$

where  $T_{6m}$  is the coordinate-transformation matrix from the reference-coordinate system of the master to the coordinate system of the matching part of the hand of the master;  $T_{6s}$  is the coordinate-transformation matrix

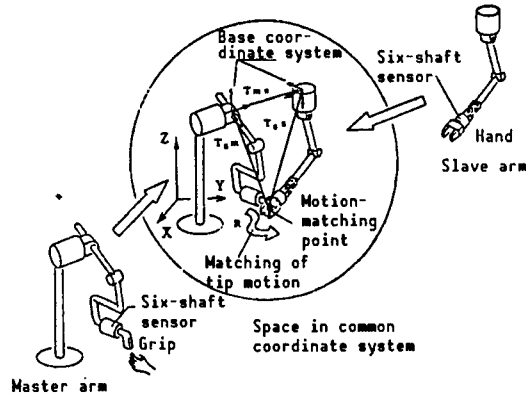


Figure 2. Tip-Motion Matching Manipulator

the reference-coordinate system of the slave to the coordinate system of the matching point of the hand of the slave;  $T_{ms}$  is the coordinate-transformation matrix from the reference-coordinate system of the master to the reference-coordinate system of the slave; and  $R$  is the rotary-transformation matrix between the coordinate system of the hand of the master and the coordinate system of the hand of the slave. The following advantages are found in this tip-motion matching system:

**a. Motion transfer between arms of different shapes**

In this system, there is no structural restriction between the master and the slave. Therefore, optimum structures can be provided, making the master arm suit human operation and the slave arm suit the task. Furthermore, many kinds of slave arms with different structures can be sequentially switched and manipulated with one master arm.

**b. Motion transfer to different-attitude arrangement**

In the manipulator of a parent-child system in which the child arm is connected to the tip of the parent arm, the attitude of the base part of the child arm changes with the attitude of the hand of the parent arm and, therefore, the movements of the hands of the master and slave do not match, making manipulation difficult. In this system, the position and the attitude of the base part of the slave arm are detected, and the movements of the master and slave can always be matched by updating the coordinate-transformation matrix  $T_{ms}$ , which indicates the relative positional relationship between both arms. Therefore, intuitive manipulation can be carried out.

**c. Scale conversion/base-point shift of motion**

The ratio of the magnitude of the motion to be transferred can be freely set by multiplying the length of the link of the master arm by a scale conversion coefficient before transferral to the common coordinate system. The relative positions of both arms in the operating region can be changed by stopping one arm, changing the configuration of the other arm, and resetting the  $T_{ms}$ . In other words, the motion can be transferred by shifting the matching points of the arms, and the base point of the arm can be moved.

Therefore, even when the operating region of the master is small and the total area of the slave cannot be covered, manipulation can be carried out by shifting the master's operating area.

### 2.3 Configuration of Entire System

The basic system is configured, as shown in Figure 3, in order to verify the functions described above. The control system is composed of an upper system, an arm control device, and a high-speed, highly free input-output control device, and has the following features:

- a. In order to process the coordinate-transformation operation at a high speed, five boards, each of which has a DSP (digital signal processor) that can perform high-speed multiplication and addition operations, are used in the operation execution part of the arm control device.
- b. The upper system (super minicomputer) acts as a system controller. It interrupts the lower system as required, and can perform supervisory control. The lower systems (the arm control device and the high-speed highly-free input-output control device) can perform operation processing and input-output processing, such as periodic servo operation and the coordinate-transformation operation at a high speed. The upper system and the lower system can operate in an asynchronous mode.
- c. The interface functions with the arms are independent and dispersed. The sensor data is preprocessed so that common formats are provided for the different kinds of arms. The data can be handled uniformly in the arm control device and the upper system.
- d. The arm control device and the high-speed highly-free input-output control device are connected with a high-speed optical fiber link in which noise resistance is high and a large amount of data can be transmitted over a long distance.

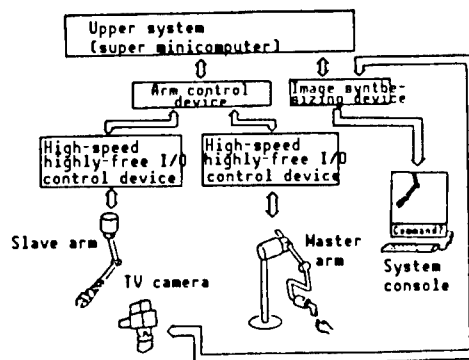


Figure 3. Structure of Smart Manipulator System

The image system is composed of the following: a TV camera; a universal head and its controller to change the view of the TV camera; an image combiner, in which the real image from the TV camera is superimposed on the image output from the computer; and a monitor to display the output of the combiner. Manipulation guidance to the operator is performed.

### 3. Elements Constituting the System

#### 3.1 Manipulator

Figure 4 illustrates the master manipulator, Table 1 shows the operating range of joint angles, and Table 2 shows specifications. For masters, two kinds of manipulators with different installation systems and different axis constitutions are used. The first is the manipulator shown in Figure 4(a). This is a wall-installation system, and the manipulator is attached to the wall at the lateral side of the operator. The freedom constitution is PRPPYR. The second is the manipulator shown in Figure 4(b). This is a floor-type installation system. The manipulator rises up from the floor so that the operator does not get an oppressive feeling. The freedom constitution is RRRPRR. The actuator is formed by combining a DC motor and a harmonic speed reducer. The transfer systems of the fourth, fifth, and sixth shafts in the wall-installation system transmit the output of the harmonic speed reducer to the hand through a wire cable.

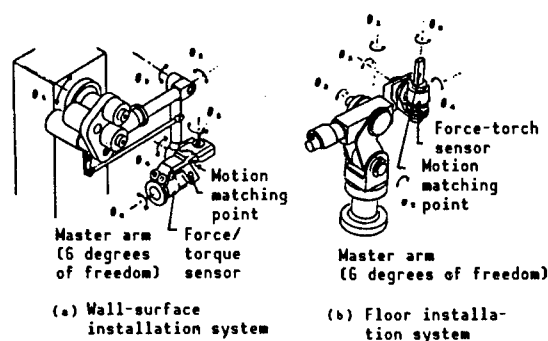


Figure 4. Master Manipulator

Table 1. Operating Range of Master Manipulator

| Systems    | Wall surface installation | Floor installation     |
|------------|---------------------------|------------------------|
| $\theta_1$ | $\pm 90^\circ$            | $\pm 90^\circ$         |
| $\theta_2$ | $\pm 45^\circ$            | $+110 \sim -70^\circ$  |
| $\theta_3$ | $\pm 60^\circ$            | $\pm 42^\circ$         |
| $\theta_4$ | $+5 \sim -85^\circ$       | $+120 \sim -180^\circ$ |
| $\theta_5$ | $+3 \sim -60^\circ$       | $\pm 135^\circ$        |
| $\theta_6$ | $\pm 40^\circ$            | $\pm 135^\circ$        |

Figure 5 illustrates the slave manipulator, Table 3 shows the operating range of the joint angles, and Table 4 shows the specifications. The freedom constitution of the slave is RPPRPY. The slave manipulator is of the suspended installation type and has a larger operating range than that of the master manipulator. The actuator is formed by combining a DC motor and a harmonic speed reducer.

Table 2. Specifications of Master Manipulator

| Systems              | Floor installation type    |
|----------------------|----------------------------|
| Degrees of freedom   | 6                          |
| Full length of arm   | 900 mm                     |
| Weight               | 25 kg                      |
| Force at tip         | 20 N                       |
| Moment at tip        | 2 Nm                       |
| Speed at tip         | 720 mm/s                   |
| Type of force sensor | 6-shaft concentration-type |

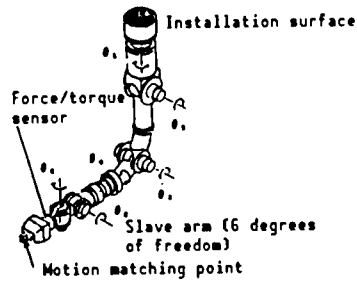


Figure 5. Slave Manipulator

Table 3. Operating Range of Slave Manipulator

| $\theta_1$      | $\theta_2$     | $\theta_3$               | $\theta_4$      | $\theta_5$     | $\theta_6$     |
|-----------------|----------------|--------------------------|-----------------|----------------|----------------|
| $\pm 150^\circ$ | $\pm 90^\circ$ | $0^\circ$<br>$180^\circ$ | $\pm 150^\circ$ | $\pm 90^\circ$ | $\pm 90^\circ$ |

A six-shaft concentrating-type force/torque sensor is arranged at the hand of each manipulator so that the force and the torque are detected highly accurately without being affected by the friction of each joint.

Position detection with any arm is based on the combination of an encoder and an up-down counter.

Table 4. Specifications of Slave Manipulator

| Systems              | Multiple-joint type        |
|----------------------|----------------------------|
| Degrees of freedom   | 6                          |
| Full length of arm   | 1,750 mm                   |
| Weight               | 38.5 kg                    |
| Force at tip         | 30 N                       |
| Moment at tip        | 4.5 Nm                     |
| Speed at tip         | 470 mm/s                   |
| Type of force sensor | 6-shaft concentration type |

### 3.2 Arm Control Device

The arm control device shown in Figure 6 is composed of the following main components: an interface portion (HIF) with the upper system; an interface portion (AIF) with the high-speed highly-free input-output control system (SIF); an operation executing portion (PE), which performs coordinate transformation and servo operation in parallel; a control portion (PUC); and a system control portion (SYS), which controls those portions. The operation executing portion (PE) is composed of parts ( $PE_0 - PE_4$ ), which execute the high-speed operation with DSP (model TMS32010). The PUC communicates between the PEs and between the SYS and the IOP. The SYS expands each command in correspondence with a macrocommand from the upper system and executes the input-output operations of the data and the commands to and from the SIF and the PE. The SYS downloads the programs from the upper system to various portions and then operates the master and the slave according to the commands from the terminals. The data (arm's position, speed, force/torque, etc.) from the SIF are input to the PE through the PUC, and the motor-command values for the arm from the PE are sent to the SIF. The input-output data to and from the SIF undergo high-speed transfer by the DMA without any connection to the SYS. The SYS is initiated by the interruption from the upper system. When access to the SIF and the PE is required, a handshake is performed by a request flag, i.e., the SIF and the PE respond to the SYS access by polling and then receive the data. Therefore, the fluctuation in time of the control-data transmission between the SIF and the PE is reduced. The transferred data between the SIF of the SYS and the PE are written in the dual-port memory (DPM) in the ATF. The SYS reading can be made with almost no delay occurring in data transfer. The upper system observes the operating state of the arms through these data and can execute control depending on the state.

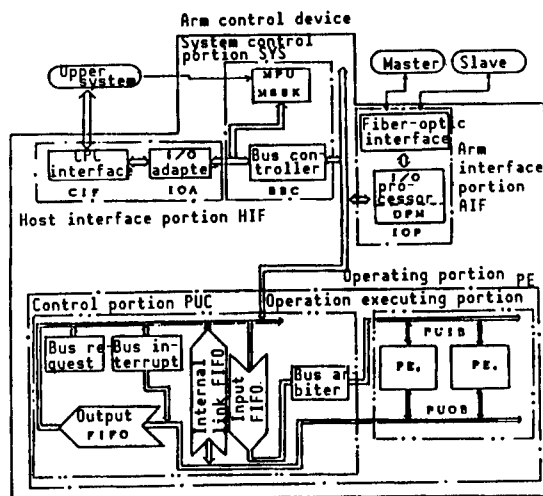


Figure 6. System Structure of Arm Control Device

### 3.3 Input-Output Control Device

The high-speed highly-free input-output control device is a high-function servo-interface so that the intelligent robot data to and from the arm

mechanisms can be handled uniformly in the upper system, both in the hardware and software modes, and only the input-output functions to and from the mechanism are independent. The block diagram of the device is shown in Figure 7. As the hardware, five kinds of sensor interface circuits, including an encoder, a potentiometer, a tachogenerator, a strain gauge, and a motor ammeter, which are frequently used in manipulators, are made compact by using dedicated ICs and are provided for eight shafts for every arm. As the software, information such as positions, speeds, and force/torque is transferred to the arm controlling device in a preset format by an internal measurement processor (SIFP). The arm control device can receive the data in the same format even for different arms. The SIFP selects, e.g., the data of the absolute angle obtained by the potentiometer and the highly accurate positional data obtained by the combination of the encoder and the counter based on the commands from the upper system, and transfers the obtained data as the positional data. Therefore, the SIFP has flexible functions. The data transmission speed between the devices is 0.8 Mbps, and the transmission capacity is 52 bytes. As transmission protocol, a simplified HDLS (high-level data-link control) procedure is used.

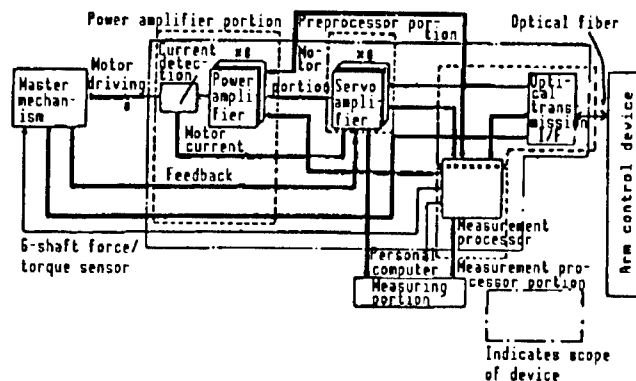


Figure 7. Block Diagram of High-Speed Highly-Free Input-Output Control Device

### 3.4 Control Function

Figure 8 shows the block diagram of the force-feedback-type bilateral servo-control system using a torque sensor. A six-shaft force/torque sensor is attached between the arms and end-effectors. The data of the positions and the forces of both arms are transferred to the common coordinate system through positive transformation, and the deviations are obtained. The deviation of the position is input to the speed servo-system of each joint as a speed command value for the joint angle of the slave arm through a reverse Jacobi operation.

The deviation in force/torque is transformed into a speed. Then the speed command signal for the joint angle of the master arm is input into the speed servo-system through the reverse Jacobi operation. Since the six-shaft force/torque sensor is not subjected to adverse effects due to the dead weight and the inertia of the arm, accurate bilateral control can be carried out.

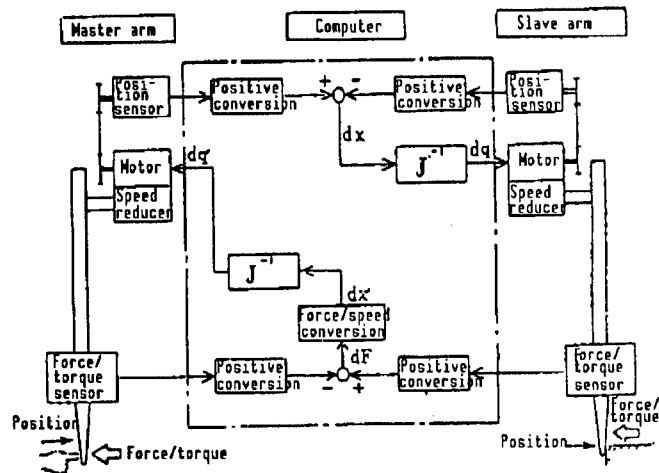


Figure 8. Block Diagram of Bilateral Servo Control System

#### 4. Result of Experiment

In the smart manipulator system comprised of the components described in Chapter 3 and thereafter, experiments involving the motion transfer between two 6 degree of freedom arms with different constitutions of freedom and the different installation attitudes were conducted. Figure 9 [not reproduced] shows photographs of those experiments. As a result, it was confirmed that the various functions described in Section 2.2 (motion transfers between arms with different configurations and different attitudes and the scale-change/base-point shift of motion) could be achieved.

#### 5. Conclusion

The motion is transferred by coupling the master arm, which has a configuration suitable for human manipulation, and the slave arm, which has a structure suitable for working, through the computer, and by matching the motions of the tips of both arms. The matching of the tip motions can be changed in various ways. Therefore, the smart manipulator, whose adaptability to environments is enhanced, has been developed. In the experiment, it was confirmed that the motions of the tips of two 6 degree of freedom arms with different structures, which were installed in different attitudes, could be matched, and that the ratio between the magnitudes of the motions to be transferred could be arbitrarily changed in this system. In the future, we would like to realize a total system, to cope flexibly with conditions.

#### References

1. T. Arai and E. Nakano, "Bilateral Control for Manipulator With Different Configurations," IECON 1984.
2. Hirai Narioki and Sato Tomomasa, "Language-Presence-Type Master-Slave Manipulator System," TRANSACTION OF THE SOCIETY OF INSTRUMENT AND CONTROL ENGINEERS, Vol 20 No 1, January 1984.

3. Iwamoto, Fujii, et al., "Study of Tip-Motion Matching Master-Slave Manipulator, Smart Manipulator (Report No 1)," 4th Robot Symposium Papers, December 1986, pp 83-84.
4. Iwamoto, Nakajima, et al., "Study of Smart Manipulator Characterized by Motion Matching of Tips of Arms Having Different Six Degree of Freedom Structures," 5th Robot Symposium Papers, November 1987, pp 103-104.

## Closed Loop Displacement Control of Multilink Dynamic Robot Arms

43064062 Tokyo 4TH INTELLIGENT ROBOTS SYMPOSIUM PAPERS in Japanese  
13/14 Jun 88 No 220 pp 251-256

[Article by Hikaru Umeno (student member of the Society of Mechanical Engineers), Graduate School, Tohoku University; and Seiji Naganami (regular member of the same Society), Tohoku University]

### [Text] 1. Introduction

In recent years, requirements such as high-speed motion, reduction in energy consumption, more portable weight, etc., have been increased for industrial robots. It is necessary to reduce the weight of an arm in order to meet these requirements. In this case, however, deflecting vibration due to the elastic deformation of the components is yielded. This vibration cannot be suppressed by a conventional control method if the arm is regarded as a rigid body. With respect to the control problem if the arm is an elastic body, many methods<sup>1</sup> have been introduced. In these methods, the displacement of the arm is expanded into modes, and control is performed for each mode. In this case, it is necessary to prove the orthogonality of the mode function. For an arm with many links and a complicated mechanism, the problem arises that analytic equations cannot be formed. On the other hand, when the control problem involving the elastic arm is theoretically analyzed in simulation, assurance that the theoretical results agree quantitatively with the experimental results is required. In this respect, Tawara, et al.,<sup>2</sup> conducted an experiment for a one-link arm, and obtained excellent coincidence between the theory and the experiment. With respect to the multilink arm, free vibration in a plane accompanied by the change in joint angle,<sup>3</sup> three-dimensional free vibration,<sup>4</sup> vibration suppression and control using strain gauges, and the output of rotary angles,<sup>5,6,7,8</sup> etc., have been analyzed. As far as these reports are concerned, apparently no research or report has been published which quantitatively compares the theoretical and experimental results with respect to the control problem involving multilink arms.

In consideration of the situation described above, the problem involving the tip position control of a two-link elastic arm, whose shoulder joint is driven, has been selected as one of the multilink arm subjects in this research, and the positioning problem for feedback control of the arm tip was analyzed theoretically and experimentally by using the tip-position data

directly measured by the sensors. Then, comparisons and examinations were carried out. In the theoretical analysis, the motion equation of the arm is formed after taking into consideration the effects of the lateral and longitudinal vibrations of the arms, internal damping, translation inertias of a joint and a tip load, rotation inertia, and the rotation inertia of a motor. As a solution, a Laplace transformation in the time domain is used. For reverse transformation, a numerical Laplace reverse transformation method demonstrated by Weeks<sup>9</sup> is used. This method's characteristics are such that proof of orthogonality is not required, even if the system becomes complicated, and residue computation is not required either. Its utility is shown in the displacement control analysis of an elastic one-link arm.<sup>2</sup> As a detailed example, the problem involving moving and stopping the tip of the stationary two-link elastic arm to an objective position  $W_d$  is studied. The experiment is conducted, and the theoretical and experimental values are compared and examined. The resulting values demonstrate excellent matching.

## 2. Analysis

In Figure 1, the model of a two-link elastic robot arm used in this analysis is shown. The mechanism portion of the robot is composed of five parts, i.e., a motor, elastic arm 1, elastic arm 2, a fixed intermediate joint, and a tip load. Each element is linked at shear force  $Q$  and moment  $M$ . Now, let us consider the following problem: torque  $T$  is applied to the root (shoulder) of the two-link elastic arm, which is fixed at a reference position, with the motor; and the tip of arm 2 is moved to the objective position  $W_d$ . As a control method, the following is used: the data of the position and speed are fed back with respect to the displacement of the tip of the arm, and the shoulder joint part is driven. In solving this problem, a Laplace transformation in time domain is used, and the answer is obtained by a numerical Laplace reverse transformation method.

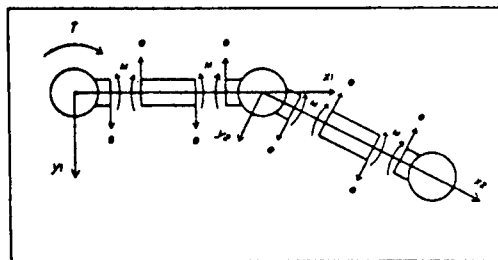


Figure 1. Model Being Analyzed

Now, with the center of the motor shaft as the original point, the  $x_1$  axis is formed along arm 1 and the  $y_1$  axis is formed at a right angle to the  $x_1$  axis. Then, with the center of the fixed joint portion as the original point, the  $x_2$  axis is formed only along arm 2 and the  $y_2$  axis is formed at a right angle to the  $x_2$  axis. The angle formed by the  $x_1$  and  $x_2$  axes is  $\theta$ . The  $x_1y_1$  plane and the  $x_2y_2$  plane are located on the same plane. Arms 1 and 2 are assumed to operate only in the  $x_1y_1$  plane. Then, the motion equations of the lateral and longitudinal vibrations are expressed, respectively, by:

$$E_j I_j \left(1 + C_j \frac{\partial}{\partial t}\right) \frac{\partial^2 w_j(x_j, t)}{\partial x_j^2} + \rho_j A_j \frac{\partial^2 w_j(x_j, t)}{\partial x_j^2} = 0 \quad (1)$$

$$E_j A_j \frac{\partial^2 u_j(x_j, t)}{\partial x_j^2} - \rho_j A_j \frac{\partial^2 u_j(x_j, t)}{\partial t^2} = 0 \quad (2)$$

( j = 1, 2 )

where P is the density of the arm, A is the cross section of the arm, E is longitudinal elastic modulus, I is the secondary moment of the cross section, C is an internal damping coefficient, w and u are lateral displacement and the longitudinal coefficient with respect to position x and time t, respectively, and j is a suffix showing the number of arms.

The arms are assumed to be stationary at t = 0. Equations (1) and (2) undergo Laplace transmission, and the following conditions are given:

$$\xi_j^* = -\frac{\rho_j A_j s^2}{E_j I_j (1 + C_j s)} \quad (3)$$

$$\gamma_j^* = \frac{\rho_j A_j s^2}{E_j A_j} \quad j = 1, 2 \quad (4)$$

Then, the general solutions are given by:

$$w_j(x_j, s) = a_j \sin \xi_j x_j + b_j \cos \xi_j x_j + c_j \sinh \xi_j x_j + d_j \cosh \xi_j x_j \quad (5)$$

$$u_j(x_j, s) = e_j \sinh \gamma_j x_j + f_j \cosh \gamma_j x_j \quad (6)$$

( j = 1, 2 )

where a<sub>j</sub> to f<sub>j</sub> represent undetermined numbers.

Now, let us consider the boundary conditions of the arms. The moment of inertia of the tip load is initially made to be J<sub>p</sub>. Based on the balance of the moments, the following equation is obtained:

$$J_p \frac{\partial^2 w_2(L_2, t)}{\partial t^2 \partial x_2} = -E_2 I_2 \left(1 + C_2 \frac{\partial}{\partial t}\right) \frac{\partial^2 w_2(L_2, t)}{\partial x_2^2} \quad (7)$$

When the mass of the tip load is M<sub>p</sub>, the balances of forces in the lateral and longitudinal directions are given, respectively, by:

$$M_p \frac{\partial^2 w_2(L_2, t)}{\partial t^2} = E_2 I_2 \left(1 + C_2 \frac{\partial}{\partial t}\right) \frac{\partial^2 w_2(L_2, t)}{\partial x_2^2} \quad (8)$$

$$M_p \frac{\partial^2 u_2(L_2, t)}{\partial t^2} = -E_2 A_2 \frac{\partial u_2(L_2, t)}{\partial x_2} \quad (9)$$

Then, the boundary conditions of the intermediate joint are studied. The relationship between the lateral and longitudinal displacements in the x<sub>1</sub>y<sub>1</sub> and x<sub>2</sub>y<sub>2</sub> coordinates are given by:

$$w_1(L_1, t) = w_2(0, t) \cos \theta + u_2(0, t) \sin \theta \quad (10)$$

$$u_1(L_1, t) = -w_2(0, t) \sin \theta + u_2(0, t) \cos \theta \quad (11)$$

When the mass of the joint is  $M_h$ , the balances of forces in the lateral and longitudinal directions are given by:

$$\begin{aligned} M_h \frac{\partial^2 w_1(L_1, t)}{\partial t^2} &= E_1 I_1 \left(1 + c_1 \frac{\partial}{\partial t}\right) \frac{\partial^2 w_1(L_1, t)}{\partial x_1^2} - * \\ &+ E_1 I_2 \left(1 + c_2 \frac{\partial}{\partial t}\right) \frac{\partial^2 w_2(0, t)}{\partial x_2^2} \cos \theta \\ &+ E_2 A_2 \frac{\partial u_2(0, t)}{\partial x_2} \sin \theta \end{aligned} \quad (12)$$

$$\begin{aligned} M_h \frac{\partial^2 u_1(L_1, t)}{\partial t^2} &= -E_1 I_1 \frac{\partial u_1(L_1, t)}{\partial x_1} + E_1 I_2 \left(1 + c_2 \frac{\partial}{\partial t}\right) \frac{\partial^2 u_2(0, t)}{\partial x_2^2} \sin \theta \\ &+ E_2 A_2 \frac{\partial u_2(0, t)}{\partial x_2} \cos \theta \end{aligned} \quad (13)$$

When the moment of inertia of the joint is  $J_h$ , the following equation is given based on the balance of the moments:

$$\begin{aligned} J_h \frac{\partial^3 w_j(L_j, t)}{\partial t^3 \partial x_j} &= -E_j I_j \left(1 + c_j \frac{\partial}{\partial t}\right) \frac{\partial^3 w_j(L_j, t)}{\partial x_j^3} \\ &+ E_j I_j \left(1 + c_j \frac{\partial}{\partial t}\right) \frac{\partial^3 w_j(0, t)}{\partial x_j^3} \end{aligned} \quad (j = 1, 2) \quad (14)$$

Finally, the boundary conditions of the shoulder joint portion are shown. Since the displacements of the root of arm 1 in the lateral and longitudinal directions are zero, the following expressions are given:

$$w_1(0, t) = 0 \quad (15)$$

$$u_1(0, t) = 0 \quad (16)$$

When the moment of inertia of the motor shaft is  $J_m$ , the viscosity damping coefficient is  $\epsilon_1$  and the torque generated by the motor is  $T$ , the following equation is obtained based on the balance of moments:

$$\begin{aligned} J_m \frac{\partial^3 w_1(0, t)}{\partial x_1 \partial t^3} + \epsilon \frac{\partial^2 w_1(0, t)}{\partial x_1 \partial t} \\ = E_1 I_1 \left(1 + c_1 \frac{\partial}{\partial t}\right) \frac{\partial^3 w_1(0, t)}{\partial x_1^3} + T \end{aligned} \quad (17)$$

When the torque constant of the motor is  $K_t$ , the torque is given by  $T = K_t i_a$ . When the position feedback gain is  $G_d$ , speed feedback gain is  $G_v$ , and objective position is  $W_d(L_2, t)$ , the circuit equation of the motor is given by:

$$\frac{L_a}{R_a} \frac{d i_a}{d t} + i_a \cdot \frac{E}{R_a} = G_d \{ w_2(L_2, t) - w_1(L_2, t) \} - G_v \frac{\partial w_2(L_2, t)}{\partial t} \quad (18)$$

where  $L_a$  is the circuit inductance,  $R_a$  is the circuit resistance,  $i_a$  is the armature current, and  $E$  is the counter electromotive force. When the counter electromotive force constant is  $K'$ ,  $E$  is expressed by:

$$E = K' \frac{\partial^2 w_1(0, t)}{\partial t^2 \partial x_1}$$

Equations (7) to (16) and equation (18) are substituted into equation (17), and the boundary-condition equation obtained undergoes Laplace transformation in the time domain. Equations (5) and (6) and their derived functions are substituted into the result, thereby obtaining the simultaneous algebraic equations, including  $a_1 - f_2$ . When  $d_1$  and  $f_1$  are eliminated, the following simultaneous equations are obtained:

$$[q_{ij}] \begin{bmatrix} a_1 \\ \vdots \\ f_2 \end{bmatrix} = \begin{bmatrix} K_t W_d(L_2, s) \\ 0 \\ \vdots \\ 0 \end{bmatrix}, \quad i, j = 1 \dots 10 \quad (19)$$

where

$$\begin{aligned} q_{11} &= \left( \frac{L_a}{R_a} s + 1 \right) (J_1 s^2 + \varepsilon s) + K_t K' \frac{s}{R_a} \xi_1 \\ q_{12} &= 2 E_1 J_1 (1 + C_1 s) \left( \frac{L_a}{R_a} s + 1 \right) \xi_1^2 \\ q_{13} &= \left( \frac{L_a}{R_a} s + 1 \right) (J_m s^2 + \varepsilon s) + K_t K' \frac{s}{R_a} \xi_1 \\ &\vdots \\ q_{14} &= J_4 s^2 \xi_1 + \cosh \xi_1 L_1 + E_1 J_1 (1 + C_1 s) \xi_1^2 \sinh \xi_1 L_1 \\ q_{16} &= E_2 J_2 (1 + C_2 s) \xi_2^2, \quad q_{17} = -E_2 J_2 (1 + C_2 s) \xi_2^2 \\ q_{18} &= -E_1 J_1 (1 + C_1 s) \xi_1^2 \sin \xi_1 L_1 \\ q_{19} &= -E_1 J_1 (1 + C_1 s) \xi_1^2 (\cos \xi_1 L_1 + \cosh \xi_1 L_1) \\ q_{20} &= -E_1 J_1 (1 + C_1 s) \xi_1^2 \sinh \xi_1 L_1 \\ q_{21} &= J_4 s^2 \xi_2, \quad q_{22} = E_2 J_2 (1 + C_2 s) \xi_2^2 \\ q_{27} &= J_4 s^2 \xi_2, \quad q_{28} = -E_2 J_2 (1 + C_2 s) \xi_2^2 \end{aligned}$$

Parts of the matrix elements have been omitted due to the restriction on the number of pages. When the inverse matrix of the 10 x 10 matrix  $[q_{ij}]$  in equation (19) is obtained, the previously undetermined coefficients are determined. When the results are substituted into equation (15), the following intelligent robot function is obtained:

$$\frac{W_1(x_1, s)}{W_d(L_1, s)} = \left\{ \frac{\Delta a_1}{\Delta} \sin \xi_1 x_2 + \frac{\Delta b_1}{\Delta} (\cos \xi_2 x_2 - \cosh \xi_3 x_2) + \frac{\Delta c_1}{\Delta} \sinh \xi_2 x_2 \right\} \frac{k_2 G_d}{s} \quad (20)$$

if

$$\Delta a_1 = \begin{vmatrix} 1 & \xi_{11} & \xi_{1n} \\ 0 & \vdots & \vdots \\ 0 & \xi_{n2} & \xi_{nn} \end{vmatrix}, \quad \Delta b_1 = \begin{vmatrix} \xi_{11} & 1 & \xi_{13} & \dots & \xi_{1n} \\ \vdots & 0 & \vdots & \vdots & \vdots \\ \xi_{1n} & 0 & \xi_{n3} & \dots & \xi_{nn} \end{vmatrix}$$

$$\Delta c_1 = \begin{vmatrix} \xi_{11} & \xi_{12} & 1 & \xi_{14} & \dots & \xi_{1n} \\ \vdots & \vdots & 0 & \vdots & \vdots & \vdots \\ \xi_{n1} & \xi_{n2} & 0 & \xi_{n4} & \dots & \xi_{nn} \end{vmatrix}, \quad \Delta = \begin{vmatrix} \xi_{11} & \dots & \xi_{1n} \\ \vdots & \vdots & \vdots \\ \xi_{n1} & \dots & \xi_{nn} \end{vmatrix}$$

The transient response characteristics of the arms are examined to study the followup property to the displacement of the tip of the elastic arm. As the input function, the step function whose magnitude is  $W_d^*$  is used, i.e.,

$$W_d(L_1, s) = \frac{W_d^*}{s} \quad (21)$$

At this time, equation (20) becomes:

$$\frac{W_1(x_1, s)}{W_d^*} = \left\{ \frac{\Delta a_1}{\Delta} \sin \xi_1 x_2 + \frac{\Delta b_2}{\Delta} (\cos \xi_2 x_2 - \cosh \xi_3 x_2) + \frac{\Delta c_1}{\Delta} \sinh \xi_2 x_2 \right\} \frac{k_2 G_d}{s} \quad (22)$$

In the numerical computation, which will be shown later, the step response change during the arm tip displacement is obtained by using a numerical Laplace reverse transformation method for equation (22). The method in Reference (9) has been adopted as the numerical Laplace transformation method.

## 9. Experiment

A diagram of the experimental apparatus used in this experiment is shown in Figure 2. The various constants of the arms and the motors used in the experiment are shown in Tables 1 to 4. The elastic arms comprise two aluminum beams, in which thickness  $B_j$ , width  $H_j$ , and length  $L_j$  ( $j = 1, 2$ ) are uniform. The first and second arms each use three inner arms of different lengths. They are designated as A-1, B-1, and C-1 for the first arm, from shorter to longer, and as A-2, B-2, and C-2 for the second arm. One end of the first arm is fixed to the motor, and the arm can be turned only in the horizontal plane with the motor shaft as the center. The other end of the first arm and the second arm are linked by the fixed joint at the

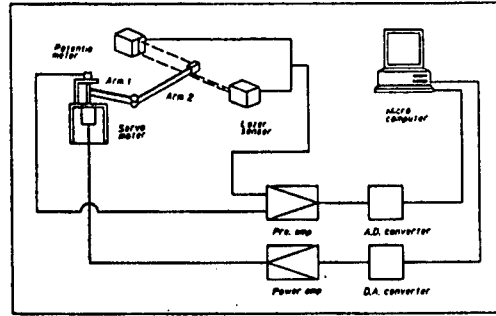


Figure 2. Schematic Diagram of Experimental System

Table 1. Tip Load Constants

| Payload                 | MA1                    | MB                     |
|-------------------------|------------------------|------------------------|
| Mp (kg)                 | $4.525 \times 10^{-2}$ | $3.030 \times 10^{-1}$ |
| Jp (kg·m <sup>2</sup> ) | $4.509 \times 10^{-6}$ | $5.826 \times 10^{-5}$ |

Table 2. Elastic Arm Constants

(a) Arm 1

|                                  | A-1                     | B-1                     | C-1                     |
|----------------------------------|-------------------------|-------------------------|-------------------------|
| $\rho_1$ (kg/m <sup>3</sup> )    | $2.6785 \times 10^3$    | $2.6843 \times 10^3$    | $2.6647 \times 10^3$    |
| B <sub>1</sub> (m)               | $3.000 \times 10^{-2}$  | $3.000 \times 10^{-2}$  | $2.998 \times 10^{-2}$  |
| H <sub>1</sub> (m)               | $3.000 \times 10^{-3}$  | $3.000 \times 10^{-3}$  | $3.000 \times 10^{-3}$  |
| L <sub>1</sub> (m)               | 0.200                   | 0.300                   | 0.449                   |
| A <sub>1</sub> (m <sup>2</sup> ) | $9.000 \times 10^{-5}$  | $9.000 \times 10^{-5}$  | $8.995 \times 10^{-5}$  |
| E <sub>1</sub> (Pa)              | $5.263 \times 10^{10}$  | $5.652 \times 10^{10}$  | $6.187 \times 10^{10}$  |
| I <sub>1</sub> (m <sup>2</sup> ) | $6.750 \times 10^{-11}$ | $6.750 \times 10^{-11}$ | $6.746 \times 10^{-11}$ |
| C <sub>1</sub> (sec)             | $2.046 \times 10^{-4}$  | $3.777 \times 10^{-4}$  | $8.836 \times 10^{-4}$  |

(b) Arm 2

|                                  | A-2                     | B-2                     | C-2                     |
|----------------------------------|-------------------------|-------------------------|-------------------------|
| $\rho_2$ (kg/m <sup>3</sup> )    | $2.7136 \times 10^3$    | $2.7090 \times 10^3$    | $2.7117 \times 10^3$    |
| B <sub>2</sub> (m)               | $2.600 \times 10^{-2}$  | $2.600 \times 10^{-2}$  | $2.600 \times 10^{-2}$  |
| H <sub>2</sub> (m)               | $2.000 \times 10^{-3}$  | $2.000 \times 10^{-3}$  | $2.000 \times 10^{-3}$  |
| L <sub>2</sub> (m)               | 0.199                   | 0.300                   | 0.449                   |
| A <sub>2</sub> (m <sup>2</sup> ) | $5.200 \times 10^{-5}$  | $5.200 \times 10^{-5}$  | $5.200 \times 10^{-5}$  |
| E <sub>2</sub> (Pa)              | $5.539 \times 10^{10}$  | $6.194 \times 10^{10}$  | $6.774 \times 10^{10}$  |
| I <sub>2</sub> (m <sup>2</sup> ) | $1.733 \times 10^{-11}$ | $1.733 \times 10^{-11}$ | $1.733 \times 10^{-11}$ |
| C <sub>2</sub> (sec)             | $2.997 \times 10^{-4}$  | $5.532 \times 10^{-4}$  | $1.060 \times 10^{-3}$  |

Table 3. Intermediate Joint Constants

|                         | 0°                     | 30°                    | 45°                    |
|-------------------------|------------------------|------------------------|------------------------|
| Mh (kg)                 | $2.700 \times 10^{-1}$ | $2.700 \times 10^{-1}$ | $2.699 \times 10^{-1}$ |
| Jh (kg·m <sup>2</sup> ) | $8.055 \times 10^{-5}$ | $8.055 \times 10^{-5}$ | $8.053 \times 10^{-5}$ |

Table 4. Motor Constants

|              |                         |                          |
|--------------|-------------------------|--------------------------|
| Jm :         | $5.5657 \times 10^{-5}$ | (kg·m <sup>2</sup> )     |
| $\epsilon$ : | $9.7004 \times 10^{-3}$ | (kg·m <sup>2</sup> /sec) |
| Kt :         | $6.2400 \times 10^{-2}$ | (N·m/A)                  |
| K' :         | $6.0925 \times 10^{-2}$ | (V·sec/A)                |
| La :         | $1.9 \times 10^{-3}$    | (H)                      |
| Ra :         | 13.2                    | ( $\Omega$ )             |

intermediate part. The attaching angle of the second arm can be changed to 0°, 30°, or 45°, depending on the kind of intermediate joints. An armature-control-type DC servomotor is employed as the motor. A direct coupling method is used for the arm connection. A load mass is attached to the tip of the second arm. Two kinds of loads ( $M_A$ ,  $M_B$ ), with different masses, for the tip load, are used. A laser sensor is used to measure the displacement. The laser sensor comprises a light emitting part and a light receiving part. The amount of light received by the arm and the output voltage of the sensor have a linear relationship. The amount of arm tip displacement is converted into the amount of light screening by slanting the tip of the arm with respect to the laser light. Now the output voltage from the sensor is amplified to  $\pm 5$  V with a preamplifier. After A/D conversion, the signal is sent to a microcomputer. A driving signal from the microcomputer undergoes D/A conversion. Then the signal is amplified through a power amplifier and an armature current is obtained which, in turn, is applied to the motor.

Since the motor is directly controlled by the armature current in this experiment, it is assumed that no effect is produced by the circuit inductance or counter electromotive force, and that  $L_a = 0$ (H) and  $K' = 0$ (V sec/A) are set.<sup>10</sup>

In the meantime, information regarding the arm tip displacement is sent to the computer from the laser sensor through an A/D converter over a constant time interval  $T$  (sampling period). When the sampling period  $T$  is long, not only can the change in the tip's position not be obtained correctly, but also arm resonance tends to occur when the tip's position is controlled. In this experiment,  $T = 3$  (m sec) has been adopted, and this is sufficiently shorter than the period of free vibration of the arm. Since the arm tip speed cannot be measured directly, the speed signal  $V_v$  at time  $i$  is obtained by:

$$V_v = (\text{position signal at time } i) - (\text{position signal at time } (i-))$$

This speed signal is used. The speed feedback gain is divided by the sampling period  $T$ , and the tip's speed is computed. Based on the position signal  $V_w$  and the speed signal  $V_v$ , obtained by the method described above, the following computation is performed for every sampling period in the computer:

$$V' = f_{gd} \cdot (V_{wd} - V_w) - f_{gv} \cdot V_v,$$

where  $V'$  is a control signal,  $f_{gd}$  and  $f_{gv}$  are the position feedback gain and the speed feedback gain used in the experiment, respectively, and  $V_{wd}$  is the objective position signal. The following relationships exist between the position and speed feedback gains in theory and experiments:

$$\begin{aligned} G_d &= 65.78 \times f_{gp} \\ G_d &= 65.78 \times f_{gv} \times T \end{aligned}$$

The value 65.78 (V/m) is the voltage-displacement of the laser sensor. In this experiment, the objective distance  $W_d^* = 3.8$  (cm).

#### 4. Numerical Computation, Experimental Examples, and Their Interpretations

Figure 3 shows the theoretical curve of the displacement of the feedback-controlled arm tip and the change in the root angle when the length of the arm is changed. When the arms of A-1 and B-2 are used, the movement of the numerous vibrations (secondary mode) appears in the root angle. The movement of a small number of vibrations (primary mode) acts about the same as the tip's displacement. After four seconds, both are converged. In Figure 3(b), however, where the longer arms B-1 and B-2 are used, the secondary mode of the root angle appears even after the tip displacement has been converged. Furthermore, when the tip load is changed from  $M_B$ , which is heavier than  $M_{A1}$  (Figure 3(c)), the tip displacement phase is delayed, but the root angle phase is not. The following can be gathered from these figures: When the length of the arm is short, elastic deformation is small and, therefore, the tip can be moved to the objective position even by the conventional feedback method for angle change, while, when the arm becomes longer,  $\theta = W/L$  does not hold true any longer and the tip's displacement cannot be controlled by the angle feedback.

In Figure 4, the theoretical and experimental values of the arm tip displacement are compared. It is found that the coincidence of the theoretical and experimental results is excellent, as shown in the figure.

Now let us observe the change in the tip displacement response when the position and speed feedback gains are changed. In Figure 5, the theoretical values of the tip displacement are shown when  $G_v$  is changed under the fixed state of  $G_d = 131.5$  A/m. In Figure 5(a), the tip displacement is quickly converged into the objective position as  $G_v$  increases. When  $G_v$  is increased further, it is found that the effect of the second mode becomes conspicuous and the tip convergence worsens, as shown in Figure 5(b).

In Figure 6, the changes in tip displacements, when the value of  $G_d$  is 131.5 A/m in Figure 6(a) and 263.1 A/m in Figure 6(c), are shown in

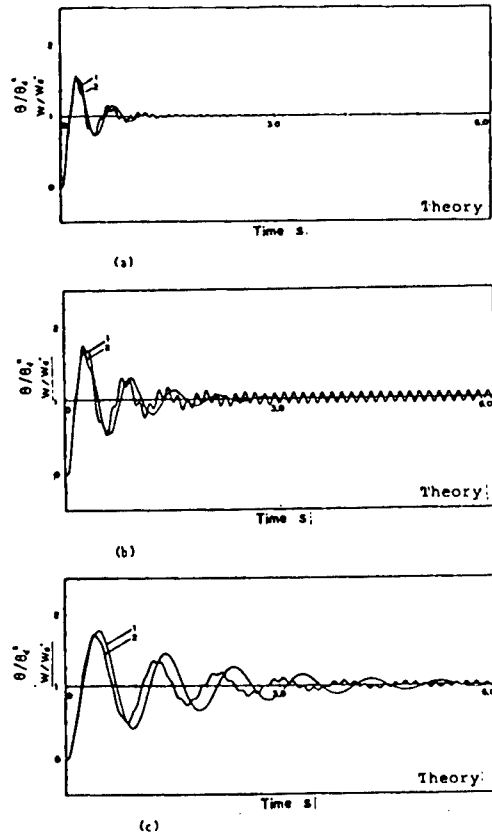


Figure 3. Step Response Change in Tip Displacement and Angle, Theoretical Values  
 (a) Arm 1: A-1, Arm 2: B-2,  $M_p$ : MA1  
 (b) Arm 1: B-1, Arm 2: B-2,  $M_p$ : MA1  
 (c) Arm 1: B-1, Arm 2: B-2,  $M_p$ : MB. Curve 1: tip displacement, Curve 2: Root angle

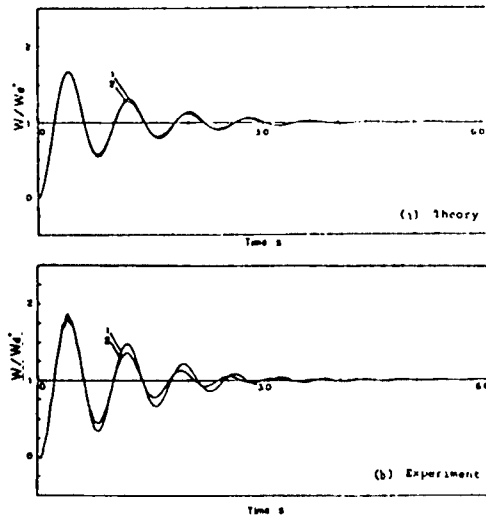


Figure 4. Step Response Change in Tip Displacement  
 Arm 1: C-1, Arm 2: A-2, M: MA1,  $\theta=0^\circ\text{C}$   $C_d=131.5$  A/m  
 Curve 1:  $C_v=0.789$  A<sub>s</sub>/m; Curve 2:  $C_v=1.579$  A<sub>s</sub>/m

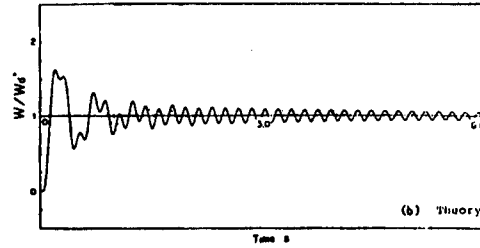
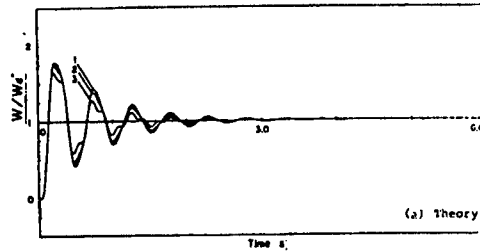


Figure 5. Step Response Change in Tip Displacement  
 Arm 1: A-1; Arm 2: C-2;  $M_p$ : MA1,  $\theta 30^\circ$ ,  
 $C_d = 131.5$  A/m  
 (a) Curve 1:  $G_v=0.789$  As/m; Curve 2:  $G_v=1.184$  As/m;  
 Curve 3:  $G_v=1.974$  As/m  
 (b)  $G_v=2.367$  As/m

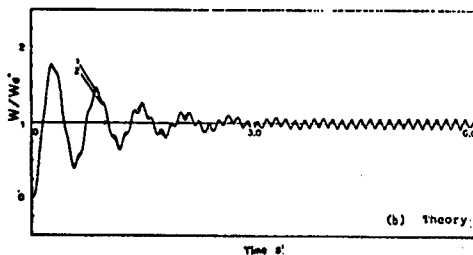
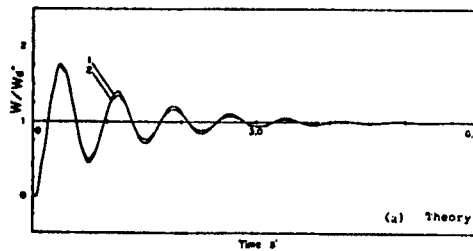


Figure 6. Step Response Change in Tip Displacement  
 Arm 1: C-1; Arm 2: B-2;  $M_p$ : MA1,  $\theta = 30^\circ$   
 (a)  $G_d$ : 131.5 A/m; Curve 1:  $G_v=0.789$  As/m;  
 Curve 2:  $G_v=1.184$  As/m  
 (b)  $G_d$ : 263.1 A/m; Curve 1:  $G_v=2.368$  As/m;  
 Curve 2:  $G_v=2.763$  As/m

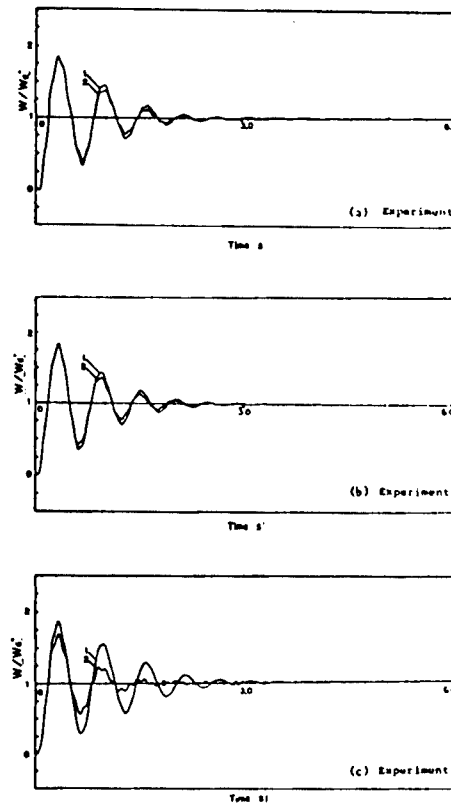


Figure 7. Step Response Change in Tip Displacement

Arm 1: B-1; Arm 2: B-2;  $M_p$ : MA1,  $C_d = 131.5$  A/m

(a)  $\theta = 0^\circ$ , Curve 1:  $G_v = 0.789$  As/m; Curve 2:  $G_v = 1.184$  As/m

(b)  $\theta = 30^\circ$ , Curve 1:  $G_v = 0.789$  As/m; Curve 2:  $G_v = 1.184$  As/m

(c)  $\theta = 45^\circ$ , Curve 1:  $G_v = 0.000$  As/m; Curve 2:  $G_v = 1.973$  As/m

theoretical values. In Figure 6(a), the value at which the tip displacement is converged to the objective position is shown. When the value of  $G_d$  is twice that in Figure 6(a), a  $G_v$  sufficient for converging the tip displacement could not be found, as shown in Figure 6(b).

Finally, the change in the tip displacement step response with respect to the joint angle change is examined. In Figure 7, the tip displacement step response when the joint angle is changed from  $0^\circ$  to  $45^\circ$ , which is obtained by the experiment, is shown. With respect to the change in the joint angle, a conspicuous change does not appear in the overshoot or in the primary mode. As the angle increases, the secondary mode tends to occur readily.

## 5. Conclusion

The problem involving the position feedback control and the speed feedback control of the tip displacement was analyzed theoretically and environmentally for a two-link elastic robot arm by directly measuring the tip's displacement using sensors. In the theoretical analysis, the motion equations of the arms were formed taking into consideration the effects of the lateral and vertical vibrations of the arms, internal damping, translation inertias of the joints and tip loads, rotation inertia, and rotation inertia of the motor.

As the solution, the Laplace transformation method in the time domain was used, while the numerical Laplace reverse transformation method was used for the reverse solution. The coincidence of the values obtained through theoretical computation and the results of the experiment was excellent, and it was found that the control problem involving the two-link elastic arm could be grasped theoretically. When both the Laplace transformation method and the numerical Laplace reverse transformation methods are used together, proof of the orthogonality of the modes is not required, nor is the residue computation. Therefore, it is believed that this method is particularly useful for analyzing the behavior of multilink arms.

If the displacement of the elastic arm is controlled, the convergence of the primary mode improves when the speed feedback gain is increased, but the effect of the secondary mode becomes greater with the increase in feedback gain. Therefore, convergence to the objective position does not occur when a certain value is exceeded. When the position feedback gain exceeds a certain value, the speed feedback gain, which has been converged to the objective position, disappears. Therefore, adequate values should be used for the position and speed feedback gains, and these values can be estimated by numerical computation utilizing simulations. Furthermore, it has been confirmed that the secondary mode tends to occur readily in the displacement of the elastic arm tips with the increase in the angle of the fixed-joint portion.

#### References

1. R.H. Cannon, Jr., and E. Schmitz, INT. J. ROBOTICS RES, Vol 3 No 3, 1984, p 62.
2. Tahara and Naganami, TRANSACTION OF THE JAPAN SOCIETY OF MECHANICAL ENGINEERS, Vol 54 No 498, c, 1988, p 363.
3. Ueno, Tahara, and Naganami, "Vibrations of Robot Arms in a Plane," Symposium Papers at the Tohoku Branch of the Society of Design and Drawing Engineers, 1986.
4. Aoshima and Naganami, "TRANSACTION OF THE JAPAN SOCIETY OF MECHANICAL ENGINEERS, C, to be published.
5. W.J. Book, et al., Trans. ASME, JOURNAL OF DYN. SYST. MEAS. CONTROL, 1975, p 424.
6. Fukuda, TRANSACTIONS OF THE JAPAN SOCIETY OF MECHANICAL ENGINEERS, Vol 51 No 468, C, 1985, p 2140.
7. Fukuda and Isogai, Ibid., Vol 53 No 487, C, 1987, p 664.
8. Fukuda and Arakawa, Ibid., Vol 53 No 488, C, 1987, p 954.
9. W.T. Weeks, ASSOCIATION COMP. MACH., Vol 13 No 3, 1966, p 419.
10. "Introduction to Servo-Technology for Mechatronics," Nikkan Kogyo Shimbunsha, 1986, p 14.

## Obstacle Avoidance Teaching Techniques for Two-Link Manipulator

43064062 Tokyo 4TH INTELLIGENT ROBOTS SYMPOSIUM PAPERS in Japanese  
13/14 Jun 88 No 221 pp 257-262

[Article by Kiyoji Muramatsu (student member of the Society of Instrument and Control Engineers (I&C), Nagoya University; Gisho Katayama and Masami Into (regular members of I&C), Nagoya University]

### [Text] 1. Introduction

In this subject, the techniques for teaching the obstacle avoidance of two-link manipulators is studied, and teaching models are proposed. With respect to the problem involving the obstacle avoidance of the manipulators, various algorithms have been proposed in robotics and computational geometry, but a definitive method has not yet been established. This is one example of problems that can be solved simply by human beings, but pose serious difficulties for computers.

A potential method<sup>1</sup> and a free-space method<sup>2</sup> are the two main approaches toward analytically solving the obstacle avoidance techniques for the manipulators. However, there are advantages and disadvantages in both methods. With the potential method, a path (the moving path of the manipulator from an initial state to an objective state) can be found by using a mathematical programming method when the potential is defined, but the problem of multiple peaks remains. Therefore, there is the risk of deadlock. With the free space method, the path can always be found if conversion to the free space is perfect. Currently, however, no perfect conversion method exists, and sometimes the path cannot be found.

Since all the problems cannot be solved using the analytical method described above, it is believed that the incomplete portion can be complemented by a teaching system, in which the human thinking process is adopted. With the analytical method, the same procedures must always be repeated and when lengthy computing time is required, the problem becomes very serious. With the method utilizing knowledge, similar problems can be solved readily by utilizing the knowledge obtained through experience.

## 2. Construction of Teaching Model<sup>3-6</sup>

### 2.1 Definition of Problem

A manipulator is to be moved in a two-dimensional plane, and the angle between the first link and the second link, which correspond to the human elbow, is set in the range of 0-180 degrees. The configurations and the number of obstacles are basically arbitrary (Figure 1).

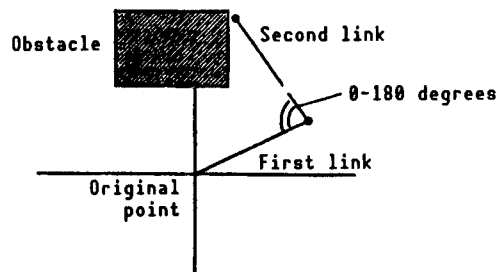


Figure 1. Two-Link Manipulator

It is assumed that the moving path of the manipulator from the initial state to the objective state can be obtained without fail, and objectives that cannot be reached are not considered. It is further assumed that the minimum required knowledge is given as a priori knowledge in order to reach the objective state. What is given as a priori knowledge is knowledge such that the manipulator advances by a specified distance when no obstacle is present, while it advances in different direction when an obstacle is present. At first, the manipulator finds the path by a trial-and-error method utilizing only a priori knowledge.

### 2.2 Introduction of Subgoal (Secondary Objective)

Several intermediate objective states are set in order to obtain a path on which the manipulator will not hit an obstacle from the initial state to the objective state. Then the operation of the manipulator up to the intermediate objective is determined. In this study, this intermediate objective is expressed as a subgoal (secondary objective). It is intended to teach the determining knowledge of the local subgoal expressed in a priori knowledge and the determining knowledge of the broad-area subgoal. The subgoal is expressed by the direction to which the manipulator is to advance next, and the current direction, with the advancing direction of the manipulator up to that point and the point of attention (explained later) as reference (Figure 1).

### 2.3 Outline of Model

The proposed teaching model is divided into two portions--an executing portion and a teaching portion. The executing portion utilizes the knowledge in a knowledge base (KB), estimates the subgoal, and finds the path from the initial state to the objective. The teaching portion creates new knowledge based on the evaluated data obtained in one trial and adds the knowledge to the KB. In the KB, a production rule, in which the present

state of the manipulator is made a conditional portion and the subgoal is an action portion, is stored as knowledge.

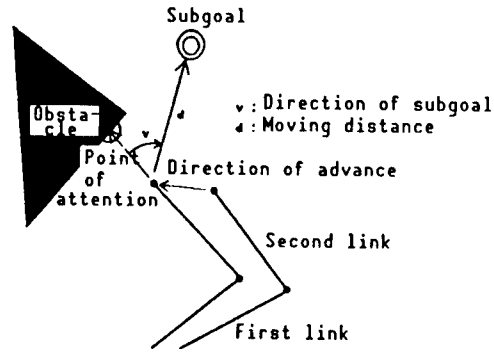


Figure 2. Definition of Subgoal

The main data flow is shown in Figure 3. The state of the subgoal, which was determined previously before and after the application, is stored in short-term memory (STM). The advancing direction of the manipulators, the obstacle as viewed from the tip of the second link, the objective point, the position of the original point, etc., which are obtainable in the STM, become the physical states. When certain knowledge is applied in tact to the current state, this state becomes a mental state. If these states are adequate, they become the subgoal, and the manipulator is moved to the subgoal. The data obtained by evaluating the manipulator operation are sequentially stored in the memory region until one trial (the entire process until one path is obtained) is finished. After the trial, the results are sent to the teaching portion.

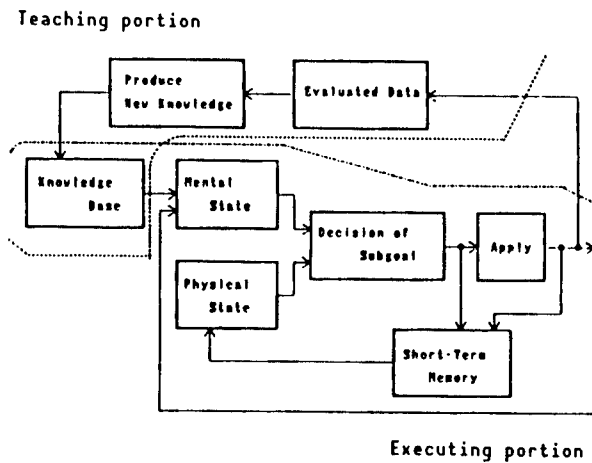


Figure 3. Teaching Model

### 3. Teaching Portion<sup>9</sup>

#### 3.1 Information Obtained From Two-Link System

Information which the manipulator can obtain directly in a two-dimensional working space is limited to local information. The source of information

is limited to the field of view. The attitudes of the manipulators and the position (relative positional relationship) in space, etc., can be listed as broad informational items. These pieces of information are difficult to obtain except when special sensors are provided. Therefore, the knowledge based on the broad-area information must be obtained indirectly by teaching.

In this study, local information will be described by introducing concepts of points of attention and characteristic points (a point indicating an objective, the position of an obstacle, etc.).

### 3.2 Expression of Knowledge

In past studies, in order to expand the scope of applications, methods of generalization of the knowledge obtained in the special state comprised the mainstream.<sup>7</sup> When a man thinks of obstacle avoidance, however, he does not make accurate measurements in each case, and the grasping of the surrounding state is quite sensory in nature. Based upon this consideration, the generalization of special knowledge is not used in this study, but the following method is adopted instead: allowance widths are provided for numerical data in advance, general knowledge, to some extent, is formed from the beginning, and this knowledge is applied. Therefore, directions are expressed only by the values of 0-7 (8 directions) and distances by 0-19 (20 stages).

The surrounding state of the tip of the second link is assigned to the condition portion of the production rule. This is because the tip of the second link is the point at which the largest informational items of the link system can be obtained. The surrounding state of the tip of the second link can be expressed by a set of elements, in which direction vector  $V$  and distance  $d$  to the characteristic point present in that state are combined into one set. Therefore, the state  $e_t$  at time  $t$  can be expressed by:

$$e_t : \bigcup_i (v_i, d_i) \quad i=1,2,3,\dots,n$$

$n$ : number of characteristic points

The character  $i$  expresses the label (number) of the characteristic point so that the obstacle is 1 and the objective point is 2. In this study, as the elements of  $e_t$ , three points, i.e., the objective point ( $i = 1$ ), one point of the nearest obstacle ( $i = 2$ ), and the original point ( $i = 3$ ), are adopted. Information regarding the original point is effective in indirectly obtaining the information of the first link.

When the manipulator moves from a certain state, the characteristic point which most strongly affects the manipulator's action must exist in the environment. In this study, this characteristic point is called the point of attention. The next action is determined, using this point as a reference. Then, as a subgoal to be applied to the manipulator in the state  $e_t$ , the point of attention  $i$ , the vector  $V_i$  in the moving direction with the point of attention as a reference, and the moving distance  $d_i$  are imparted into the action portion. The subgoal  $b_t$  can then be expressed by:

$$b_t: (i, v_{it}, d_{it}) \\ i = 1, 2, \text{ or } 3$$

Therefore, application of  $b_t$  in the state  $e_t$  at time  $t$  is expressed as:

$$(e_t, b_t)$$

This also expresses the knowledge as the form of the production rule.

### 3.3 Inference of Subgoal

Inference of the subgoal is carried out by selecting one knowledge item, based on matching the present state to the condition portion, and by applying the knowledge to the present state.

In order to seek the knowledge efficiently, the set of knowledge (knowledge base) is classified into two portions. One is the set of knowledge provided at first as a priori knowledge. Since this knowledge is given as the minimum required knowledge for a manipulator to avoid an obstacle, the actual situation is not considered, and the knowledge, which will not be used in the future, is included. The other is the set of the knowledge obtained as a result of teaching. Since this knowledge is formed based on the actual state of the manipulator, it is more specific than a priori knowledge, and the possibility of future application is high. Therefore, the set of knowledge with high application possibilities and which has been obtained as a result of teaching is used as the first-stage seeking space. When suitable knowledge has not been found, the set of knowledge provided as a priori knowledge is used as the second-stage seeking space, and one item of knowledge is selected.

In the first-stage seeking process, only the knowledge for which the condition portion agrees perfectly with the current state is selected. For the a priori knowledge, however, it is not always possible for knowledge agreeing perfectly with the current state to exist. Therefore, when knowledge for which the condition portion agrees with the current condition is not found at the second stage, the item of knowledge most suitable for the current state is selected by using evaluative information. Since the knowledge is expressed by a simple integer at this time, knowledge with the same value appears if only one evaluative function is used, and contention occurs. Multiple evaluative functions are used to eliminate the contention, and the seeing space is narrowed when one evaluative function is applied. When the number of knowledge items in the space is reduced to one, this item is adopted as the selected knowledge. In this study, the following three evaluative functions are used sequentially. "Difference," as used in the following explanation, refers to the difference between the current state and the element corresponding to the condition portion of the knowledge. The functions are:

$$f_1 = \sum_{i=1}^3 (w_i \cdot \Delta v_i) + \Delta d_2$$

$\Delta v_1$ : difference in directions to objective point  
 $\Delta v_2$ : difference in directions to obstacle

$\Delta v_3$ : difference in directions from original point  
 $\Delta d_2$ : difference in distances to obstacle  
 $w_1$ : positive constant

$$f_2 = \Delta d_1$$

$\Delta d_1$ : Difference in distances to objective point

$$f_3 = [\text{distance from tip of second link after application of knowledge to objective point}]$$

#### 4. Teaching Portion<sup>9</sup>

##### 4.1 Evaluating Functions and $h_t$ Graph

In order to acquire knowledge by learning and to develop techniques, it is important to repeat a trial. However, techniques are not improved solely through repeating the trial. It is important that the results of each trial be confirmed and evaluated. The evaluation is called "knowledge results: (KR)" or "feedback." The fact that learning does not occur if the KR is not imparted has been confirmed in the experiments conducted by many psychologists, such as Bilodean, et al., (1959), and Reynolds and Adams (1953).<sup>8</sup>

In this study, evaluative functions are introduced in which each step (a process from the determination of one subgoal to the movement to the subgoal) in one trial is evaluated. Since the information obtained in each step is local information, the evaluative functions produce only the local evaluation. Here, the objective that the tip of the second link reaches the objective point is emphasized, and the evaluative function  $h_t$  time  $t$  is defined as follows:

$$h_t = \sum_{i=1}^2 c_i (d_{it} - d_{it-1})$$

$t$ : time  
 $d_{it}$ : distance is characteristic point  $i$   
 $c_i$ : 1 ( $i = 1$ , objective point)  
       -1 ( $i = 2$ , obstacle)

The value of  $h_t$  becomes large when the objective is approached and small when the obstacle is approached.

The graph which plots the values of the evaluative function  $h_t$  with time is called a  $h_t$  graph (Figure 4). When operating the manipulator, not only the current state but also "what action did the manipulator take in the previous state?" is always described. The  $h_t$  graph is one index showing such a relation. In the  $h_t$  graph, positive values denote proper operation, while negative values denote incorrect operation. When the application of  $b_t$  at  $e_t$  is successful, the evaluation produces a value greater than zero. When the knowledge applications are successful from the initial state to the objective state, the  $h_t$  graph holds high values in the positive region.

Conversely, when all the applications fail, the values remain in the negative region. Therefore, the knowledge ( $e_t$ ,  $b_t$ ), as applied at time  $t$ , is adjusted so that a high level is maintained in the  $h_t$  graph, and the knowledge formed here becomes that obtained by learning. Therefore, the operation of the manipulator is improved by repeating the trial.

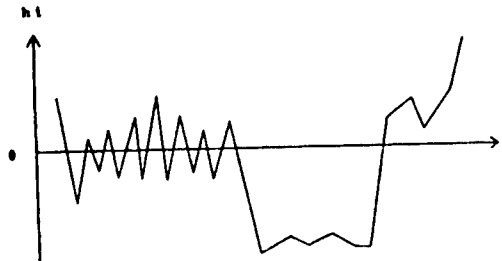


Figure 4.  $h_t$  Graph

#### 4.2 Extraction of Broad-Area Information

Since only local information is utilized by the evaluation function  $h_t$ , it is difficult to evaluate a series of operations over a broad area. When the features of the  $h_t$  graph are grasped, however, the broad-area information can be extracted, and the evaluation can be corrected (post correction) by utilizing the information. Deadlocks and backtracking are used as the most characteristic examples, and the extraction and utilization of the broad-area information will be described.

Deadlock refers to the state in which the manipulator cannot move in any direction (so-called fumble state). Immediately before falling into this state, the manipulator tries to find the possible path many times. Therefore, the positive and negative values appear many times. The fact that the evaluation is high, even if the manipulator is in the deadlock state, is definitely not good. This evaluation must be corrected by a post evaluation. In backtracking, the manipulator goes back after it has been recovered from the deadlock state, and is brought to a remote point from the objective point. During this period, low evaluation continues. When the manipulator goes back to a certain point and finds a path toward the objective point again, the evaluation becomes high and the path seeking continues. Figure 4 illustrates the  $h_t$  graph of the deadlock and backtrack states.

As featured in the  $h_t$  graph for the deadlock, the values in the range from the DLP, which is the starting point of the deadlock state, to the DLX, which is the end point, are lowered.

Now, let us consider the similar path shown in Figure 5. Figure 5(a) shows the path when the deadlock has occurred, and (b) shows the corresponding  $h_t$  graph. When only the deadlocked portion is extracted and the evaluation is lowered, the deadlock state can be avoided. The fact that the manipulator approaches the deadlock state is not changed, and the fundamental improvement is not achieved. To solve this problem, it is necessary to find the point of cause of the deadlock fault and to remove the cause. The point

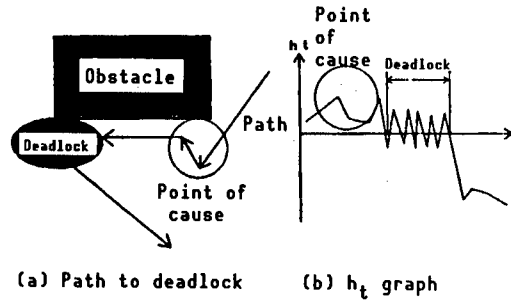


Figure 5. Point of Cause of Deadlock

of cause is difficult to spot on the  $h_t$  graph. Now the point of cause (DLE) is defined in accordance with the following consideration.

When the path is traced back from the deadlock state, a point must exist at which the operation of the manipulator changes, as shown by the path in Figure 5(a). If the manipulator had taken another path, it would not have fallen into the deadlock. Therefore, the path is traced back from the point where the deadlock begins, and the point on the path at which the large change occurred for the first time is considered to be the point of cause. The change in the path appears as the change in values on the  $h_t$  graph. Therefore, the point of the cause of deadlock on the  $h_t$  graph is the first point at which the change appears on the graph when the path is traced back from the DLP. When the path is traced back from the DLP, and the initial point is reached without finding the point of cause, it can be thought that the manipulator has operated incorrectly from the start. Based on the above description, the DLE is defined as follows:

$$\alpha = \frac{\sum_{t=1}^{DLP-1} h_t}{(DLP-1)},$$

where  $\alpha$  is the average value from the initial point to the DLP. The path is traced back, and the point at which the evaluated value intersects  $\alpha$  is defined as the DLE (Figure 6). When the evaluation at DLE + DLX is lowered, the value at the deadlock state is corrected to an adequate one, as is its cause.

A low evaluation can be imparted for the backtracking state only when local information is used and the cause is believed to be the deadlock. Therefore, only the deadlock is noted in this study, and the features are extracted.

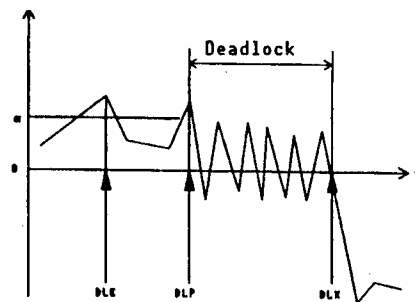


Figure 6. Definition of Point of Cause DLE

### 4.3 Teaching Utilizing $h_t$ Graph

Based on the  $h_t$  graph, which is corrected by the method described in the previous section, a method for creating new technology (macro operator) will be described.

The evaluative point at time  $t$  is  $p(t)$ . The point at which erroneous operation is carried out appears at the minimum point on the graph. This point becomes the object point for teaching. The point at time  $t_0$  is the minimum point, and the two maximum points on either side of  $p(t_0)$  are  $p(t_1)$  and  $p(t_2)$ . The knowledge applied between time  $t_1$  and time  $t_2$  is regarded as the incorrect knowledge applied at  $(t_1-1)$  is believed to be the cause of the erroneous operation. Therefore, the macro knowledge, which can go straight from  $p(t_1-1)$  to  $p(t_2)$ , is created (Figure 7).

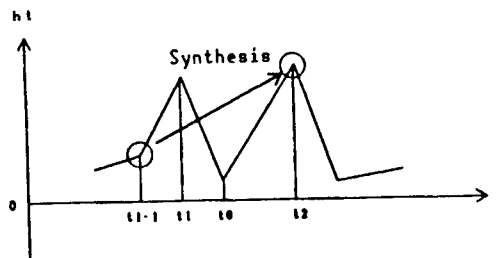


Figure 7. Creation of Macro Knowledge

The condition portion of the knowledge applied at time  $(t_1-1)$  is used. The action portion is the vectorially synthesized action portion of the knowledge. Therefore, the knowledge to be obtained can be expressed by:

$$(e_t, \sum_{t=t_1-1}^{t_2-1} b_t)$$

$t_1, t_2$ : Maximum points on either side of minimum point  
 $t_1-1$ : Point of cause

The procedure described above is performed for each minimum point, and the newly-created knowledge is added to the knowledge base.

### 5. Simulation

Simulation is carried out on a personal computer PC09801VX(NEC), and the program is described with Optimizing C 86.

The results of the simulation are shown in Figure 8. Figure 8(a) and (b) show the results before teaching and after five trials. On the link path after the five trials, the link's useless operations have been decreased from those existing before the teaching. This is shown by the heights of the values on the  $h_t$  graph.

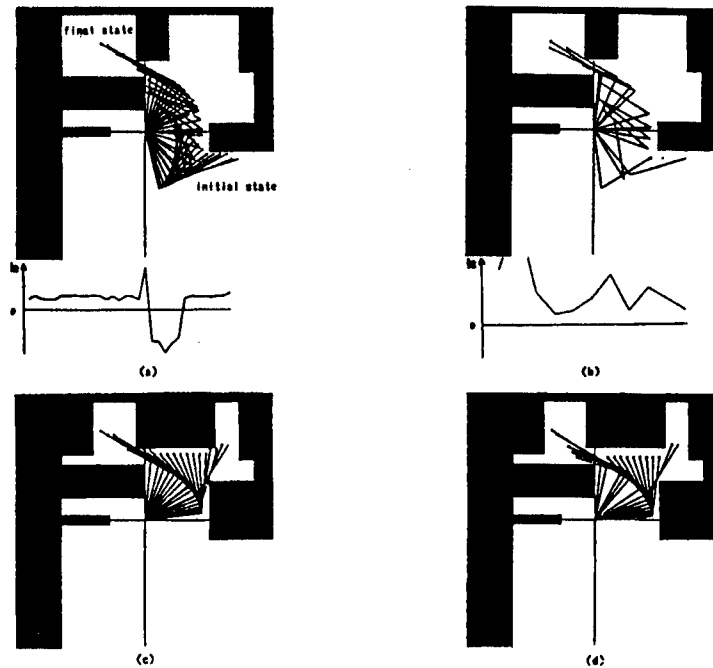


Figure 8. Simulation Results

Figure 8(c) and (d) show the results when the configurations of the obstacles are changed and the operations are executed. In (d), the knowledge obtained in (b) is applied intact to this obstacle, and a more efficient path is obtained than that in (c). This demonstrates that the knowledge obtained in one environment can be utilized effectively in another environment.

## 6. Conclusion

In this study, the role of action in the "recognition-action" cycle which is the basis for the model of teaching techniques, has been treated, taking the teaching of obstacle-avoidance operation of two-link manipulators as the subject matter.

The results obtained in this study are summarized as follows:

- (1) Methods utilizing teaching models for the obstacle-avoiding operation of manipulators have rarely been proposed in the past. In this study, this method is proposed for a two-link manipulator.
- (2) The knowledge for obstacle-avoidance operation of the two-link manipulator is shown by a simple expression comprising only the direction and the distance. Since the modularity of each element is high, this expression is useful when the knowledge has been corrected.
- (3) A means for plotting the graph of the local evaluation data and for creating the macro-knowledge, including broad-area information to some extent, by utilizing the graph is proposed.

(4) The fact that the knowledge obtained in one environment can be effectively utilized in another environment is shown by the simulation.

Problem areas in this study are described as follows:

(1) In this study, the information obtained in a given environment is described by using fixed simple features. It is necessary, however, to study teaching and inference in the information recognition process (characteristic extracting process) and to actively obtain information.

(2) The newly-created macro-knowledge is not always correct, as is apparent during the knowledge formation process. Therefore, it is necessary to examine the adequacy of the created knowledge.

#### References

1. Okutomi and Mori, "Determination of Robot Operation Using Potential Field," NIPPON ROBOT GAKKAISHI, Vol 1 No 3, October 1983, pp 226-232.
2. T. Lozano and Prez, "A Simple Motion-Planning Algorithm for General Robot Manipulators," IEEE JOURNAL OF ROBOTICS AND AUTOMATION, Vol RA-3, June 1987.
3. J.L. Growley, "Path Planning and Obstacle Avoidance," "Encyclopedia of Artificial Intelligence," Vol 2, 1987, pp 708-715.
4. Anzai, "Models for Teaching and Adapting Functions for Production System," KEISOKU TO SEIGYO, Vol 18 No 4, 1979, pp 303-311.
5. Anzai Yuichiro, "Cognitive Control of Real-Time Event-Driven System," COGNITIVE SCIENCE, Vol 8, 1984, pp 221-254.
6. J.R. Anderson, "Acquisition of Cognitive Skill," PSYCHOLOGICAL REVIEW, Vol 89 No 4, 1982, pp 369-406.
7. Hirukawa and Kitamura, "Modeling of Teaching Process of Manipulator Operation Based on Adaptation Production System," BIOMECHANISM, Vol 8, 1986, pp 67-76.
8. Yamanouchi and Haruki (editors), "Learning Psychology-Action and Recognition," Science Co., 1985.
9. Muramatsu, Kayanuma, and Ito, "Utilization of Knowledge in Obstacle Avoidance," SICE, Reference Material for 6th Artificial Intelligence Symposium, October 1987, pp 33-36.

- END -